



UNIVERSITY OF
BIRMINGHAM

Bis-homoleptic, Terdentate, Cyclometalates of Group 8 and 9

By

Thomas Wheildon Rees

A thesis submitted to

The University of Birmingham

For the degree of

DOCTOR OF PHILOSOPHY

School of Chemistry

University of Birmingham

Edgbaston

B15 2TT

September 2016

Abstract

Cyclometalates have been the focus of much attention in recent years and have applications ranging from photovoltaics to cancer therapies. Many heteroleptic terdentate complexes are known in the literature however bis-homoleptic terdentate cyclometalates remain rare. The metals of group 8 and 9 are of particular interest due to the excellent optoelectronic properties of their organometallic complexes.

In this work our initial focus was the synthesis of a novel series of substituted phenylbipyridine ligands. We then developed and optimised a new protocol for the cyclometalation of ruthenium. This gave access to a unique series of bis-homoleptic terdentate cycloruthenates. These complexes were characterised by UV-Vis absorption and cyclic voltammetry and found to be suitable for use in photovoltaic devices. Selected complexes were tested in dye-sensitized solar cells with the best device achieving an efficiency of 4.30%.

We next turned our attention to the synthesis of a second generation of ligands. This included 2,2',6',3''terpyridines, a pyrimidylbipyridine and a 2-quinolyl-6-phenylpyridine. This work allowed access to a second generation of bis-homoleptic terdentate ruthenium complexes which were characterised by UV-Vis absorption spectroscopy and cyclic voltammetry.

The third area on which we concentrated was further expansion of the series of complexes by variation of the metal centre. Initial work with osmium gave bis-homoleptic terdentate complexes with very broad absorption profiles. In a collaborative theoretical work we used the data obtained to explore the effect of spin-orbit coupling on the optoelectronic properties of such complexes. The work continued with the synthesis of heteroleptic bis-cyclometalates of iridium which were characterised by UV-Vis absorption and emission spectroscopy. Finally, preliminary investigations into the synthesis of bis-homoleptic terdentate cyclometalates of iron, rhodium and cobalt were undertaken.

Acknowledgements

I would like to thank my supervisor Dr Etienne Baranoff for giving me the opportunity to study for a PhD. Thank you for your invaluable support and advice for the last four years. I would also like to thank the other members of the Baranoff group, in particular Yanouk Cudré and Antoine Herbaut. We had an amazing time building the lab together, working hard and playing hard. Thanks also go to the School of Chemistry and the University of Birmingham for providing an excellent research environment. Thanks to all the analytical facilities staff and support staff for their help, in particular Dr Louise Male for the crystal structures. Special thanks go to all my friends and family for their love and support for the last 8 years, especially my parents. Most of all, thanks to Cassie for being so patient. I love you so very much.

Contents

General Introduction	1
1 Cyclometalates	1
2 Cycloferrates	1
3 Cyclocobaltates	2
4 Cycloruthenates	3
5 Cycloosmates	5
6 Cyclorhodates	6
7 Cycloiridates	7
8 Bis-homoleptic terdentate cyclometalates	8
9 Aim of the project	10
Chapter 1: Cycloruthenates for Dye-Sensitised Solar Cells	11
1 Introduction	11
1.1 The Global Demand for Energy	11
1.2 Photosynthesis	12
1.3 Inorganic Solar Cells	13
1.4 Dye-sensitised Solar Cells	15
1.5 Requirements of the Dye	16
1.6 The Archetypal Dyes N3 and N719	17
1.7 Champion Dyes	19
1.8 Dyes Containing Terdentate Cyclometalated Ligands	21
2 Aims	23
3 Results and Discussion	25
3.1 Synthesis of Ligands	25
3.2 Synthesis of the first generation of cycloruthenated complexes	42

3.3	Characterisation of the Complexes.....	52
3.4	Device Testing.....	58
4	Conclusion.....	59
Chapter 2: The Second Generation; a New Series of Ligands.....		60
1	Introduction.....	60
1.1	A cobalt based electrolyte.....	60
1.2	Addition of thiophene based chromophores.....	62
1.3	Substitution of pyridine for quinoline.....	65
2	Aims.....	68
3	Results and Discussion.....	69
3.1	Variation of the cyclometalating moiety C.....	69
3.2	Variation at the 4-pyridyl position B.....	77
3.3	Variation of the terminal pyridyl moiety A.....	82
4	Conclusion.....	91
Chapter 3: Bis-terdentate Cyclometalates of Group 8 and 9.....		92
1	Introduction.....	92
1.1	Terdentate cycloosmates.....	92
1.2	Terdentate cycloferrates for DSSC.....	96
1.3	Terdentate cycloiridates for emissive materials.....	97
2	Aims.....	100
3	Results and Discussion.....	101
3.1	Toward osmium based complexes.....	101
3.2	Toward iron based complexes.....	109
3.3	Toward iridium based complexes.....	110
3.4	Toward rhodium based complexes.....	115

3.5	Toward cobalt based complexes.....	117
4	Conclusion	121
	Concluding remarks	122
	Experimental.....	123
1	Instrumentation	123
2	Characterisation-Chapter 1	124
3	Characterisation-Chapter 2	167
4	Characterisation-Chapter 3	184
5	Crystallographic data	192
	References.....	195

List of Abbreviations

br	broad
°C	degrees Celsius
d	doublet
dba	dibenzylideneacetone
DMF	<i>N,N</i> -dimethylformamide
DMSO	dimethylsulfoxide
DSSC	dye-sensitised solar cell
EI	electron impact
eq	equivalent(s)
ES	electrospray ionization
Et ₂ O	diethyl ether
EtOH	ethanol
g	gram(s)
h	hour(s)
HOMO	highest occupied molecular orbital
HRMS	high resolution mass spectrometry
Hz	hertz
IPA	<i>isopropyl</i> alcohol
<i>i</i> Pr	<i>isopropyl</i>
IR	infrared (spectroscopy)
<i>J</i>	coupling constant
L	litre(s)
LUMO	lowest unoccupied molecular orbital

m	milli or multiplet
M	molar
m/z	mass to charge ratio
M^+	parent molecular ion
MeOH	methanol
MIDA	methyliminodiacetic acid
min	minute(s)
mp	melting point
<i>n</i> Bu	<i>normal</i> butyl
NMP	<i>N</i> -Methyl-2-pyrrolidone
NMR	nuclear magnetic resonance
<i>n</i> Pr	<i>normal</i> propyl
pH	hydrogen ion concentration in aqueous solution
Ph ₂ O	diphenyl ether
ppm	parts per million
q	quartet
R_f	retention factor
rt	room temperature
s	seconds, singlet or strong
t	triplet
<i>t</i> Bu	<i>tertiary</i> butyl
TBA	tetrabutylammonium
TGDME	tetraethylene glycol dimethyl ether
THF	tetrahydrofuran
TLC	thin layer chromatography

w	weak
δ	chemical shift
μ	micro
μ wave	microwave
XPhos	2-dicyclohexylphosphino-2',4',6'-triisopropylbiphenyl

General Introduction

1 Cyclometalates

Cyclometalates are compounds containing a cyclical structure, in which resides a carbon-metal σ bond. These compounds have been known since the 1960s and thereafter have seen much attention due to their interesting properties. A huge library of examples exists in the literature for most of the transition metals. The majority of these are from the platinum group metals (Ru, Os, Rh, Ir, Pd, and Pt). Complexes of this type have been developed for a wide array of purposes including: catalysis, optoelectronic devices, and biological applications. The complexes consist of a metal bound to a bidentate or higher denticity ligand with a donor atom (such as N, O, P, S etc.) as at least one coordination site and a carbon atom as one or more of the others. The mechanism of cyclometalation varies depending on the metal, ligand, and starting materials, and for some, despite numerous examples, it is not always fully understood (Ru complexes in particular). In general, coordination to the heteroatom is the first step allowing an intramolecular activation of a C-H or C-X bond by the metal centre allowing subsequent metallacycle ring closure.¹⁻⁴

2 Cycloferrates

Iron is a desirable metal for many applications particularly as an alternative to the more commonly used and more expensive platinum group metals. Although iron complexes are well known and exist in many forms, cyclometalates of iron are relatively scarce in the literature.

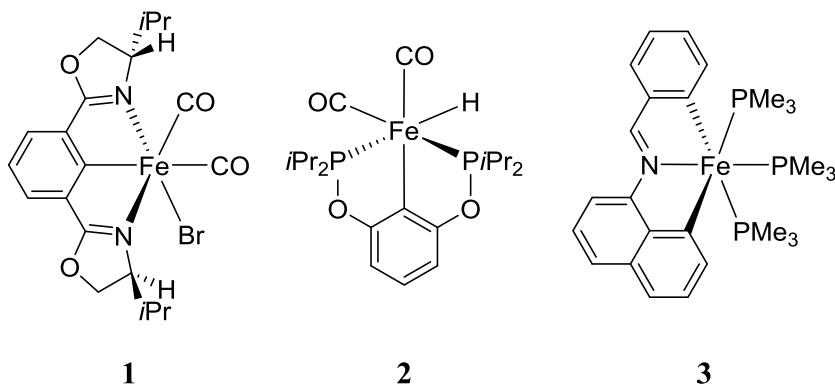


Fig. 1: Examples of cycloferrates which display catalytic activity 1-3.

Fig. 1 shows three recent examples developed in the area of catalysis. All three of the iron(II) complexes contain a terdentate “pincer” ligand where the two flanking coordination sites are the same and the central one differs. **1** is a NCN-type pincer complex of iron, formed by the oxidative addition of $\text{Fe}_2(\text{CO})_9$ to the 2-bromo substituted bis-(oxazolinyl)phenyl ligand. The complex is chiral and is able to catalyze the asymmetric hydrosilylation of phenylketones.⁵ Complex **2** has a PCP pincer ligand and is accessed *via* the reaction of $\text{Fe}(\text{CO})_5$ and the bis-phosphonite ligand. In this work by Jiang *et al.* a series of catalysts was synthesised based on this design with varying alkyl groups attached to the phosphonate moieties. Complex **3** was a particularly successful example showing high yield and selectivity as a catalyst for the dehydrogenative borylation of styrene.⁶ The third example differs to the others in that whilst it contains a pincer ligand the iron is biscyclometalated by a CNC coordinated ligand. Klein *et al.* reacted *N*-benzylidene-1-naphthylamine with $\text{Fe}(\text{CH}_3)_2(\text{PMe}_3)_4$, the loss of two molecules of methane helping to provide the driving force for the formation of this metallobicycle.⁷

3 Cyclocobaltates

Cobalt, iron’s group 9 neighbour has been the focus of similar investigations into first row transition metal catalysts as alternatives to the platinum group metals.

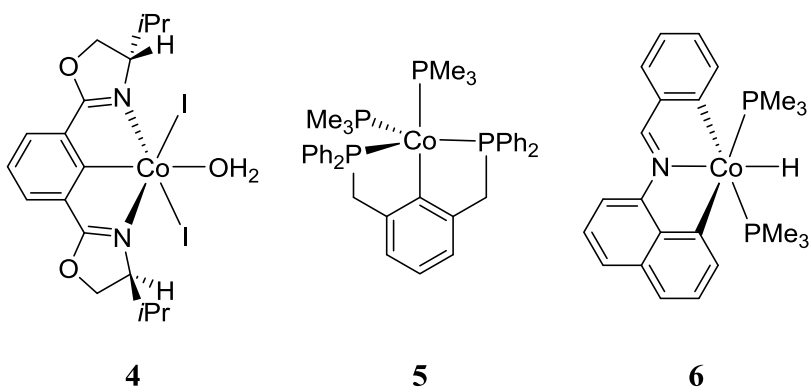


Fig. 2: Examples of cyclocobaltate pincer complexes 5-6.

In Fig. 2 we can see comparable terdentate pincer complexes have been synthesised. The NCN example **4** (as well as its iron analogue **1**) was developed by the Nishiyama group. As with the iron based example, complex **4** was accessed by reaction of the 2-bromo form of the ligand with $\text{Co}_2(\text{CO})_8$. They have yet to report the catalytic activity of **4**.⁸ The trigonal bipyramidal PCP complex **5** reported by Kent *et al.*, was synthesised by transmetalation of $[\text{CoCl}(\text{PMe}_3)_3]$ with the

2-lithiated ligand as well by insertion into the C-H bond of the normal ligand by reaction with $[\text{Co}(\text{CH}_3)(\text{PMe}_3)_3]$.⁹ A similar method was utilised by Zhou *et al.* to access CNC pincer complex **6**. Again reaction of the ligand with $[\text{Co}(\text{CH}_3)(\text{PMe}_3)_3]$ gave the complex which was shown to be an effective catalyst for the hydrosilylation of a variety of aryl aldehydes and ketones.¹⁰

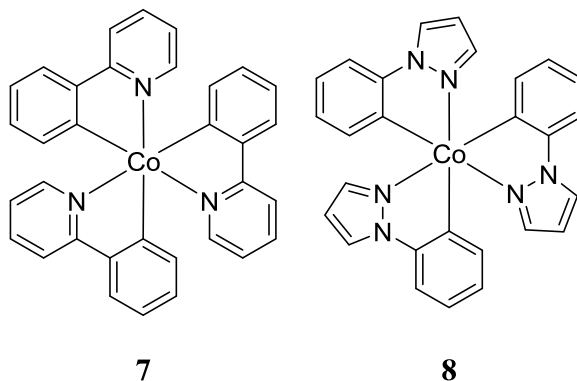


Fig. 3: Potential hole-transport materials tris-homoleptic cyclocobaltates **7** and **8**.

Although polypyridyl complexes of iron and cobalt are well known,¹¹⁻¹³ their cyclometalated analogues are rare. Tris-homoleptic bidentate cyclocobaltates **7** and **8** were first reported in 1991 by Dreves (Fig. 3).¹⁴ More recently they were investigated as potential hole-transport materials for organic light-emitting diodes (OLEDs). The synthesis of these complexes is quite involved requiring the preparation of an unusual cobalt starting material in situ which may be why very few examples of this type have been reported. OLEDs were constructed with the materials and **7** gave a stable device, although some efficiency loss was attributed to the absorption properties of the complex.¹⁵

4 Cycloruthenates

Ruthenium complexes are some of the most well studied organometallic complexes, garnering particularly strong attention in recent years for applications including catalysis, photovoltaics and medicine.¹⁶ Regarding complexes **9** and **10** (Fig. 4) we can see the same structural motifs utilised for iron and cobalt have been applied to ruthenium catalysts. The NCN pincer complex another example by the Nishiyama group is an effective catalyst for the enantioselective hydrogenation of ketones.¹⁷ The PCP complex **10** is one example from many that were synthesised by Conner *et al.* in an investigation into coordinatively unsaturated ruthenium complexes.¹⁸ Complex **11** differs somewhat as although it is a CNC coordinated pincer complex, *N*-heterocyclic carbenes

rather than phenyl groups are utilised for cyclometalation. In fact relatively few examples of biscyclometalated ruthenium exist in the literature aside from carbenes. The compound was shown to be an excellent catalyst for the oxidative cleavage of olefins.¹⁹

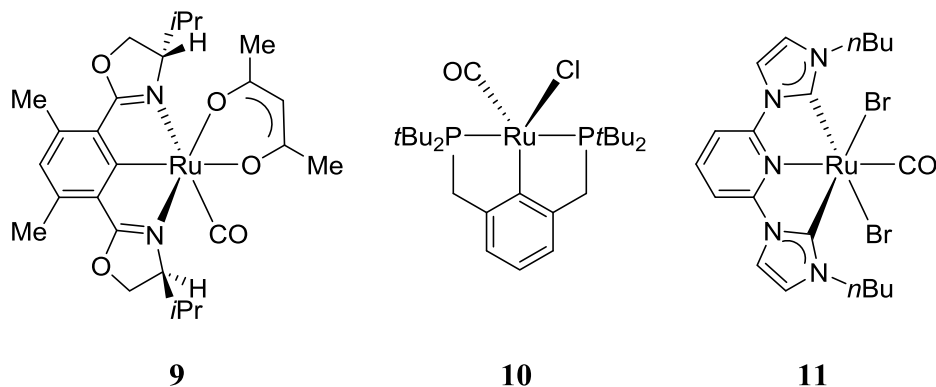


Fig. 4: Examples of cycloruthenate pincer complexes **9-11**.

Ruthenium(II) tris(2,2'-bipyridine) ($\text{Ru}(\text{bpy})_3$) and its terdentate analogue ruthenium(II) bis(2,2',6,2''-terpyridine) ($\text{Ru}(\text{tpy})_2$) are some of the most well studied complexes of ruthenium.²⁰⁻²² Their optical and electronic properties have been investigated and utilised for many applications. Fig. 5 shows the monocyclometalated CN and CNN analogues **12** and **13** first reported in the late 80s/early 90s.^{23, 24} These compounds are also well known in the literature and many analogues have been developed as well as many synthetic routes to the complexes.

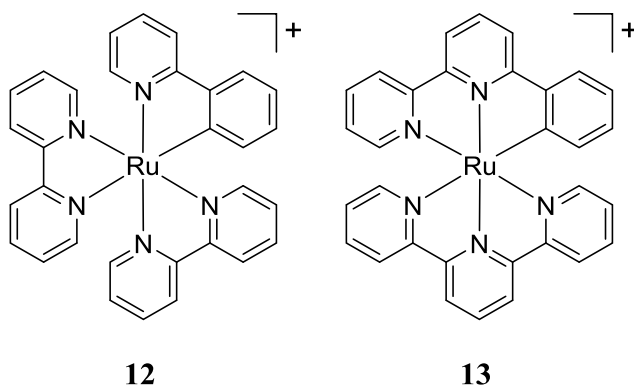


Fig. 5: Complexes **12** and **13**. Monocyclometalated derivatives of ruthenium polypyridyl complexes.

The main difference between the polypyridyl complexes and their cyclometalated equivalents is the reduction in oxidation potential and red-shifted absorption due to the destabilisation of the HOMO. Both complexes, as well as hundreds of their derivatives, have been investigated for

many applications including cancer therapy,²⁵⁻²⁹ photovoltaics^{2, 30, 31} and molecular electronics.^{32,}
33

5 Cycloosmates

Osmium has a relatively similar chemistry to its group 8 homologue ruthenium and has often been investigated for similar applications. Fig. 6 shows two examples of terdentate PCP and CNC pincer complexes **14** and **15**. As with ruthenium the CNC complex contains a carbene ligand. Both examples were synthesised in order to investigate osmium pincer compounds and their characteristics.^{34, 35}

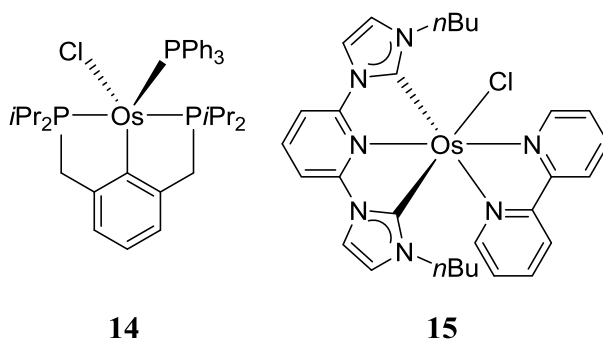


Fig. 6: Examples of terdentate cycloosmate complexes **14** and **15**.

In Fig. 7 we see the simple monocyclometalated polypyridyl complexes of osmium **16** and **17**. Both were synthesised by reaction of an osmium dichloride dimer in acetonitrile.^{36, 37}

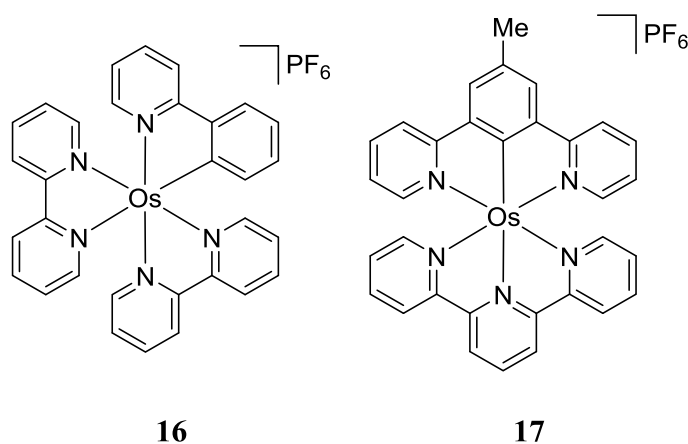


Fig. 7: Complexes **16** and **17**. The monocyclometalated derivatives of osmium polypyridyl complexes.

These particular examples were developed for biological applications and other similar complexes have been investigated for molecular electronics,³⁸⁻⁴⁰ and emissive materials for OLEDs.⁴¹ Compared to ruthenium these complexes have broader absorption profiles and lower oxidation and reduction potentials.

6 Cyclorhodates

Examples of rhodium cyclometalates exist in all the same general areas as for its group 8 and 9 neighbours ruthenium and iridium. In Fig. 8 some examples of rhodium pincer complexes are presented. Complex **18** developed by Wang *et al.* is an effective catalyst for both the enantioselective allylation of aldehydes and the reaction of trifluoropyruvates with alkenes.⁴² The PCP complex **19** was synthesised in an unusual fashion, by insertion of the metal into a C-O bond. The 2-Methoxy ligand was prepared and reacted with chlorobis(cyclooctene)rhodium(I) dimer to give pincer complex **19**.⁴³ As in the case of ruthenium and osmium CNC pincer complexes, **20** is a carbene. The cyclorhodate exhibited good catalytic activity for both hydrosilylation of alkynes and hydrogenation of ketones.⁴⁴

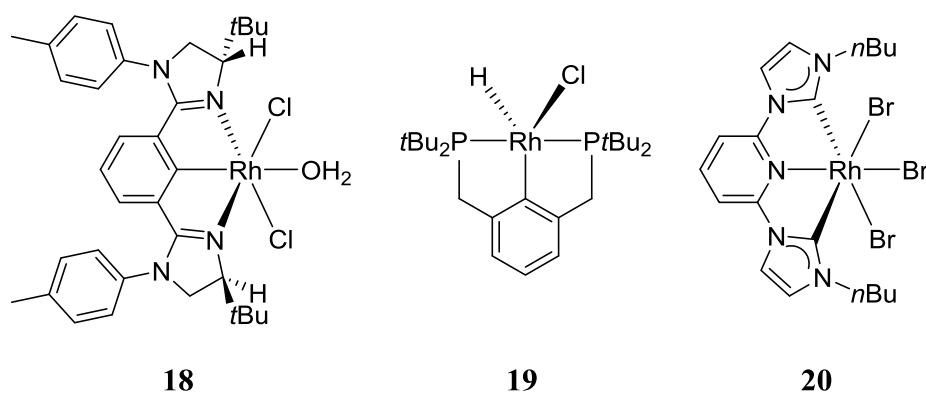


Fig. 8: Terdentate cyclorhodate pincer complexes **18-20**.

The bis and tris-homoleptic bidentate cyclorhodates **21** and **22** have been known since the late 80s/early 90s.⁴⁵⁻⁴⁷ However since then they have been investigated very little. Compared to their ruthenium and osmium analogues they have narrower absorption profiles and more intense emission in the visible spectrum. Both complexes were synthesised in two steps, firstly synthesis of rhodium bis(phenylpyridine) chloro-bridged dimer from RhCl₃, then subsequent reaction with a further equivalent of ligand to give bis and tris-cyclometalated **21** and **22**.

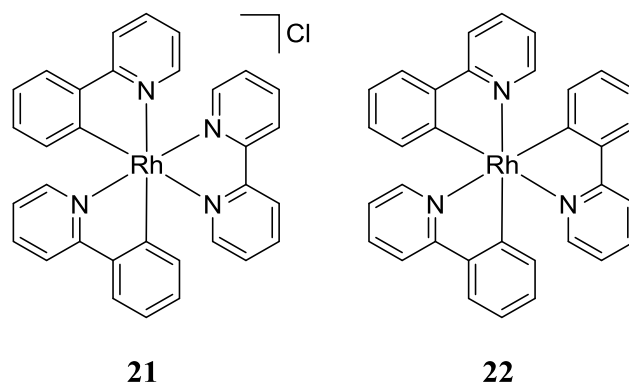


Fig. 9: Bis and tris-cyclorhodates **21** and **22**

7 Cycloiridates

Although few examples of NCN and CNC iridium catalysts have been reported the cyclometalated iridium PCP pincer catalysts **23** and **24** have shown excellent catalytic properties for aliphatic dehydrogenations and the reduction of aryl halides.^{48, 49}

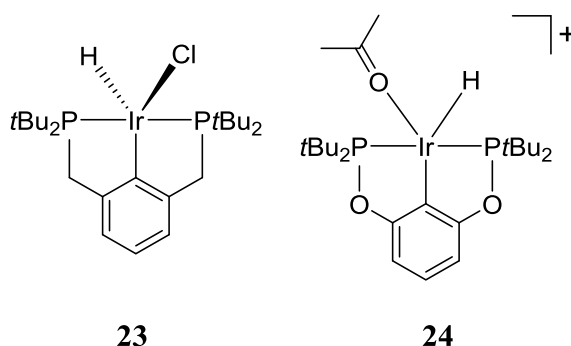


Fig. 10: Terdentate cycloiridate PCP pincer catalysts **23** and **24**.

Iridium polypyridyl complexes and their cyclometalated derivatives are currently an area of great interest due to their excellent and highly tuneable emissive properties. Bis and tris-homoleptic cyclometalates **25** and **26** were first developed at the same time as their rhodium analogues and display similar absorption and emission properties.^{46, 47, 50} Also like their rhodium analogues they are synthesised *via* a chloro-bridged dimer intermediate. Since it was first demonstrated that the tris-cyclometalated complex **26** (Ir(ppy)₃) could be used in highly efficient lighting devices, it and its derivatives have been the subject of intense research.^{51, 52}

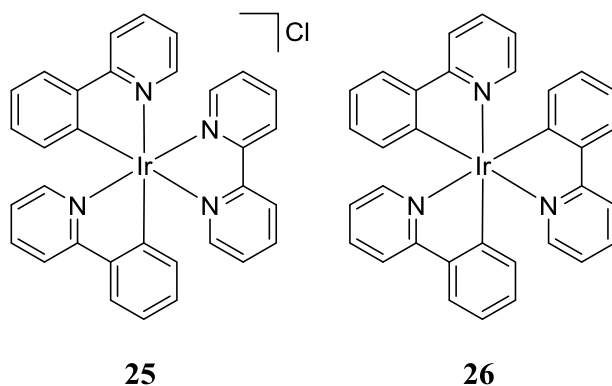


Fig. 11: Bis and tris-cycloiridates **25** and **26**.

8 Bis-homoleptic terdentate cyclometalates

There are innumerable examples of cyclometalated complexes from group 8 and 9 including examples with terdentate ligands for all of the metals. Homoleptic cyclometalates are much rarer although the tris-homoleptic bidentate cyclometalated complexes of rhodium and iridium are well known. A family that as yet has received very little attention is bis-homoleptic terdentate cyclometalates. To date there are no examples of iron, cobalt, ruthenium or osmium bis-terdentate homoleptic cyclometalates in the literature. At least two attempts at synthesising homoleptic phenylbipyridine complexes of ruthenium have been reported, however only the dichloride **27** and monocyclometalate **28** were obtained.^{53, 54} In fact even bis-cyclometalates of ruthenium with phenylpyridines are rare with **29** one of few examples in the literature.⁵⁵

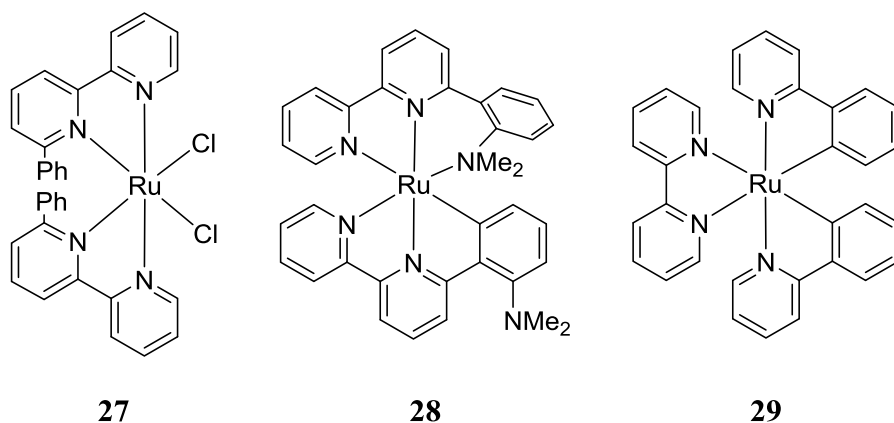
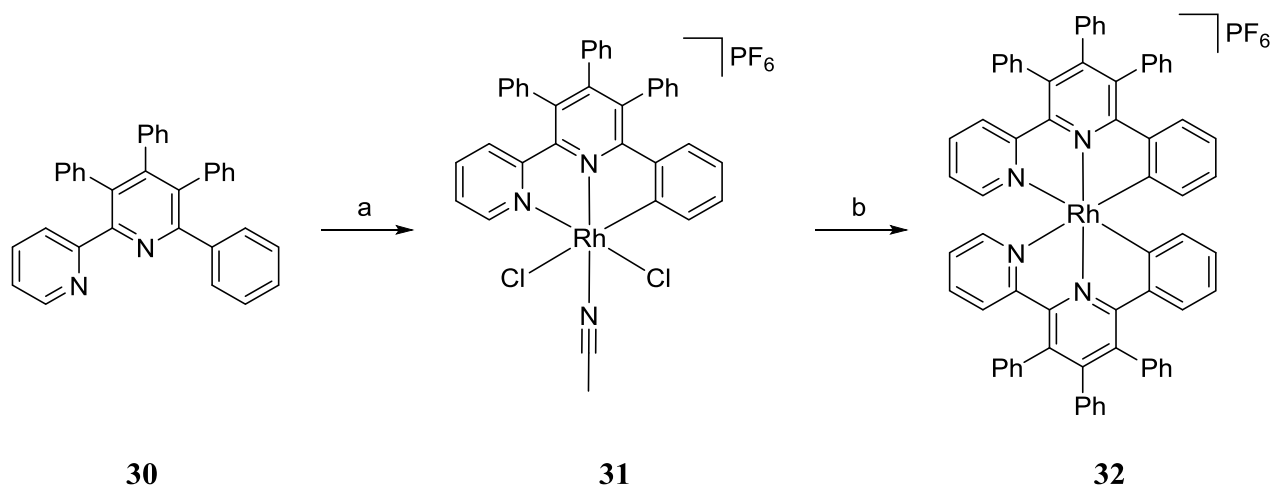


Fig. 12: Ruthenium polypyridyl mono and bis-cyclometalated complexes **28-29**.

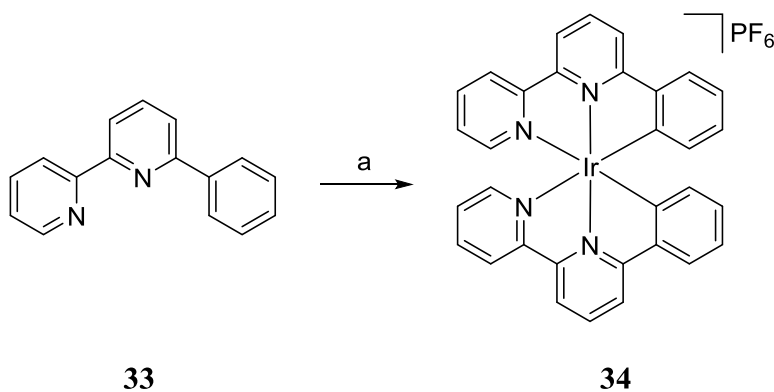
A single example of a bis-homoleptic terdentate cyclorhodate exists in the literature. Synthesis was achieved in several steps. The ligand was reacted with RhCl_3 in MeCN to form the

monocyclometalated complex **31**. This was then reacted with an additional equivalent of ligand as well as AgNO_3 in acetone/EtOH to give the biscyclometalate **32**.⁵⁶



Scheme 1: Synthesis of homoleptic terdentate cyclorhodate **32**. Reaction conditions: (a) $\text{RhCl}_3 \cdot \text{H}_2\text{O}$, MeCN reflux, 16 h (b) AgNO_3 , Acetone/EtOH, reflux 19 h.

There is also at least one example for iridium in the literature. Complex **34** was obtained directly by reflux of the ligand **33** with IrCl_3 , in ethylene glycol for 90 hours.⁵⁷



Scheme 2: Synthesis of homoleptic terdentate cycloiridate **34**. Reaction conditions: (a) $\text{IrCl}_3 \cdot 4\text{H}_2\text{O}$, ethylene glycol, 175 °C, 90 h

The absorption spectra of the complex is reported (Fig. 13) and compared to the biscyclometalated bidentate analogue **25** as well as the DFT predicted spectra for **34**. We can see the absorption profile is broadened for **34** with respect to **25**.

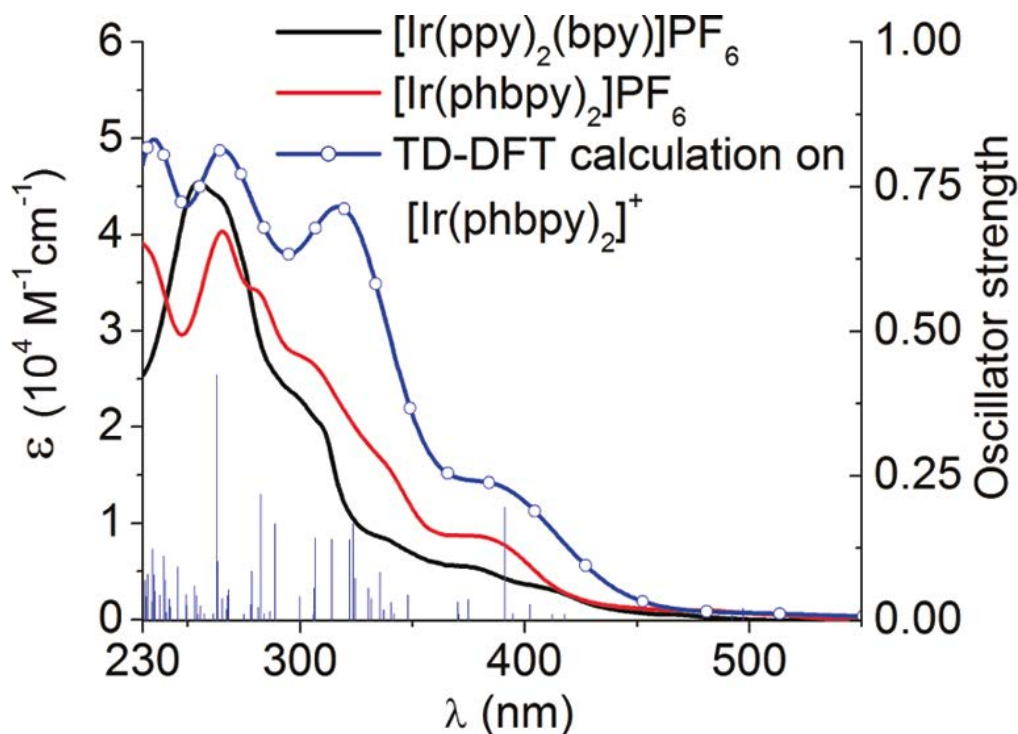


Fig. 13: UV-Vis absorption profile of **34** (red line) and **25** (black line) compared to the theoretical spectra for **34** (blue line) in MeCN.⁵⁷

9 Aim of the project

Here we have introduced a few of the diverse range of cyclometalates of group 8 and 9. This huge library of compounds has been investigated for a wide range of applications. Despite this the area of bis-homoleptic terdentate cyclometalates represents a huge area of as yet unexplored chemical space with great potential.

In this project we planned to investigate this relatively unknown family of compounds and use the information gathered to generate complexes with properties that could be applied to an array of applications. We were particularly interested in the challenges of synthesis of these complexes. Attempts to access bis-homoleptic terdentate cycloruthenates in the literature had so far been unsuccessful.^{54,55}

Our initial focus was to design a new series of complexes for a single application. This would give us the tools to then explore the field of bis-homoleptic terdentate cyclometalates further as well as the information on their properties which could better inform our future designs. To this end we began with an investigation into cycloruthenates for dye-sensitised solar cells.

Chapter 1: Cycloruthenates for Dye-Sensitised Solar Cells

1 Introduction

1.1 The Global Demand for Energy

The past century has seen a vast rise of the global consumption of energy. Driven by a variety of factors, the demand for energy in the future will only increase. Currently the majority is produced from fossil fuels and nuclear power (Fig. 14).⁵⁸ These sources are not sustainable; fossil fuels are a finite resource and their use produces massive amounts of pollution while nuclear power creates waste, which is costly and dangerous to manage. Although renewable energy sources have seen a large increase in recent years, they still account for only a small percentage of total energy production. We need to see a huge increase in their use if the future energy demands of the world are to be met in a sustainable manner.

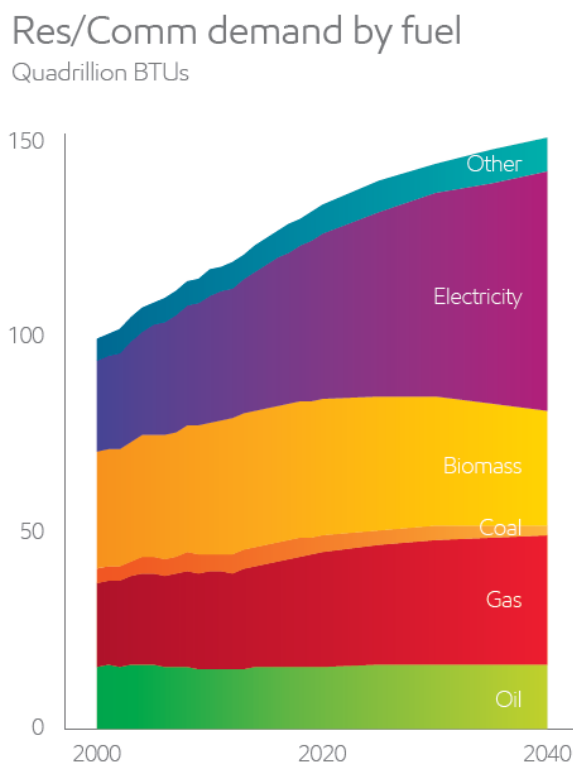


Fig. 14: Residential and commercial energy demand by fuel 2000-2040 (Exxon Mobil, 2013).⁵⁸

Sunlight is by far the most abundant energy source on the planet. More solar energy reaches the surface of the earth in one hour than the total energy consumed by the world in one year. Current energy demand could be satisfied by 10% efficiency solar cells covering approximately 0.1% of the earth's surface.⁵⁹

1.2 Photosynthesis

Conversion and storage of solar energy is already in widespread use in the natural world. Plants harness sunlight, water and carbon dioxide to create sugar, a store of energy which can be later consumed through respiration. Indeed this process is fundamental to almost all forms of life on earth.

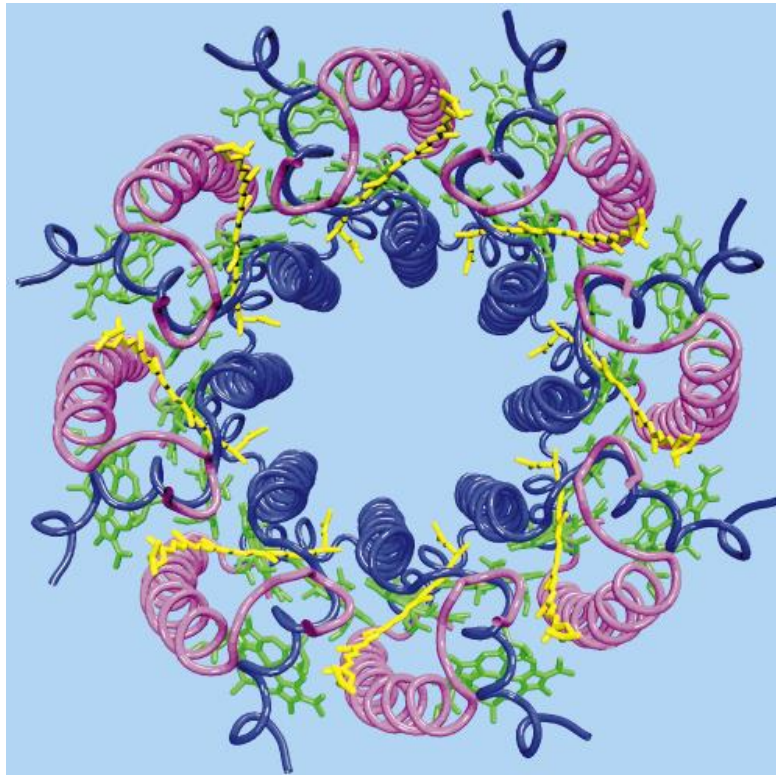


Fig. 15: The light harvesting complex of *Rhodospirillum rubrum*.⁶⁰

In Fig. 15 we see the crystal structure of the light harvesting complex in the bacteria *Rhodospirillum rubrum*.⁶⁰ The pigments (carotenoids in yellow and chlorophylls in green) are organised into what are known as photosynthetic antennae which are arranged around a reaction centre. In Fig. 16 we see the absorption profiles of the photosynthetic pigments; β -

carotene⁶¹ and chlorophylls a and b.⁶² The chlorophylls absorb between around 300 nm and 500 nm and also between 550 nm and 700 nm whilst β -carotene has a broad absorption band between 350 nm and 550 nm. Pigments such as these, which can absorb different portions of the electromagnetic spectrum, work in concert to achieve a more efficient absorption of available photons. The absorption of light by the antennae causes a series of electron transfer reactions which are focused toward the reaction centre. There, the electrons are used to split water into hydrogen and oxygen which are subsequently used to convert carbon dioxide into sugar.

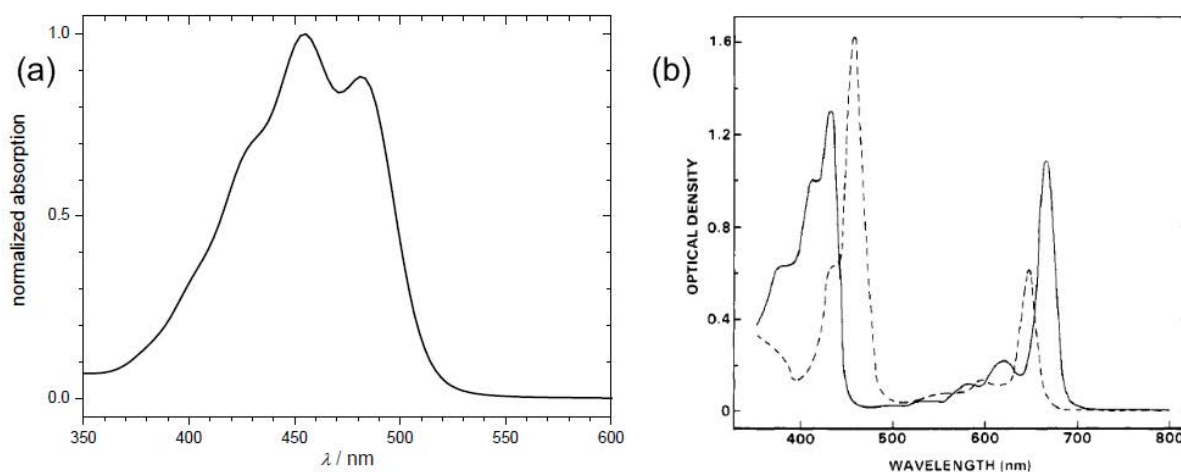


Fig. 16: (a) Absorption spectrum of β -carotene in acetone. (b) Absorption spectra of chlorophyll a (solid line) and chlorophyll b (dashed line) in CHCl_3 .^{61, 62}

1.3 Inorganic Solar Cells

The idea for the silicon based photo-voltaic (PV) cell was first patented in 1941 by Russell Ohl,⁶³ later work reported in 1954 by Chapin *et al.*, gave a device with an efficiency of 6%.⁶⁴ These cells are now widely used for various applications including supplementing residential electricity supply. Silicon PV cells contain both p-type and n-type silicon semiconducting layers. The interface between the layers is known as a p-n junction and this is the key to the device. Electrons are excited by the absorption of light from the valence band to the conduction band in the p-type semiconductor. This creates an electron-hole pair. They are separated by the movement of the electrons across the p-n junction and the holes toward the electrode creating a potential difference (Fig. 17).⁶⁵

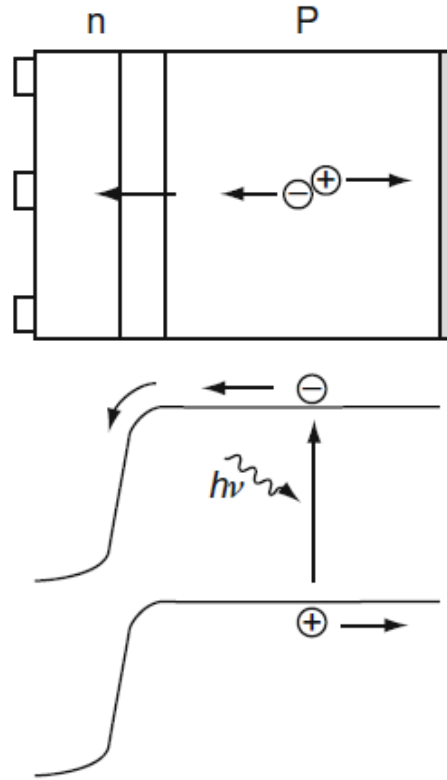


Fig. 17: Schematic of a silicon PV cell and the p-n junction.

Silicon based devices have some key advantages over other types of solar cell. The modern cells can obtain relatively high efficiencies (as much as 25%)⁶⁶ and show good longevity.⁶⁷ There is a high abundance of silicon on the earth (it is the second most abundant element in the earth's crust after oxygen).⁶⁸ There is also a large and well established silicon semiconductor industry. However they have some issues preventing their use to satisfy large scale energy demand. Silicon based PV cells operate best in high intensity light, and therefore have reduced efficiency in low light applications.⁶⁹ Conversion of the raw material to a high quality silicon semiconductor suitable for PV cells is very expensive.⁷⁰ The cells produced are often inflexible and fragile.⁷¹ Due to the production techniques used, silicon based PV cells have a very high embodied energy. The time taken for the cell to pay this energy back (EPBT) was recently estimated at 3.1 years for a polycrystalline silicon cell.⁷² An alternative to silicon PV cells are thin film PV cells, these fall into three types, gallium arsenide (GaAs), copper indium gallium diselenide (CIGS) and cadmium telluride (CdTe). All three types also contain a thin film of cadmium sulfide. Although these cells have better EPBT values than silicon based PV cells (e.g.

1 year for CdTe),⁷² they contain toxic and/or rare elements. When the cells are no longer useful, they will have to be carefully disposed of.⁷³ They are therefore a less than ideal alternative for future use on a large scale.

1.4 Dye-sensitised Solar Cells

The Dye-sensitised solar cell (DSSC) is a newer technology first developed by Michael Grätzel and Brian O'Regan, in 1991.⁷⁴ Also known as the Grätzel cell, DSSCs (Fig. 18) offer a possible substitute for conventional technologies. Unlike silicon PV cells, they display similar efficiency at all light intensities. This is ideal for applications in low light conditions. DSSCs may also be manufactured on flexible materials utilising relatively facile techniques.² The energy intensive purification of the raw material as in silicon PV cells is not required and the energy payback time of a 10% efficiency cell has been estimated at 0.74 years.⁷⁵

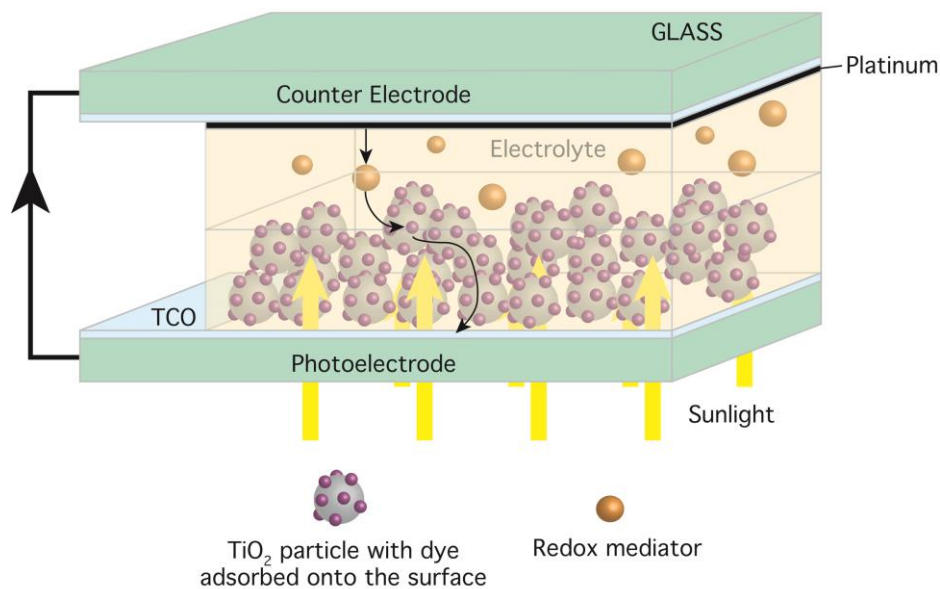


Fig. 18: The dye-sensitised solar cell.

The operating principle of the DSSC is related to that of photosynthesis. It contains a light harvesting material which transfers electrons to a semiconductor similar to the way the pigments in the photosynthetic antennae absorb light and transfer electrons to the reaction centre. A typical DSSC (Fig. 19) is made up of titanium oxide (TiO_2) nanoparticles sensitised by a dye at the anode, a platinum coated cathode and an electrolyte. Absorption of a photon by the dye leads the excitation of an electron which is then transferred to the conduction band (E_{CB}) of the TiO_2 . The

electrons are collected at the anode before performing work and then pass on to the cathode where at the platinum surface the electrolyte is reduced. The electrolyte then acts as a redox mediator transferring the electrons back to regenerate the dye and complete the circuit.⁷⁶

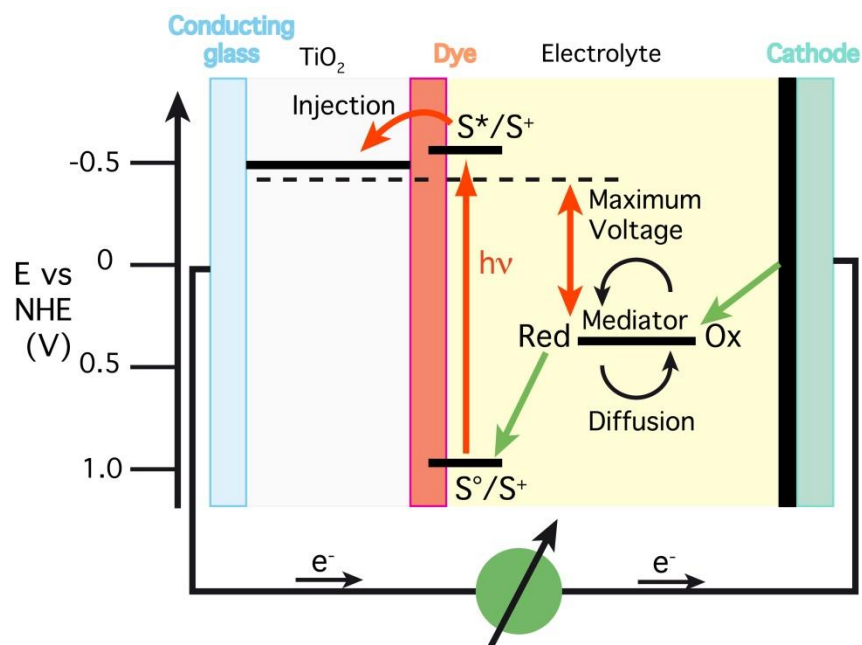


Fig. 19: Operating principle of the DSC.

1.5 Requirements of the Dye

A range of factors determine the efficiency of the cell, however the key component of the device is, as the name suggests, the sensitiser or dye. It is this molecule which plays the most crucial role in DSSCs. The dye dictates the amount of light harvested and is a key component of the electron transfer processes necessary for efficient use of the light collected. The following is a list of requirements for the ideal dye.

1. Strongly binds to TiO_2 in order to efficiently transfer electrons to the E_{CB} of the TiO_2 .
2. The energy of the excited electron must be higher than the E_{CB} of TiO_2 to favour injection.
3. The HOMO energy level must be lower than that of the redox couple and higher in energy than the valence band of TiO_2 to allow efficient regeneration of the dye.
4. The dye should be panchromatic i.e. show a good absorption of photons in the near IR and UV/Vis range (energies greater than 920 nm).

- The directionality of the ligand should be so that the LUMO is on the anchoring ligand and the HOMO is on the ligands away from the TiO₂ toward the electrolyte.
- Photochemically, thermally, and electrochemically stable.
- The dye is not so bulky that the surface coverage of TiO₂, and thus efficiency of the cell, is reduced, but not small enough to allow I₃⁻ access to the TiO₂ or cause problems with aggregation.

1.6 The Archetypal Dyes N3 and N719

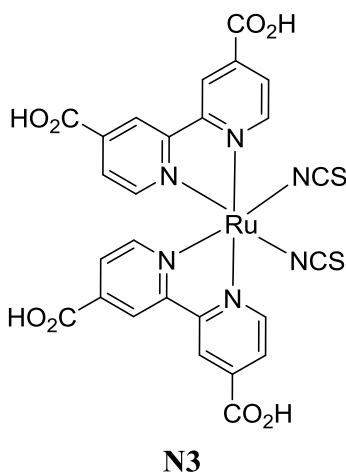
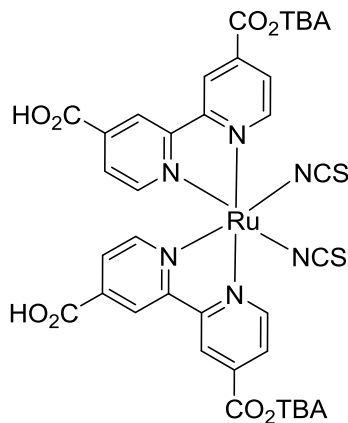


Fig. 20: The archetypal dye N3

The first dye to satisfy the majority of the requirements in **2.1** was **N3** (Fig. 20). The carboxylic acid groups give strong binding to the TiO₂ surface and the thiocyanate ligands tune the electronic properties of the complex by lowering the energy of the HOMO. The dye has a broad absorption spectrum due to a series of metal to ligand charge transfer (MLCT) transitions. The directionality of the dye is good, with the LUMO on the bipyridine dicarboxylate ligands and the HOMO on the ruthenium and thiocyanate ligands. The thiocyanate ligands interact well with the triiodide electrolyte aiding the regeneration of the dye. Most importantly this results in a power conversion efficiency (η) of 10%.⁷⁷ Due to the excellent performance of **N3** it has become one of the archetypal dyes for DSSCs with many later dyes based on its design.



N719

Fig. 21: The archetypal dye N719.

The anchoring groups of the dye donate their protons to the TiO_2 upon binding. This causes a positive charge at the TiO_2 surface aiding the transfer of electrons and increasing the absorbance of the dye. The Fermi level of the semiconductor is however lowered which decreases the gap between the Fermi level and that of the iodide/triiodide redox couple. This has the effect of decreasing the overall efficiency of the system. The Grätzel group investigated this effect and compared **N3**, **N719**, and the fully deprotonated version **N712**, the results showed that **N719** with two equivalents of tetrabutylammonium (TBA), was an effective compromise with an improved η compared to **N3**, of 11.18%.^{78,79} In Fig. 22 we can see the absorption profile of **N719** with varied pH. We see two peaks corresponding to MLCT transitions at around 380 nm and 520 nm and the absorption extends beyond 700 nm.

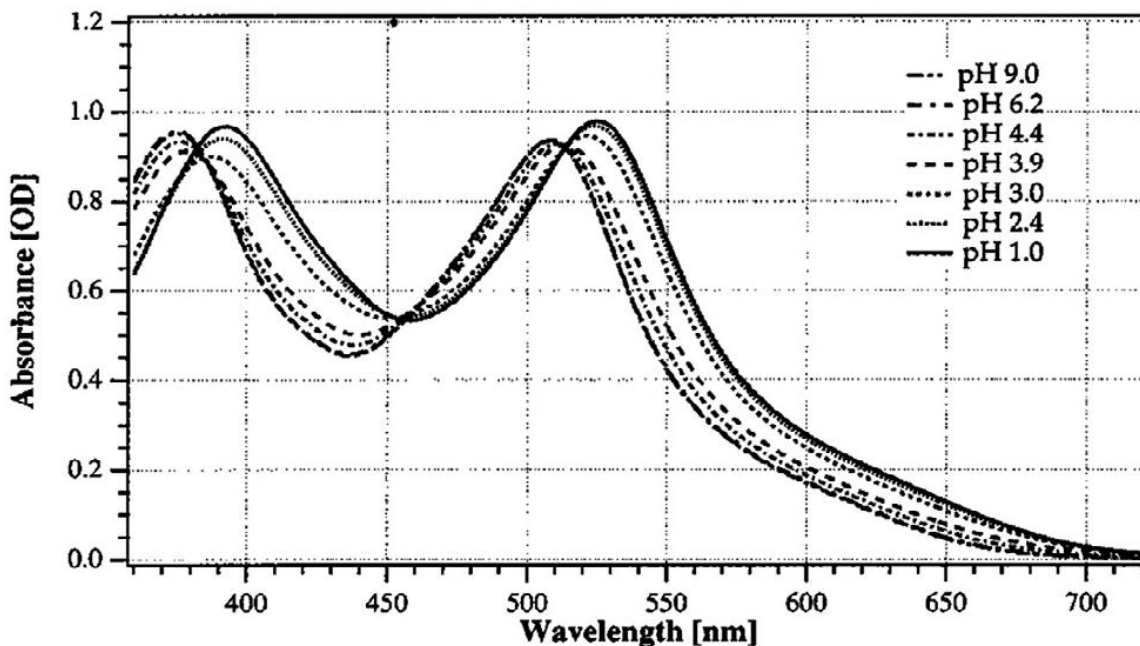


Fig. 22: Absorption spectra with varied pH of **N719**.⁷⁹

1.7 Champion Dyes

Dyes which satisfy the requirements set out in 2.1, and which achieve an η of 10% or more, have become known as champion dyes. The main drawback of the **N3** and **N719** dyes is although they show a high incident photon to current conversion efficiency (IPCE) (80-85% for **N3**),^{77,80} they exhibit little to no absorption in the red and near IR region. The ideal dye should be panchromatic (as described in 2.1). To address this issue the Grätzel group synthesised **N749** (also known as black dye) (Fig. 23), successfully creating a dye which absorbs up to the threshold 920 nm value (Fig. 24) The rationale behind a design utilising a terpyridine ligand alongside three thiocyanate ligands was to synthesise a dye with improved absorption in the near IR whilst avoiding significant alterations to the HOMO and LUMO which would negatively affect the efficiency of the dye. The η of **N749** at 10.4% is not however significantly greater than that of **N3**, and is less than that of **N719** despite the improved absorption.⁸¹

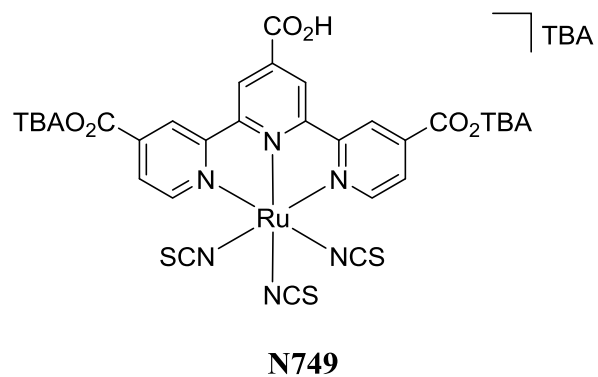


Fig. 23: The panchromatic sensitizer **N749** (black dye).

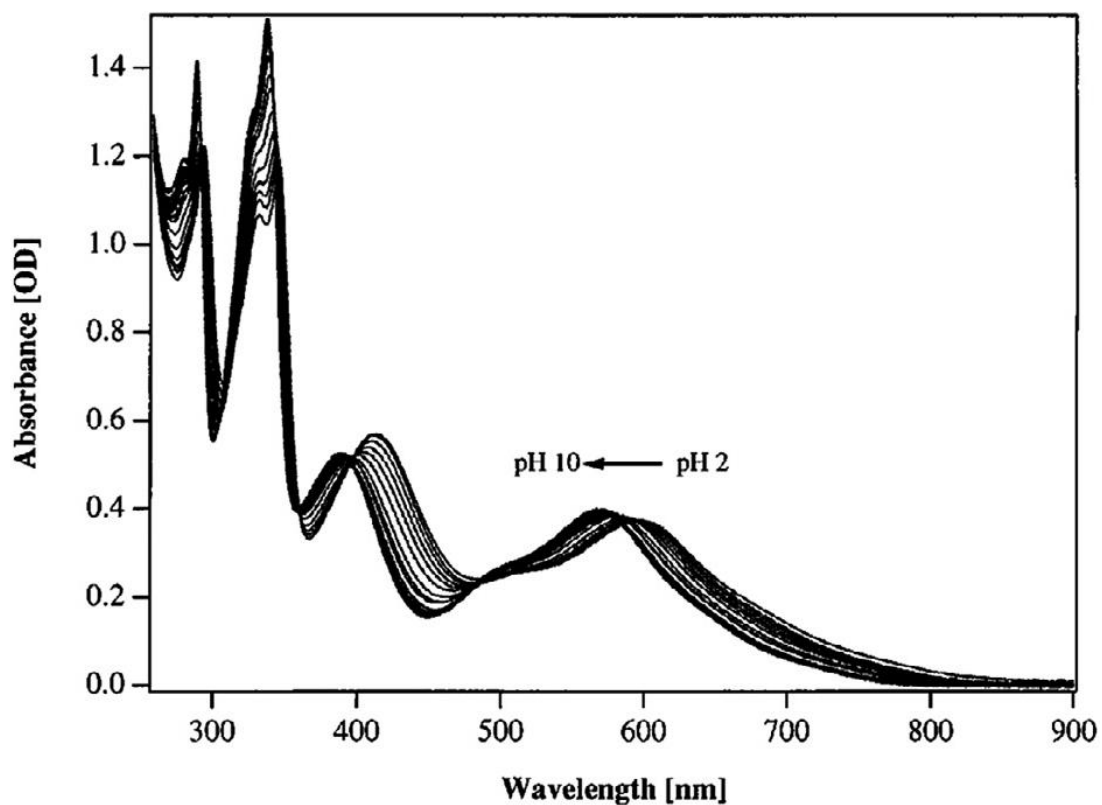
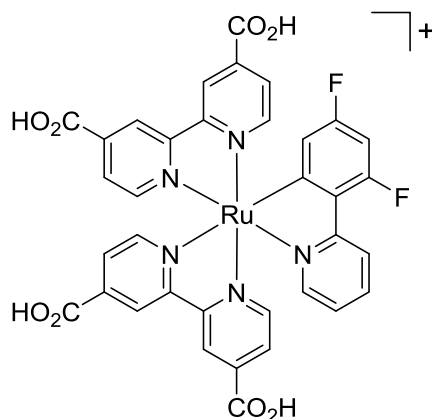


Fig. 24: Absorption spectra of the sensitizer **N749** (black dye) on variation of pH.⁸¹

Despite the excellent characteristics of the dyes detailed so far, they all have one issue in common. The use of thiocyanate ligands affords an effective tuning of the HOMO, yet the ligand itself has two disadvantages. Firstly the ligand is ambidentate; coordination of the sulfur instead of the nitrogen causes linkage isomerism. Secondly the ligand is monodentate and can more easily disassociate than a polydentate ligand. Overall thiocyanate ligands reduce the stability and therefore the longevity of the sensitiser.⁸²



YE05

Fig. 25: The first thiocyanate-free ruthenium based champion dye YE05.

The dye **YE05** reported by Bessho *et al.*, was the first thiocyanate-free, ruthenium based, champion dye. Based on the **N3** archetype a cyclometalated difluorophenylpyridine ligand was used in place of the two thiocyanate ligands. The η of **YE05** is 10.1% almost identical to **N3** proving the thiocyanate ligand is not a necessary component in a successful dye.⁸³

1.8 Dyes Containing Terdentate Cyclometalated Ligands

Utilisation of a terpyridine ligand as in **N749** not only allows an increased range of absorption but also a greater stability compared to ligands of a lower denticity. However use of two terpyridine ligands has an overall negative effect. The excited states become too low for injection of electrons to be efficient, the distorted octahedral geometry causes a decrease in the gap between the metal-to-ligand and metal-centred states allowing decay of photo-excited states,⁸⁴ and the increased symmetry causes a narrowing of the absorption spectrum.⁸⁵ The van Koten group demonstrated the first use of terdentate cyclometalating ligands in a ruthenium dye (Fig. 26).

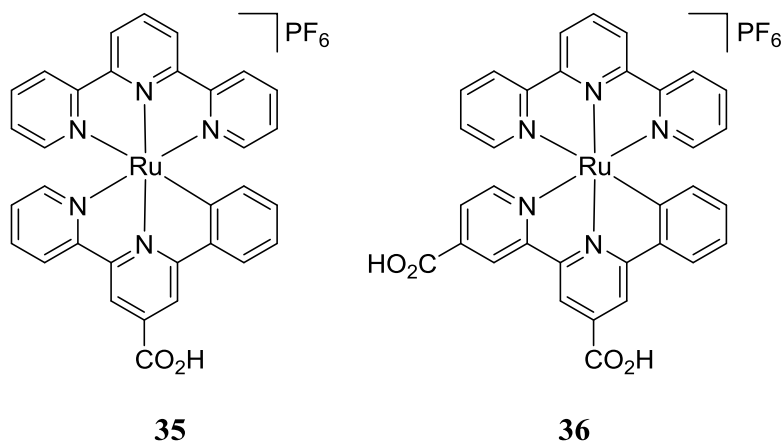


Fig. 26: Bis-terdentate cyclometalated dyes by van Koten and co-workers

However the efficiencies of the devices were only in the region of 2%. This nevertheless revealed an effective method to overcome the deficiencies present in a bis-terpyridine complex.⁸⁶ The use of terdentate cyclometalated ligands not only gives the advantage of stability over thiocyanate ligands but can also allow independent tuning of the HOMO and π^* -based LUMO.⁸⁷ A further improvement is that the HOMO of the dye is expanded over the metal and anionic section of the ligand whilst the LUMO remains on the polypyridyl ligands. This gives an array of metal-to-ligand and ligand-to-ligand transitions resulting in a broad absorption of incident photons.⁸⁵

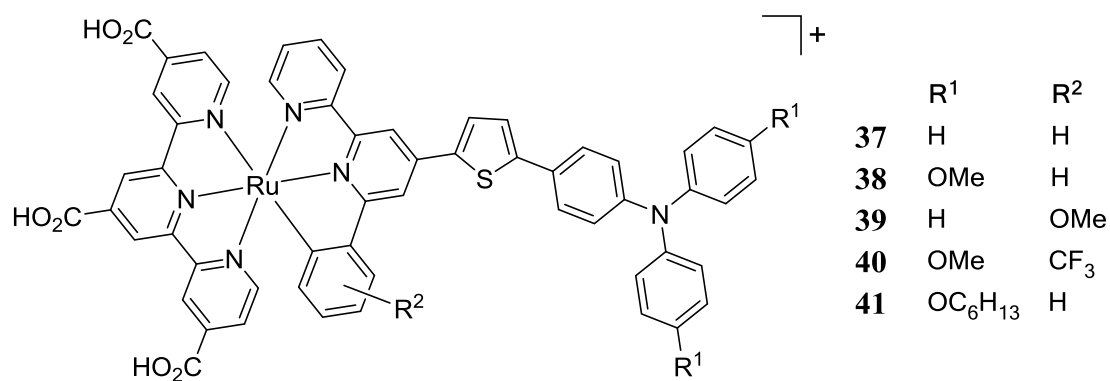
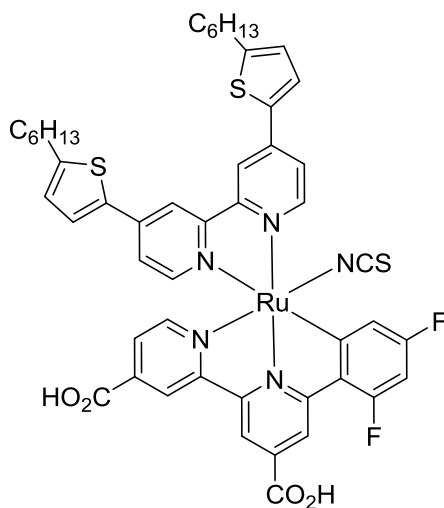


Fig. 27: Series of bichromic cyclometalated dyes by the Berlinguette group.

In a continuation of the work by van Koten and co-workers, the Berlinguette group performed an investigation of dye **36**, showing that the absorption profile of a dye could be tuned by choice of substituents.⁸⁸ Building on this work and inspired by the success of organic dyes containing a triphenylamine (TPA) moiety, the Berlinguette group synthesised a range of dyes **37-41** (Fig.

27). Aiming to produce an improved absorption, TPA as a secondary chromophore attached at the 4' position, with the ability to tune the reduction potential by alteration of the substituents on both the cyclometalating ligand and the TPA unit,^{89,30} however the group is yet to show an enhanced device performance, despite promising preliminary results.² A cyclometalated dye with an η greater than 10% has been reported by the Ko group. **JK-206** (Fig. 28) contains thiophene units in order to increase the absorption of the dye and a single thiocyanate ligand to enhance the dye regeneration. A cyclometalated difluorophenyl bipyridine ligand affords a broad and red-shifted absorption and a HOMO which is raised in energy.⁹⁰



JK-206

Fig. 28: Mixed-denticity, heteroleptic cyclometalated dye, JK-206.

2 Aims

Given our focus on bis-homoleptic terdentate cyclometalates and their properties we were interested in investigating this structure for the application of dyes in DSSC. In our initial work we aimed to synthesise a new family of dyes based on the **N3** archetype, with an improved design. Our strategy was to synthesise homoleptic, terdentate, cycloruthenated dyes in an effort to improve stability, simplify the synthetic route, and to create dyes with improved performance.

The use of cyclometalating ligands has been proven an effective strategy in the work by the Grätzel, van Koten, Berlinguette and Ko groups.^{85,89,90} Tuning of the electronic properties by altering the substituents on the ligands avoids the use of less stable thiocyanate ligands and the

absorption of the dyes should be broad and red shifted. We hypothesised terdentate ligands would afford complexes which have greater stability than those containing lower denticity ligands. In order to keep the synthesis of such dyes simple our aim was to create bis-terdentate homoleptic dyes. Utilising only one type of ligand would reduce the length of the synthesis. It would also avoid any issues of scrambling or isomerism which can occur with heteroleptic complexes, which reduce yield and complicate purification.

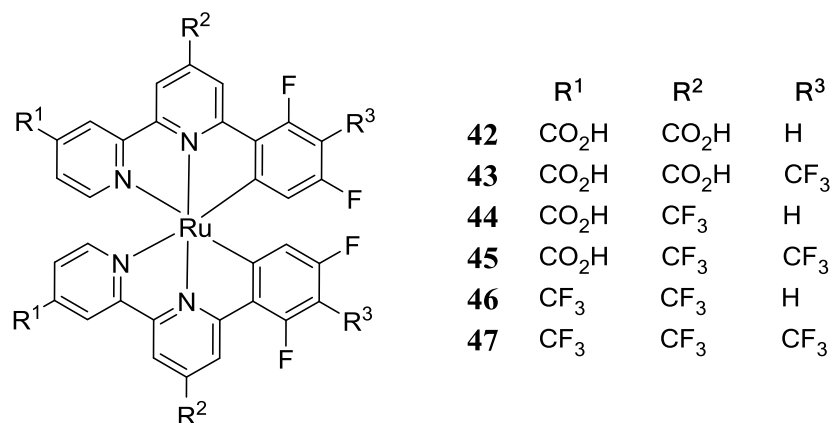


Fig. 29: First generation of Homoleptic, terdentate, cycloruthenated dyes **42-47**.

Our initial focus was on the synthesis and characterisation of complexes **42-47** the first generation in a new family of dyes (Fig. 29). Complexes **42** and **43** are similar in design to **YE05** with bipyridine dicarboxylate moieties to provide binding to the TiO₂ surface and a LUMO with an appropriate energy level and orientation for electron transfer. The difluorophenyl portion of the ligands was designed to provide a HOMO extended from the metal centre onto the ligand with an energy level in the region required for regeneration of the dye. The addition of an electron withdrawing trifluoromethyl group at the 3-phenyl position in complex **43** was to reduce the oxidation potential of the complex compared to **42**. We expected this to increase its stability in ambient conditions and potentially improve its properties as a dye.

The carboxylic acid groups of the dye are an essential component for binding to the TiO₂ layer in a DSSC, as highlighted in **1.4**. It has been shown in IR spectra studies by Finnie *et al.*⁹¹ that the dye molecules only bind *via* two carboxylate groups. The ideal orientation for the dye is for the LUMO to be in close proximity to the TiO₂ surface and the HOMO facing outward into the electrolyte. This allows the most efficient electron transfer. The 4' carboxylic acid groups on the

ligands in **42** and **43** should therefore ideally be those bound to the TiO₂. It is probable however that a mixture of binding modes would occur with these complexes due to the total of four carboxylate groups present (Fig. 30).

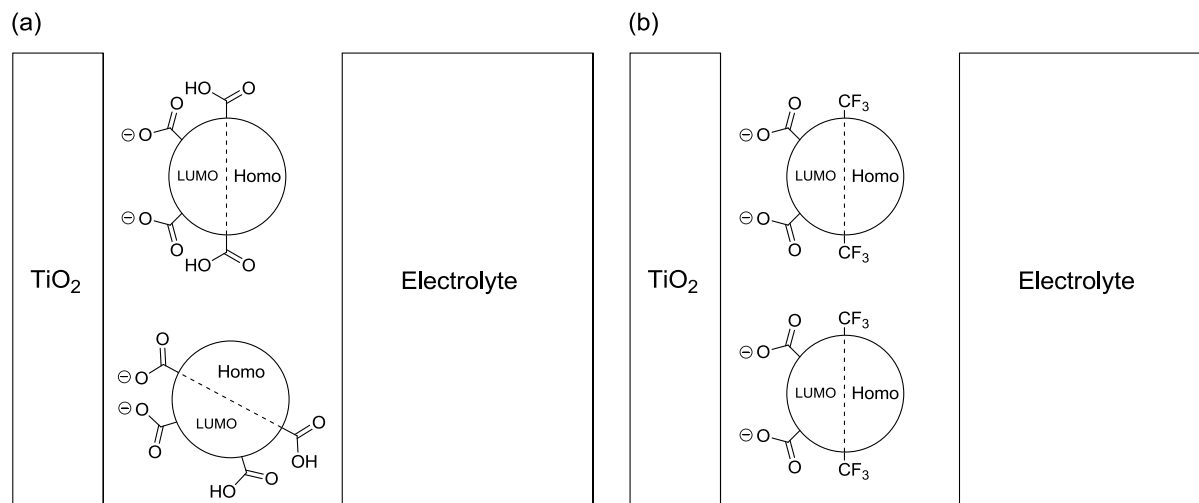


Fig. 30: (a) Shows the mixture of binding modes occurring in dyes with 4 carboxylic acid groups causing non-ideal orientation of the HOMO and LUMO for some of the dye molecules. (b) In dyes with just 2 carboxylic acids at the 4' positions, only the preferred binding mode can occur.

With this knowledge in mind we also aimed to synthesise **44** and **45** which only have two carboxylate groups positioned at the preferred 4' position. We anticipated this would lead to only one binding mode and thus increase the efficiency of the dye. The trifluoromethyl groups at the 4 position were added to give similar electronic effects to carboxylate groups (as shown by the Hammett parameters)⁹² without binding to the TiO₂. In addition complexes **46** and **47** would complete the series and allow us to see the optoelectronic effects of continuing the trend toward extremely electron withdrawing ligands.

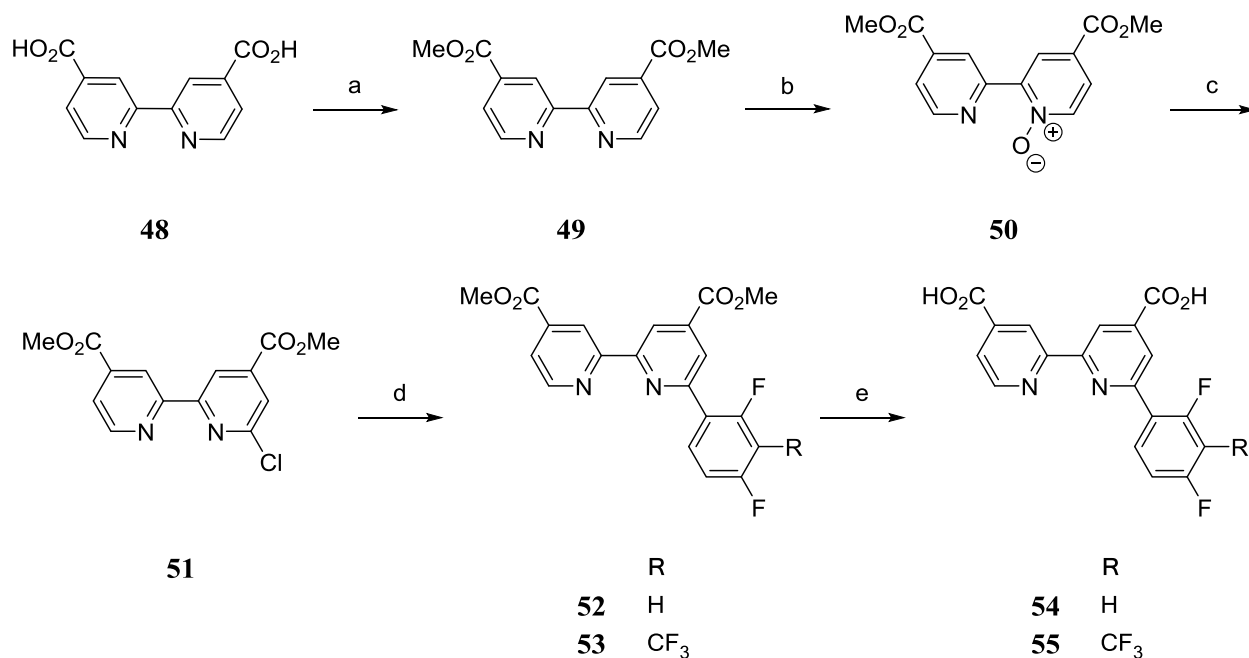
3 Results and Discussion

3.1 Synthesis of Ligands

3.1.1 Synthesis of the Ligands **54** and **55**

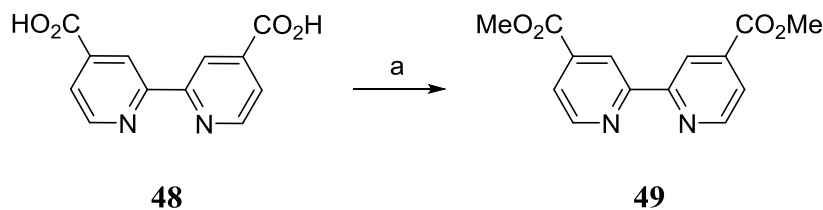
The first target was the synthesis of ligands **54** and **55** which were accessed *via* the same methodology used by Kim *et al.* in their synthesis of **JK-206** (Scheme 3).⁹⁰ One of the benefits of this method is that both **54** and **55** can be accessed in two steps from **51**. The esters **52** and **53** provide a possible alternative strategy for the synthesis of the complexes i.e. synthesis of the

complexes from **52** and **53** followed by ester hydrolysis. This route therefore allows both strategies to be attempted.



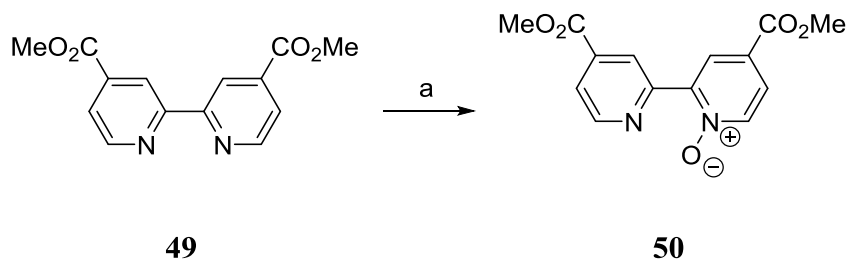
Scheme 3: Synthetic route to our initial targets **54** and **55**. Reaction conditions: (a) H₂SO₄, MeOH; (b) *m*CPBA, CH₂Cl₂; (c) POCl₃; (d) 2,4-difluorophenylboronic acid/2,4-difluoro-3-(trifluoromethyl)phenylboronic acid, Pd(PPh₃)₄, Na₂CO₃; (e) KOH, aqueous MeOH.

The synthesis began with a protection of the carboxylic acid groups of 2,2'-bipyridine-4,4'-dicarboxylic acid, by methylation in H₂SO₄ and MeOH (Scheme 4).



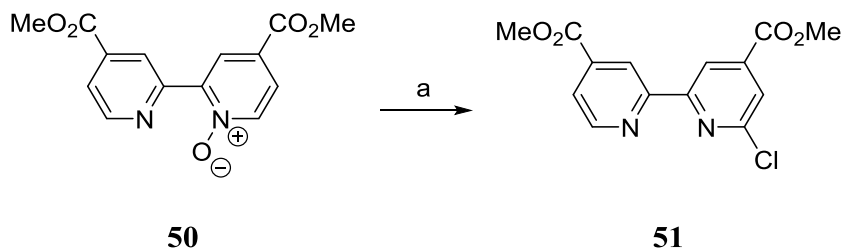
Scheme 4: Esterification. Reaction conditions: (a) H₂SO₄, MeOH, 85 °C 46 h 85%.

This was followed by oxidation one of the pyridine moieties with *m*-chloroperbenzoic acid (*m*CPBA) in preparation for the following chlorination (Scheme 5).



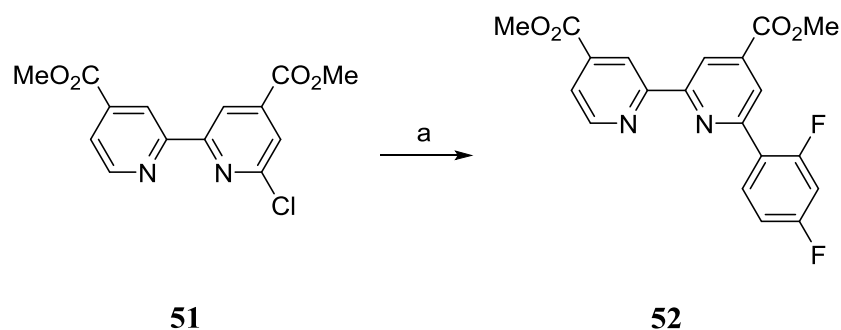
Scheme 5: Oxidation. Reaction conditions: (a) *m*CPBA, CHCl₃, rt, 10 h.

The product, **50**, proved difficult to purify, column chromatography was attempted on both silica and alumina however the compound was unstable and reacted with UV light on the column giving a yellow impurity which was not removed. Recrystallization in CH₂Cl₂ and precipitation by addition of a concentrated solution of **50** in CH₂Cl₂ added to hexane was attempted, but were unsuccessful. The impure product was carried forward to the next step. Chlorination of **50** was achieved by reflux in phosphorus(V) oxychloride (POCl₃), (Scheme 6). A poor yield was obtained over these two steps mainly due to the instability of **51** and the various attempts at purification.



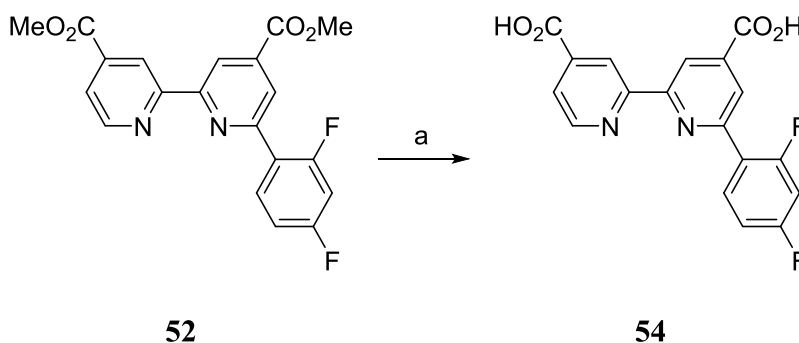
Scheme 6: Chlorination. Reaction conditions: (a) POCl₃, 120 °C, 2 h, 12% over 2 steps.

Addition of the difluorophenyl unit was achieved *via* Suzuki coupling of the chloride **51** to 2,4-difluorophenylboronic acid (Scheme 7).



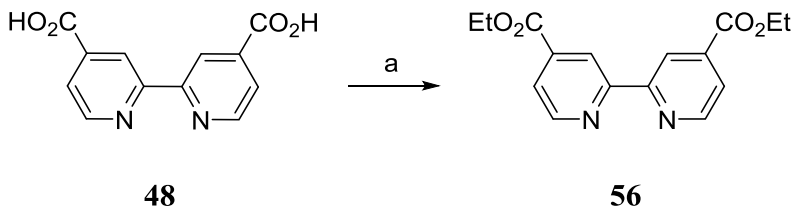
Scheme 7: Suzuki coupling. Reaction conditions: (a) 2,4-difluorophenylboronic acid, Pd(PPh₃)₄, Na₂CO₃, THF/H₂O 5:1, 70 °C, 21 h, 60%.

Reaction of **52** with potassium hydroxide (KOH), MeOH and H₂O afforded the diacid ligand **54** in 79% yield (Scheme 8).



Scheme 8: Deprotection of the acid groups. Reaction conditions: (a) KOH, aqueous MeOH, 85 °C, 18 h 79%.

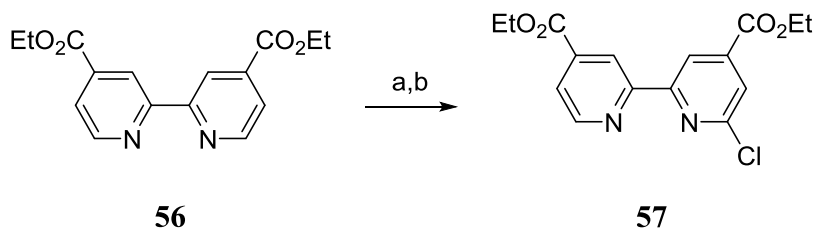
In order to improve the synthetic method, the first three steps were repeated with alterations. To aid the solubility of compounds in organic solvents, the esterification was carried out with EtOH to give the diethyl ester **56** (Scheme 9).



Scheme 9: Esterification. Reaction conditions: (a) H₂SO₄, EtOH, 100 °C, 72 h, 72%.

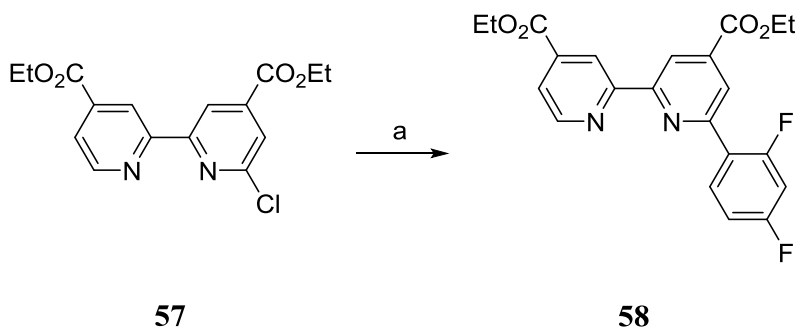
The oxidation and chlorination steps were then combined, avoiding the unsuccessful purification which had dramatically decreased the yield. The oxidation was performed at a higher temperature of 30 °C in an attempt to increase yield, and the *m*CPBA was added as a solution

rather than a solid to prevent synthesis of the dioxide. The crude oxide produced was washed with aqueous Na_2CO_3 solution to remove any remaining *m*CPBA and immediately refluxed with POCl_3 . These modifications furnished an improved yield of 35% over 2 steps (Scheme 10).



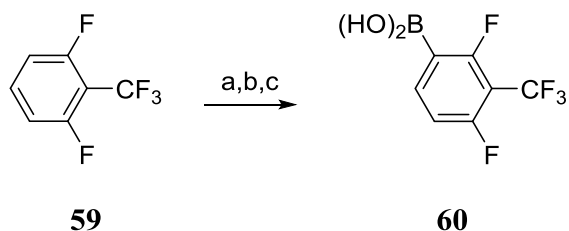
Scheme 10: Two step synthesis of chloride **57**. Reaction conditions: (a) *m*CPBA, CHCl_3 , 30 °C, 10 h, (b) POCl_3 , 120 °C, 2 h, 35% over 2 steps.

Coupling of the difluorophenyl moiety was achieved in the same fashion as before with an improved yield of 73%.



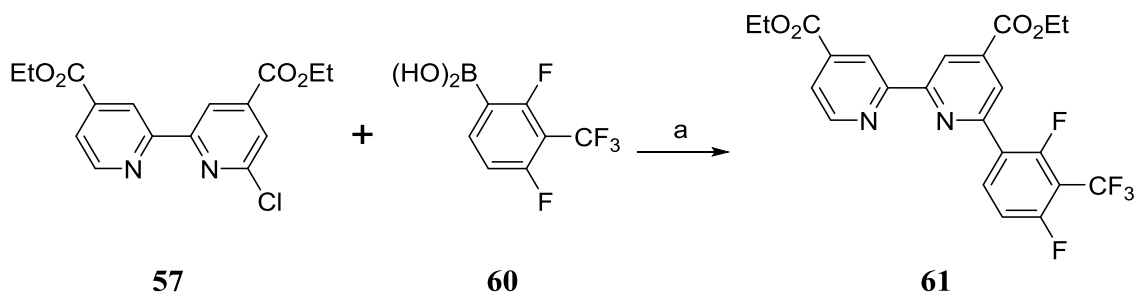
Scheme 11: Suzuki coupling. Reaction conditions: (a) 2,4-difluorophenylboronic acid, $\text{Pd}(\text{PPh}_3)_4$, Na_2CO_3 , THF/ H_2O 5:1, 70 °C, 16 h, 73%.

Synthesis of 2,4-difluoro-3-(trifluoromethyl)phenylboronic acid was achieved by reaction of 2,4-difluorobenzotrifluoride **59** with *n*butyllithium and trimethylborate. The crude product was carried forward.



Scheme 12: Synthesis of **60**. Reaction conditions: (a) 2,6-difluorobenzotrifluoride, *n*BuLi, THF, -78 °C 1 h, (b) B(OMe)₃, -78 °C → 20 °C 16 h, (c) HCl, 1h.

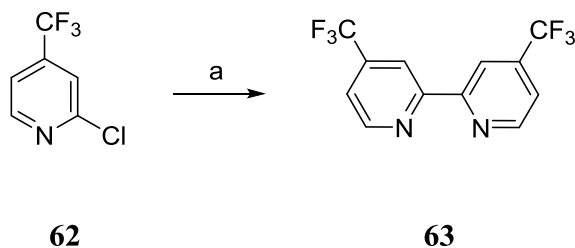
Coupling of **57** to **60** was again achieved using a similar method with a similar yield of 67%.



Scheme 13: Suzuki coupling. Reaction conditions: (a) Pd(PPh₃)₄, Na₂CO₃, THF/H₂O 5:1, 70 °C, 21 h, 67%.

3.1.2 Synthesis of Ligands **67** and **68**

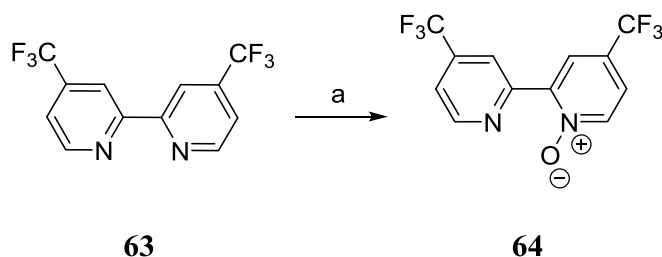
The strategy for the synthesis of ligands **67** and **68** was the same as for the previous ligands. The main difference was the initial bipyridine precursor **63** is not available commercially. Synthesis of **63** was achieved by the homocoupling reaction of chloride **62** with dibromonickel(II)bis(triphenylphosphine), zinc and tetraethylammonium iodide, to give a yield of 33%.



Scheme 14: Synthesis of bipyridine **63**. Reaction conditions: (a) Ni(PPh₃)₂Br₂, Zn, TEAI, 50 °C, 100 h, 33%.

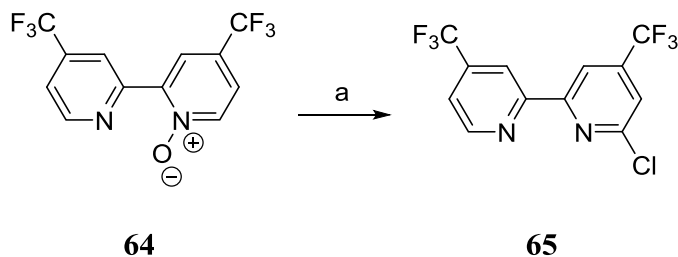
N-oxide **64** was synthesised using the method previously identified however a higher temperature of 50 °C was required for decent levels of conversion. As with the other bipyridyl *N*-

oxides investigated, this compound proved highly unstable toward light on silica and alumina. The crude was carried forward after aqueous work up.



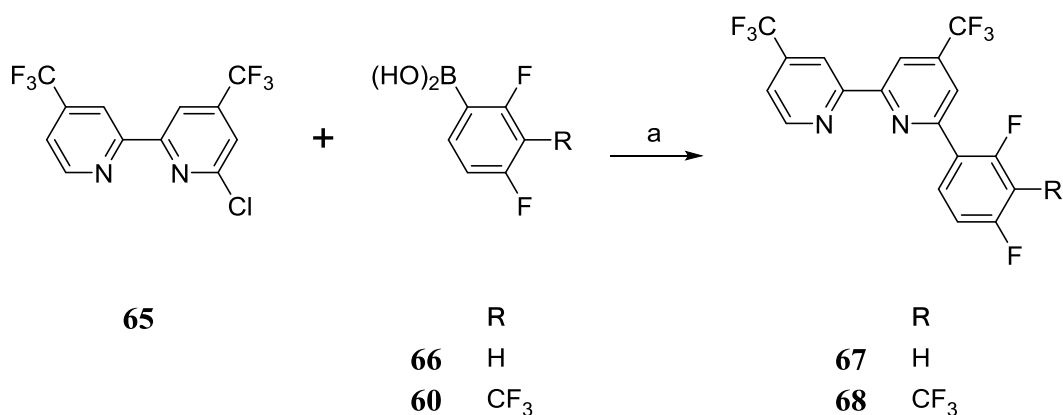
Scheme 15: Synthesis of *N*-oxide **64**. Reaction conditions: (a) *m*CPBA, CHCl₃, 50 °C, 16 h.

Chlorination of **65** was performed by reaction with POCl₃. A reaction time of 1.5 h (as for **51** and **57**) gave inconsistent results. A longer reaction time of 5 h, gave **65** in 37% yield over two steps.



Scheme 16: Synthesis of chloride **65**. Reaction conditions: (a) POCl₃, 120 °C, 5 h, 37% over two steps.

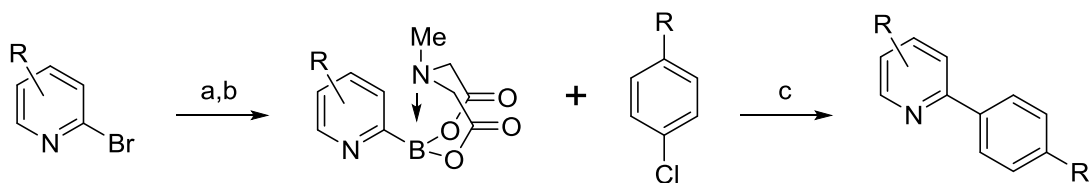
Synthesis of phenylbipyridines **67** and **68** was achieved in the previously reported manner, by Suzuki coupling with the desired boronic acid. The chlorides were particularly active toward coupling with yields for **67** and **68** of 96% and 93% respectively.



Scheme 17: Synthesis of phenylbipyridine **67** and **68**. Reaction conditions: (a) Pd(PPh₃)₄, Na₂CO₃, THF, H₂O, 5:1, 70 °C, 16 h, 96% and 93% respectively.

3.1.3 Synthesis of Ligands **77** and **78**

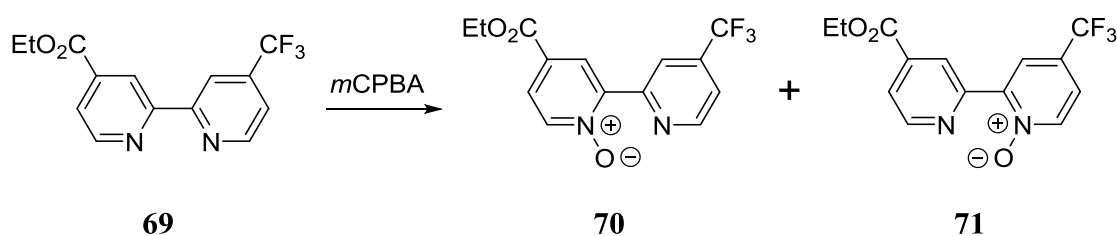
Ligands **58**, **61**, **67** and **68** were accessed relatively simply following the strategy used by Kim *et al.*⁹⁰ Ligands **77** and **78** would present more of a problem. Ideally we would proceed via the same route. First synthesise the asymmetrical bipyridine moiety, oxidise, chlorinate and then react with the relevant boronic acids to obtain the ligands. The first problem with this strategy was forming the 2,2'-bipyridyl bond. Standard Suzuki coupling is not sufficient to this task, as 2-pyridyl boronic acids are particularly unstable to protodeborylation. The classic solution is to use the Stille coupling method. This however would require the use of highly toxic organostannanes and the more expensive bromide rather than chloride for the cross-coupling reaction. A rather neat solution to this problem is the method developed by the Burke group (Scheme 18). A stabilised boronic acid analogue is produced by reaction of the unstable 2-pyridyl boronic acid directly with methyliminodiacetic acid (MIDA). This can then be coupled with aryl chlorides under specialised palladium catalysed cross-coupling conditions. Some of these stabilised boronic acid analogues are even available for purchase from the manufacturer Sigma Aldrich.^{93,94}



Scheme 18: Synthesis of MIDA boronates. Reaction conditions: (a) *n*BuLi, (*i*PrO)₃B, -78 °C, 1h, then 23 °C 3 h (b) MIDA, DMSO, 115 °C, 1 h (c) XPhos, Pd₂dba₃, Cu(OAc)₂, K₂CO₃, DMF/IPA 100 °C, 4 h.

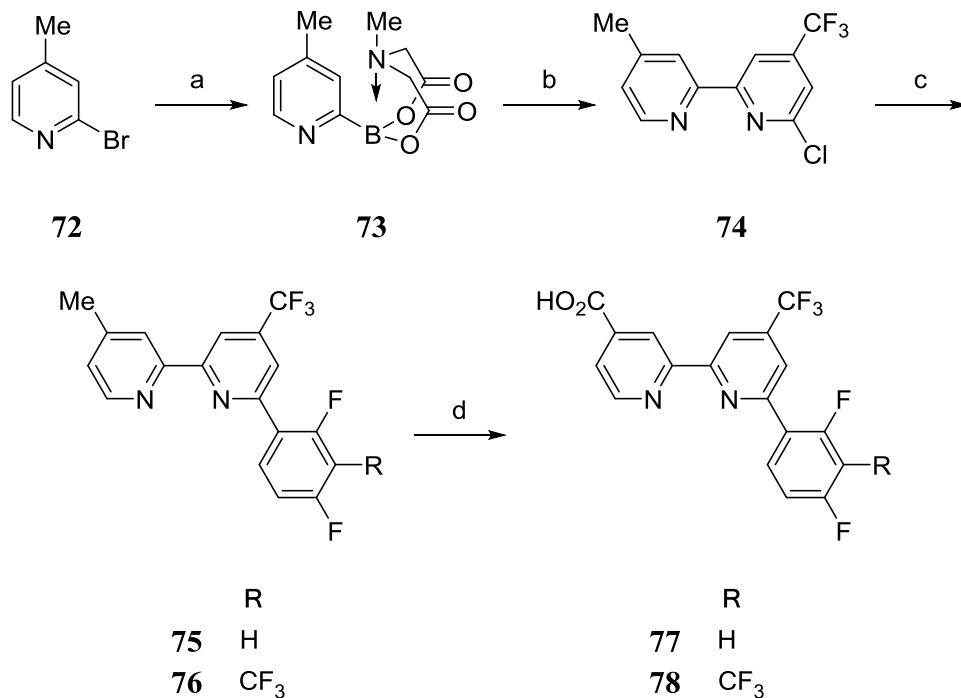
In order to utilise this method we would have to use 2-bromo-4-methylpyridine to make the boronate, as the acid or ester would not tolerate the lithiation. Oxidation of the methyl group could then be performed at a later stage in the synthesis to allow access to the desired acid.

The second challenge to overcome to access ligands **77** and **78** involves the oxidation step. Assuming you have the correct bipyridine in hand we would wish to selectively oxidise on one of the pyridyl nitrogens. One would predict that if you attempted the oxidation of **69** (the potential bipyridine precursor for ligands **77** and **78**), the likely product would be a mixture of both possible oxides (Scheme 19), and would even favour the non-desired product due to the more electron-withdrawing trifluoromethyl group being deactivating. Indeed the 4,4'-(trifluoromethyl)bipyridine **63**, required a higher temperature to give conversion to the *N*-oxide compared to the bipyridine-4,4'-dicarboxylate **56**.



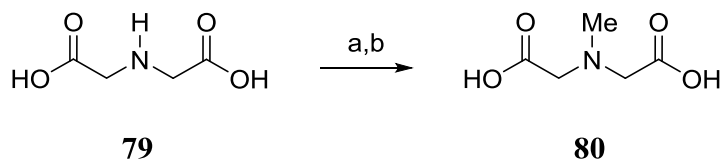
Scheme 19: Predicted outcome of the oxidation of the asymmetric bipyridine **69**.

In order to overcome this issue we were interested to see if it were possible to use stoichiometric control to perform a mono-coupling to a dihalide using the burke boronate to access the chloride **74** directly. Our strategy was devised around these techniques along with the methyl to acid oxidation method used by Nazeeruddin *et al.* in their synthesis of **N749** using potassium dichromate ($K_2Cr_2O_7$) and H_2SO_4 (Scheme 20).⁸¹



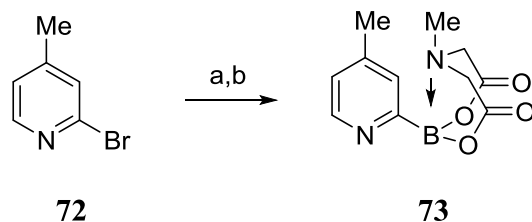
Scheme 20: Synthetic route to our secondary target ligands **77** and **78**. Reaction conditions: (a) (i) *n*BuLi, (*i*PrO)₃B (ii) MIDA, DMSO; (b) 2,6-dichloro-4-(trifluoromethyl)pyridine, Pd₂dba₃, XPhos, K₂CO₃, Cu(OAc)₂; (c) 2,4-difluorophenylboronic acid/2,4-difluoro-3-(trifluoromethyl)phenylboronic acid, Pd(PPh₃)₄, Na₂CO₃; (d) K₂Cr₂O₇, H₂SO₄.

MIDA was synthesised by reaction of iminodiacetic acid, formaldehyde and formic acid, a simple reaction on a large scale with an acceptable yield of 84%.



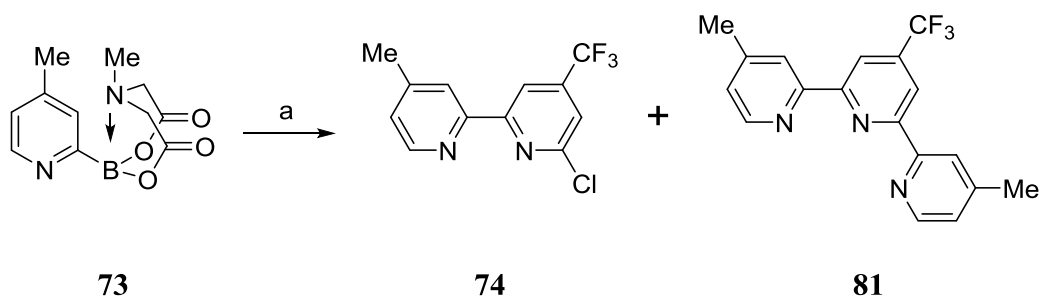
Scheme 21: Synthesis of **80**. Reaction conditions: (a) Iminodiacetic acid, formaldehyde 90 °C, 30 min (b) formic acid 90 °C, 1h. 84%.

Synthesis of the MIDA boronate **73** was achieved successfully although in much lower yield than that reported in the literature. (25% vs. 42%). This is possibly due to the sensitivity of the 2-pyridylboronic acid *isopropyl* ether intermediate to H₂O, as the DMSO used was not anhydrous.



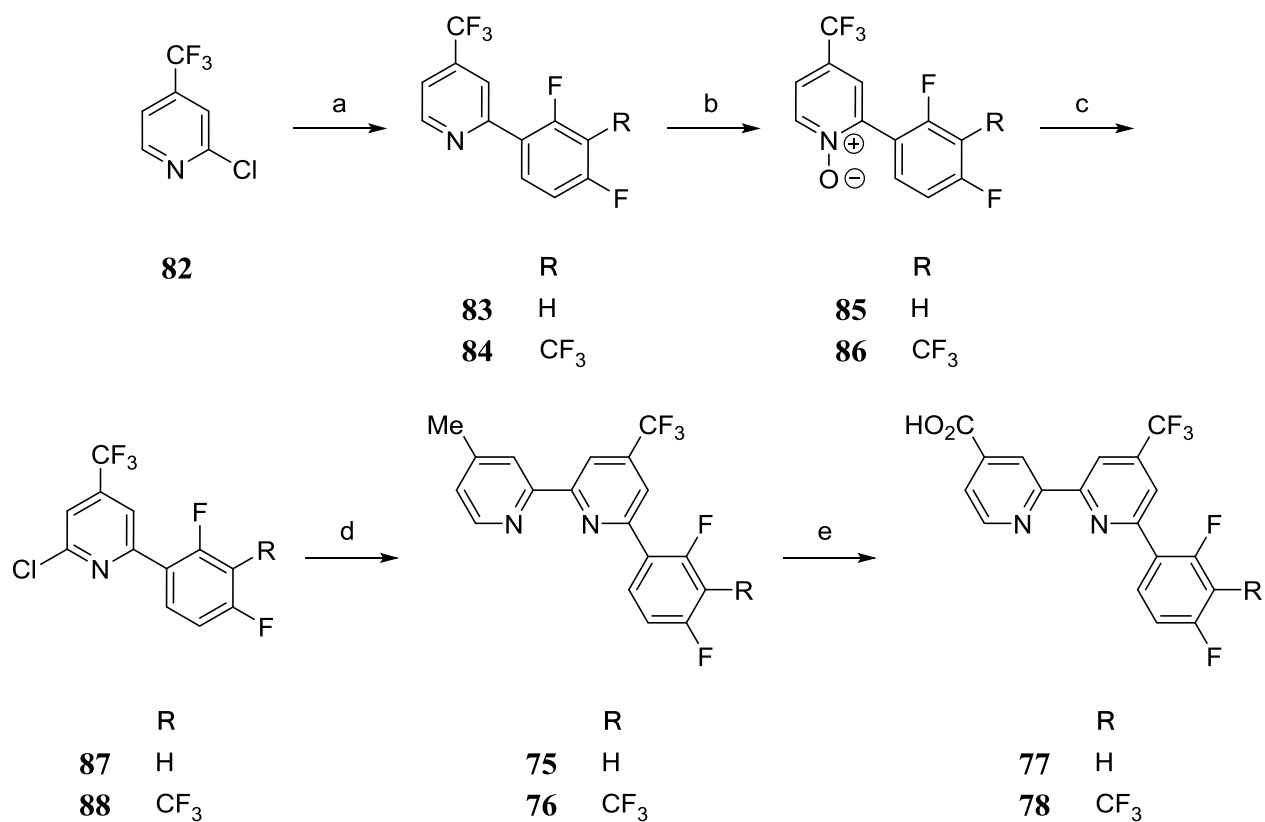
Scheme 22: Synthesis of MIDA boronate **73**, (Method 1). Reaction conditions: (a) *n*BuLi, (*i*PrO)₃B, -78°C, 1h, then 23 °C 3 h (b) MIDA, DMSO, 115 °C, 1 h, 25%.

The slow-release cross-coupling was attempted next, in an alteration to the literature method a dihalide (2,6-dichloro-4-(trifluoromethyl)pyridine) was used and to avoid two portions of the boronate reacting with one of the halide, stoichiometric control was employed (Scheme 23).



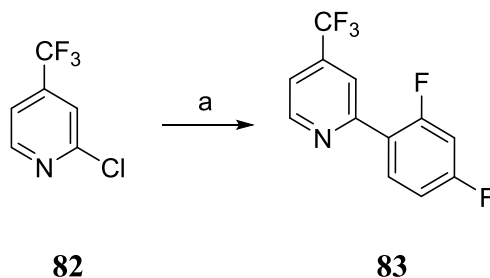
Scheme 23: Synthesis of **81**. Reaction conditions: 2,6-dichloro-4-(trifluoromethyl)pyridine, Pd₂dba₃, XPhos, K₂CO₃, Cu(OAc)₂, DMF, 100 °C, 4h.

The major product of the reaction was however the unexpected disubstituted product, in a low yield of 30% whilst only trace quantities of the desired product were observed. The obvious route to avoid problems with the selectivity of oxidation of the bipyridyl moiety is to proceed via the phenylpyridines **83** and **84**. Oxidation occurs at only one site, subsequent chlorination gives a suitable partner for cross-coupling with the MIDA boronate **73** to give the phenylbipyridine which can be oxidised to give the desired acids **77** and **78** (Scheme 24). However as the two ligands vary only on the phenyl portion introduction of this moiety in the first step effectively doubles the amount of steps to access both ligands.



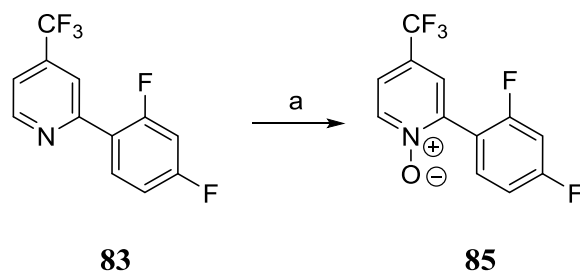
Scheme 24: Revised Synthetic route to our secondary target ligands **77** and **78**. Reaction conditions: (a) 2,4-difluorophenylboronic acid/2,4-difluoro-3-(trifluoromethyl)phenylboronic acid, Pd(PPh₃)₄, Na₂CO₃; (b) *m*CPBA; (c) POCl₃; (d) Pd₂dba₃, XPhos, K₂CO₃, Cu(OAc)₂; (e) K₂Cr₂O₇, H₂SO₄.

The synthesis began with the cross coupling reaction between **82** and 2,4-difluorophenylboronic acid to give **83** in 71% yield.



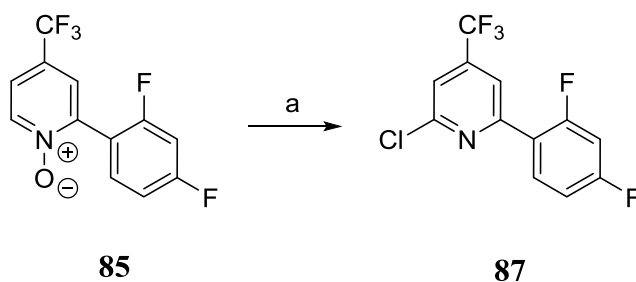
Scheme 25: Suzuki coupling. Reaction conditions: (a) 2,4-difluorophenylboronic acid, Pd(PPh₃)₄, Na₂CO₃, THF/H₂O 5:1, 70 °C, 21 h, 71%.

The next step was the oxidation of the 1-position of **83** with *m*CPBA (Scheme 26).



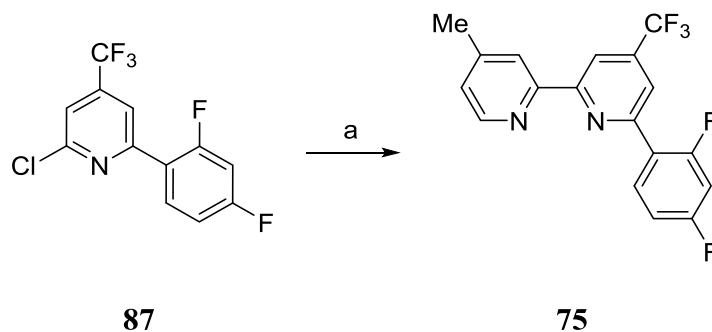
Scheme 26: Oxidation of **83**. Reaction conditions: (a) *m*CPBA, CH₂Cl₂, 30 °C, 16 h, 89%.

This reaction proceeded with much improved yield to that achieved previously with the same methodology. When using the same method for the mono-oxidation of **56**, it was found that column chromatography on silica or alumina caused degradation of the product. In this instance a column was not required, as only one possible oxidation product was formed. Instead **85** was easily purified by precipitation in hexane from a concentrated solution in Et₂O.



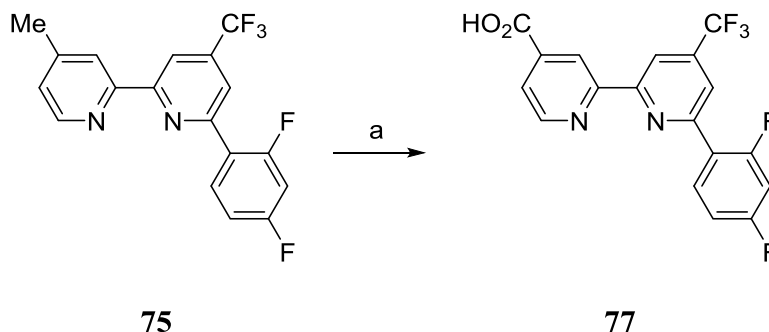
Scheme 27: Chlorination of **85**. Reaction conditions: (a) POCl₃, 120 °C, 2 h, 40%.

The oxide **85** was then refluxed in POCl₃ for 2 h to obtain the chloride **87** (Scheme 27). In order to attach a further pyridine moiety, **87** was coupled with **73**, under slow release conditions over four hours (Scheme 28).



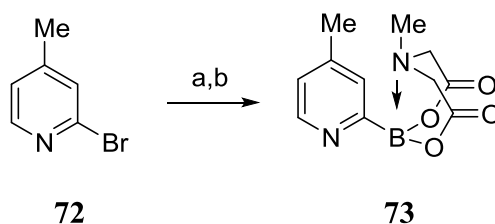
Scheme 28: Slow release cross coupling. Reaction conditions: (a) 2-MIDA-boronate-4-methylpyridine, Pd₂dba₃, XPhos, K₂CO₃, Cu(OAc)₂, DMF/IPA (4:1), 100 °C, 4 h, 30%.

A poor yield was achieved and a significant quantity of starting material was observed by TLC in the crude product. This could indicate that a longer reaction time is required. The final step in the sequence was the oxidation of the methyl group of **75** with $K_2Cr_2O_7$ and H_2SO_4 (Scheme 29).



Scheme 29: Oxidation of the methyl group of **75**. Reaction conditions: (a) $K_2Cr_2O_8$, H_2SO_4 , $70^\circ C$, 2 h, 34%.

The reaction was successful, albeit in a poor yield of 34%. It is possible the trifluoromethyl group is sensitive to the oxidation method. The amphiphilic nature of this compound also meant it was difficult to dissolve, purify and therefore analyse by NMR. Overall this revised synthetic route was successful in producing the desired phenylbipyridine **77**. Unfortunately poor yields were obtained throughout, particularly the synthesis of MIDA boronate **73**, a key starting material obtained in only 25% yield. In order to improve upon this, the reaction was repeated with anhydrous DMF as a solvent replacing DMSO (Scheme 30). We predicted that as the 2-pyridylboronic acid isopropyl ether intermediate is very sensitive to H_2O , anhydrous solvent would perform better. Also as DMF can be removed by rotary evaporation, the method would be simpler and far quicker.

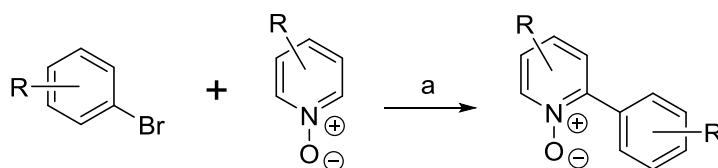


Scheme 30: Synthesis of MIDA boronate **73** (Method 2). Reaction conditions: (a) $nBuLi$, $(iPrO)_3B$, $-78^\circ C$, 1h, then $23^\circ C$ 3 h (b) MIDA, DMF, $115^\circ C$, 1 h, 25%.

Although the method was significantly more efficient in terms of time, the yield was unchanged by this alteration. The low yields of this method and the synthetic route as a whole, as well as its

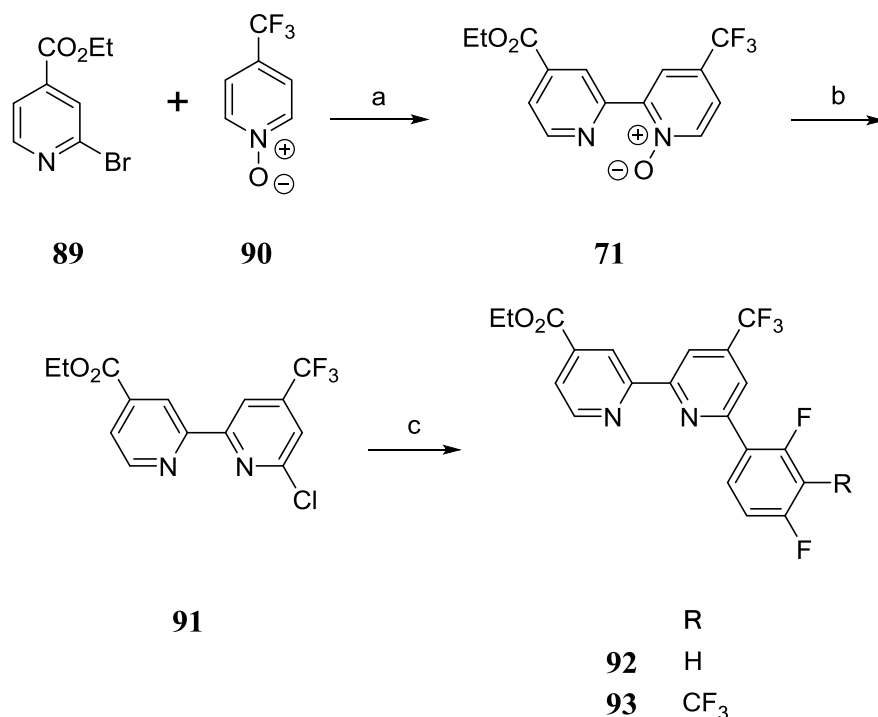
non-ideal divergent nature with a large number of steps lead us to consider utilising a different method for coupling at the 2-pyridyl position.

In a paper published by Campeau *et al.* 2-pyridyl cross-coupling is achieved without the use of boronic acids or esters but rather using an oxidised pyridine.⁹⁵ This reacts with an aryl bromide and a palladium catalyst to form a new carbon-carbon bond and the pyridyl nitrogen remains oxidised in the product (Scheme 31).



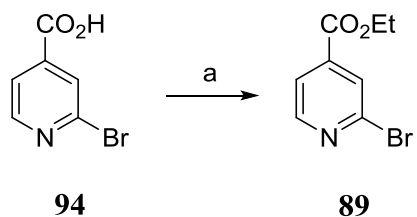
Scheme 31: General scheme for pyridyl oxide cross-coupling by Campeau *et al.* Reaction conditions: Pd(OAc)₂, P^tBu₃-HBF₄, K₂PO₃, Toluene, 110 °C.

We hypothesised earlier that if you attempted the oxidation of **69** the likely product would, at best, be a mixture of both possible oxides. Using the method by Cameau *et al.* we planned to access the desired oxide intermediate **71** avoiding any issues of selectivity. The chlorination product **91** can then be coupled to the phenyl moiety using standard Suzuki coupling allowing access to both **92** and **93** (Scheme 32).



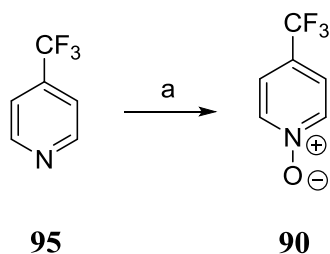
Scheme 32: Simpler synthetic route to **92** and **93**. Reaction conditions: (a) Pd(OAc)₂, P^tBu₃-HBF₄, K₂PO₃ (b) POCl₃ (c) 2,4-difluorophenylboronic acid/2,4-difluoro-3-(trifluoromethyl)phenylboronic acid, Pd(PPh₃)₄, Na₂CO₃.

This synthetic route is simpler, more convergent and significantly shorter. One drawback is the *N*-oxide cross-coupling reaction needs at least two equivalents of the oxide to proceed. However the excess reactant can be reclaimed by chromatography. It would theoretically be possible to avoid chlorination altogether and couple the bipyridyl-oxide with a phenylbromide and then reduce to give the ligand. There are several reasons why we did not attempt this. Firstly proceeding via the chloride feeds nicely into the synthetic route used for ligands **58**, **61**, **67** and **68**, allowing us to use the same boronic acids and reagents rather than purchasing/synthesising the phenyl halides. We would also have to use two equivalents of the bipyridyl-oxide per phenyl compound reducing yield with respect to the bipyridine. Finally, the Fagnou group reported poor yields for these reactions in the presence of very electron-withdrawing substituents, and extended aromatic systems. The ethyl ester **89** was accessed from commercially available 2-bromoisonicotinic acid in 63% yield using a similar method to that used for **56** (Scheme 33).



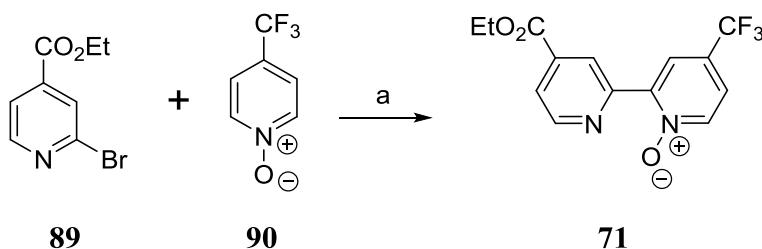
Scheme 33: Synthesis of ester **51**. Reaction conditions: (a) H_2SO_4 , EtOH, 80°C , 24 h, 63%.

The *N*-oxide **90** was accessed from the parent pyridine **95** by reaction with *m*CPBA. Due to its sensitivity to light when adsorbed on silica, the crude obtained after aqueous work-up was carried forward without purification.



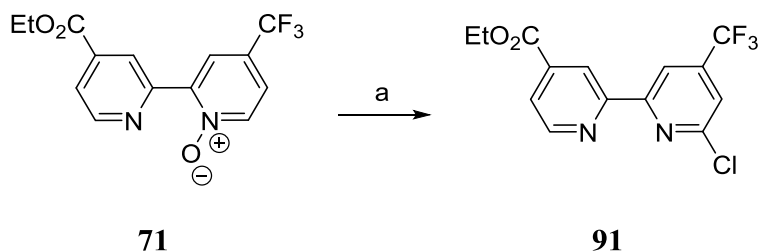
Scheme 34: Synthesis of *N*-oxide **90**. Reaction conditions: (a) *m*CPBA, CH_2Cl_2 30°C , 16 h.

Synthesis of **71** was achieved by the palladium catalysed cross-coupling reaction of bromide **89** and *N*-oxide **90** (Scheme 35).



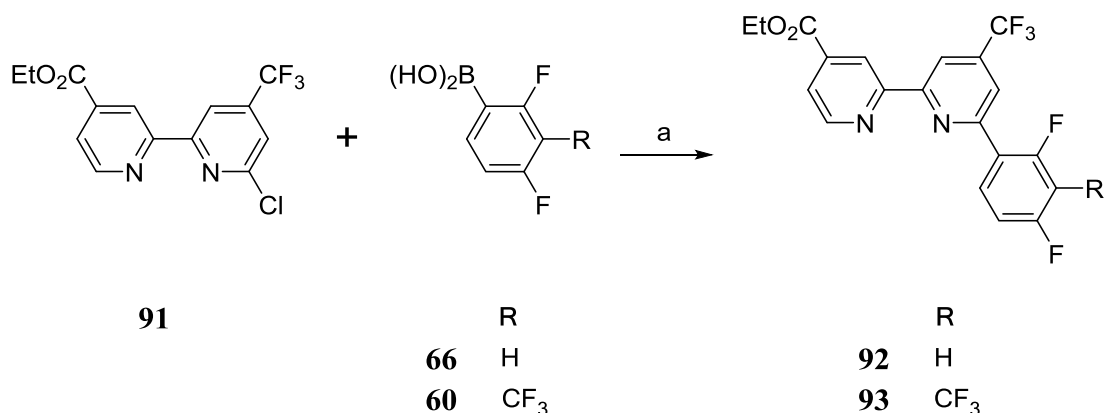
Scheme 35: Synthesis of oxide **90**. Reaction conditions: (a) $\text{Pd}(\text{OAc})_2$, $\text{P}^t\text{Bu}_3\text{-HBF}_4$, K_2PO_3 , PhMe, 110°C , 16 h. 63%.

The crude product was obtained by aqueous work-up. Purification on a silica column was found to be successful but ultimately gave a poorer yield due to decomposition of the oxide on the column when exposed to light. The crude product was therefore carried forward. Crude **71** was then chlorinated by reaction with phosphorous oxychloride to provide **91** in 32% yield over two steps (Scheme 36).



Scheme 36: Synthesis of chloride **91**. Reaction conditions: (a) POCl₃, 120 °C, 2 h. 32% over two steps.

Phenylbipyridines **92** and **93** were then acquired *via* Suzuki coupling of **91** with boronic acids **66** and **60** (Scheme 37). This synthetic strategy proved an elegant solution to the problems faced when synthesising a phenylbipyridine containing an asymmetrical bipyridine moiety, allowing access to a new family of ligands.



Scheme 37: Suzuki coupling. Reaction conditions: (a) Pd(PPh₃)₄, Na₂CO₃, THF, H₂O, 70 °C, 20 h. **92**, 60%, **93** 55%.

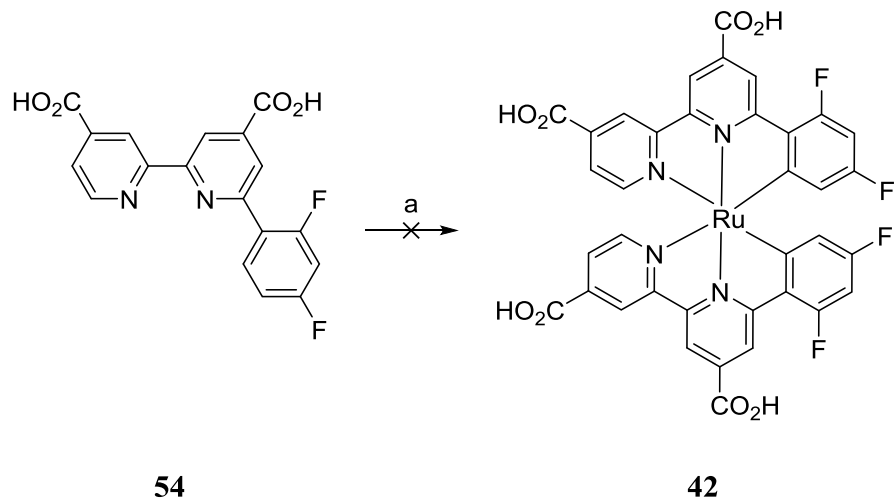
3.2 Synthesis of the first generation of cycloruthenated complexes

A review of the literature concerning the synthesis of cyclometalated, ruthenium, osmium and iridium complexes gave us some indications of the reagents and conditions required, although there are no examples of bis-homoleptic terdentate cycloruthenates. The literature methods, (of which there are many) include generally polar solvents, addition of a base and/or silver salts, or high boiling point alcohols. They mostly use either the trichloride or a chloro-bridged dimer as the metal source. As most are heteroleptic, stepwise addition of ligands is often involved. Table 1 shows a few examples.

Table 1: Example literature methods for synthesising terdentate cyclometalates.

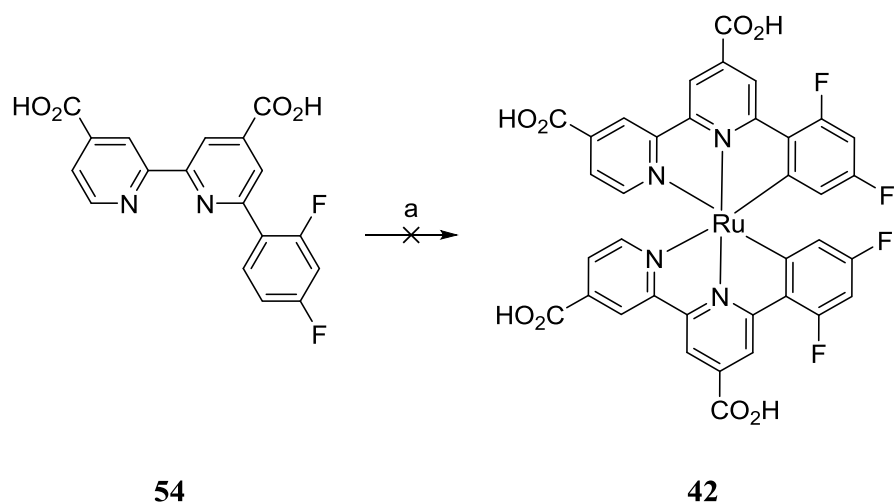
Metal	Solvent	Base	Temp (°C)	Duration (h)	Ref
Ir	Ethylene glycol	-	175	90	57
Ir	Glycerol	K ₂ CO ₃	200	2	96
Ru	DMF	-	160	4	90
Ru	<i>n</i> Butanol	-	118	3	32
Ru	Ethylene glycol	<i>N</i> -Methylmorpholine	200	1	54
Ru	MeOH/H ₂ O	<i>N</i> -Ethylmorpholine	45	14	2
Ru	CH ₃ CN	NaOH	82	72	29
Os	CH ₃ CN	NaOH	82	72	37

As the most similar example in terms of the ligand was the work by Kim *et al.*⁹⁰ we first attempted the method they had used, simply ruthenium(II) *p*-cymene dichloride dimer and DMF, at 80 °C for 4h then 160 °C for 4 h (in our case, with an additional equivalent of ligand) (Scheme 38). Large amounts of unreacted ligand remained in the mixture and a secondary reflux in ethylene glycol was performed and TBAOH added as a base to aid deprotonation. Purification by column chromatography on Sephadex LH20 was attempted. The different fractions obtained contained many different compounds and clear evidence of the compound was difficult to observe, whilst some very broad signals indicated possible oxidation to paramagnetic Ru³⁺.



Scheme 38: Attempted synthesis of complex **42** (Method 1). Reaction conditions: (a) $[\text{Ru}(p\text{-Cymene})\text{Cl}_2]_2$, DMF, 80 °C, 4 h, then 160 °C, 4 h.

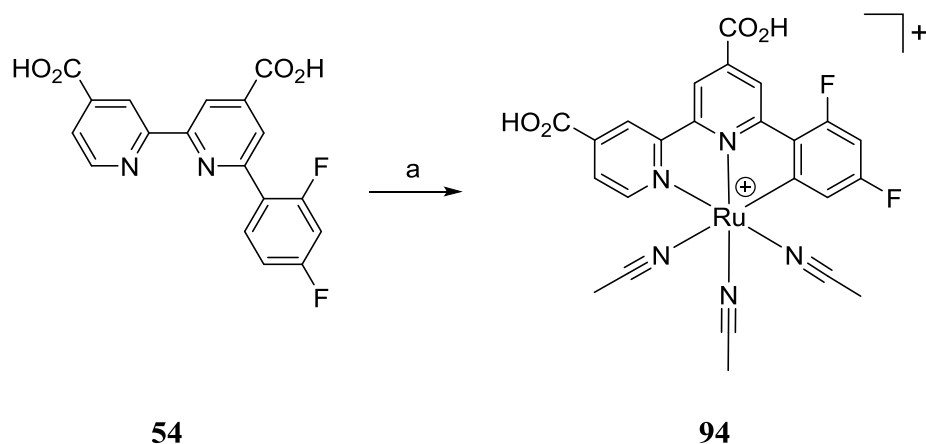
A patent published by the Grätzel group in May 2013 during the time this research was being performed, showed a synthesis of **42**, by refluxing **54** with $[\text{Ru}(p\text{-cymene})\text{Cl}_2]_2$ in DMF for 48 h.⁹⁷ Similar to the method we had already tried but with a longer reaction time. This method was attempted (with the reaction time extended) but was however unsuccessful (Scheme 39). The crude obtained was a mixture of so many products that purification proved impossible, and the resulting yield would have been, in any case, extremely poor.



Scheme 39: Synthesis of **42** (Method 2). Reaction conditions: (a) $[\text{Ru}(p\text{-Cymene})\text{Cl}_2]_2$, DMF 160 °C, 72 h.

The next approach was to access the complex in a stepwise fashion, using the same method as the Pfeffer group.²⁹ This involved a lower temperature and longer time, a strong base to aid in

cyclometalation as well as a solvent (acetonitrile) which could act as a labile ligand to aid in abstraction of the chlorides from the dimer. To prove that we could proceed to the bis-cyclometalated product via the tris-acetonitrile complex **94**, the reaction of **54** with $[\text{Ru}(p\text{-cymene})\text{Cl}_2]_2$ in acetonitrile was attempted at 45 °C for 72h (Scheme 40). The mass spectrum of the crude showed a signal at 581 m/z with the correct isotope pattern for the $[\text{M}+\text{H}]^+$ ion of **94**. A significant signal showing unreacted ligand was also present.



Scheme 40: Synthesis of cyclometalated intermediate **94**. Reaction conditions: (a) $[\text{Ru}(p\text{-cymene})\text{Cl}_2]_2$, MeCN, KOH, KPF_6 , 45 °C, 72 h.

The crude was then combined with acetonitrile and refluxed overnight to see if more of the remaining ligand could be converted to complex **42**. The mass spectra showed that at this higher temperature the tris-acetonitrile complex degrades and a mixture of complexes is observed. As adding just one equivalent of ligand required such long reaction times and the di/tetra acid products are so difficult to separate and study, we decided to investigate the cyclometalation of the esters of the ligands giving new targets **95-98** (Fig. 31).

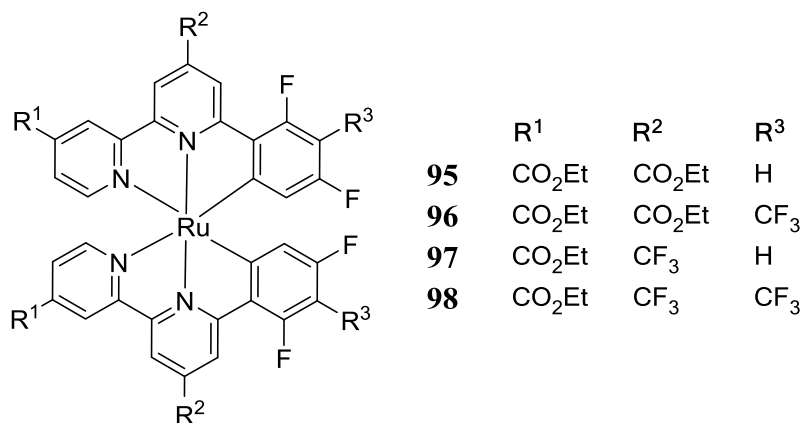
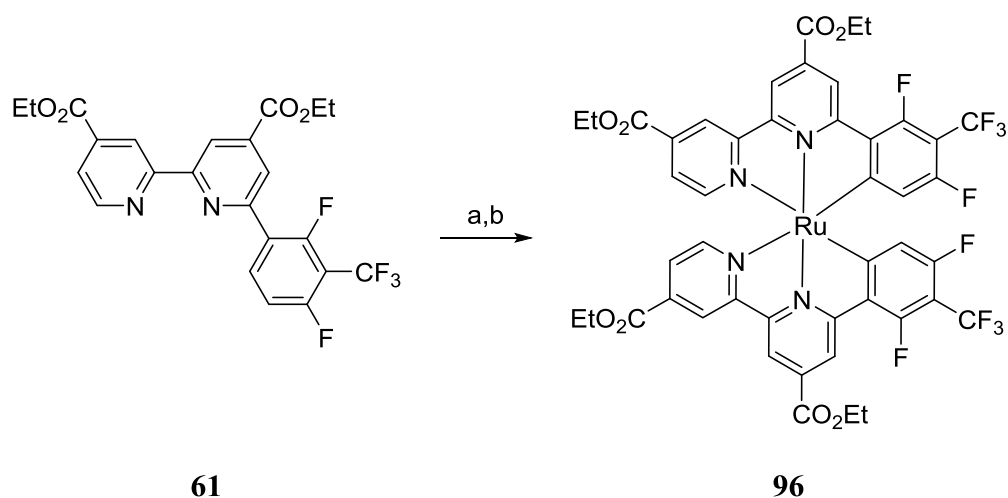


Fig. 31: New target cycloruthenates **95-98**.

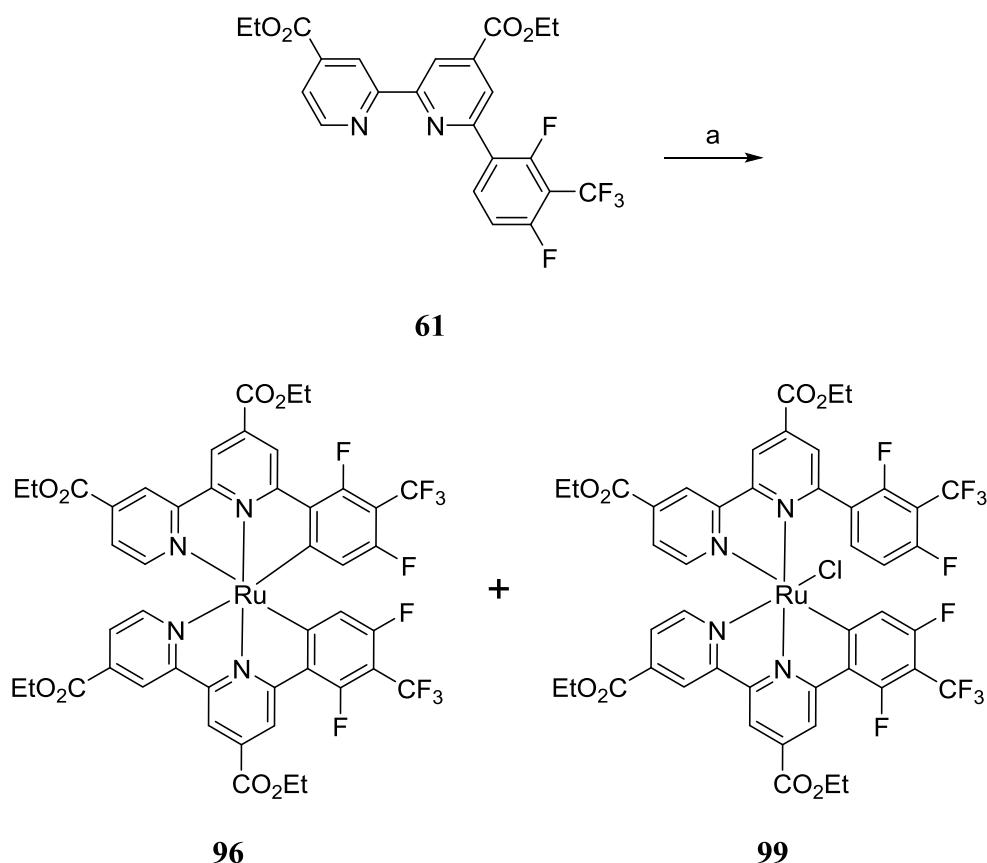
Using the method by Fetzer *et al.* we were able to access **96** in two steps (Scheme 41).²⁹ The product was purified by preparative chromatography on silica. The yield was however only 5%.



Scheme 41: Synthesis of **95** (Method 1). Reaction conditions: (a) [Ru(*p*-Cymene)Cl₂]₂, KOH, KPF₆, MeCN, 45 °C, 72 h. (b) *N*-Ethylmorpholine, EtOH, 80 °C, 16 h, 5%.

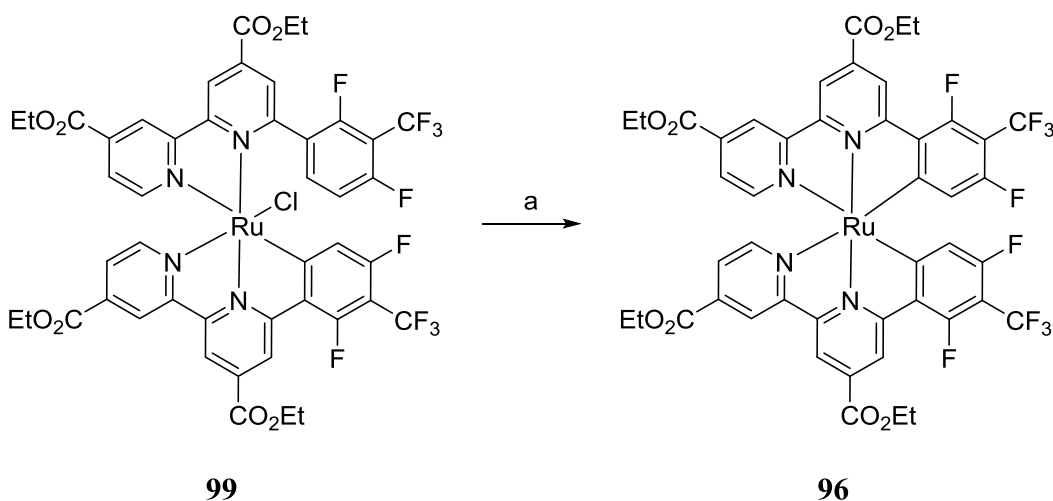
We then began to work on optimisation of this method. Analysis of the side products indicated significant deesterification was occurring. A one step approach in MeCN with *N*-ethylmorpholine instead of KOH and an extra equivalent of ligand was more successful, with an improved yield of 23%. It was also observed that the major side product was the monocyclometalated chloride complex **99** in a yield of 27%. The reaction was attempted again with a longer reaction time and a stronger base than *N*-ethylmorpholine (NEt₃) in an attempt to increase the yield of bis-cyclometalated product and decrease the amount of monocyclometalate

produced. The ratio of bis to mono was improved, however the yield was extremely poor for both (2.7% and 1.4% respectively) (Scheme 42). As increasing cyclometalation by increasing basicity was unsuccessful we posited that increasing the reaction temperature could overcome the activation energy barrier of cyclometalation. As we had observed the tris-acetonitrile intermediate by mass spec and had very little success with DMF, we theorised that the coordination properties of the solvent were important. We chose butyronitrile (*n*PrCN) as a solvent in order to retain the excellent coordination properties displayed by MeCN whilst allowing higher reaction temperature. Surprisingly the yield of bis-cyclometalated product was decreased to 11%. Clearly *n*PrCN is less effective at aiding the removal of the chloride than MeCN. A dramatic increase in the yield of the monocyclometalated complex to 74% was observed, indicating that formation of the first carbon metal bond was indeed favoured by higher temperatures.



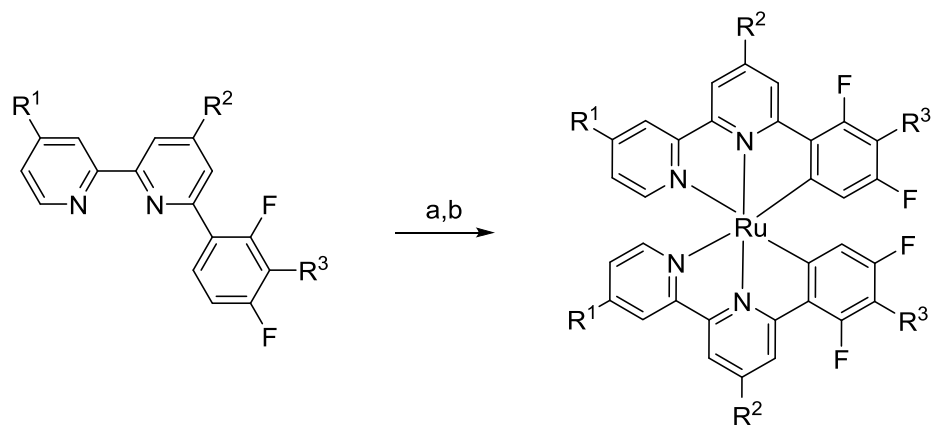
Scheme 42: Synthesis of **99** (Method 2, 3, and 4). Reaction conditions: (a) [Ru(*p*-Cymene)Cl₂]₂, *N*-Ethylmorpholine, MeCN, 80 °C, 144 h, **96** 23%, **99** 27%. (b) [Ru(*p*-Cymene)Cl₂]₂, NEt₃, MeCN, 80 °C, 162 h, **96** 2.7%, **99** 1.5%. (c) [Ru(*p*-Cymene)Cl₂]₂, *N*-Ethylmorpholine, *n*PrCN, 120 °C, 96 h, **96** 11%, **99** 72%.

Several literature methods including some in Table 1, involve heating to 200 °C in ethylene glycol. The monocyclometalated complex **99** obtained from the reaction in *n*PrCN was refluxed for 2 h in ethylene glycol to determine whether accessing even higher temperatures would improve the conversion of monocyclometalate to bis-cyclometalate. An almost total conversion from mono to bis-cyclometalated complex was observed (Scheme 43).



Scheme 43: Synthesis of **96** (Method 5). Reaction conditions: (a) Ethylene glycol, 200 °C, 2h, 90%.

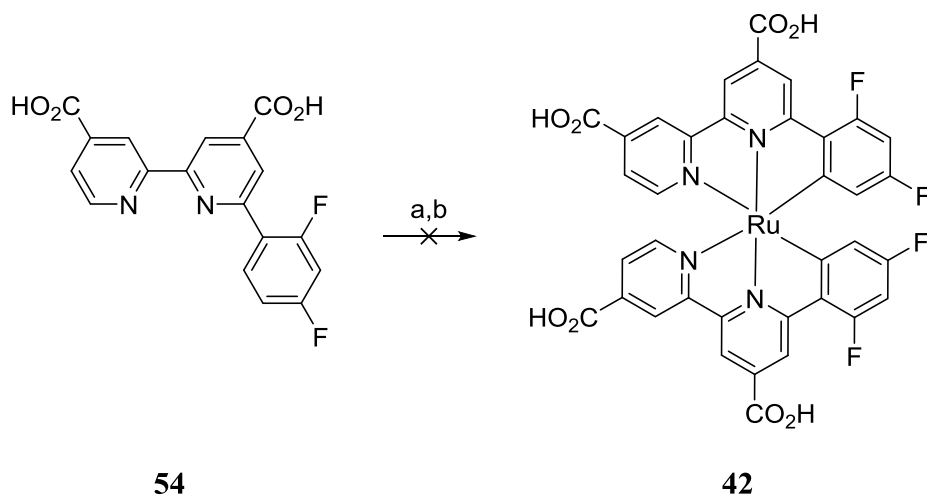
Armed with this information a two-step strategy was devised. Reflux in *n*PrCN with *N*-ethylmorpholine at 120 °C for 16 h, removal of solvent and base under reduced pressure, followed by addition of ethylene glycol and subsequent reflux at 200 °C for 2 h. This method allowed access to **95-98** and **46-47** in yields from 41-80% (Scheme 44).



	R ¹	R ²	R ³		R ¹	R ²	R ³	Yield %
58	CO ₂ Et	CO ₂ Et	H	95	CO ₂ Et	CO ₂ Et	H	65
61	CO ₂ Et	CO ₂ Et	CF ₃	96	CO ₂ Et	CO ₂ Et	CF ₃	41
67	CO ₂ Et	CF ₃	H	97	CO ₂ Et	CF ₃	H	49
68	CO ₂ Et	CF ₃	CF ₃	98	CO ₂ Et	CF ₃	CF ₃	80
92	CF ₃	CF ₃	H	46	CF ₃	CF ₃	H	32
93	CF ₃	CF ₃	CF ₃	47	CF ₃	CF ₃	CF ₃	37

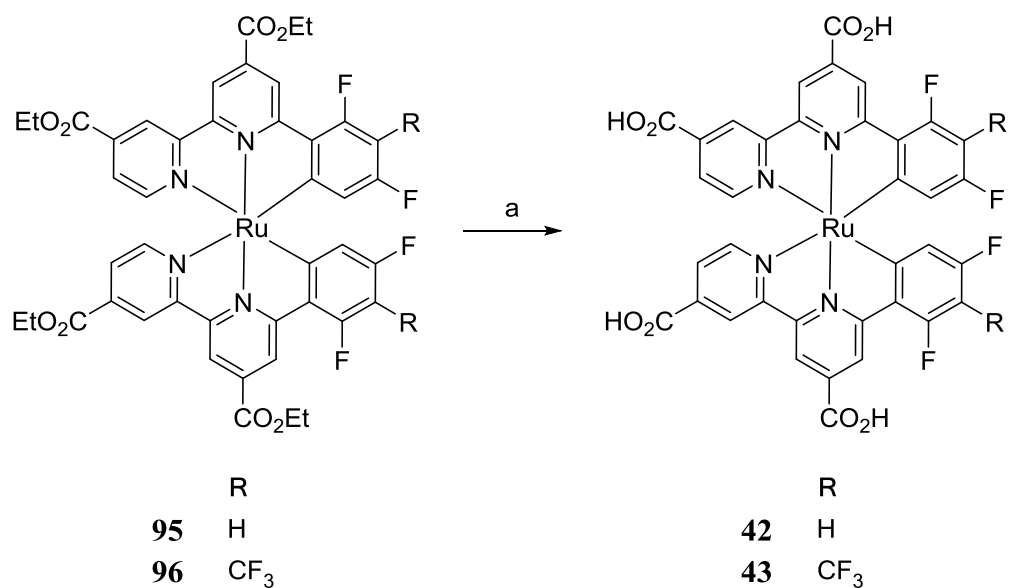
Scheme 44: Synthesis of **95-98** and **46-47** (Method 6 for **96**). Reaction conditions: (a) [Ru(*p*-Cymene)Cl₂]₂, *N*-ethylmorpholine *n*PrCN, 120 °C, 16 h. (b) Ethylene glycol, 200 °C, 2h.

Having determined a successful method for accessing the ester complexes, synthesis using this method directly with the ligand **54** was attempted. Unfortunately similarly poor results were obtained to all previous attempts to access **42** directly (Scheme 45).



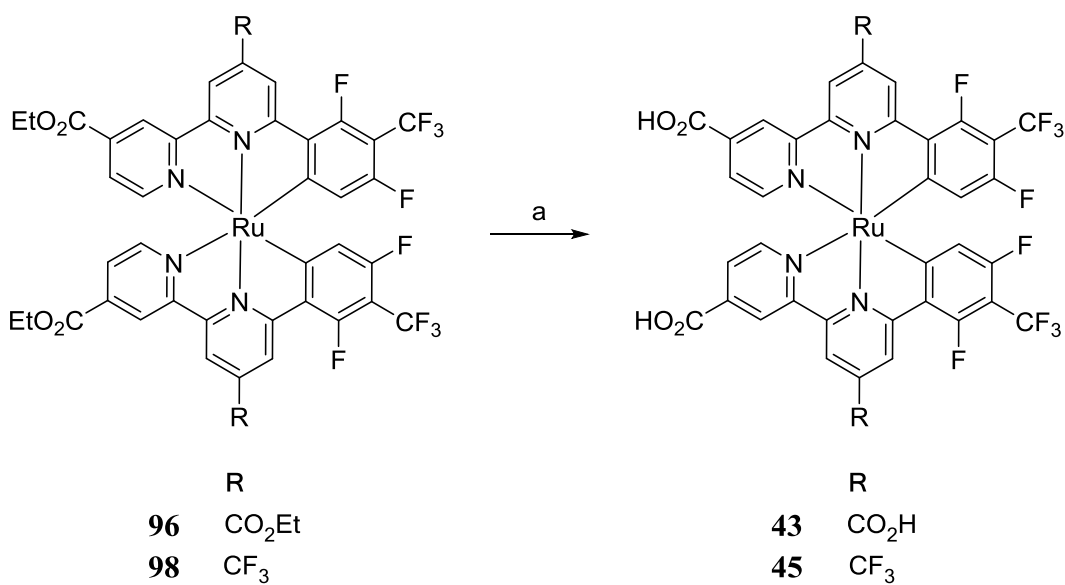
Scheme 45: Synthesis of **42** (Method 4). Reaction conditions: (a) $[\text{Ru}(\textit{p}\text{-Cymene})\text{Cl}_2]_2$, *N*-ethylmorpholine *n*PrCN, 120 °C, 16 h. (b) Ethylene glycol, 200 °C, 2h.

We turned our attention to synthesis of **42** and **43** by de-esterification of **95** and **96**. The Grätzel group have published a method for this with a complex with two ethyl ester moieties, using DMF, H₂O and NEt₃ in a 3:1:1 mix. This method was attempted for both **42** and **43**. The product obtained was far superior to that obtained directly from the ligand **54**. The vast majority of the crude material was the desired product with some small amounts of complex with some ethyl ester still present. Purification on sephadex LH20 allowed removal of these complexes however some impurities remained which could not be removed by chromatography on sephadex, or by precipitation from a solution of excess TBAOH in H₂O by addition of HNO₃. The complexes **42** and **43** (**42** in particular), are very easily oxidised to ruthenium(III) making manipulation difficult (Scheme 46).



Scheme 46: Synthesis of **42** (Method 5) and **43**. Reaction conditions: (a) DMF/NEt₃/H₂O, 3:1:1, 110 °C, 16 h.

Synthesis of complexes **43** and **45** was achieved with better results using the method by Chou *et al.*, reflux in acetone with 2M KOH (aq) (Scheme 47).⁹⁸



Scheme 47: Synthesis of **43** and **45**. Reaction conditions: (a) 2M KOH (aq) Acetone, 60 °C, 16 h, **43** 88%, **45** 85%.

Purification by precipitation from H₂O and washing the filtrand with H₂O, CH₂Cl₂ and hexane gave the acids **43** and **45** in 88% and 85% yields respectively.

3.3 Characterisation of the Complexes

3.3.1 UV-Vis absorption profiles.

Due to the difficulty in preparation of the acid complexes, the low oxidation states and poor solubility in organic solvents, the di and tetra-ester complexes **95-98** as well as the complexes **46** and **47** were investigated in terms of their optical and electronic properties. Characterisation of the series by UV-Vis spectroscopy was performed in CH_2Cl_2 solution (Fig. 32).

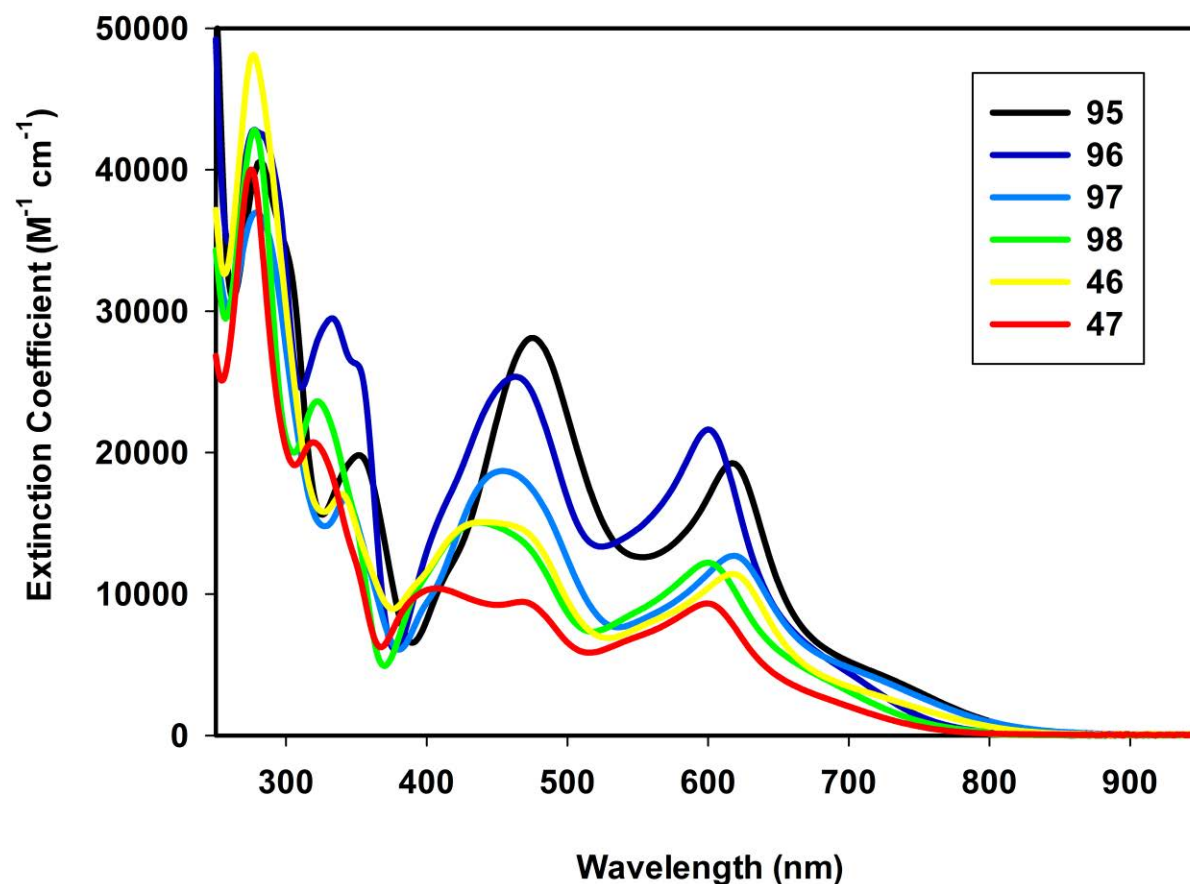


Fig. 32: Absorption spectra of **95-98** and **46-47** in CH_2Cl_2 between 250 and 950 nm.

The absorption profiles of all six first generation complexes are both very broad and intense. They absorb from 250 nm to above 850 nm and (aside from the spectrum of **47**) the maxima have extinction coefficients in excess of $10000 \text{ M}^{-1} \text{ cm}^{-1}$. The tetra-ester complexes **95** and **96** are the most intensely absorbing, with maxima between 400 nm and 600 nm in excess of $20000 \text{ M}^{-1} \text{ cm}^{-1}$. The entire series has relatively similar profiles, the peaks of which can be divided into two main environments: firstly the ligand centred $\pi-\pi^*$ transitions between 250 and 400 nm, and

secondly the peaks associated with MLCT transitions between 400 and 800 nm. There is a clear trend across the series from **95** to **47**. This is due to the trend of increasing electron-withdrawing nature of the ligand. The effect is that the intensity of the MLCT transitions are decreased with respect to the π - π^* transitions (which remain roughly similar throughout). This is likely due to the withdrawal of electron density onto the ligand and the subsequent reduction in metal character of the transitions. The replacement of the auxochromic ester substituents (which extend the conjugation of the system) with trifluoromethyl groups (which do not), probably also plays a role. All of the complexes show peaks at around 450 nm, 600 nm and a shoulder at around 750 nm. As we progress through the series from **95-47** we see the addition of electron withdrawing moieties to the ligand causes the peak at 450 nm to gradually blue-shift and broaden until in **47** it appears to split into two. The gradual change is indicative of a strong involvement of the bipyridyl portion of the ligand in this transition as this is gradually altered through the series by changing the esters to the slightly more electron withdrawing trifluoromethyl groups. The peak at around 600 nm behaves very differently as we progress through the series. The maxima for **95**, **97** and **46** are the same, at around 617 nm. The peaks for **96**, **98** and **47** are also the same as one another at around 600 nm. The gradual blue shift observed for the peak at around 450 nm is not replicated in this part of the spectrum. Instead we see a shift of the peak back and forth as we go through the series. This corresponds to the change between the cyclometalating moieties, with and without the trifluoromethyl group at the 3-phenyl position. It is clear this transition strongly involves the phenyl moiety of the ligand and is largely unaffected by the changes elsewhere in the complex. The shoulder at approximately 750 nm is observed for all the complexes and could be explained as a spin forbidden 3 MLCT transition resulting from spin-orbit coupling.

3.3.2 Cyclic voltammetry

Analysis of the complexes by cyclic voltammetry gave the oxidation and reduction potentials (Table 2). As with the absorption profiles two main effects are observed: firstly an overall gradual change of the oxidation potentials through the series as each ester is replaced by a trifluoromethyl group. We see the difference between **95** and **97** is 0.05 V. The second is the stronger effect of the trifluoromethyl group on the cyclometalating phenyl ring, which we see causes a large change in oxidation potential between **95** and **96** of 0.20 V. This is because the HOMO is based mainly on the metal and phenyl portion of the complex and the oxidation is primarily a metal based process. The reduction potentials follow the same pattern. The difference

between the oxidation and reduction potentials $E^{\text{ox-red}}$ is barely affected by changes to the bipyridyl portion of the ligand, with a change of only 0.02 V between **97** and **46**. The alteration of the phenyl group again gives a more significant change of around 0.10 V. This shows how we can tune the HOMO, the LUMO and the HOMO-LUMO gap.

Table 2: Oxidation and reduction potentials of **95-98** and **46-47**. Recorded in 0.1 M solution of TBAPF₆ in CH₂Cl₂ vs Fc/Fc⁺.

Complex	$E^{\text{ox}}_{1/2}$ (V)	$E^{\text{red}}_{1/2}$ (V)	$E^{\text{ox-red}}$ (V)
95	0.00	-1.92	1.92
96	0.20	-1.83	2.03
97	0.05	-1.87	1.92
98	0.24	-1.76	2.00
46	0.09	-1.85	1.94
47	0.29	-1.74	2.03

3.3.3 X-ray crystallography

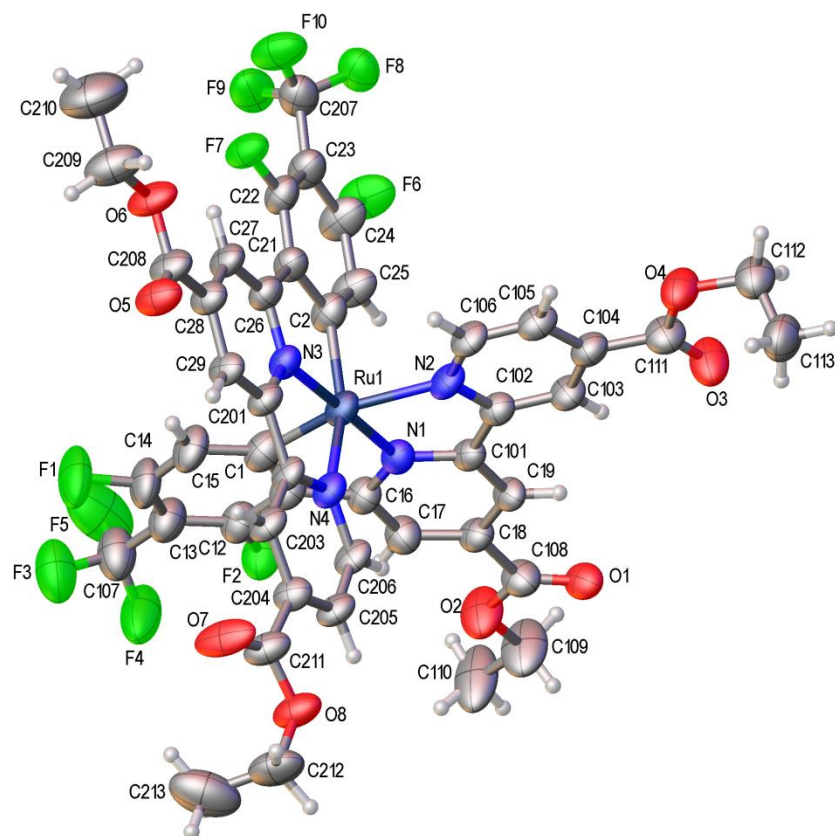


Fig. 33: Ortep of **96** with ellipsoids drawn at the 50 % probability level. The ethyl group C(109)-C(110)/C(09')-C(10') is disordered over two positions with the refined percentage occupancy ratio of 56(2):44(2). A molecule of dichloromethane solvent is present at 20 % occupancy and is disordered over two positions. The minor component of the disordered ethyl group and the solvent have been omitted for clarity.

Single crystals of **95**, **96**, and **98** were obtained by slow diffusion of hexane into a concentrated solution of the complexes in CH_2Cl_2 . The crystals were analysed by x-ray diffraction. In Fig. 33 we see the structure of **96** in detail as an example. The bond lengths and angles around the ruthenium centre are given in tables 3 and 4. The structure is a distorted octahedron with shortening of the central Ru-N(1) and Ru(N3) bonds (1.983 and 1.982 Å respectively) and lengthening of the flanking Ru-N and Ru-C bonds due to the angles C(1)-Ru-N(2), and C(2)-Ru-N(4) (both 157.6 °) which are significantly less than 180 °. This is a consequence of the rigid structure of the ligand. The Ru-C bonds (Ru-C(1), 2.015 and Å, Ru-C(2), 2.020 Å) are shorter than the Ru-N(2) and N(4) bonds (2.139 and 2.109 respectively) in the flanking pyridines due to the strong trans influence of the anionic Ru-C bonds.

Table 3: Bond lengths of the distorted octahedron around the ruthenium centre of **96**.

Bond	Bond length (Å)	Bond	Bond angle (Å)
C(1)-Ru(1)	2.015	N(2)-Ru(1)	2.139
C(2)-Ru(1)	2.020	N(3)-Ru(1)	1.982
N(1)-Ru(1)	1.983	N(4)-Ru(1)	2.109

Table 4: Bond angles of the distorted octahedron around the ruthenium centre of **96**.

Bond	Bond angle (°)	Bond	Bond angle (°)
N(3)-Ru(1)-N(1)	178.7	C(1)-Ru(1)-N(4)	89.0
N(3)-Ru(1)-C(1)	99.0	C(2)-Ru(1)-N(4)	157.6
N(1)-Ru(1)-C(1)	80.1	N(3)-Ru(1)-N(2)	103.3
N(3)-Ru(1)-C(2)	79.6	N(1)-Ru(1)-N(2)	77.6
N(1)-Ru(1)-C(2)	101.5	C(1)-Ru(1)-N(2)	157.6
C(1)-Ru(1)-C(2)	92.9	C(2)-Ru(1)-N(2)	90.0
N(3)-Ru(1)-N(4)	78.1	N(4)-Ru(1)-N(2)	96.8
N(1)-Ru(1)-N(4)	100.9		

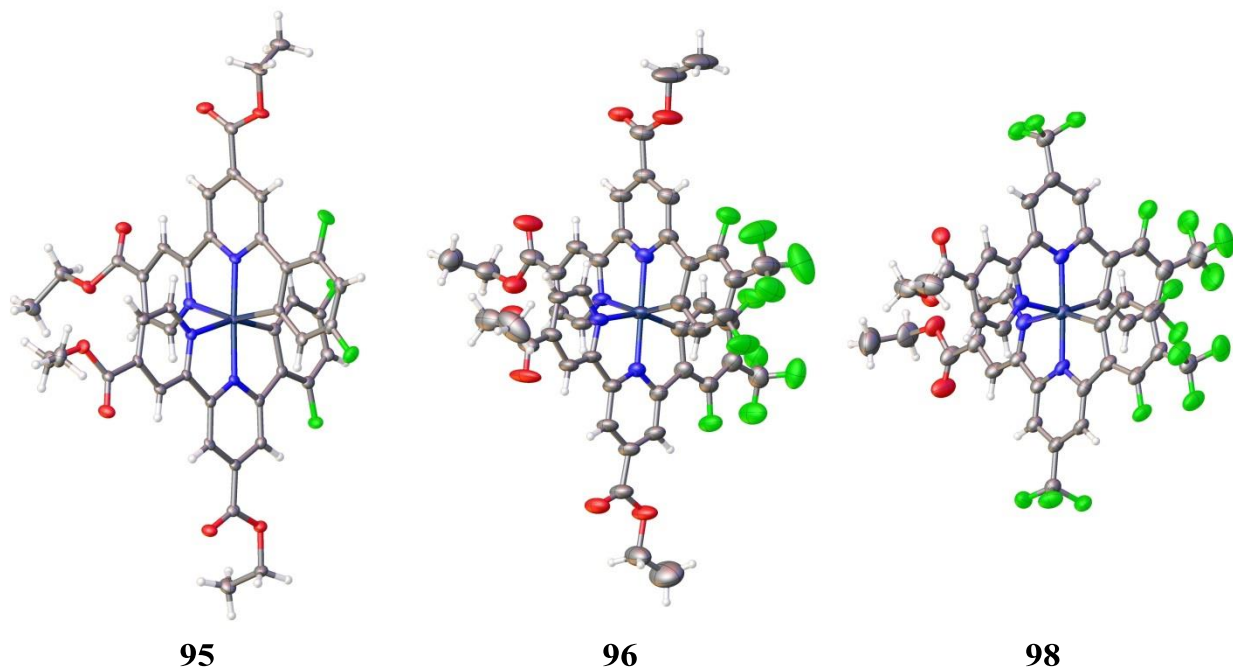


Fig. 34: Ortep diagrams of **95**, **96** and **98** with ellipsoids drawn at the 50 % probability level. Disordered substituents are omitted for clarity.

In Fig. 34 the structures of complexes **95**, **96** and **98** are compared. We see the same general structure for all three. A slightly compressed octahedron where the axial Ru-N(1) and Ru-N(3) are shortened and the remaining Ru bonds are lengthened. In table 5 we see a comparison between similar bonds across the three structures. We see very little variation, the axial Ru-N(1) bond remaining 1.98 Å for all three and variation within a range of only 0.02 Å for the other bonds.

Table 5: Comparison of sample bond lengths for the crystal structures of **95**, **96** and **98**.

Bond	Bond length (Å)		
	95	96	98
C(1)-Ru(1)	2.04	2.02	2.03
N(1)-Ru(1)	1.98	1.98	1.98
N(2)-Ru(1)	2.12	2.14	2.12

3.4 Device Testing

In collaboration with Dr Alessandro Sinopoli at the University of Huddersfield complexes **43** and **45** were tested in DSSCs. The DSSCs were fabricated using **43**, **45** and **N719** as sensitizers, iodine/iodide redox shuttles, and platinum as cathodes. The dye coated film was realised using multi-layered commercial titanium oxide pastes. Platinic FTO glass was used as the counter electrode and a solution LiI 0.1 M and I₂ 0.05M, in acetonitrile/valeronitrile (1:1, v:v) mixture together with 0.6M N-methyl-N-butyl imidazolium (BMII) and 0.5M *tert*butyl pyridine. The cell was thermally sealed before taking measurements. Photovoltaic measurements were performed on AM 1.5 solar simulator (100 mW cm⁻²). The incident light was calibrated by using a Si photodiode reference. The main photovoltaic parameters are listed in Table 6.

Table 6: Device performance data for complexes **43** and **45** in comparison with archetypal dye N719.

Dye	V _{oc} (V)	J _{sc} (mAcm ⁻²)	FF	η (%)
43	0.20	0.35	0.33	0.02
45	0.59	11.2	0.61	4.30
N719	0.63	18.4	0.58	6.84

In a device, complex **45** achieved an efficiency just under two thirds of that obtained with the archetype **N719** (4.30% and 6.84% respectively). Both dyes gave devices with similar V_{oc} but the device with **45** had a lower current density. Complex **45** performed significantly better than **43** which had gave an efficiency of only 0.02%. One possible reason is the decrease in driving force for regeneration of the dye for complex **43** as its di ester analogue **45** has a higher oxidation potential (0.20 Vs 0.24). However the difference in oxidation potentials is slight, whilst the difference in η is relatively large (4.30 Vs 0.02). A contributing factor could be the effect of the orientation of the dye as posited in section 2.

4 Conclusion

In this work we successfully synthesised a new family of phenylbipyridine ligands. An efficient synthetic route to access phenylbipyridines containing an asymmetric bipyridine moiety was developed based on the cross-coupling method by the Fagnou group.

We also developed a new method to access bis-homoleptic terdentate cycloruthenates. This was then used to access the first generation of a novel series of complexes. These complexes displayed excellent absorption characteristics with intense profiles extending above 800 nm. Their oxidation potentials (between 0.00 and 0.29 V Vs Fc/Fc^+) and reduction potentials (between -1.92 and -1.74 V Vs Fc/Fc^+) are suitable for use in DSSCs. Crystal structures were obtained for complexes **95**, **96** and **98** which revealed their distorted octahedral structure.

Preliminary testing of **43** and **45** gave devices which achieved efficiencies of 0.02% and 4.30% respectively.

Chapter 2: The Second Generation; a New Series of Ligands

1 Introduction

In **Chapter 1** we discussed the synthesis and characterisation of the first generation of a new family of cycloruthenated dyes. These dyes have excellent absorption properties, but have oxidation potentials a little too low for optimal performance in device. In order to improve the second generation we return to the literature to investigate some of the different strategies that have been utilised in dye design.

1.1 A cobalt based electrolyte

The iodide/triiodide electrolyte system has been the benchmark for DSSCs giving excellent results with correctly tuned dyes. This however limits the dyes which can be used to those with compatible oxidation and reduction potentials. Furthermore the electrolyte will absorb some light reducing the efficiency of the cell. The electrolyte is also extremely corrosive increasing the cost and complexity of the device.⁹⁹ Several other systems have been tried including bromide/tribromide,¹⁰⁰ thiocyanate/trithiocyanate¹⁰¹ and copper(I/II).¹⁰² One that is particularly of interest is a cobalt(II/III) system. The main advantage of this is (in a similar fashion to ruthenium dyes) the electrolyte can be tuned by judicious choice of ligands and/or ligand substituents to obtain redox potentials suited to a particular dye. The first reported example by the Grätzel group was **100** a cobalt(II) complex.¹⁰³ The standard potential of the bis-homoleptic cobalt complex is +0.36 V Vs NHE which is comparable to that of iodide/triiodide (+0.35 V Vs NHE). Initial testing with **N719** gave poor results, however a device sensitised by **Z316** with **100** as the electrolyte achieved an efficiency of 5.2% (Fig 35). This is attributed to the reduction of the negative charge density on the semiconductor surface for **Z316** compared to **N719**.

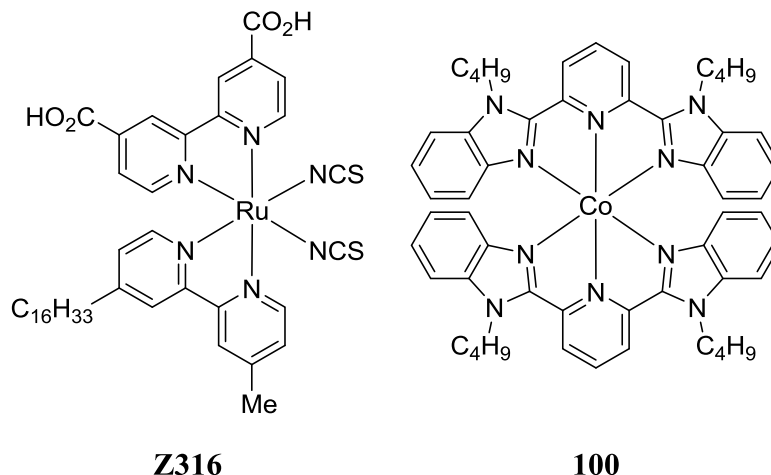


Fig. 35: Cobalt redox mediator **100** and dye **Z316**.

In later work by the Grätzel group a zinc porphyrin dye **YD2-*o*-C8** in a device with cobalt(II) tris(bipyridine) **101** achieved an efficiency of 12.7% (Fig. 36).^{104, 105} In this case the tris-bipyridyl cobalt complex forms part of an optimised electrolyte mixture named **AY1** with a standard potential of +0.54 V Vs NHE (more positive than iodide/triiodide). **YD2-*o*-C8** has an oxidation potential of +0.82 V Vs NHE (less positive than **N719** at +1.1 V Vs NHE). This constitutes a reduction in the driving force of the regeneration of the dye compared to a standard **N719** and iodide/triiodide system. The improved efficiency is in part attributed to long alkyloxy chains reducing the electrolytes proximity to the titania and thus preventing unwanted charge recombination from the conduction band of TiO₂ to the electrolyte.

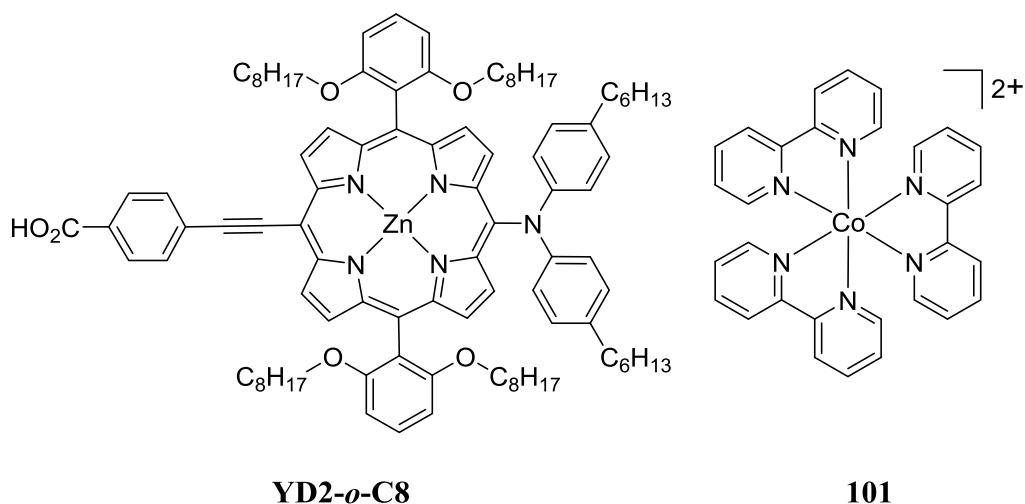


Fig. 36: Cobalt redox mediator **101** and dye **YD2-*o*-C8**.

The Grätzel group were subsequently able to achieve relatively high efficiency for a ruthenium complex with the cobalt mediator **104** (standard potential 0.62 V Vs NHE). Utilizing a 2',6'-dimethoxy-2,3'-bipyridine ligand and its bis(dodecyloxy) analogue in complexes **102** and **103** (Fig. 37) achieving efficiencies of 4.7% and 8.6% respectively.¹⁰⁵ In this example the effect of long alkoxy chains is clearly demonstrated. The two dyes **102** and **103** have virtually identical oxidation and reduction potentials as well as absorption profiles, however the dye with longer dodecyloxy chains **103** performs almost twice as efficiently. Importantly the efficiency for **103** in a device with a cobalt based electrolyte was comparable to that of a device with the standard iodide/triiodide mediator (8.7%).

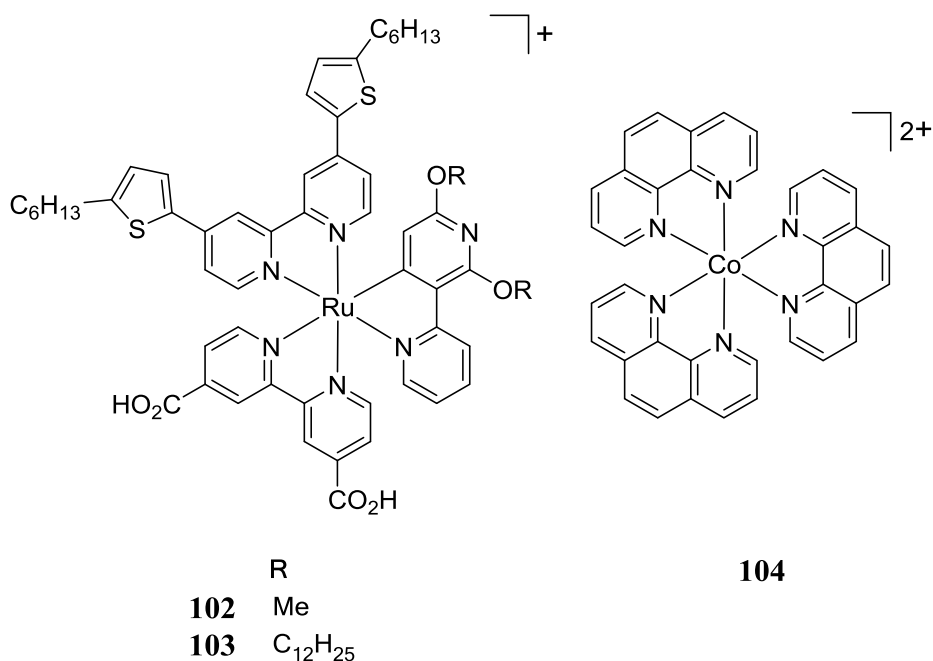


Fig. 37: Cobalt redox mediator **104** and dyes **102** and **103**.

1.2 Addition of thiophene based chromophores

In the introduction to **Chapter 1** we discussed some archetypal dyes, including the panchromatic sensitiser **N749** or black dye. It is an example which has been investigated thoroughly in the literature and many analogous complexes have also been synthesised and characterised. This body of work can help give us an insight into the effect of variations to the ligand structure. In the above examples as well as in **Chapter 1** we have already discussed some dyes with thiophene moieties added to improve dye absorption. Here we examine the effects more closely. The Chou group synthesised and studied complexes **PRT-11-14** (Fig. 38).¹⁰⁶ In Fig. 39 we see

the comparison of the absorption spectra of the complexes compared with **N749**. In **PRT-11** one of the carboxylic acid groups of **N749** is replaced with a proton. In the absorption spectra we see this change results in an overall decrease in the intensity of absorption as the acid groups contribute to the absorption of the complex. A concurrent decrease in oxidation potential leads to a slight decrease in device efficiency (8.0%) compared to **N749** (8.5%). The remainder of the complexes (**PRT-12-14**) display a marked increase in absorption above 350 nm due to the addition of chromophores at the 5'' position of the ligand. This translates to moderate gains in efficiency in device for **PRT-12** (9.1%) and **PRT-13** (10.3%). Conversely for **PRT-14**, despite having the most intense absorption with a very broad intense band between 300 and 550 nm, this trend begins to reverse as the device efficiency was only 8.8%. This is explained in a paper published later by the group. They show the efficiency of injection of electrons for **PRT-14** (72%) is slightly reduced compared to **PRT-12** (85%) and **PRT-13** (78%). The coverage of the titania is also greatly reduced for **PRT-14** ($3.4 \times 10^{-8} \text{ mol cm}^{-2}$) compared to **PRT-12** ($8.5 \times 10^{-8} \text{ mol cm}^{-2}$) and **PRT-13** ($8.1 \times 10^{-8} \text{ mol cm}^{-2}$). These effects are attributed to the bulk of the TPA group.¹⁰⁷

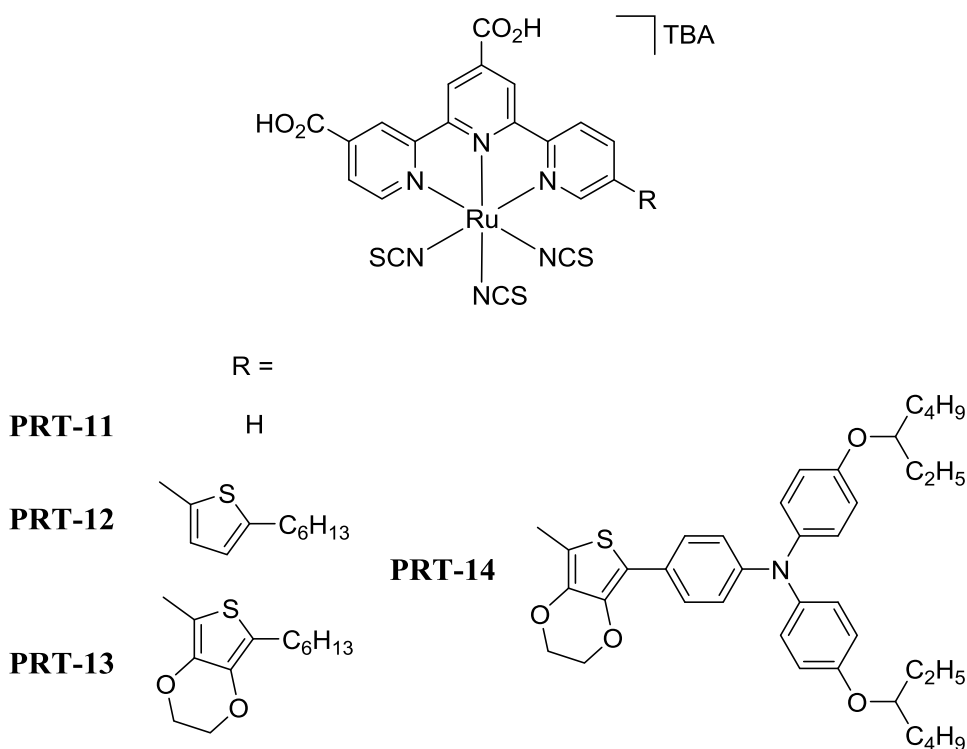


Fig. 38: Black dye derivatives including additional chromophores **PRT-11-15**.

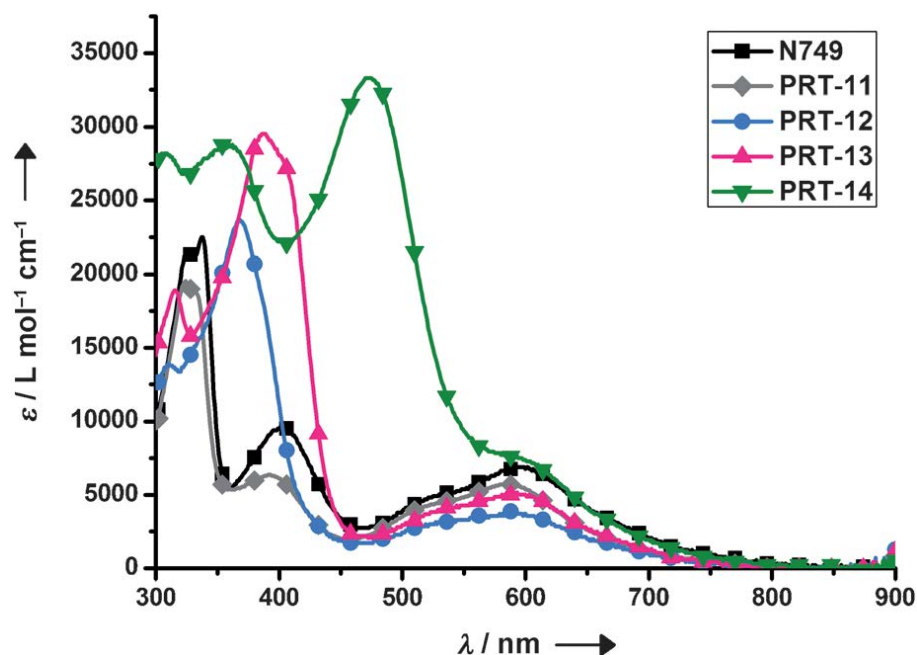


Fig. 39: Absorption spectra of **PRT-11-15** in comparison with **N749** in methanol.¹⁰⁷

The Chou group continued their work on ruthenium dyes for DSSC and later published the series **TF-1-4** (Fig. 40).³¹ Here the thiocyanate groups have been replaced by a bis(pyrazolyl)pyridine ligand. In the absorption spectra (Fig. 41) we see a gain in intensity for **TF-1** at 500 nm and a loss compared to **N749** at 600 nm. Overall the performance is similar in device for **TF-1** (9.1%) and **N749** (9.2%). As with the **PRT** series we see an increase in absorption and accompanying increase in performance for **TF-2-4**. All three have similar efficiencies, 10.5% for **TF-2** and **TF-4**, and 10.7% for **TF-3** again a trade-off between absorption intensity and efficiency of injection due to auxochrome size could be the reason for this trend.

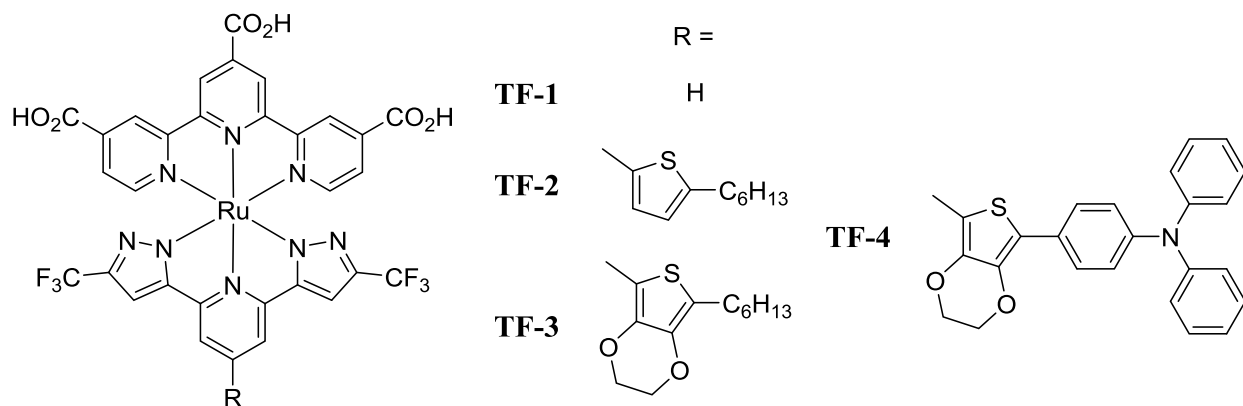


Fig. 40: Dyes containing a bis (pyrazole) pyridine ligand **TF1-4**.

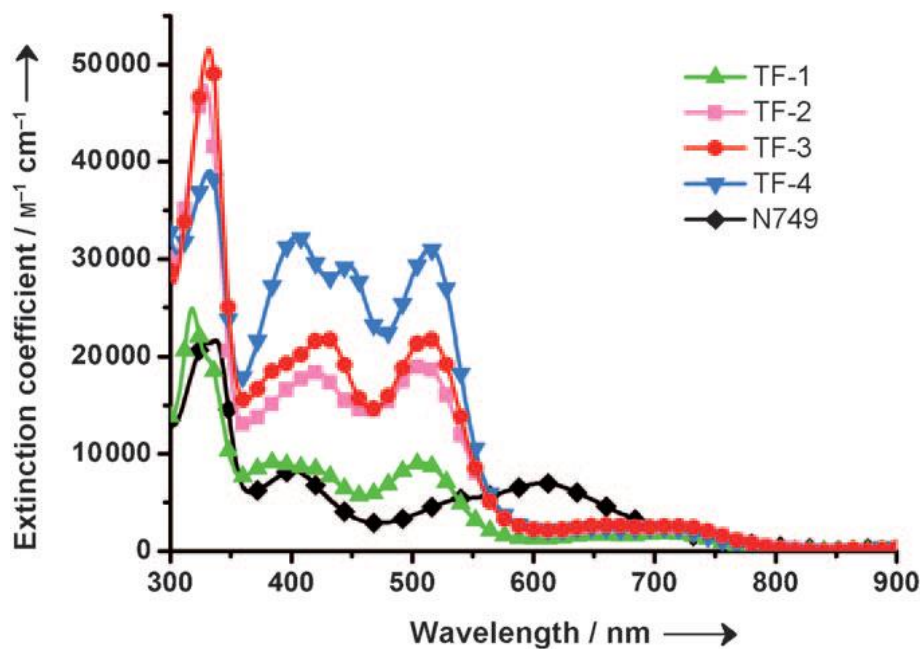


Fig. 41: Absorption spectra of **TF-1-4** in comparison with **N749** in DMF.³¹

1.3 Substitution of pyridine for quinoline

In the below example Onozawa-Komatsuzaki *et al.* investigated the dye **105**. The core aromatic structure of the terpyridyl ligand of **N749** has been extended in order to increase the light harvesting properties of the dye in the form of a bis(quinolyl)pyridine ligand (Fig. 42).^{108, 109}

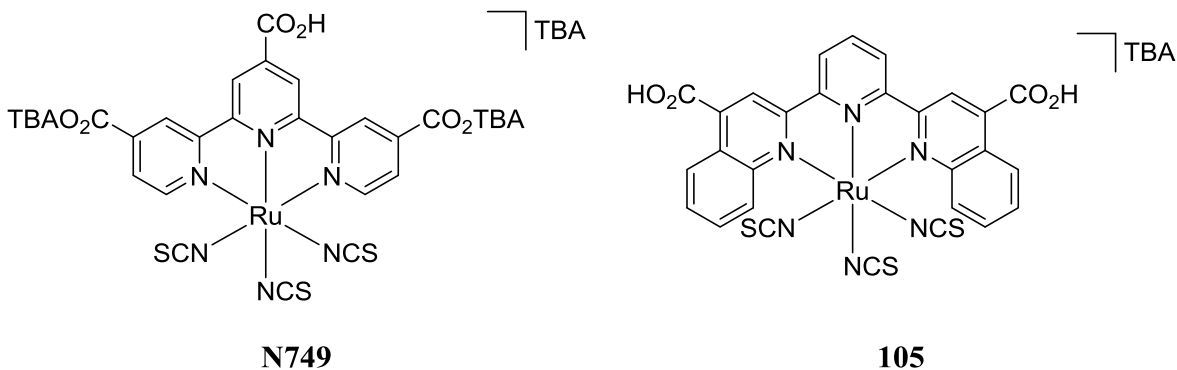


Fig. 42: **N749** (or black dye) and 2,6-di(quinolin-2-yl)pyridine based dye **105**.

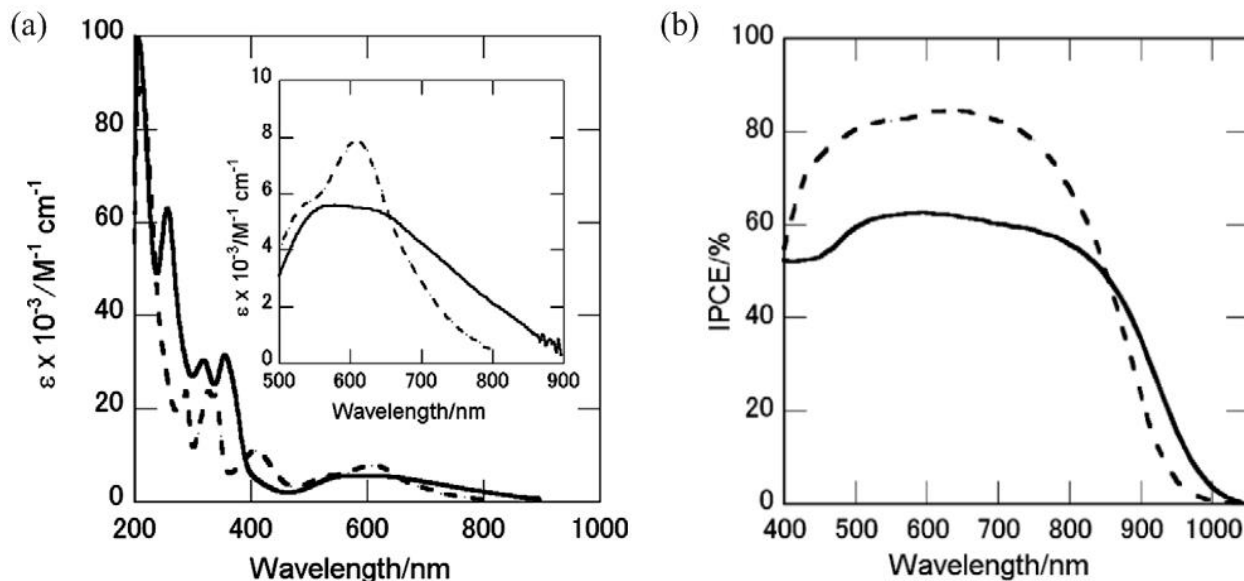


Fig. 43: Comparison of **N749** (dashed line) and **105** solid line. (a) Absorption spectra of **N749** in ethanol and **105** in methanol. (b) Photocurrent action spectra of DSSCs sensitised by **N749** and **105**.¹⁰⁸

In Fig. 43 (a) we see the comparison of the absorption spectra of **N749** and **105**. The changes to the aromatic ligand result in a complex with more intense absorption between 250 and 400 nm and extension of the absorption deep into the infrared region. **N749** absorbs more intensely in the region between 400 and 650 nm. In the photocurrent action spectra for DSSCs sensitised by the two dyes (Fig. 43 (b)) we can see the changes in absorption for **105** have not translated to significant gains in efficiency. **N749** is much more efficient between 400 and 850 nm and **105** is only marginally better above 850 nm than **N749**. The LUMO of **N749** is relatively low for efficient injection of electrons into the conduction band of titania, the stabilisation of the LUMO in **105** results in a further reduction in injection efficiency. Overall the efficiency of a DSSC with **105** is only 3.0% compared with 6.3% for the same device with **N749**.

The Chou group have investigated a large series of efficient dyes based on **TF-1** a complex with the same terpyridyl ligand as black dye but where the thiocyanate ligands have been replaced with a 2,6-bis(5-pyrazolyl)pyridine ligand. **TF-30-33** are a series of derivatives of **TF1** where a terminal pyridine of the terpyridyl ligand has been replaced by a quinoline coordinated at the 8-position creating a ligand with a markedly altered bite-angle and extended aromatic system.⁹⁸

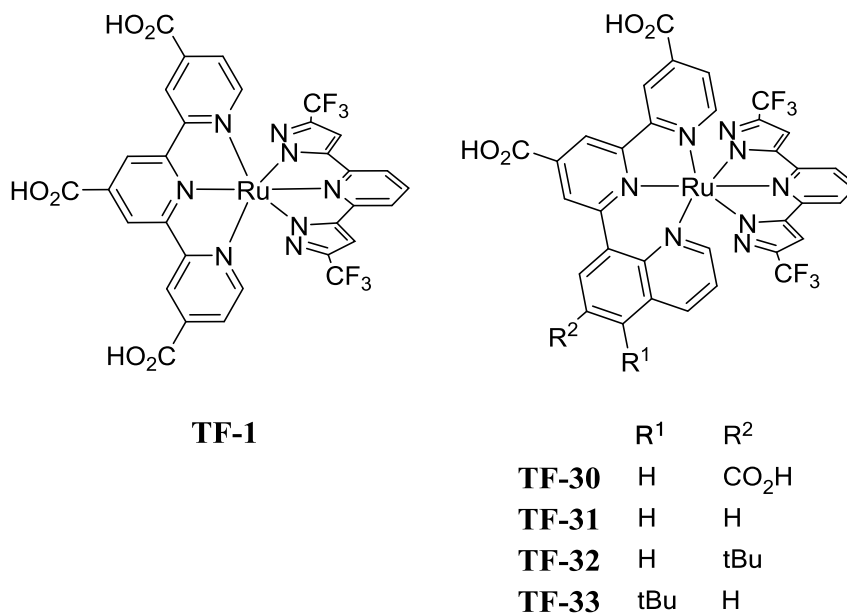


Fig. 44: 2,6-(5-pyrazolyl)pyridine complexes **TF-1** and **TF-30-33**.

In Fig. 45 we see the comparison of **N749** (black dye), **TF-1** and **TF-30-33**. The substitution of the bis-pyrazolylpyridine ligand for the thiocyanate ligands in the case of **TF-1** compared to **N749** causes an increase in the absorption between 375 and 550 nm but there is a concurrent reduction in absorption between 550 and 700 nm. In the case of **TF-30-33** the quinoline containing dyes all have broadly similar absorption profiles with comparable absorption intensity to **TF-1** at lower wavelengths and increased absorption compared to **TF-1** at longer wavelengths. As in the case of **105** the quinoline moiety stabilises the LUMO due to the extension of the aromatic core and we see a reduction in device efficiency for **TF-30** (8.2%) and **TF-31** (8.8%) compared to devices with **TF-1** (9.2%) and **N749** (9.2%). However in **TF-32** and **TF-33** the *t*-butyl group counters this effect, giving improved performances in device of 10.2% and 10.0% respectively.

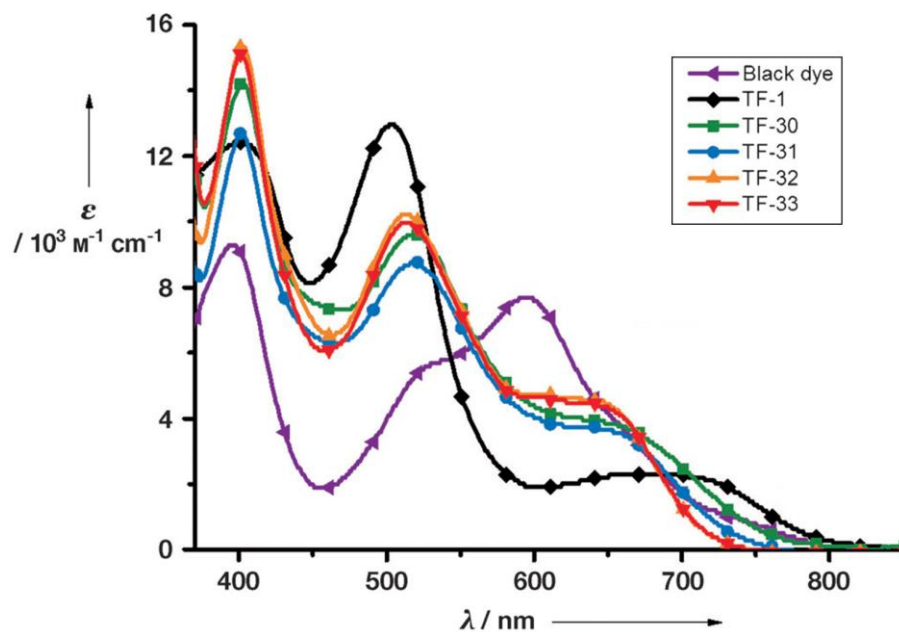


Fig. 45: Absorption spectra of complexes TF-1 and TF-30-33 in comparison to N749 (black dye).⁹⁸

2 Aims

In the first part of this work we accessed a series of complexes with very broad and intense absorption profiles and with redox properties suitable for use in DSSC. In the next stage in our work we were interested in expanding this new family of complexes by altering the ligand in various ways to adjust these interesting properties possibly leading to better dyes for use in photovoltaic devices.

To improve upon the first generation of complexes, we would ideally increase the breadth and intensity of absorption as well as the oxidation potential. In the initial results however we see a trade-off between the two properties. In order to address the issue of oxidation potential whilst maintaining the absorption properties we devised two main strategies. The first was to adjust the dye for compatibility with a cobalt redox mediator. With a correctly tuned mediator even dyes with relatively low oxidation states can achieve high efficiencies in device. This would require the addition of electron donating alkyl or alkoxy chains to the ligand which could potentially lower the oxidation state even further. This would also therefore require adjustments to increase the electron withdrawing nature of the ligand to counteract this effect. The second strategy was to increase the absorption of the ligand by the addition of thiophene chromophores with pendant

alkyl chains. Again these would have to be introduced to the ligand in a fashion that did not compromise the oxidation potential of the complex.

Having developed an effective synthetic strategy to access the first generation of bis-homoleptic, terdentate cycloruthenates; we centred our strategy for improvement on the same basic structure (Fig. 46). The ligand is divided into three main areas: the terminal *N*-coordinating moiety (**A**), the central *N*-coordinating moiety (**B**) and the terminal cyclometalated moiety (**C**).

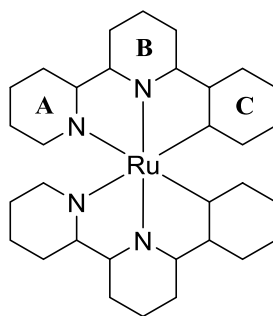


Fig. 46: General design of the bis-homoleptic, terdentate, cycloruthenated dyes.

The possibility of variation at these three positions gives rise to many possible developments based on results from the first series and the literature. In this work we investigated several different avenues involving variation at each position.

3 Results and Discussion

3.1 Variation of the cyclometalating moiety C

In the first generation of dyes the addition of a trifluoromethyl group to the cyclometalating phenyl portion of the ligand caused the greatest change to the oxidation potential and the breadth of the absorption profile. We were interested therefore in introducing heteroatoms into the cyclometalating ring, and the effect this would have. The ligand 2',6'-dimethoxy-2,3'-bipyridine has been shown to be an effective cyclometalating ligand with interesting properties for DSSC.¹⁰⁵ In particular it and its bis(dodecyloxy) derivative showed excellent performance in a device with a cobalt redox mediator. We were interested in exploring the terpyridine analogues as well as the even more electron withdrawing pyrimidylbipyridine ligand giving us preliminary targets **106-107** (Fig. 47).

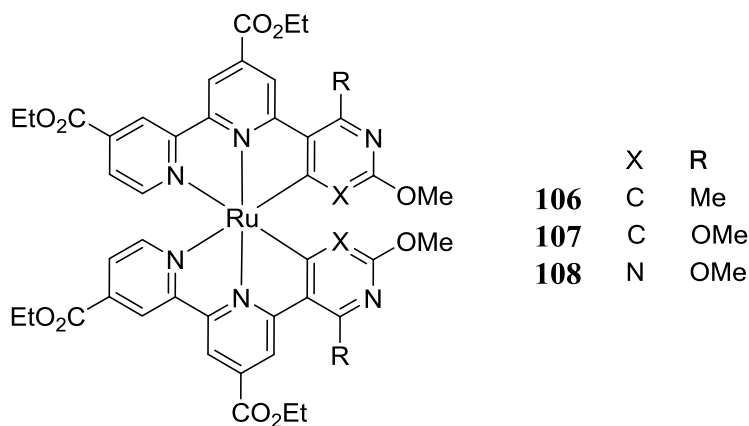
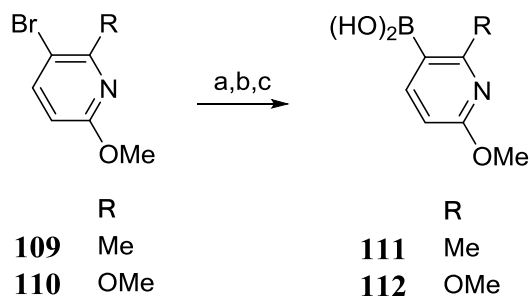


Fig. 47: Second generation targets with heterocyclic cyclometalating moieties: **106-108**

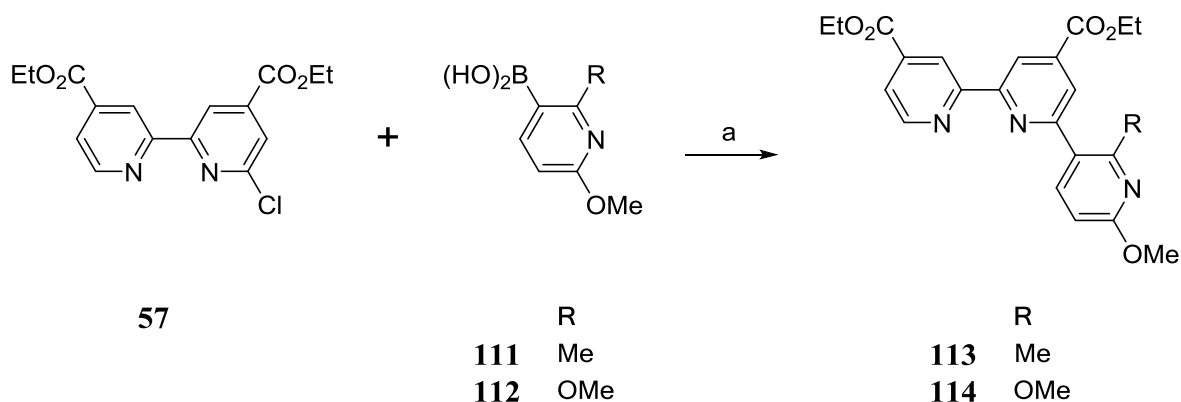
3.1.1 Synthesis of the terpyridine ligands

In order to access the two desired terpyridine ligands we were able to use the same procedures as for the ligands **58** and **61** in **Chapter 1** section 3.1.1. Our first steps would be synthesis of the desired boronic acids, followed by Suzuki coupling to the bipyridyl chloride **57**. Boronic acids **109** and **110** were obtained by reaction of the relevant bromide with *n*butyllithium and trimethylborate (Scheme 48). The crude products were carried forward.



Scheme 48: Synthesis of **111** and **112**. Reaction conditions: (a) *n*BuLi, THF, -78 °C 1 h, (b) B(OMe)₃, -78 °C → 20 °C 16 h, (c) HCl, 1h.

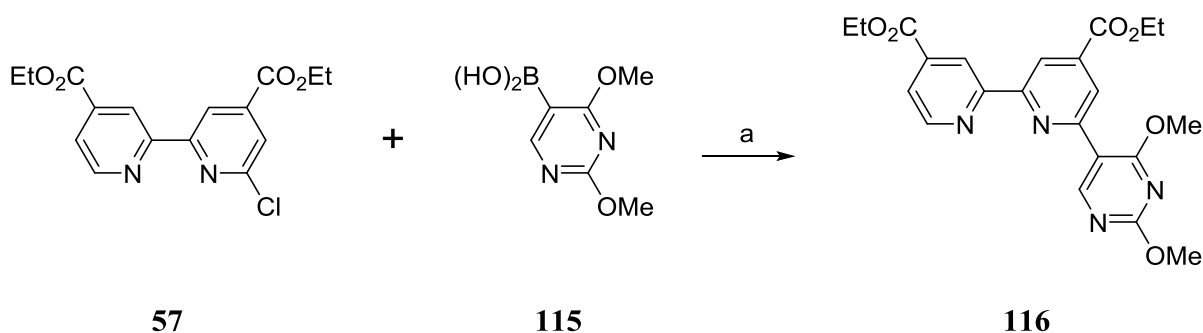
Terpyridines **113** and **114** were then accessed *via* Suzuki coupling of chloride **57** with the boronic acids **111** and **112** in good yields (Scheme 49).



Scheme 49: Suzuki coupling. Reaction conditions: (a) Pd(PPh₃)₄, Na₂CO₃, THF, H₂O, 70 °C, 20 h. **113**, 86%, **114** 85%.

3.1.2 Synthesis of the pyrimidylbipyridine ligand

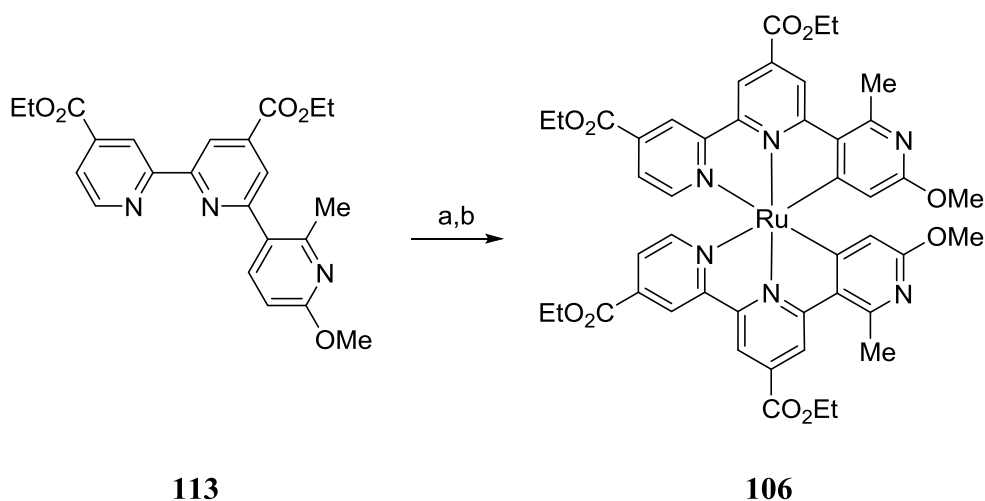
For the synthesis of pyrimidylbipyridine **116** the boronic acid **115** was purchased commercially. The synthesis was first attempted in dioxane/H₂O and with potassium carbonate as the base (Scheme 50) as this method had been successfully used for another ligand using the same boronic acid **115**. However a yield of only 9% was obtained. The majority of the product appeared to have reacted further to make a compound far more polar and with a mass of 28 g mol⁻¹ less than the target, possibly due to loss of two methyl groups and the addition of two protons. The Suzuki coupling method used for the phenylbipyridine ligands with THF/H₂O and sodium carbonate gave a much improved 66% yield. Possibly the more polar dioxane favoured the de-etherification reaction.



Scheme 50: Synthesis of pyrimidylbipyridine **116**. Reaction conditions: Method 1 (a) Pd(PPh₃)₄, K₂CO₃, 1,4-dioxane:H₂O 2:1, 80 °C, 16 h, 9%. Method 2(a) Pd(PPh₃)₄, Na₂CO₃, THF:H₂O 5:1, 70 °C, 16 h, 66%.

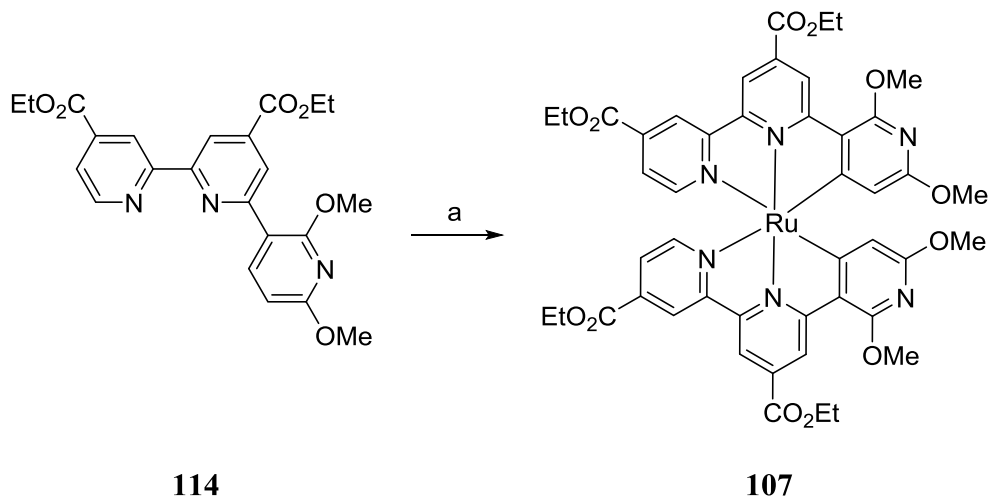
3.1.3 Synthesis of the complexes

Synthesis of the ruthenium complex **106** was attempted using the method that had been successful for the first generation of complexes (Scheme 51). Only trace amounts of product were observed. It appears that the oxidation potential is very low. Attempts to purify on silica also led to protonation of the product which could not be removed from the silica.



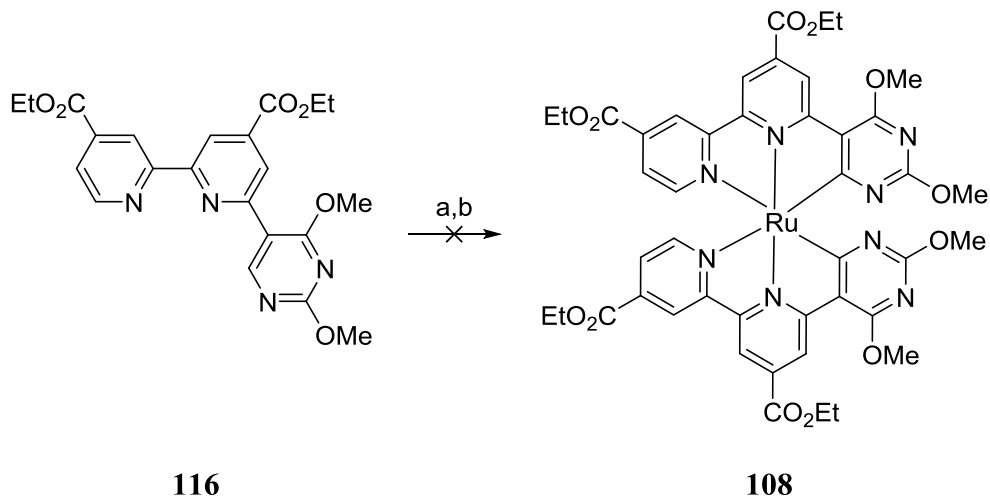
Scheme 51: Synthesis of **106**. Reaction conditions: (a) [Ru(*p*-Cymene)Cl₂]₂, *N*-ethylmorpholine *n*PrCN, 120 °C, 16 h. (b) Ethylene glycol, 200 °C, 2h, trace.

We anticipated that the oxidation potential of **107** would be higher than **106** and should therefore be more easily isolable. As we had had some success with a new method of synthesis using a microwave reactor (see **Chapter 3** section **3.1** for details of the development) this method was attempted. The purification was performed on neutral alumina and we were able to access complex **107** in 14% yield.



Scheme 52: Synthesis of **107**. Reaction conditions: (a) $[\text{Ru}(p\text{-Cymene})\text{Cl}_2]_2$, *N*-ethylmorpholine, EtOH, 150 °C, μwave , 16 h, 14%.

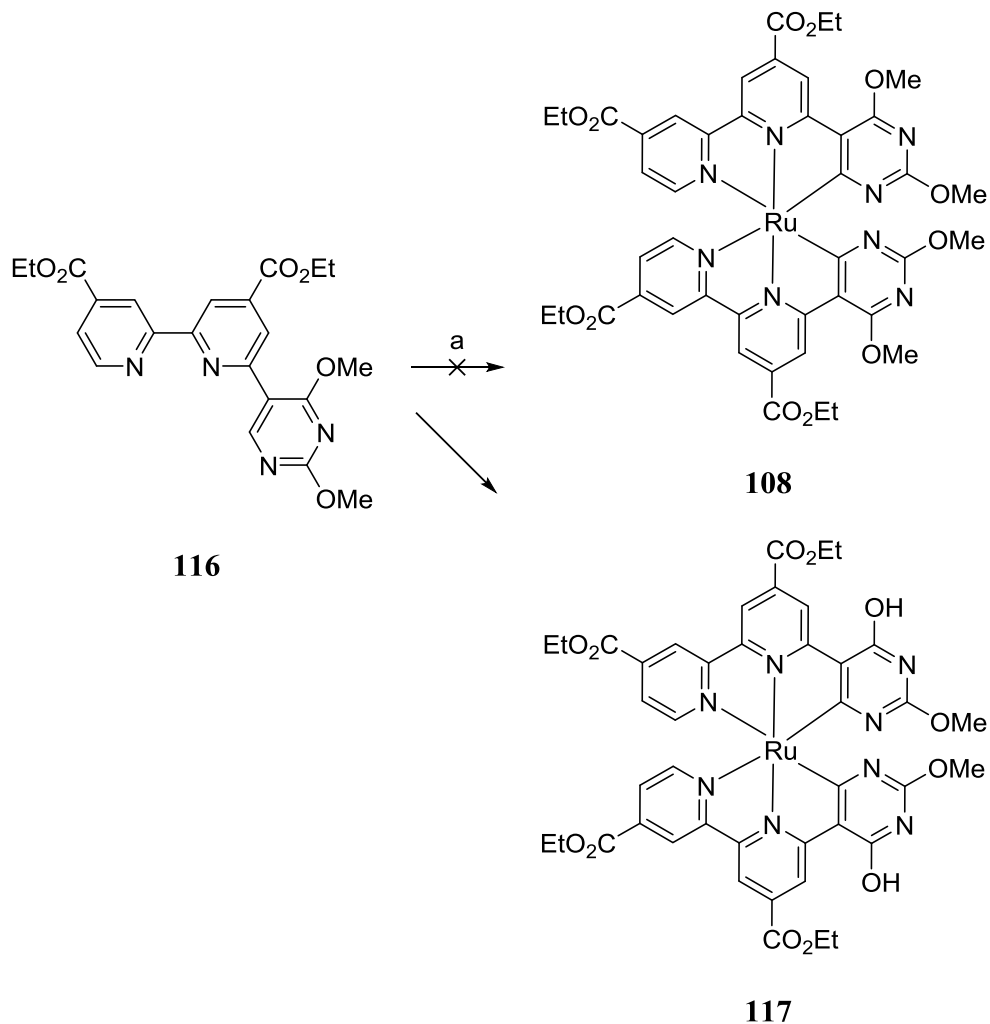
The pyrimidylbipyridine ligand was reacted with the ruthenium dimer in butyronitrile followed by ethylene glycol. Again this did not provide the product but a mixture of transesterified and demethylated versions of both the mono and bis-cyclometalated complexes were identified by mass spectrometry.



Scheme 53: Synthesis of **108**. Reaction conditions: (a) $[\text{Ru}(p\text{-Cymene})\text{Cl}_2]_2$, *N*-ethylmorpholine *n*PrCN, 120 °C, 16 h. (b) Ethylene glycol, 200 °C, 2h.

Synthesis of **108** was also attempted using the microwave method, however the desired product was not observed. Instead complex **117** was isolated, the result of a double demethylation. We hypothesise that the pyrimidyl nitrogen situated between the two methoxy groups is very readily

protonated. As the proton is held adjacent to the methoxy groups this lowers the activation energy for the ether cleavage a similar effect to that observed when synthesising the ligand in dioxane.



Scheme 54: Synthesis of **117**. Reaction conditions: (a) $[\text{Ru}(p\text{-Cymene})\text{Cl}_2]_2$, *N*-ethylmorpholine, EtOH, 150 °C, μwave , 16 h, 15%.

3.1.4 Characterisation of the complexes **107** and **117**

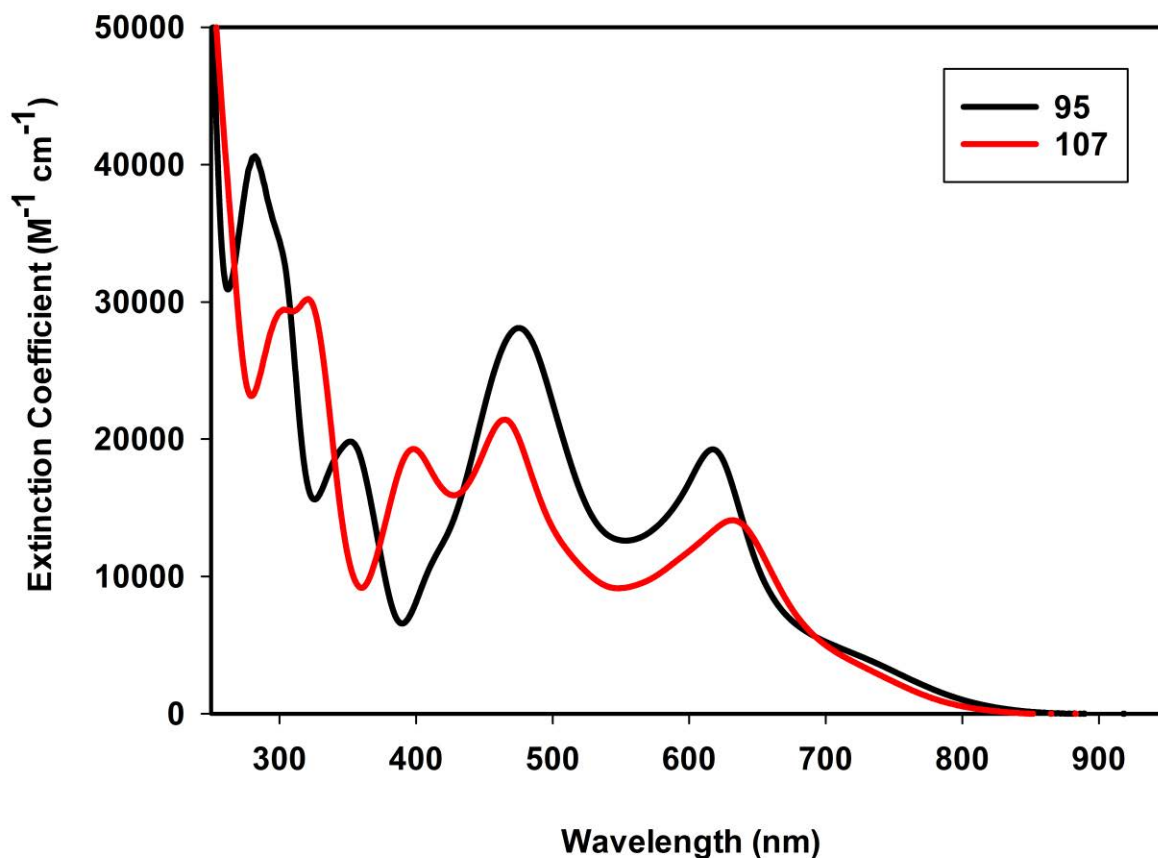


Fig. 48: Absorption spectra of **107** vs **95** in CH_2Cl_2 .

In Fig. 48 we see the absorption profiles of dye **107** in contrast with **95** the broadest and most intense absorber from the first generation of complexes. We can see that the profiles are similar although **107** has consistently lower intensity of absorption across the spectrum. The peaks which correspond to the ligand centred transitions are shifted significantly toward the red whilst the MLCT peaks are only slightly changed. The peak between 450 and 500 nm is slightly blue shifted for **107** whereas the peak at 617 nm for **95** is marginally red shifted to 633 nm for **107**.

Table 7: Oxidation and reduction potentials of **107** and **95**. Recorded in 0.1 M solution of TBAPF_6 in CH_2Cl_2 vs Fc/Fc^+ .

Complex	$E^{\text{ox}}_{1/2}$ (V)	$E^{\text{red}}_{1/2}$ (V)	$E^{\text{ox-red}}$ (V)
95	0.00	-1.92	1.92
107	-0.06	-1.93	1.87

The oxidation and reduction potentials of **107** and **95** are shown in Table 7. We can see the slight red shift of the absorption corresponds to a slight decrease in oxidation potential. The reduction potential remains almost the same and therefore the $E^{\text{ox-red}}$ is slightly reduced.

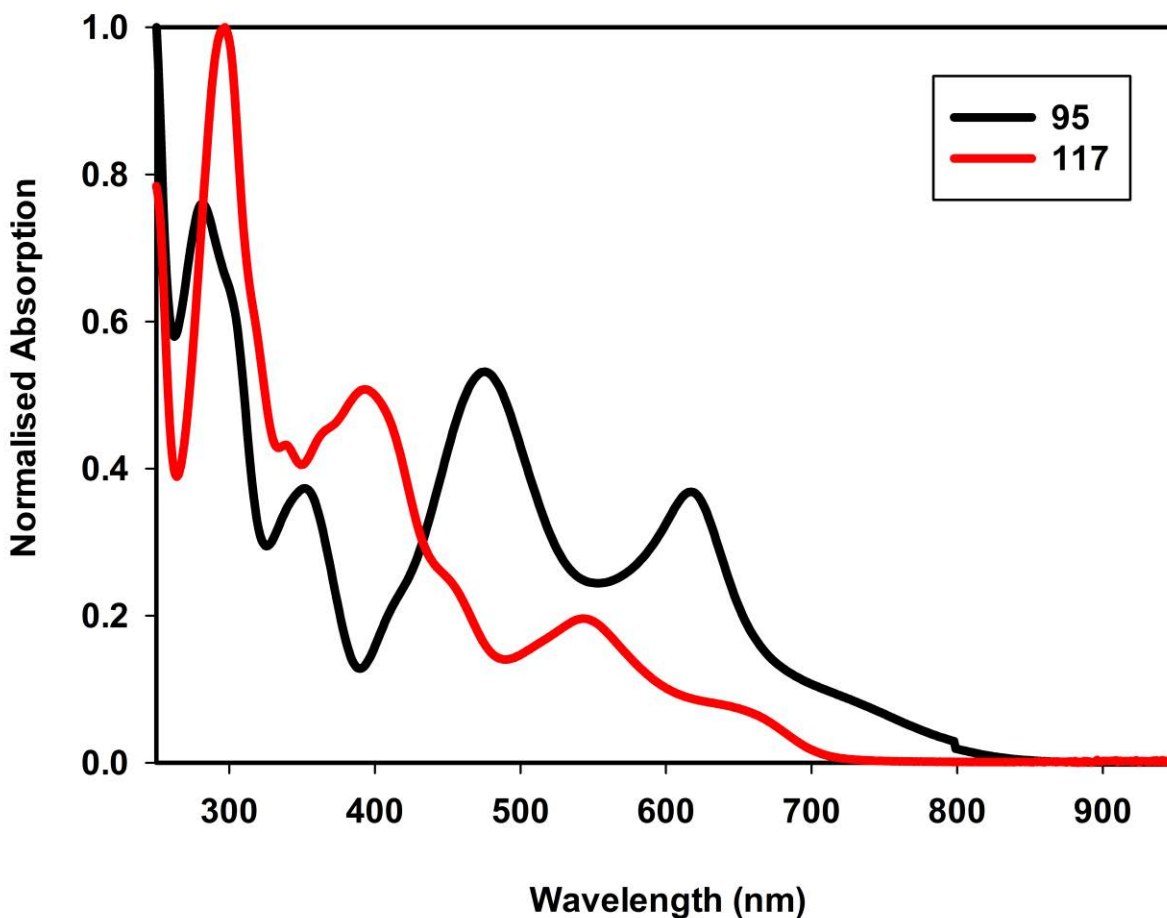


Fig. 49: Normalised absorption spectra of **117** vs **95** in CH_2Cl_2 .

In Fig. 49 the absorption profile of **117** is compared with **95**. We can see that the exchange of the 2,4-difluorophenyl moiety for 2-hydroxy-4-methoxypyrimidine has had a significant effect on the absorption profile of the dye. The ligand centred transitions are much more intense and the MLCT bands are reduced in intensity relative to each other. Moreover the MLCT bands are considerably blue-shifted with the onset of absorption reduced from 850 to 750 nm. Although we anticipate the oxidation potential of this dye to be increased, there is a simultaneous decrease in both breadth and intensity of absorption at longer wavelengths.

3.2 Variation at the 4-pyridyl position B

In **Chapter 1**, Section 2 we hypothesised that complexes with only two coordinating carboxylate groups might be more efficient compared to those with four, due to the orientation of the dye when adsorbed onto titania, indeed comparison of the performance of complexes **43** and **45** in device showed the diacid dye performed significantly better than the tetra acid dye. Analysis of complexes **96** and **98** by UV-Vis spectroscopy showed that replacing an ester with a trifluoromethyl group at the 4-pyridyl position leads to a decrease in the absorption intensity in the MLCT region. To investigate this effect we were interested in replacing the trifluoromethyl group with other moieties which will also not bind to titania but extend the conjugation of the ligand as the ester/acid does. The two functional groups we considered were acetyl, and cyano, which are less and more electron withdrawing than a trifluoromethyl group respectively. We had developed a method for the synthesis of such phenylbipyridines containing asymmetrical bipyridine moieties. This investigation would allow us to test the scope of the method with differently functionalised pyridine starting materials. If successful it would also be possible to attach electron donating substituents at the 4-pyridyl position via a ketone functional group to avoid compromising the oxidation potential. This would allow the addition of longer alkyl chains (for compatibility with cobalt redox mediators) or chromophores (to increase the absorption of the dye). This gave us two initial targets; complex **118** and **119** (Fig. 50).

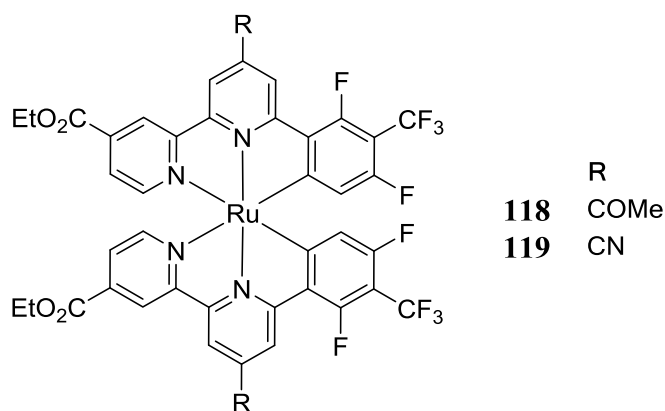
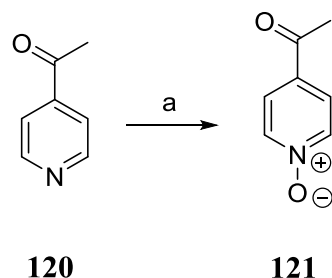


Fig. 50: Second generation targets varied at the 4-pyridyl position: **118** and **119**.

3.2.1 A ligand containing a 4-Acetylpyridyl moiety

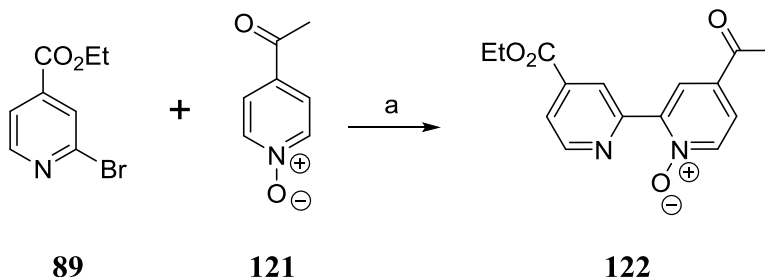
Having developed the synthesis outlined in 3.1.3 where the ethoxycarbonyl group was replaced with a trifluoromethyl group, we aimed to expand this method to other functional groups. Using

the same methodology we first focused on the acetyl analogue. *N*-Oxide **121** was synthesised by oxidation with *m*CPBA in CH₂Cl₂. The crude oxide was carried forward (Scheme 55).



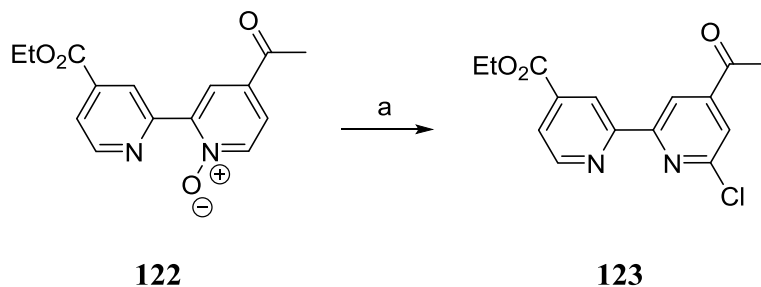
Scheme 55: Synthesis of *N*-oxide **121**. Reaction conditions: (a) *m*CPBA, CH₂Cl₂ 30 °C, 16 h.

121 was then coupled with bromide **89** to furnish the bipyridine oxide **122** (Scheme 56). The sensitivity of this product to light on silica was even more pronounced than that of **121** and the crude was therefore carried forward with minimal purification.



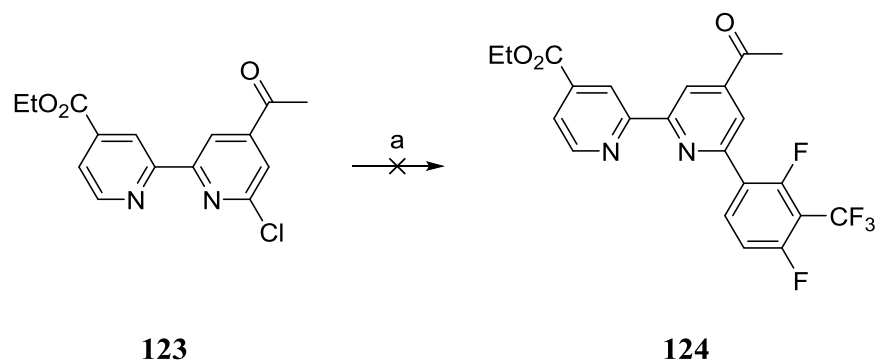
Scheme 56: Synthesis of oxide **122**. Reaction conditions: (a) Pd(OAc)₂, P^tBu₃-HBF₄, K₂PO₃, PhMe, 110 °C, 16 h. 63%.

122 underwent chlorination to provide **123** in the very low yield of 1.6% over two steps (Scheme 57). This is again possibly due to the sensitivity of the bipyridyl-*N*-oxide to the harsh conditions of the chlorination process, as well as the reactivity of the acetyl group in palladium catalysed reactions.



Scheme 57: Synthesis of chloride **123**. Reaction conditions: (a) POCl_3 , 120°C , 2 h. 1.6% over two steps.

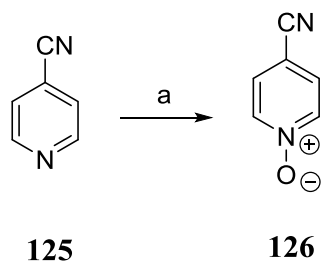
Synthesis of the phenylpyridine was attempted using the standard Suzuki coupling technique however no product was obtained. This is possibly due to the reactivity of the acetyl group to palladium catalysed cross-coupling reactions.



Scheme 58: Synthesis of phenylbipyridine **124**. Reaction conditions: (a) **123**, $\text{Pd}(\text{PPh}_3)_4$, Na_2CO_3 , THF, H_2O , 5:1, 70°C , 16 h.

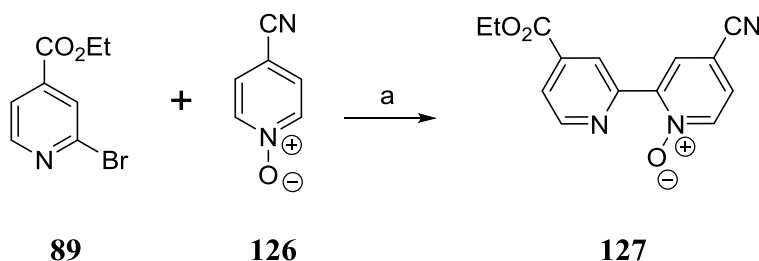
3.2.2 A ligand containing a 4-Cyanopyridyl moiety

The second target in this series was the ligand containing a 4-cyanopyridyl moiety. Synthesis of oxide **126** was achieved by oxidation with *m*CPBA in CH_2Cl_2 with 69% yield (Scheme 59).



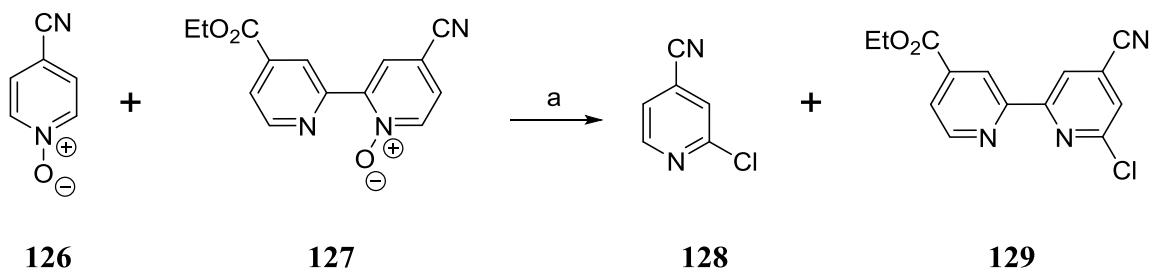
Scheme 59: Synthesis of oxide **126**. Reaction conditions: (a) *m*CPBA, CH_2Cl_2 , rt, 16 h.

Synthesis of bipyridyl-*N*-oxide **127** was achieved by the palladium catalysed cross-coupling reaction of bromide **89** and *N*-oxide **126** (Scheme 60).



Scheme 60: Synthesis of oxide **127**. Reaction conditions: (a) Pd(OAc)₂, P^tBu₃-HBF₄, K₂PO₃, PhMe, 110 °C, 16 h. 63%.

The crude product was obtained by filtration over celite followed by aqueous work-up. The resultant oxide **127** was extremely sensitive to light when absorbed on silica, rapidly turning yellow. Chlorination of the crude mixture of oxides **126** and **127** was performed using the previously described method with POCl₃ (Scheme 61), however separation of the desired chloride **129** and the side product **128** by column chromatography proved unsuccessful.

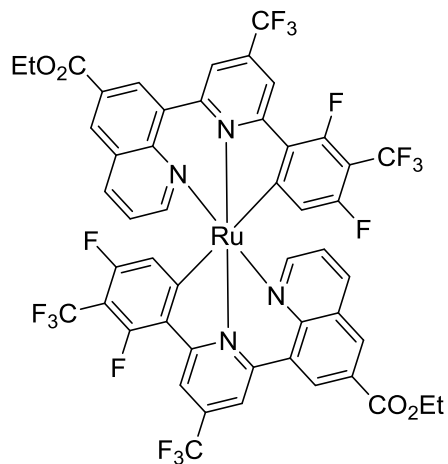


Scheme 61: Synthesis of chloride **129**. Reaction conditions: (a) POCl₃, 120 °C, 2 h.

Ligand **131** was obtained by reaction of the crude mixture of pyridyl chloride **128** and bipyridyl chloride **129** with phenyl boronic acid **60**. The phenylpyridine and phenylbipyridine products proved readily separable by column chromatography on silica.

3.3 Variation of the terminal pyridyl moiety A

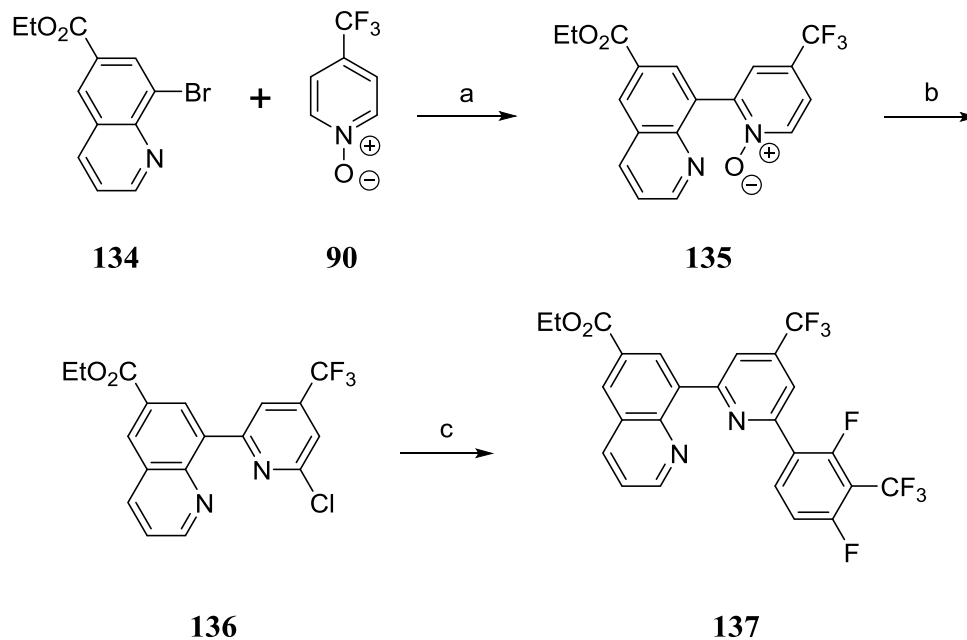
With the method developed by Campeau *et al.* and our work in **Chapter 1** we should be able to couple a variety of halides at the 2-pyridyl position.⁹⁵ We anticipated that coupling of a pyridyl-*N*-oxide with an 8-bromoquinoline would give the relevant precursor to access a (phenylpyridyl)quinoline ligand. This would provide an extended aromatic system for enhanced absorption and a more electron withdrawing ligand to raise the oxidation potential of the complex. The bite angle would also be decreased with respect to that of the phenylbipyridine complexes, causing a more elongated octahedral shape, and possible destabilisation of the HOMO and a resulting red-shift in absorption. The increase in oxidation potential may also allow for the addition of electron donating chromophores and/or long alkyl chains in future work based on this design. From this we developed the target **133** (Fig. 51).



133

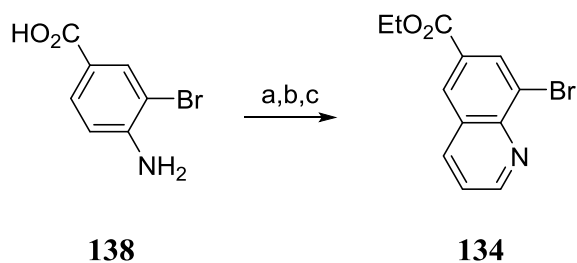
Fig. 51: Second generation target **133** with a quinolyl moiety.

In order to investigate a ligand with a different bite angle and an extended aromatic core we aimed to synthesise ligand **137**. To access the target ligand we planned to use the method which had allowed us to synthesise asymmetric bipyridines in **Chapter 1** section 3.1.3 (Scheme 64).



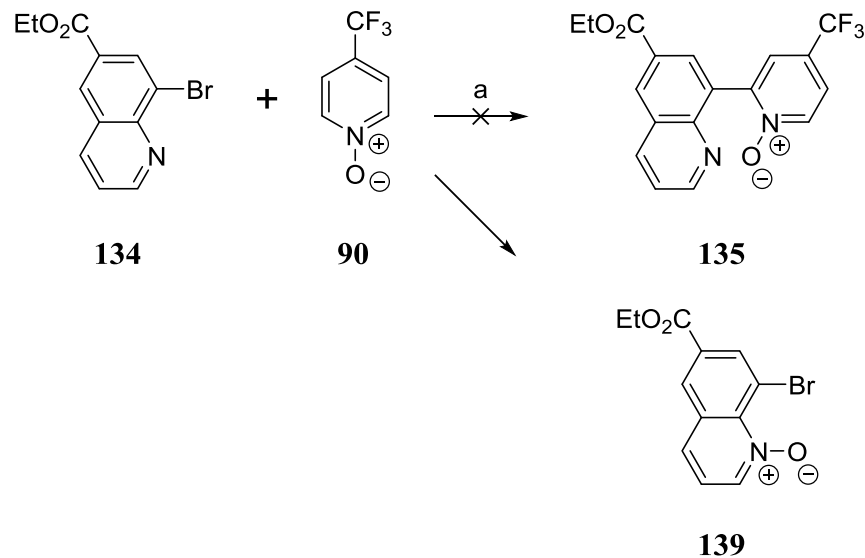
Scheme 64: Synthetic route to ligand **137**. Reaction conditions: (a) Pd(OAc)₂, P^tBu₃-HBF₄, K₂PO₃, PhMe; (b) POCl₃; (d) Pd(PPh₃)₄, Na₂CO₃, THF, H₂O.

Quinoline **134** was successfully accessed in 42% yield from amine **138**, an improvement on the literature yield of 37%.⁹⁸



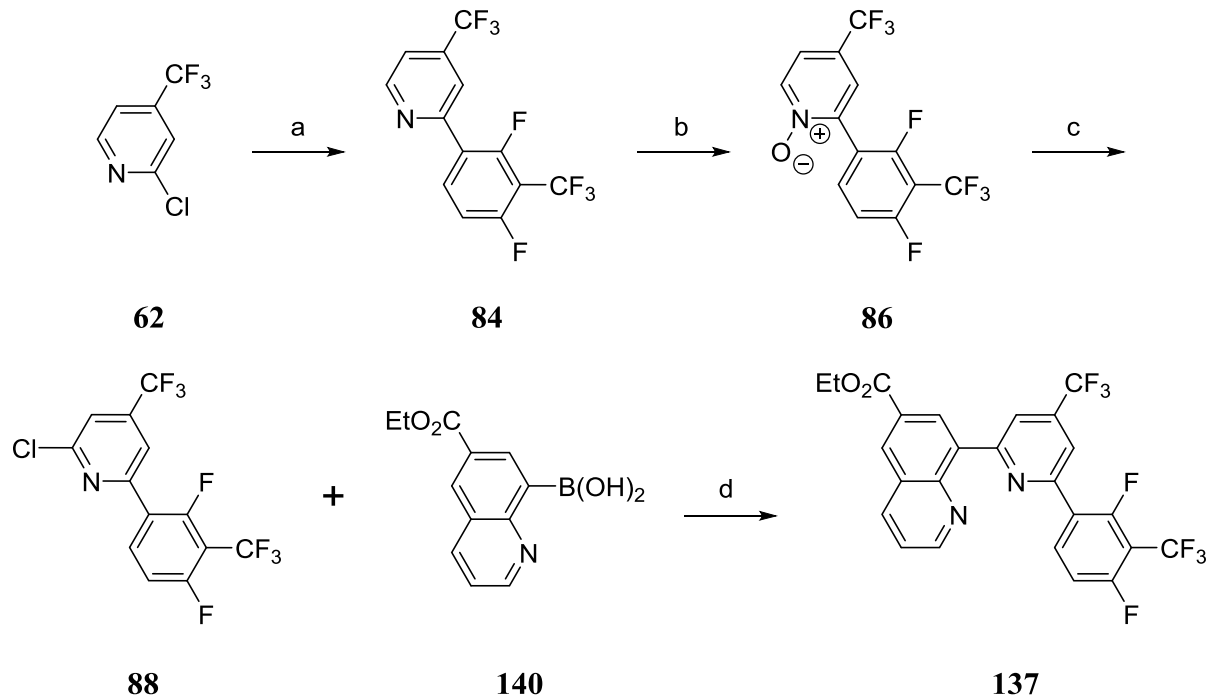
Scheme 65: Synthesis of **134**. Reaction conditions: (a) sodium *m*-nitrobenzene sulfonate, glycerol, H₂SO₄ 100 °C, 3 h (b) 140 °C 4 h, (c) EtOH, 60 °C 12h, 42%

Synthesis of **135** was attempted by the palladium catalysed cross-coupling reaction of bromide **134** and *N*-oxide **90** (Scheme 66). However the majority of the quinoline starting material was converted into the quinolyl-*N*-oxide.



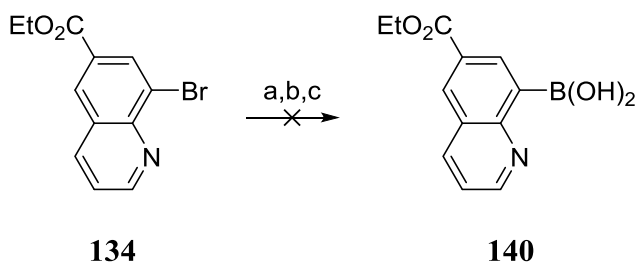
Scheme 66: Synthesis of oxide **139**. Reaction conditions: (a) Pd(OAc)₂, P^tBu₃-HBF₄, K₂PO₃, PhMe, 110 °C, 16 h. 63%.

As we could not use the method which had allowed us to synthesise asymmetric bipyridines in **Chapter 1**, we decided instead to proceed by the route outlined in Scheme 67. Here we would synthesise the quinoline-8-boronic acid **140** and couple it to the 2-chloro-6-(2-(trifluoromethyl)-5-(2,4,6-trifluorophenyl)pyridin-3-yl)pyridine **88**.



Scheme 67: Second synthetic route to ligand **137**. Reaction conditions: (a) Pd(PPh₃)₄, Na₂CO₃, THF, H₂O; (b) mCPBA, CH₂Cl₂; (c) POCl₃; (d) Pd(PPh₃)₄, Na₂CO₃, THF, H₂O.

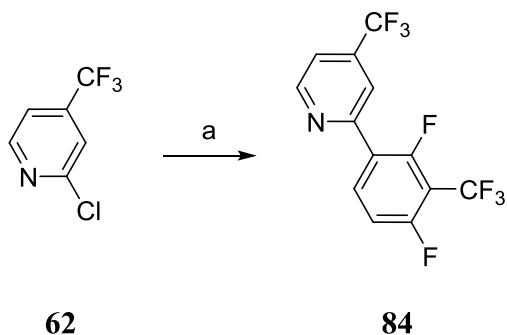
Synthesis of **140** was attempted by formation of a Grignard followed by quenching with trimethylborate (Scheme 68), using a method designed to react with an aryl halide preferentially in the presence of an ester. Isopropyl magnesium chloride was first reacted with Bis[2-(*N,N*-dimethylamino)ethyl] ether to form a complex which would prevent reaction of the magnesium with the ester moiety. After the Grignard was formed the reaction was quenched with trimethyl borate. It seems that this step was not successful. The reaction was repeated allowing a longer time for the boronate to react however only the starting material was recovered.



Scheme 68: Synthesis of boronic acid **140**. Reaction conditions: (a) *i*PrMgCl, Bis[2-(*N,N*-dimethylamino)ethyl] ether, THF, 15 °C 30 min; (b) B(OMe)₃ 0-20 °C, 1 h (c) 0.1 M HCl, rt, 1h.

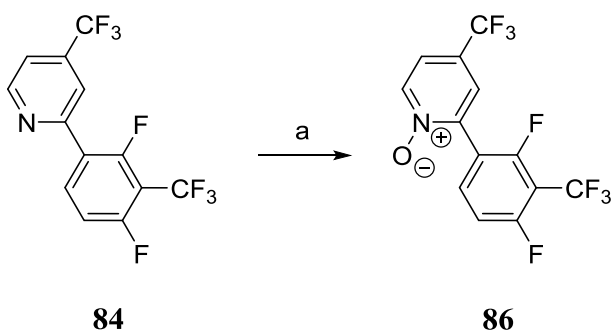
As we had no success with the above strategies we turned to the classic Stille coupling method used by Chou *et al.* in the synthesis of their quinolylbipyridine ligand.¹¹⁰

Phenylpyridine **84** was synthesised in the same manner as previously described by the reaction of boronic acid **66** and Chloride **62**.



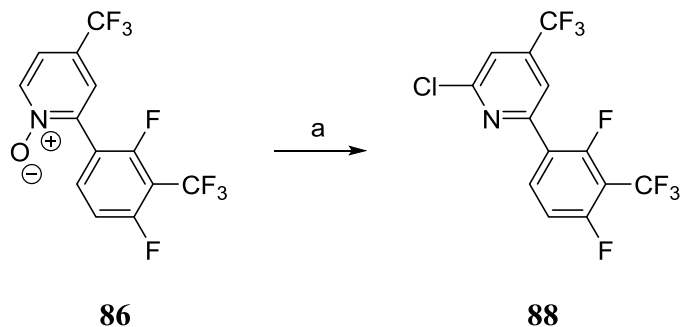
Scheme 71: Suzuki coupling. Reaction conditions: (a) **60**, Pd(PPh₃)₄, Na₂CO₃, THF/H₂O 5:1, 70 °C, 21 h, 62%.

N-oxide **86** was accessed *via* oxidation of **84** with *m*CPBA. Initially the reaction was attempted using a method proven successful for bipyridines, at room temperature in CH₂Cl₂ for 16 h. However analysis of the reaction by TLC showed the majority of the starting material remaining. This is possibly due to deactivation by the strongly electron withdrawing groups as well as a slower reaction rate than a bipyridine due to half the number of reaction sites. Steric hindrance by the phenyl moiety could also be a factor. The solvent was removed and the reaction mixture combined with CHCl₃ and heated to 50 °C for 16 h, giving yield of 73%.



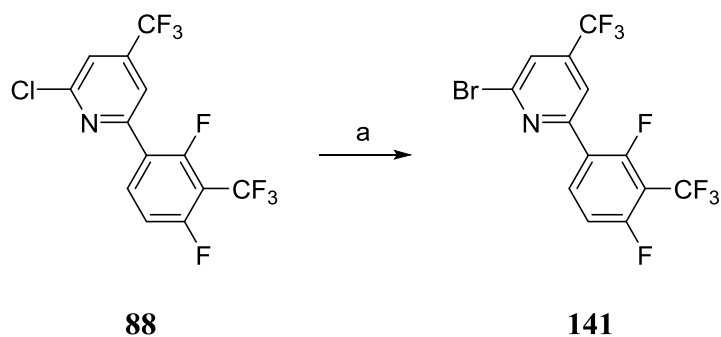
Scheme 72: Synthesis of *N*-oxide **86**. Reaction conditions: (a) *m*CPBA, CHCl₃, 50 °C, 16 h, 73%.

The *N*-oxide **86** was subsequently chlorinated by reaction with POCl₃ (Scheme 73).



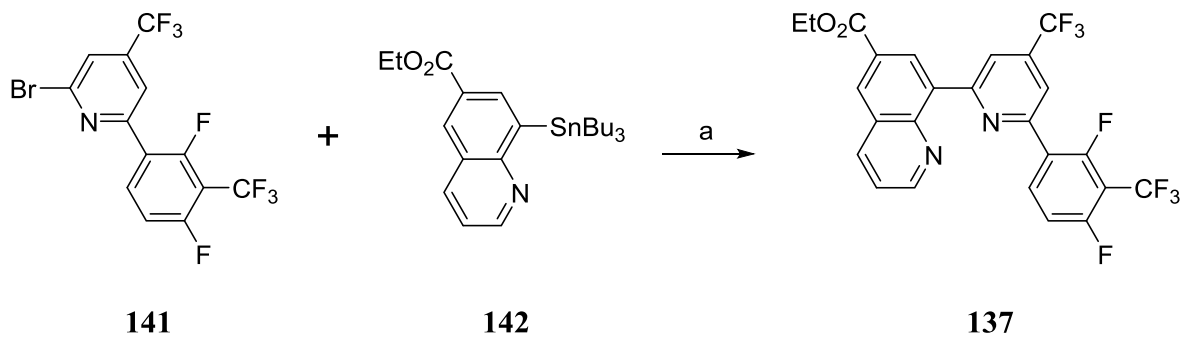
Scheme 73: Synthesis of chloride **88**. Reaction conditions: (a) POCl₃, 120 °C, 1.5 h, 35% over two steps

Bromination by reaction with bromotrimethylsilane followed (Scheme 74). The solvent was removed under reduced pressure after reflux and the crude carried forward.



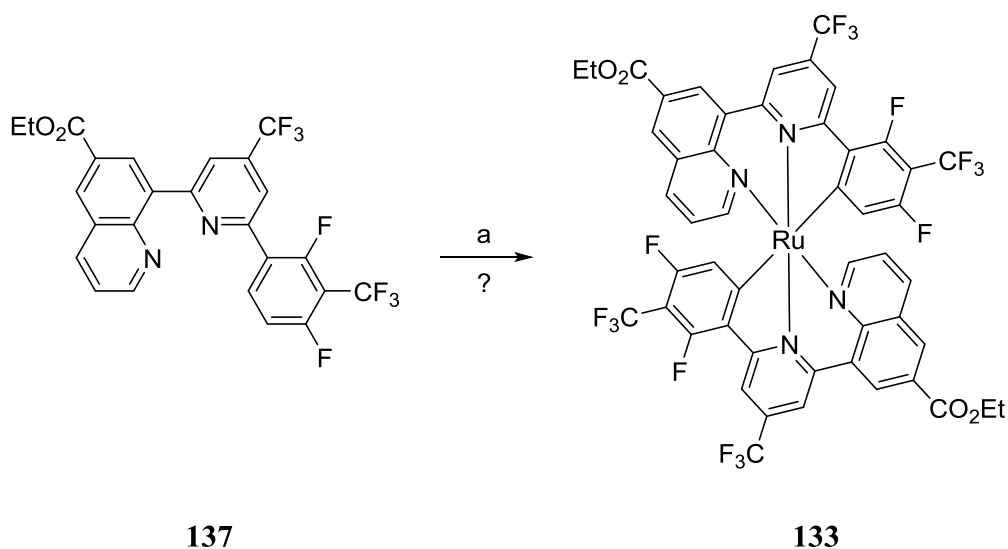
Scheme 74: Synthesis of bromide **141**. Reaction conditions: (a) BrSiMe₃, *i*PrCN, 80 °C, 100 h.

The stannane **142** underwent a Stille cross-coupling with bromide **141** to give ligand **137**. The yield was extremely poor, only 13%.



Scheme 75: Synthesis of ligand **137**. Reaction conditions: (a) Pd(PPh₃)₂Cl₂, DMF, 110 °C, 24 h, 13%.

The ligand **137** was reacted with the ruthenium dimer using the method developed in **Chapter 1**. A mixture of complexes was produced with most of the ligand unreacted. The products were separated by preparative TLC, however sub-milligram quantities were obtained. The main black fraction was analysed by ^1H NMR and mass but no signal was observed in ^1H NMR and the mass data indicated several complexes including a signal corresponding to the desired product.



Scheme 76: Synthesis of complex **133**. Reaction conditions: (a) $[\text{Ru}(\text{p-cymene})\text{Cl}_2]_2$, *N*-ethylmorpholine, *n*PrCN, 120°C 20 h, (b) Ethylene glycol 200°C , 2h.

The product was analysed by UV-Vis absorption spectroscopy. Fig. 52 (a) shows the normalised absorption spectra compared with **95**. We can see a broad absorption profile between 400 nm and 900 nm which extends further into the IR than **95**. The MLCT region of **133** is significantly less intensely absorbing than the bands below 400 nm. For **95** they are comparable. In Fig. 52 (b) we can see the absorption spectra of literature complex **105** compared to black dye. Complex **105** has a similarly broad MLCT region extending above 900 nm but with a low intensity of absorption.

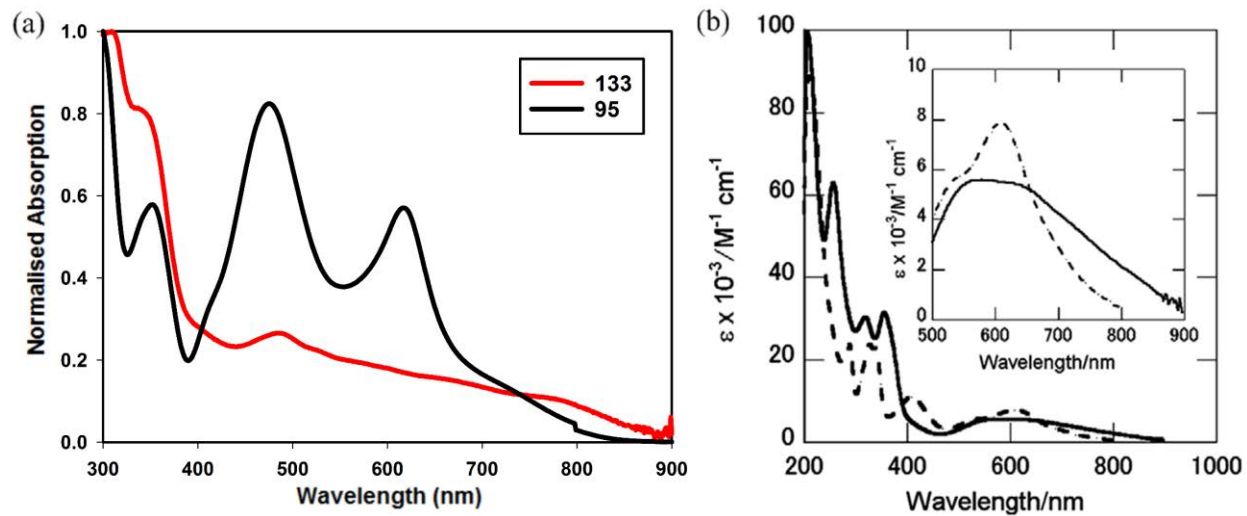


Fig. 52: (a) UV-Vis absorption spectra of complexes **133** and **95** in CH_2Cl_2 , (b) UV-Vis absorption spectra of **105** (solid line) in methanol Vs **N749** (dashed line) in ethanol.¹⁰⁸

4 Conclusion

A series of investigations were undertaken to access a second generation of bis-homoleptic terdentate cycloruthenated complexes, with enhanced properties for DSSC. We demonstrated the synthetic methods previously used could be expanded to access 2,2',6,3'' terpyridines as well as pyrimidylbipyridines. These ligands were used to access a new series of ruthenium complexes. Complex **107** had a broad absorption profile similar to its first generation analogues with intense absorption extending to the near-IR. The oxidation potential was slightly lower than the first generation complexes (-0.06 V vs Fc/Fc⁺). Complex **117** had a blueshifted absorption due to the strongly electron withdrawing pyrimidyl based ligand.

Attempts were made to investigate the effects of different substituents at the 4-pyridyl position of phenylbipyridine ligands. Target ligand **124** could not be accessed with the methodology which was developed in **Chapter 1** however novel 4-cyanopyridyl compound **131** was obtained. This ligand proved unsuited to cyclometalation with ruthenium.

A novel quinolyphenylpyridine ligand **137** was synthesised. The methods used in **Chapter 1** could not be applied to this problem, and a method based on the Stille cross-coupling reaction was used. Initial attempts to synthesise a bis-homoleptic cycloruthenate with this ligand were only partially successful. Traces of the complex **133** were identified by mass spectrometry. Analysis by UV-Vis absorption spectroscopy indicates a broadly absorbing complex was produced.

Chapter 3: Bis-terdentate Cyclometalates of Group 8 and 9

1 Introduction

In **Chapters 1** and **2** we have discussed at length the properties of ruthenium terdentate cyclometalates and their application as dyes for DSSC. Cycloruthenates have also been widely investigated in other areas such as molecular electronics, catalysis and medicinal chemistry. Indeed various cyclometalates from all the first three rows of groups 8 and 9 are reported in the literature. Here we discuss a few examples of terdentate cyclometalates and their potential applications.

1.1 Terdentate cycloosmates

1.1.1 Optoelectronic properties

As with ruthenium the main focus of the attention cycloosmates have received is due to their redox and absorption properties. Bimetallic complexes of ruthenium and osmium have been investigated for molecular electronics as building blocks for molecular wires. In a work by Nagashima *et al.* terdentate cyclometalated complexes of osmium were compared to their ruthenium analogues.¹¹¹

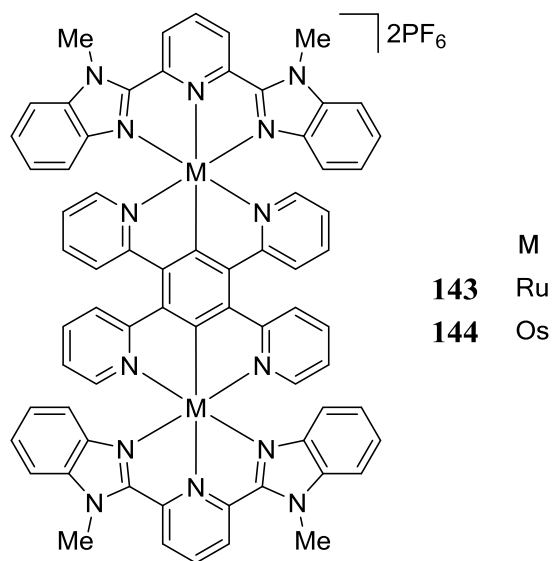


Fig. 53: Bimetallic, terdentate cyclometalated molecular wires of ruthenium and osmium **143** and **144**.

Fig. 53 shows an example pair **143** and **144**. The redox chemistry and the absorption profiles of the two complexes are compared in Table 8. The oxidation and reduction potentials are comparable to ruthenium but lower. The absorption data shows the profile for the osmium complex is less intense but significantly broader with the longest wavelength peaks for **143** and **144** at 856 and 992 nm respectively.

Table 8: Oxidation and reduction potentials of **143** and **144** vs Fc/Fc⁺ and absorption maxima. All data recorded in 0.1 M solution of TBAPF₆ in MeCN.¹¹¹

Complex	M ^{II} -M ^{II} /M ^{III} -M ^{II} (V)	E ^{red} _{1/2} (V)	λ _{max} /nm (ε/10 ³ M ⁻¹ cm ⁻¹)
143	-0.40	-1.82	308 (76.4), 318 (92.8), 351 (47.4), 388 (24.6), 408 (26.2), 484 (29.1), 527 (25.2), 616 (18.2), 688 (17.4), 856 (10.4)
144	-0.53	-1.76	303 (57.9), 335 (33.4), 349 (39.6), 409 (15.0), 492 (24.4), 574 (14.6), 720(10.7), 992 (3.5)

In a similar work by Shao *et al.* a series of monometallic cycloosmates was compared to their ruthenium analogues.¹¹² Again similar results were obtained slightly reduced oxidation potentials

and broadened absorption profiles. In Fig. 54 and Table 9 an example of the data is given for complexes **145** and **146**.

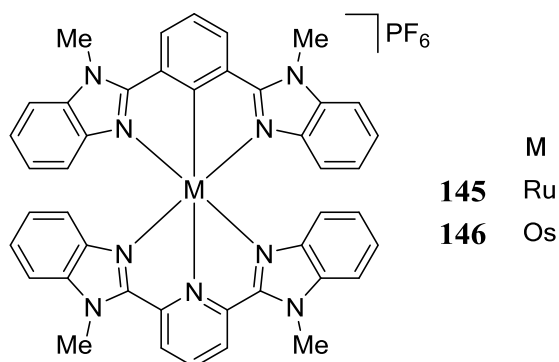


Fig. 54: Terdentate cyclometalated complexes of ruthenium and osmium **145** and **146**.

Table 9: Oxidation and reduction potentials of **145** and **146** vs Fc/Fc⁺ and absorption maxima. All data recorded in MeCN.¹¹²

Complex	$E^{\text{ox}}_{1/2}$ (V)	$E^{\text{red}}_{1/2}$ (V)	$\lambda_{\text{max}}/\text{nm}$ ($\epsilon/10^3 \text{ M}^{-1} \text{ cm}^{-1}$)
145	-0.19	-2.05	334 (32), 353 (27), 515 (13), 571 (7.7)
146	-0.41	-2.08	354 (23), 510 (16), 590 (5.7)

The absorption data of the cyclometalates were also compared to their non-cyclometalated analogues (Fig. 55). Here we can see the cyclometalated complexes have a broader absorption in the region between 300 and 600 nm and the profiles extend further into the near-IR than their non-cyclometalated counterparts.

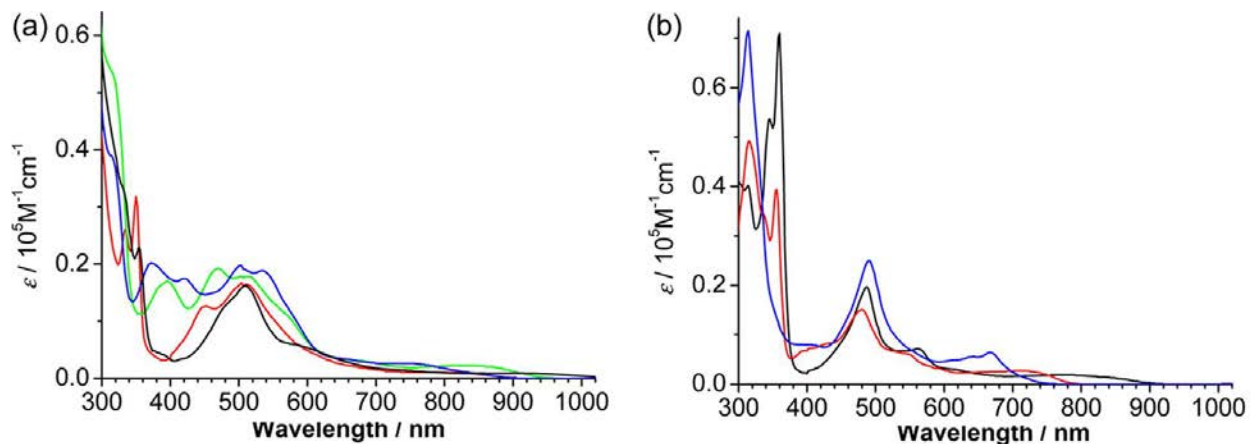


Fig. 55: Absorption profiles (a) a series of cyclometalated osmium complexes (b) their non-cyclometalated analogues. Recorded in MeCN.¹¹²

1.1.2 Terdentate cycloosmates for cancer therapies

Terdentate cycloosmates have also been investigated for their cancer cell cytotoxicity properties.

In a study by Boff *et al.* a series of cycloosmates was synthesised and tested.³⁷

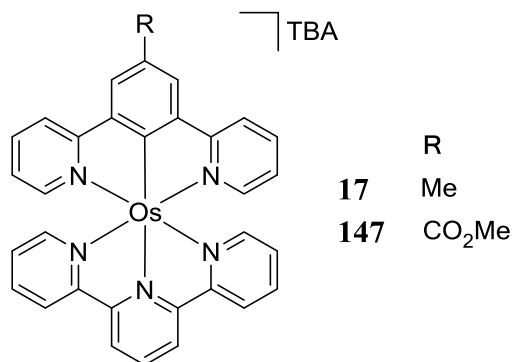


Fig. 56: Terdentate cycloosmates with excellent cytotoxic properties **17** and **147**.

The bis-terdentate complexes **17** and **147** (Fig. 56) showed the highest activities with IC₅₀ values an order of magnitude better than cis-platin. This excellent activity is attributed to the high lipophilicity (Log(*P*_{o/w})) of the complexes allowing a high level of cell uptake as well as an E^{ox}_{1/2} suited to the generation of radical oxygen species (Table 10).

Table 10: IC₅₀ values, for **17**, **147** and *cis*-platin, Oxidation and reduction potentials of **17** and **147** vs Fc/Fc⁺ and recorded in 0.1 M solution of TBAPF₆ in MeCN. Log(*P*_{o/w}) for octanol/water.³⁷

Complex	IC ₅₀ (μM)	E ^{ox} _{1/2} (V)	Log(<i>P</i> _{o/w})
17	0.8 ± 0.1	0.45	1.95 ± 0.3
147	0.3 ± 0.1	0.30	2.64 ± 0.03
<i>Cis-platin</i>	5.0 ± 0.5	-	-

1.2 Terdentate cycloferrates for DSSC

Although no bis-terdentate cyclometalates of iron are known in the literature, in a work by Mukherjee *et al.* the potential of iron(II) bis(2,2',6,2''-terpyridine) (Fe(tpy)₂) and its cyclometalated analogues for use as photosensitizers for DSSC was investigated in a theoretical study.¹¹³ In Fig 57 we see three of the bis-cyclometalated complexes studied **148-150**. In this work the predicted absorption profiles of the complexes were compared with that of the model complex [Fe(tpy)₂]²⁺ (Fig. 58).

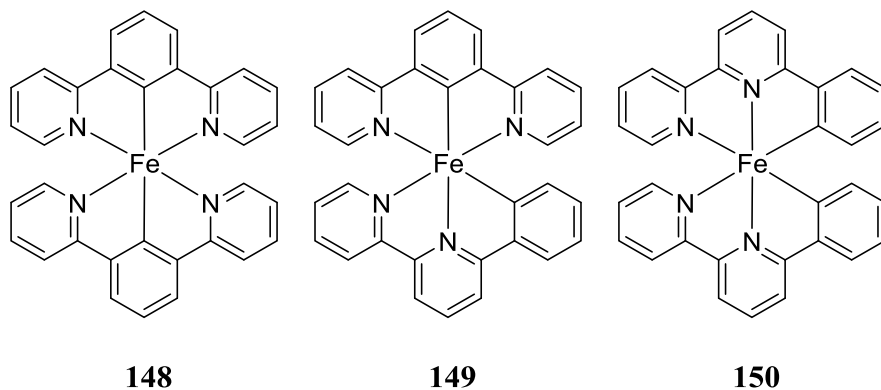


Fig. 57: Terdentate bis-cycloferrates **148-150**.

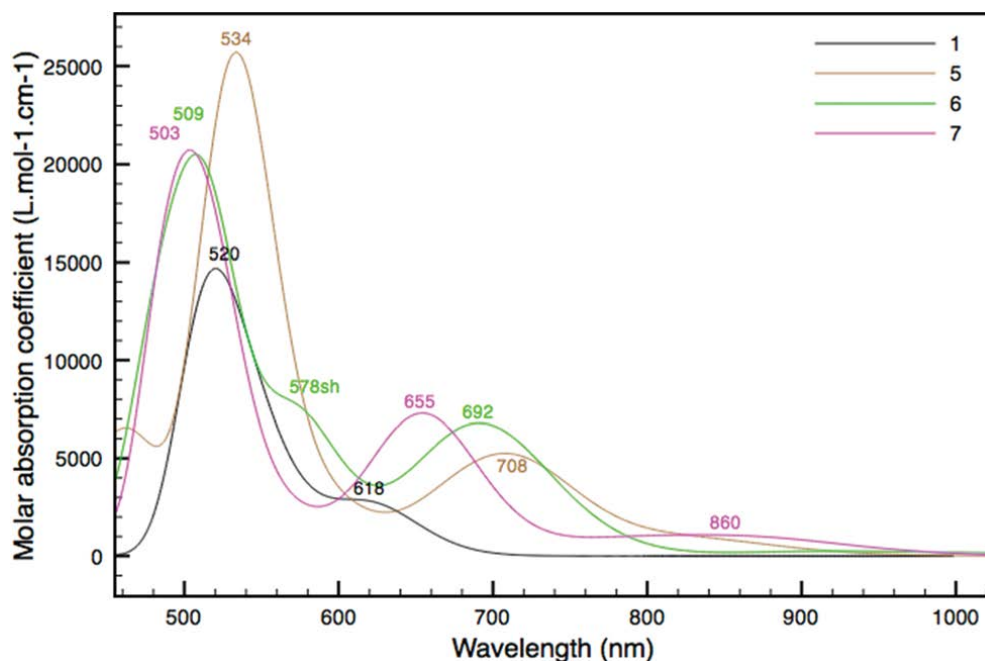
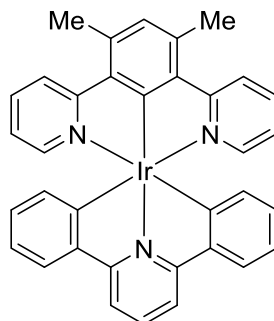


Fig. 58: Predicted absorption profiles of terdentate bis-cycloferrates **148** (orange), **149** (green) and **150**, (pink) vs $\text{Fe}(\text{tpy})_2$ (black).¹¹³

The predicted absorption profiles show all three bis-cyclometalates have broader and more intense absorption profiles than $[\text{Fe}(\text{tpy})_2]^{2+}$. Of the three we can see the bis-homoleptic cycloferrate **150** containing two phenylbipyridine ligands has the broadest absorption extending deep into the near-IR.

1.3 Terdentate cycloiridates for emissive materials

Concentrated efforts to develop efficient luminescent polypyridyl complexes of iridium have been ongoing since the early work on the tris-homoleptic bidentate cycloiridate **26**. Wilkinson *et al.* synthesised a bis-terdentate analogue of this compound, the tris-cyclometalated complex **151** (Fig. 59).¹¹⁴



151

Fig. 59: Bis-terdentate heteroleptic tris-cycloiridate **151**.

In Fig. 60 the absorption and emission profiles for **151** are displayed. The complex absorbs between 200 and 560 nm with relatively intense absorption from 200 to 340 nm and weak absorption above 340 nm. The emission profile shows a maximum in the orange region at 585 nm. This preliminary work indicated the potential of these types of complexes as emitters for devices such as OLEDs.

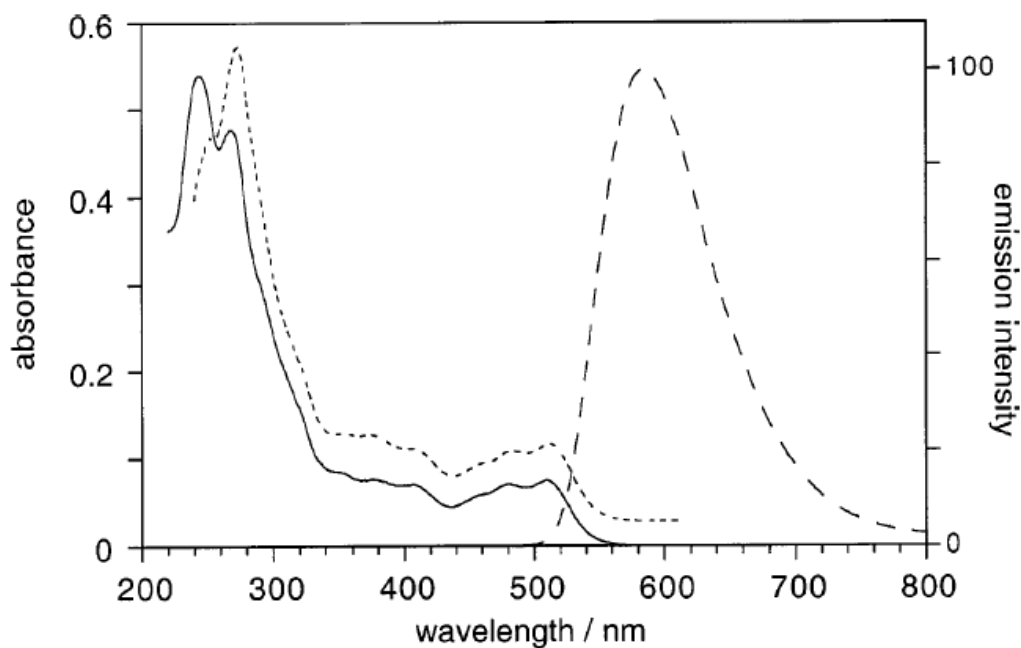
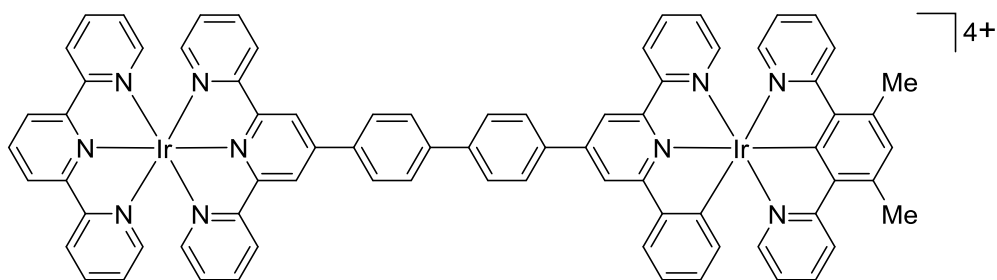


Fig. 60: Absorption spectrum of tris-cycloiridate **151** (solid line), emission spectrum (dashed line) and excitation spectrum (dotted line) in MeCN.¹¹⁴



152

Fig. 61: Bimetallic terdentate cycloridate **152**.

Bimetallic terdentate cyclometalates of iridium have also been investigated for their optoelectronic properties. Complex **152** (Fig. 61) was investigated by Whittle and Williams.¹¹⁵ The redox potentials and absorption maxima are shown in Table 11. The absorption and emission data are displayed in Fig. 62. The absorption data show very intense absorption between 200 and 450 nm, with weak absorption up to almost 600 nm. The emission maximum for **152** is at 607 nm and is orange.

Table 11: Oxidation and reduction potentials of **152** vs Fc/Fc⁺ and absorption maxima. All data recorded in MeCN.¹¹⁵

Complex	$E_{1/2}^{\text{ox}}$ (V)	$E_{1/2}^{\text{red}}$ (V)	$\lambda_{\text{max}}/\text{nm}$ ($\epsilon/10^3 \text{ M}^{-1} \text{ cm}^{-1}$)
152	1.08	-1.21	382 (62), 354 (56), 308 (96.8), 280 (109), 250 (116)

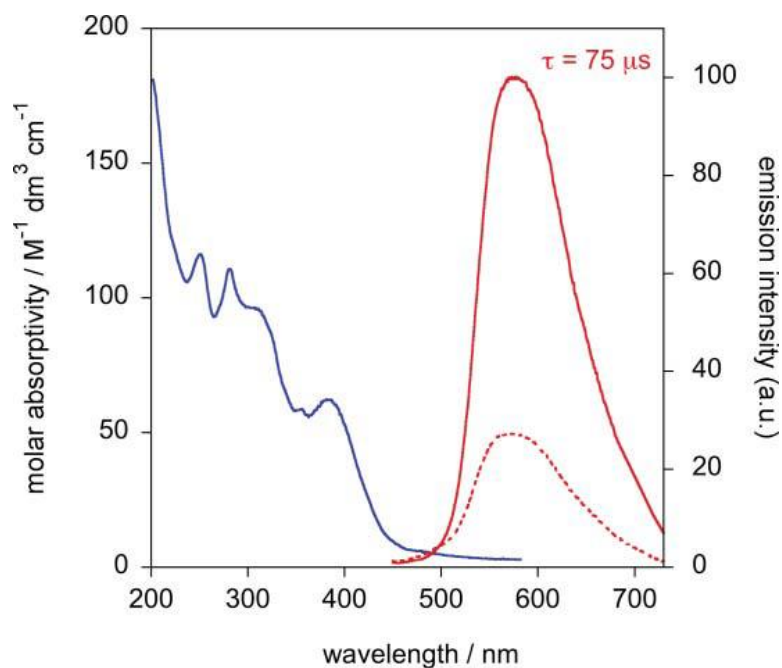


Fig. 62: Absorption spectrum of bimetallic cycloiridate **152** (blue), emission spectrum in degassed H₂O (red) and in air equilibrated H₂O (dotted line).¹¹⁵

2 Aims

In the **General Introduction** as well as the introduction to this chapter we have discussed a plethora of terdentate cyclometalates of groups 8 and 9. The broad range of applications makes them extremely interesting compounds for investigation. Bis-homoleptic terdentate cyclometalates of group 8 and 9 represent an almost entirely unexplored area of chemical space. The development of methods to synthesise them and investigation of their properties is therefore highly desirable. Having successfully synthesised a series of bis-homoleptic terdentate cycloruthenates, we aimed to apply the methods we had developed to access a novel series containing examples for each of the metals in the first three rows of group 8 and 9. Our strategy was to take one example of ligand (**61**) and attempt to synthesise the complexes **153-157** shown in Fig. 63.

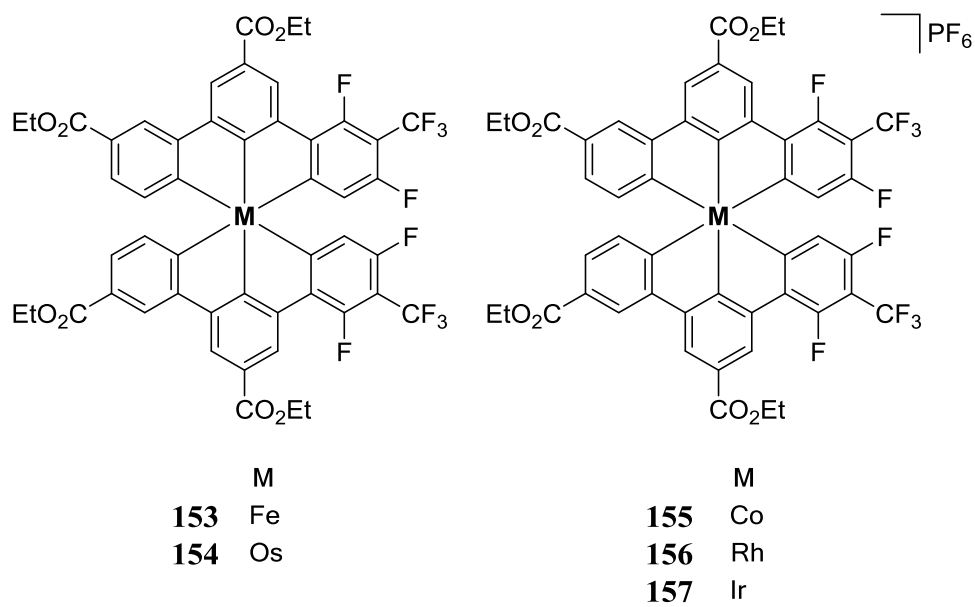


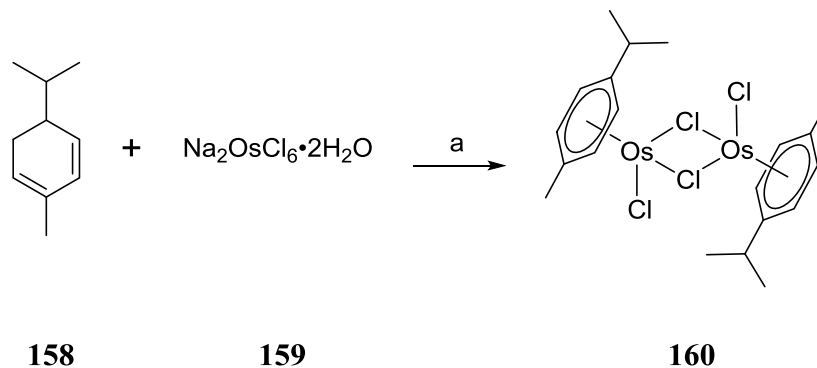
Fig. 63: Target complexes for a new series of bis-homoleptic terdentate cyclometalates **153-157**.

3 Results and Discussion

3.1 Toward osmium based complexes

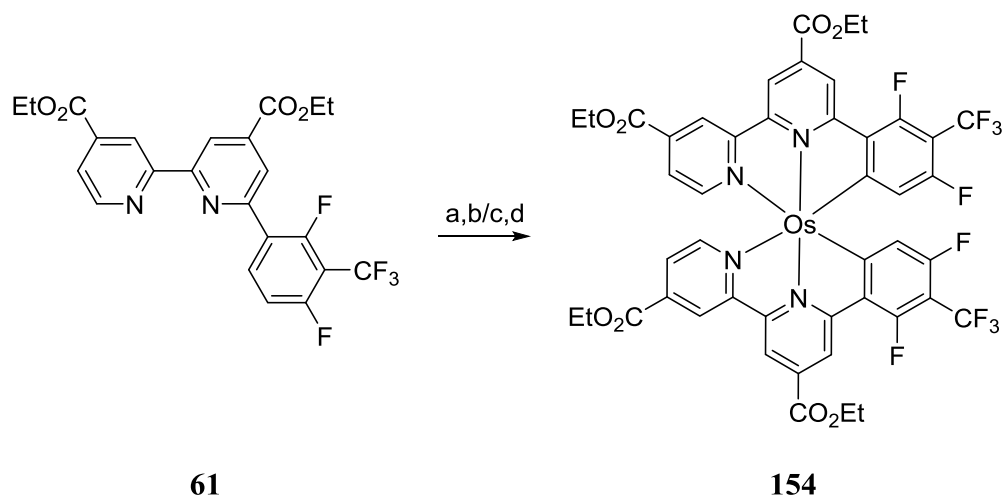
3.1.1 Synthesis of the complexes

As we expected the reactivity of osmium to be similar to ruthenium we aimed to proceed using the same methodology to access the complex **160**. The osmium(II) *p*-cymene dichloride dimer was not commercially available, this was therefore the first step in the synthesis. Following a method by Romanov *et al.* we were able to access **160** in 3 h with a 57% yield by utilising a microwave reactor.¹¹⁶



Scheme 77: Synthesis of osmium dimer **160**. Reaction conditions: (a) EtOH, H₂O, μ wave 100 °C, 3 h, 57%.

Following this we attempted to synthesise the bis-homoleptic cycloosmate **154** using the method developed in **Chapter 1**, section **3.2** to access cycloruthenates. Although this method was ultimately successful, high levels of transesterification led to a mixture of products which were difficult to separate by chromatography and a dramatically reduced yield of 6%.



Scheme 78: Synthesis of **154**. Reaction conditions: (a) **160**, *N*-ethylmorpholine, *n*PrCN, 120 °C, 16 h. (b) Ethylene glycol, 200 °C, 2h. 6 %. (c) **160**, *N*-ethylmorpholine, *n*PrCN, 120 °C, 16 h. (d) Ph₂O, 200 °C, 2h, 10%.

In order to avoid this problem a high boiling point solvent was required which could not undergo transesterification. The reaction was repeated with reflux in diphenyl ether replacing the reflux in ethylene glycol as a second step. An improved yield of 10% was obtained (Scheme 78). The major side products of the reaction were identified as heteroleptic terdentate cyclometalated **161** (6%) and the monocycloosmate **162** (12%) (Fig. 64). The remaining ligand amounted to 42% and the majority of the rest was a mixture of Os(III) complexes. The heteroleptic bis-cyclometalated complex was unexpected and clearly the result of an insertion into the C-F bond. Cyclometalation by activation of C-X bonds is well known in the literature including activation of C-F bonds.¹¹⁷ Although examples of osmium insertion into C-F bonds are rare, there are some reported.¹¹⁸ Recently several examples of similar reactions with iridium have also been reported.¹¹⁹⁻¹²² The proposed mechanisms vary, however preliminary results indicated high temperatures and polar solvents favour the process. As these are the same conditions required for cyclometalation by C-H insertion it seems difficult to avoid some yield loss to the heteroleptic complex. In order to improve the efficiency of the synthesis of the osmium complex **154**, a variety of solvents and conditions were investigated including using the microwave reactor

(Table 12). We aimed to find a single step method which avoided the issues of transesterification. Fig. 64 shows the main components of the reaction mixture after the experiment: **154** the desired product, **161** the heteroleptic bis-cycloosmate, **162** the monocyclometalated chloride and **61** the unreacted ligand.

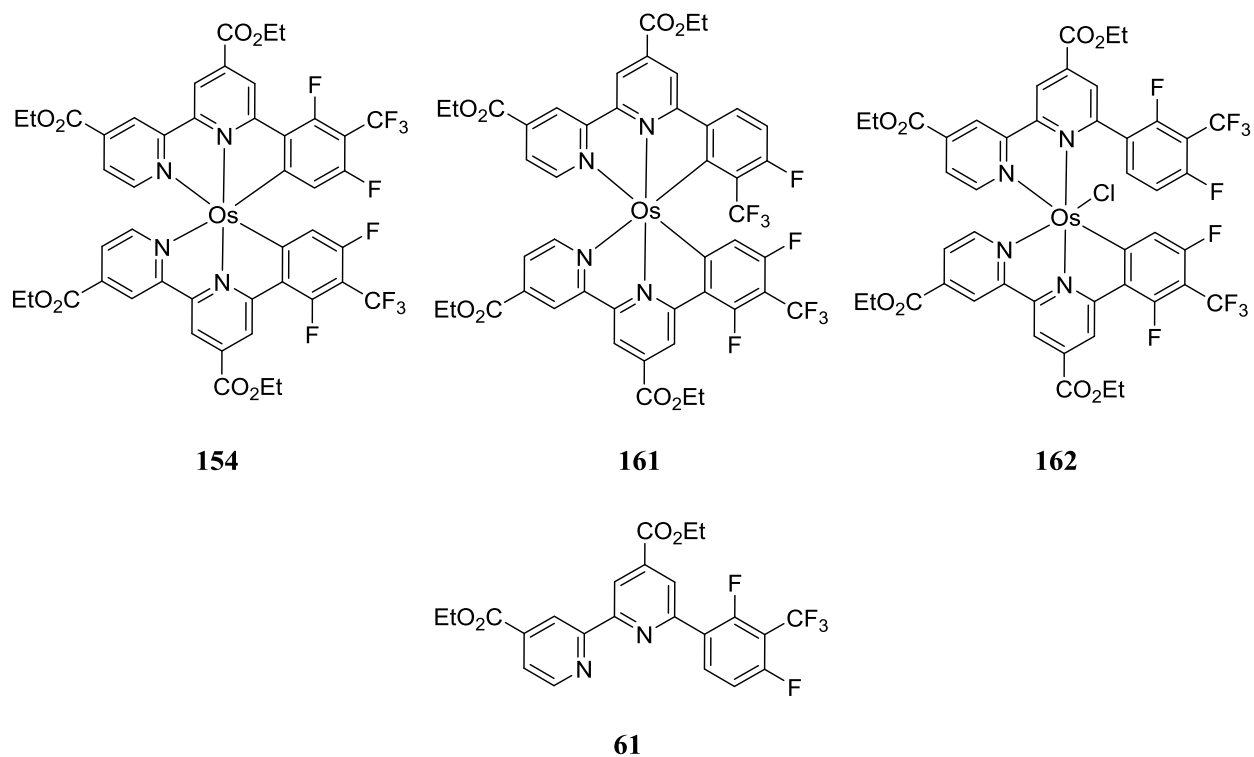


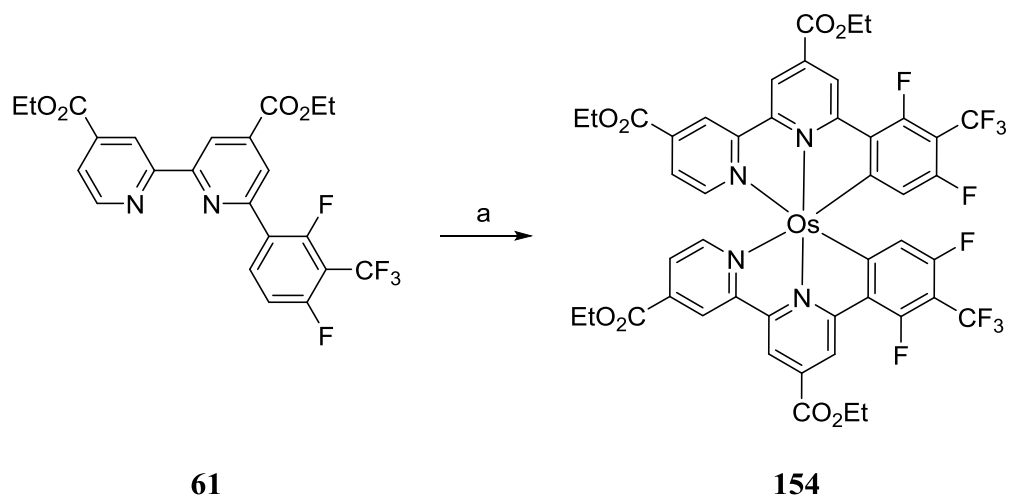
Fig. 64: Synthesis of Osmium complex **154**. Reaction contents: Bis-cyclometalated **154**, C-F bond insertion product **161**, mono-cyclometalated **162**, unreacted ligand **61**.

Table 12: Reaction conditions and results for the synthesis of osmium complex **154**.

Solvent	Base	Method	T (°C)	t (h)	Yield (%)				Majority of Remainder
					154	161	162	61	
TGDME	None	Thermal	215	2	0	0	0	*	Oxidised
Ph ₂ O	N-EM [#]	Thermal	245	2	0	0	0	0	Deesterified
NMP	None	μwave	200	3	0	0	0	*	Oxidised
NMP	KOH	μwave	200	3	0	0	0	0	Deesterified
EtOH	None	μwave	100	1	-	-	-	-	No reaction
EtOH	None	μwave	150	1	-	-	-	-	No reaction
EtOH	N-EM [#]	μwave	150	3	14	10	20	35	Oxidised
EtOH	N-EM [#]	μwave	150	14	19	12	22	34	Oxidised

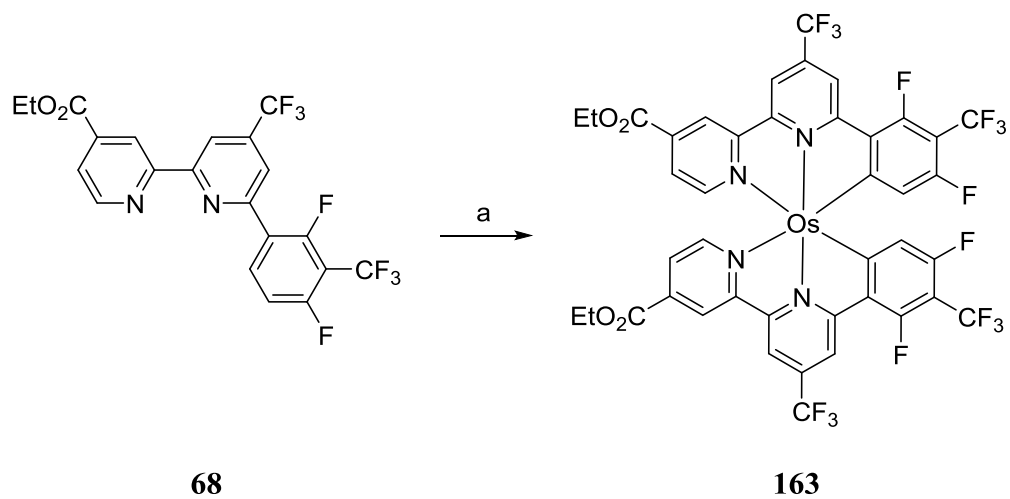
* No data, [#]*N*-ethylmorpholine

The results of the optimisation tests indicated that at higher temperatures and with strong bases the reaction predictably proceeded to the deesterified product. Furthermore in NMP and TGDME at high temperatures without a base the product was oxidised. Heating in the microwave in ethanol at 100 °C and 150 °C gave no reaction but the combination of ethanol and *N*-ethylmorpholine at 150 °C in the microwave for 3 h gave an increased yield of 14%. We also observed a concurrent increase in the amount of C-F insertion and monocyclometalated product. Extension of the reaction time to 14 h gave a further yield increase to 19% with a smaller increase in the amount of **161** and **162** produced. The reaction was also attempted under the same conditions but at 180 °C, however a decrease in yield to 13% was observed. A final effort was carried out with a fourfold increase in concentration. This gave a yield of 26%.



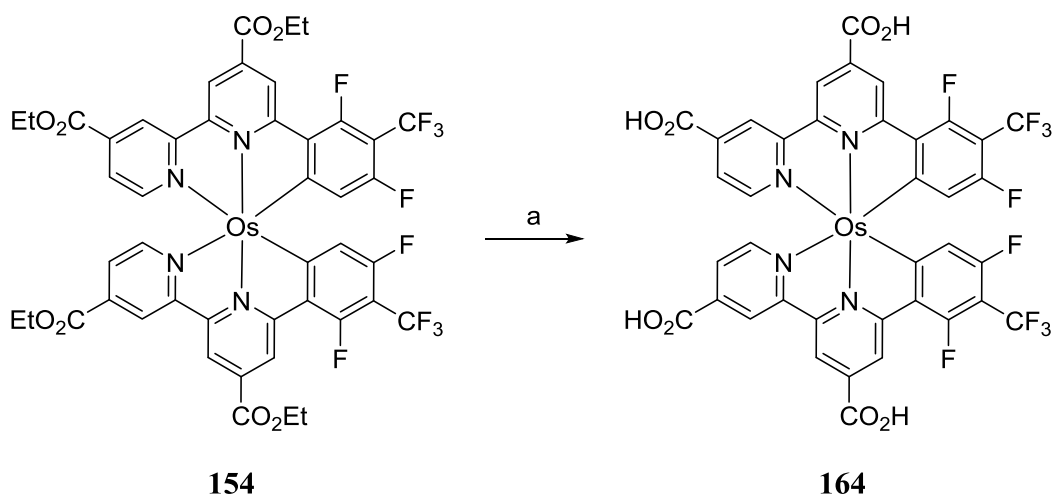
Scheme 79: Synthesis of **154**. Reaction conditions: (a) **160**, *N*-ethylmorpholine, EtOH, 150 °C, μ wave, 16 h, 26%.

Having developed a more efficient synthesis its scope was tested by application to the synthesis of complex **163** which was accessed in 15% yield (Scheme 80).



Scheme 80: Synthesis of **163**. Reaction conditions: (a) **160**, *N*-ethylmorpholine, EtOH, 150 °C, μ wave, 16 h, 15%.

The tetra acid **164** was also synthesised by the same method used for complexes **43** and **45**.



Scheme 81: Synthesis of **164**. Reaction conditions: (a) 1M KOH (aq), acetone, 60 °C, 16 h, 85%.

3.1.2 Characterisation of the complexes

In Fig. 65 we can see the UV-Vis absorption of osmium complexes **154** and **163**, in comparison to their ruthenium homologues **96** and **98**. We can see that the spectra between 250 and 400 nm are almost identical for complexes with the same ligands as these absorption bands represent ligand centred transitions. All four complexes have a MLCT peak at around 450 nm, although for the osmium complexes it is slightly blue-shifted and more intense. Above 500 nm the spectra begin to look significantly different on exchange of Ru for Os. The second MLCT peak for the Ru complexes is at 600 nm. For **154** this peak is considerably blue-shifted (approx. 80 nm). For **163** we see a more complex signal with two overlapping broad peaks at around 510 and 560 nm. As osmium is in the row below ruthenium it has an additional complement of orbitals including an f-orbital. This results in the Os orbitals being larger and more diffuse leading to more overlap with the ligand orbitals. This in turn leads to greater stabilisation of the HOMO by the cyclometalating portion of the ligand. We also see the addition of a peak at 780 nm for both Os complexes we hypothesised this represented a spin forbidden $^3\text{MLCT}$ transition. Again as Os has these larger more diffuse d-orbitals we expect to see stronger spin-orbit coupling (SOC) effects.

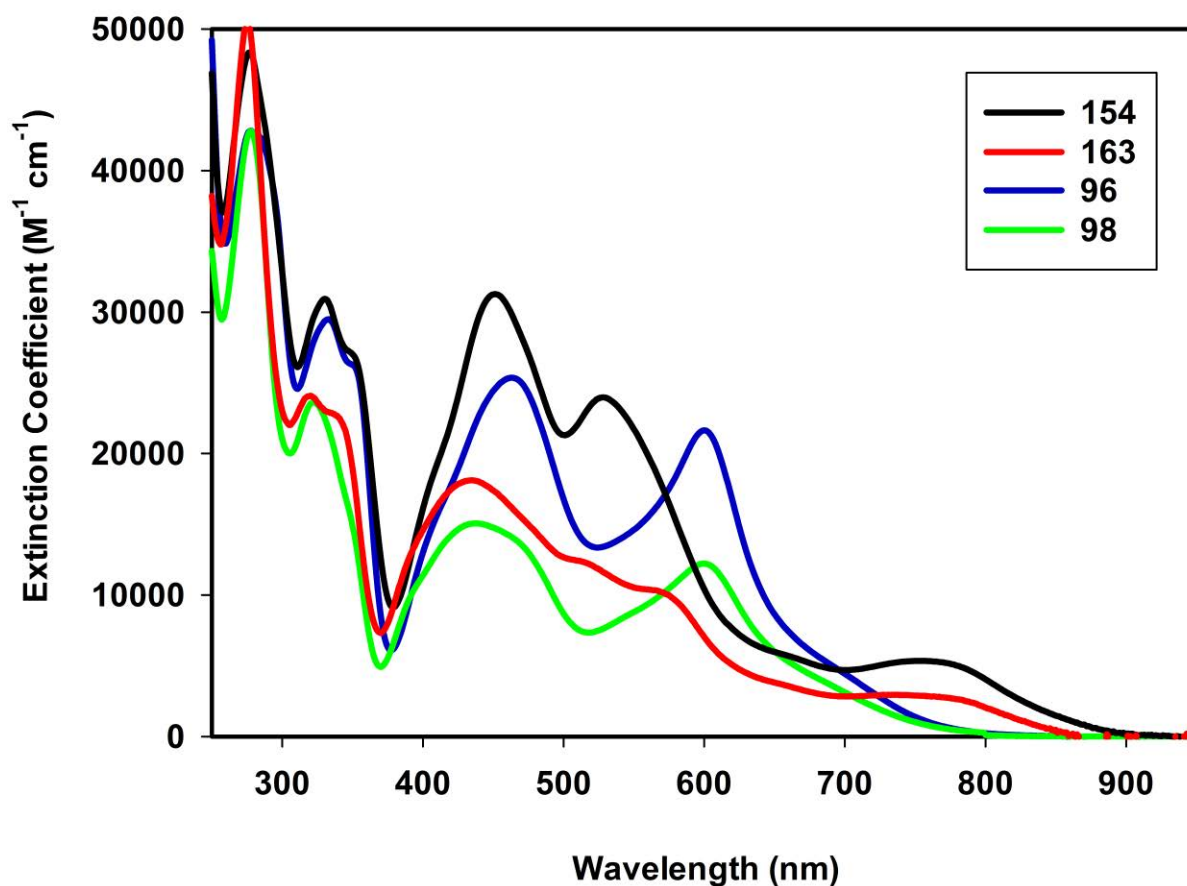


Fig. 65: Absorption spectra of **154** and **163** in comparison to **96** and **98** in CH₂Cl₂

In collaboration Dr Basil Curchod (Bristol University) we investigated this theory. Fig. 66 shows the experimentally derived absorption spectrum of **154** in comparison with the theoretical spectra both with and without SOC. It is clear that the calculations with SOC predict the experimentally obtained spectrum far more accurately.

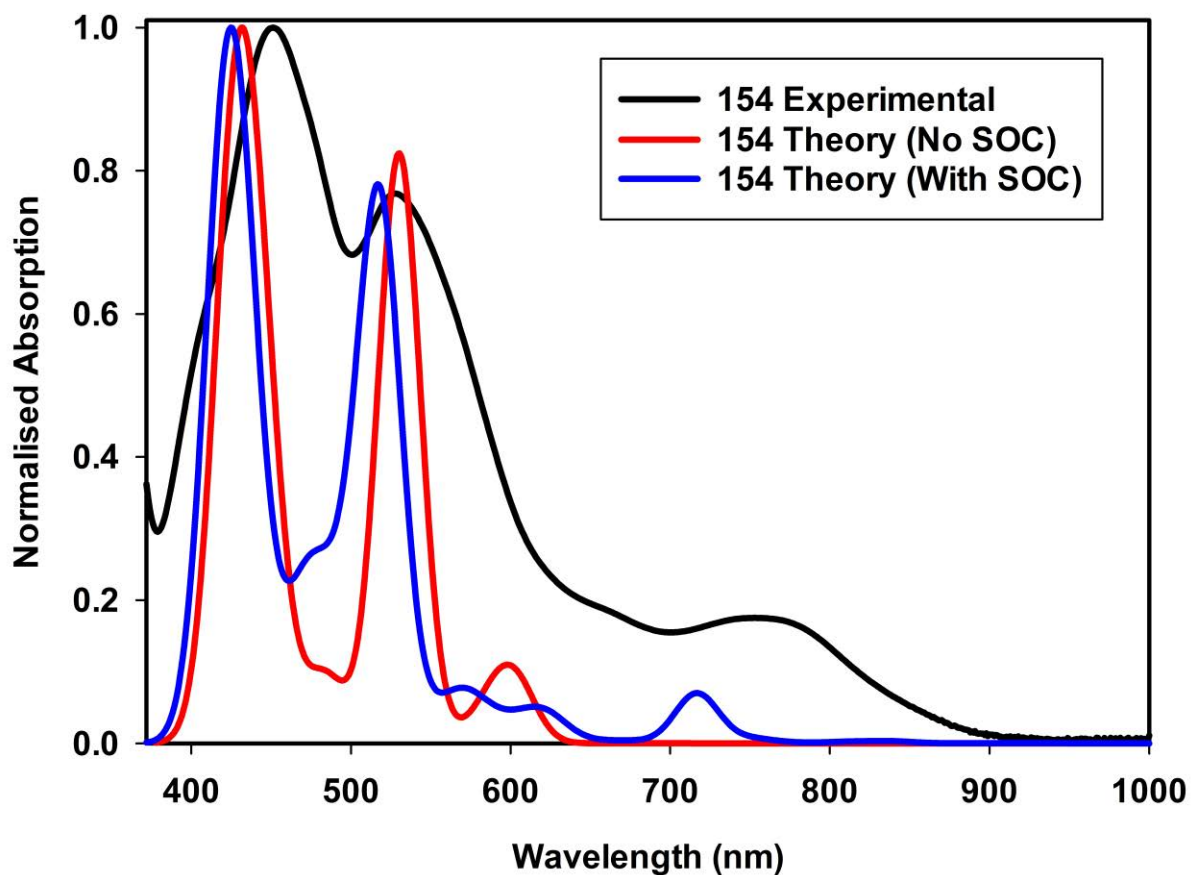


Fig. 66: Comparison of experimental spectrum with theoretical spectra (with and without SOC) of **154**.

The electrochemical data for **154** was acquired by cyclic voltammetry. Table 13 compares **154** with its ruthenium counterpart **96**. We can see that compared to **96** the cycloosmate has a lower oxidation potential and a lower reduction potential with an overall decrease in the redox gap.

Table 13: Oxidation and reduction potentials of Ru complex **96** and Os complex **154**. Recorded in 0.1 M solution of TBAPF₆ in CH₂Cl₂ vs Fc/Fc⁺.

Complex	$E_{1/2}^{\text{ox}}$ (V)	$E_{1/2}^{\text{red}}$ (V)	$E^{\text{ox-red}}$ (V)
96	0.20	-1.83	2.03
154	0.11	-1.75	1.86

3.1.3 Device testing

The osmium complex **164** was tested in DSSCs along with the ruthenium complexes **43** and **45** (**Chapter 1**, section 3.4) in collaboration with Dr Allesandro Sinopoli (University of Huddersfield). Table 14 shows the performance data compared with a device made with **N719**.

Table 14: Device performance data for ruthenium complexes **43** and **45**, as well as osmium complex **164** in comparison with archetypal dye **N719**.

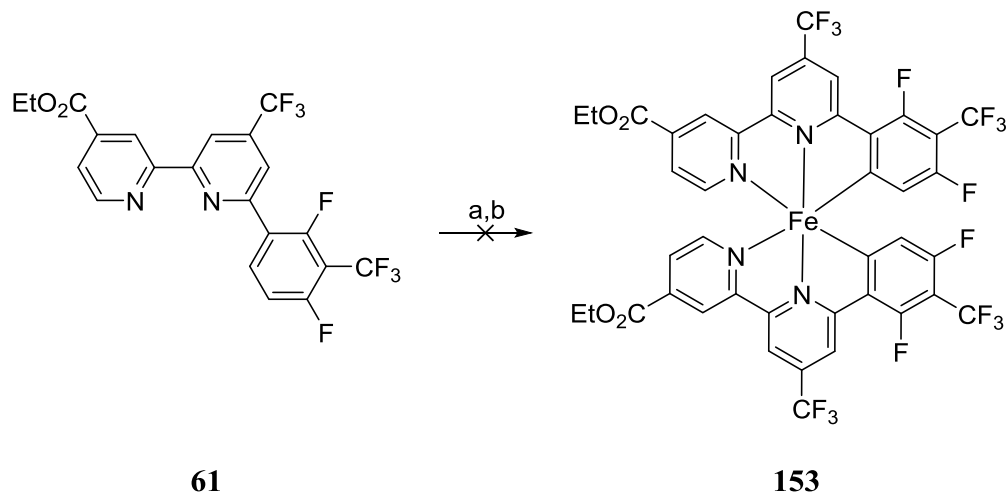
Dye	V _{oc} (V)	J _{sc} (mAcm ⁻²)	FF	η (%)
164	0.40	0.34	0.45	0.06
43	0.20	0.35	0.33	0.02
45	0.59	11.2	0.61	4.30
N719	0.63	18.4	0.58	6.84

Despite its increase in breadth and intensity of absorption the device with **164** achieved an efficiency of only 0.06%. This is an improvement compared to a device made with the ruthenium analogue **43**. As the oxidation potential of the osmium complex is lower we might expect a loss in efficiency due to the reduction in driving force for dye regeneration. Clearly the increased breadth and intensity of absorption profile counteracts this effect allowing comparable results.

3.2 Toward iron based complexes

3.2.1 Synthesis of the complexes

Having developed an improved method for the synthesis of bis-cyclometalated osmium complexes it was tested on iron based complexes. As RuCl₃, and IrCl₃ are common starting materials for the synthesis of cyclometalates, and as an iron(II) *paracymene* dichloride dimer is unknown in the literature FeCl₃ was used as the source of iron. The chloride was reacted in the microwave in ethanol along with the ligand, *N*-ethylmorpholine as base and AgNO₃ to aid in abstraction of the chloride. No reaction was observed. The solvent was removed and the reaction mixture combined with ethylene glycol and heated to 200 °C for 100 h. The reaction mixture was then analysed by mass spectrometry. No trace of any organoferrates was observed.

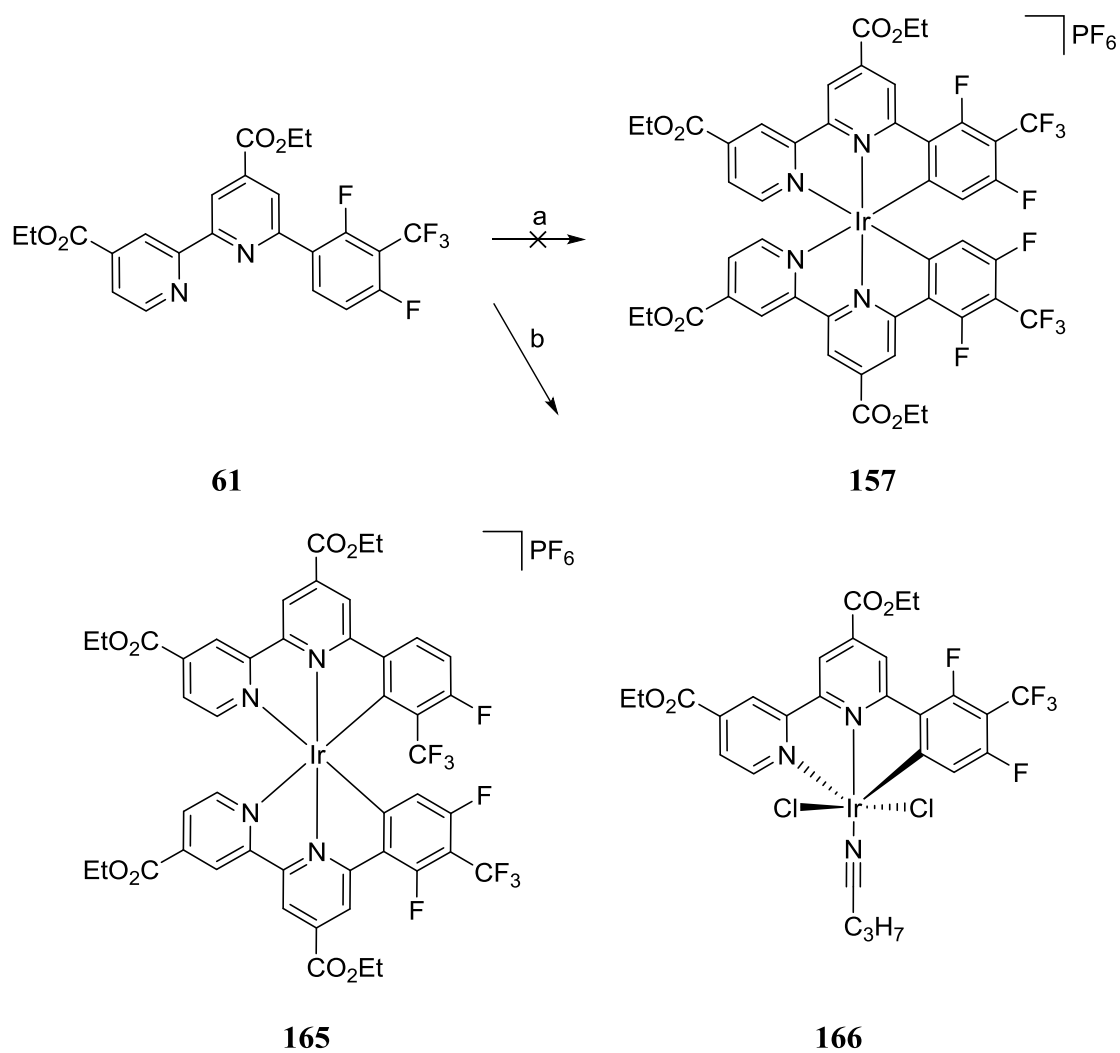


Scheme 82: Synthesis of **165**. Reaction conditions: (a) FeCl₃, *N*-ethylmorpholine, AgNO₃, EtOH, 150 °C, μ wave, 3 h, (b) ethylene glycol, 200 °C, 100 h.

3.3 Toward iridium based complexes

3.3.1 Synthesis of the complexes

The synthesis of iridium complex **166** was first attempted using the method developed by Baranoff *et al.*, by reaction of the ligand with the iridiumcyclooctadiene chloride dimer in ethoxyethanol. The reaction gave a large conversion to an inseparable mixture of highly luminescent yellow iridium complexes which were shown by mass and NMR to be products of transesterification of the ligand with ethoxyethanol similar to the case observed with osmium. A second attempt was made using butyronitrile as the solvent. This gave less conversion of reactants to complexes, however two main products were purified and characterised (Scheme 83).



Scheme 83: Attempted synthesis of an iridium complex. Reaction conditions: (a) $[\text{Ir}(\text{COD})\text{Cl}]_2$, Ethoxyethanol, 130°C , 16 h. (b) $[\text{Ir}(\text{COD})\text{Cl}]_2$, *n*PrCN, 120°C , 16 h, **165** 7%, **166** 5%.

NMR and mass spectrometry show that **165** and **166** are produced. The mass in concert with the ^1H and ^{19}F NMR (Fig 67 and 68) prove that the major product is cyclometalated once by insertion into a C-H bond, and once by insertion into the C-F bond as was observed in the case of osmium complex **161**.

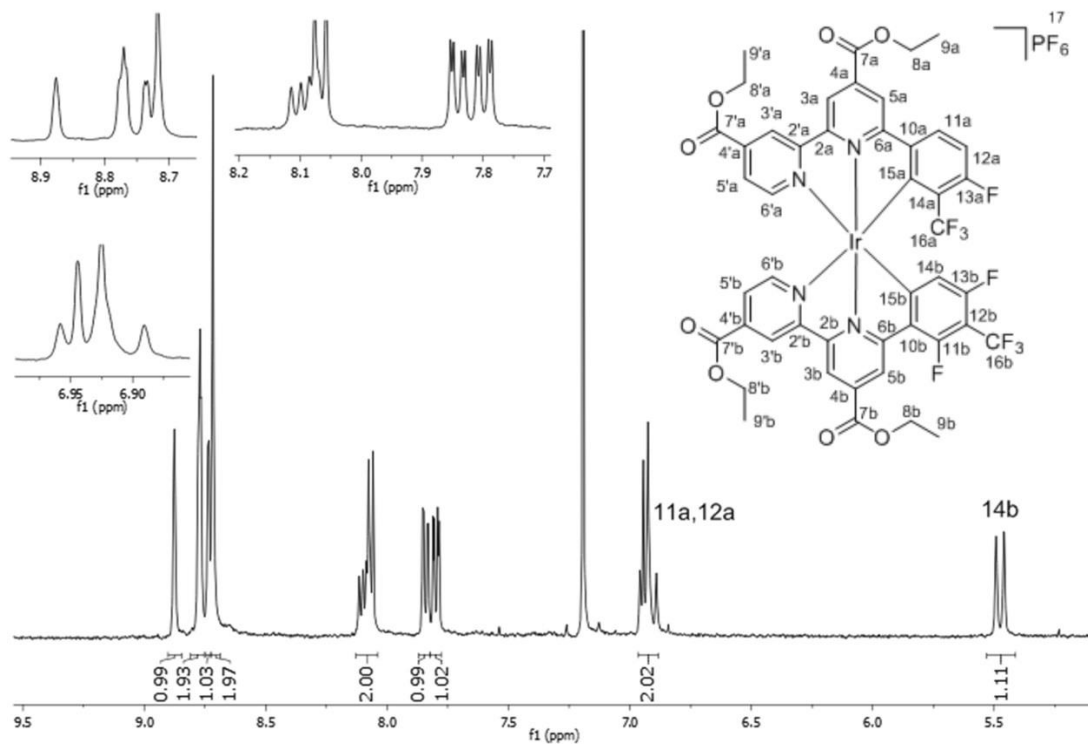


Fig. 67: ^1H NMR of heteroleptic terdentate cycloiridate **165** in CDCl_3 .

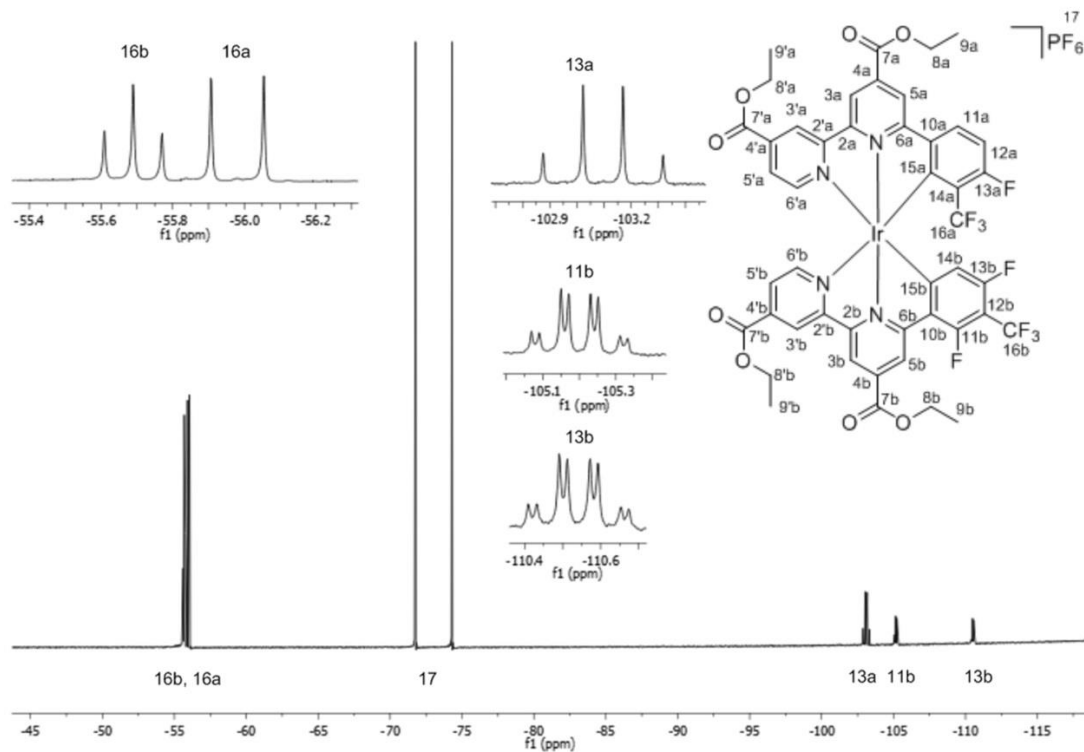
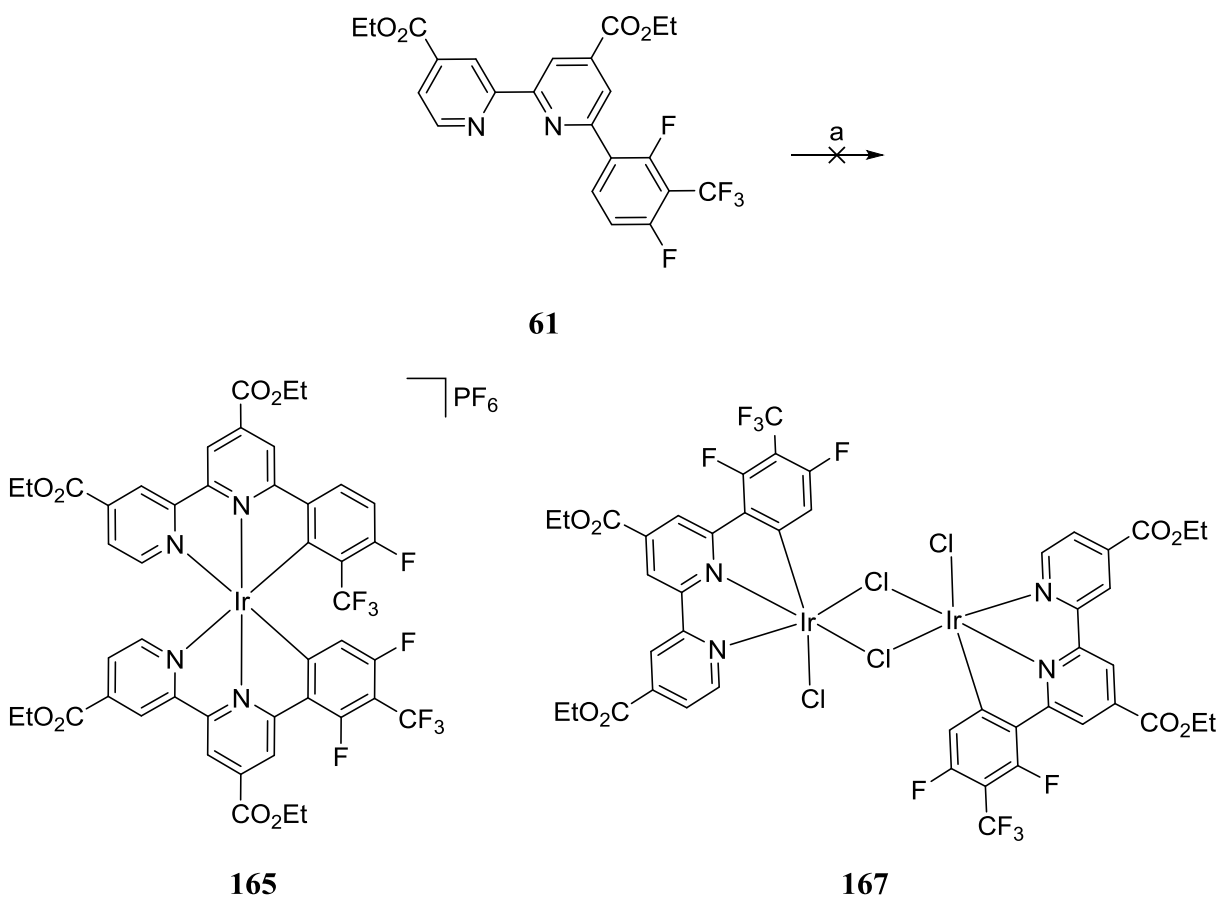


Fig. 68: ^{19}F NMR of heteroleptic terdentate cycloiridate **165** in CDCl_3 .

Fig. 67 and 68 show the ^1H and ^{19}F NMR of **165**. In the proton NMR we can see there are 13 environments in the aromatic region, too many for the homoleptic complex. Three unique environments are apparent: At 5.5 ppm there is a doublet split by a neighbouring fluoride and characteristically shifted up-field due to the adjacent carbon-metal bond. We can see that the integration is only one, corresponding to position 14b. At 7 ppm we see two overlapping environments, a doublet and a triplet with integration of one each. These correspond to 11a and 12a respectively. The ^{19}F NMR further supports the formation of this complex. We see a triplet/doublet of doublets at -55.7 ppm which is the trifluoromethyl group with 2 adjacent fluorides 16b. The neighbouring signal is only a doublet corresponding to 16a with only one fluoride in proximity. We also see only 3 fluoride environments. At -105 and -110 ppm there are two quartet of doublets consistent with 11b and 13b in the 2,4-difluoro(3-trifluoromethyl)phenyl environment. At 102 ppm there is a quartet equivalent to position 13a.

The other product **166** is the neutral complex with one equivalent of ligand, one of butyronitrile and two chlorides. With this knowledge inspection of the NMR of the mixture of transesterified complexes from the reaction in ethoxyethanol would indicate the same C-F insertion has taken place. As previously mentioned several examples in the literature exist where a cycloiridated 2,4-difluorophenyl moiety appears to lose a fluoride upon heating to high temperatures. As in this case the trifluoromethyl group is present we can see that in-fact this is due to an insertion into the C-F bond rather than by abstraction of the fluoride. As one of the literature examples with iridium report this phenomenon only at high temperatures for their complex we attempted the same reaction at room temperature.¹²² Within seconds the reaction turns bright yellow as it proceeds directly to the heteroleptic bis-cycloiridate **165** after stirring for 20 hours at room temperature the mixture was purified to give **165** and the dimer **167** (Scheme 84).



Scheme 84: Attempted synthesis of an iridium complex. Reaction conditions: (a) $[\text{Ir}(\text{COD})\text{Cl}]_2$, EtOH, rt, 20h, **165** 7%, **167** 6%.

3.3.2 Characterisation

Bis-heteroleptic cycloiridate **165** and the monocyclometalated **166** were investigated by absorption and emission spectroscopy (Fig. 69). The data shows that the complexes absorb intensely in the region between 250 and 400 nm. Indeed **166** is almost twice as intensely absorbing, which is expected due to the extra equivalent of ligand in the complex. Both complexes absorb weakly above 400 nm with the bands extending up to above 500 nm. The Emission profiles for both complexes are normalised so no comparison of intensity can be made. Qualitative examination was performed by excitation by UV light (365 nm) of solutions of comparable concentration of the two complexes. Bis-cycloiridate **165** is significantly more intensely emissive than **166** again as is expected due to the extra equivalent of ligand allowing for more emissive transitions. The bis-cyclometalates emission is yellow in colour with a

maximum at 545 nm. The emission of **166** is significantly red-shifted, orange in colour with a maximum at 610 nm.

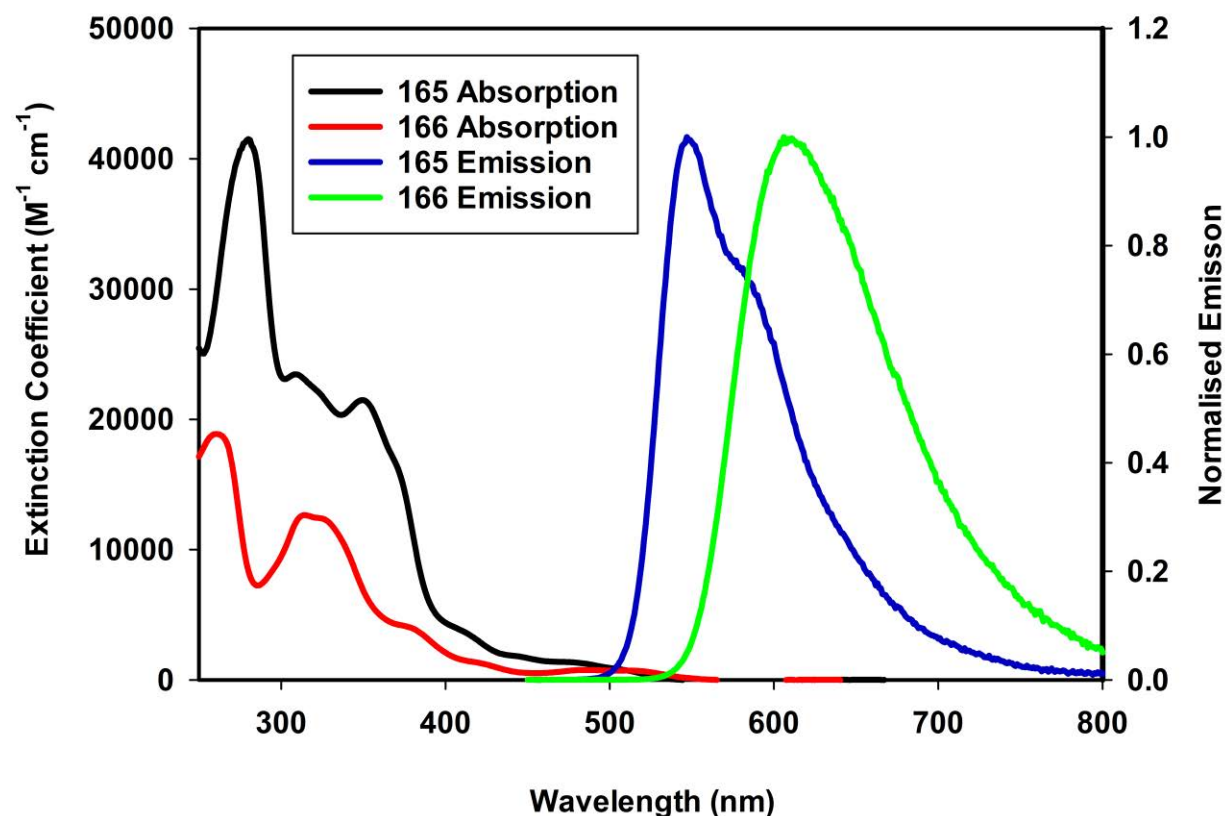
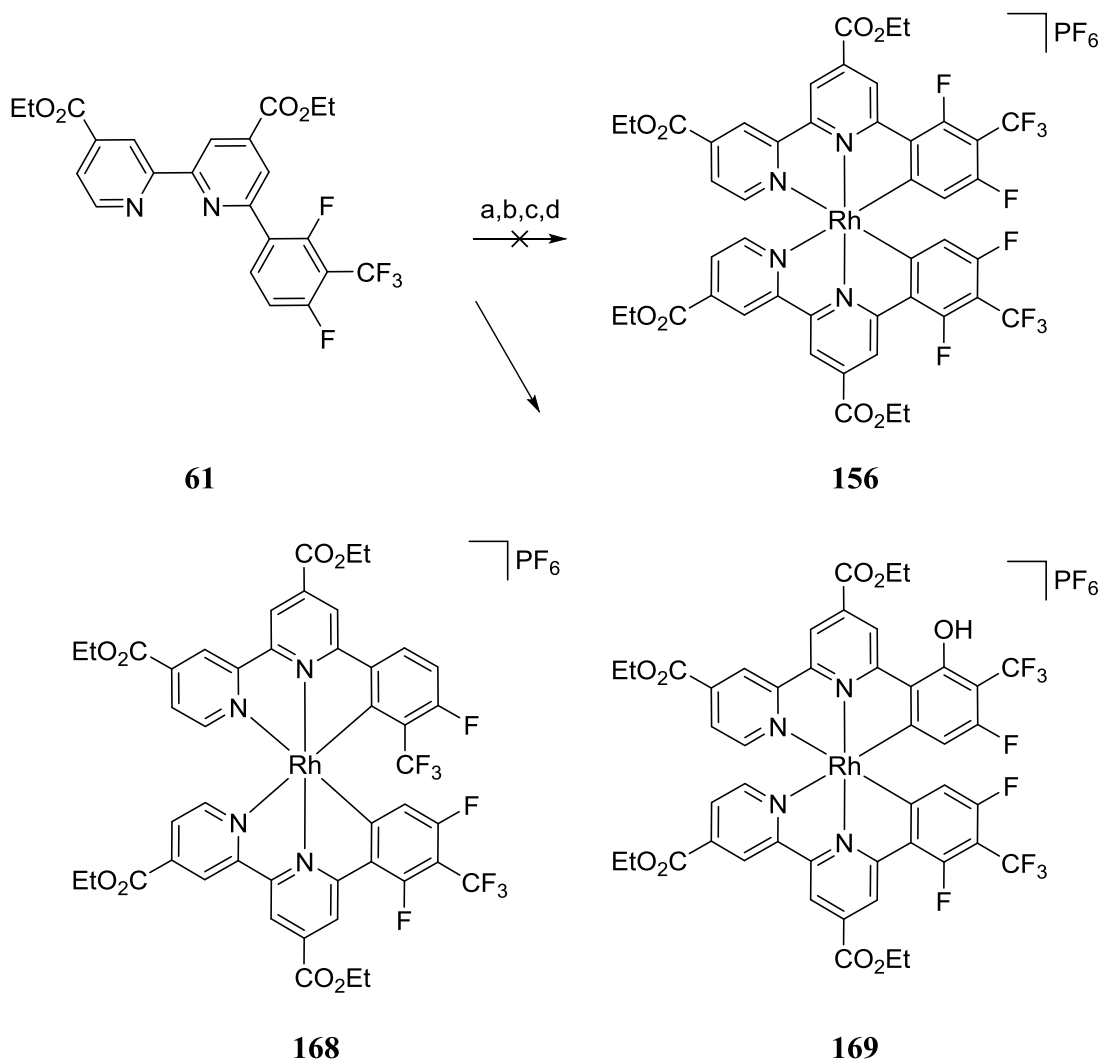


Fig. 69: Absorption and normalised emission spectra of **165** and **166** in CH₂Cl₂.

3.4 Toward rhodium based complexes

3.4.1 Synthesis of the complexes

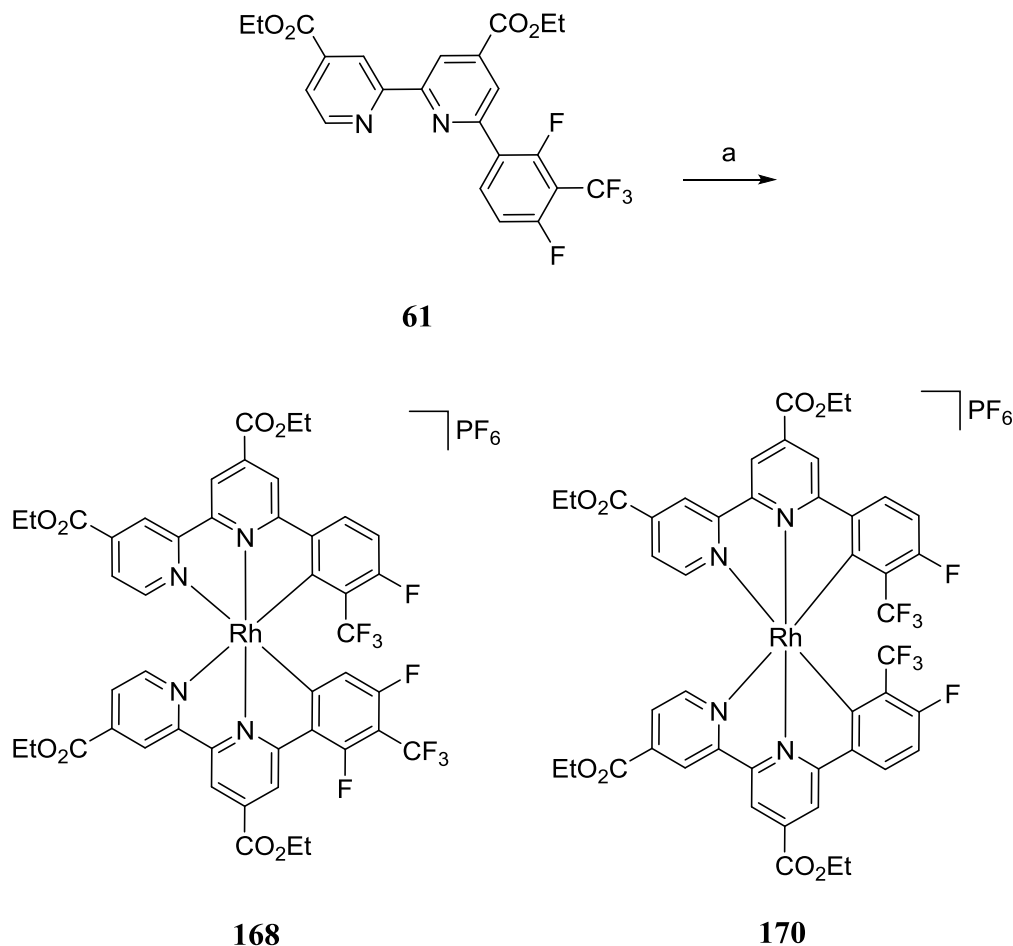
The synthesis of the rhodium based complex **156** was attempted using a variation of a literature method (rt in CH₂Cl₂ overnight). No reaction was observed. The mixture was subsequently refluxed in acetonitrile overnight, and then butyronitrile overnight. In both cases no change was observed. Reflux in ethylene glycol at 200 °C for 2 h was then attempted and a very small amount of conversion to new complexes occurred. The two main products were isolated by preparative TLC and submitted for mass spectrometry as too little was obtained for ¹HNMR.



Scheme 85: Attempted synthesis of a rhodium complex. Reaction conditions: (a) [Rh(COD)Cl]₂, CH₂Cl₂, rt, 16 h. (b) MeCN, 80 °C, 16 h (c) *n*PrCN, 120 °C, 16 h. (d) ethylene glycol, 200 °C, 2 h,

The mass spec data revealed that the two main products were the same C-F insertion product seen with iridium **168** (m/z 1043.5 (100), 1044.5 (48), 1045.5 (9)) as well as a complex which appears to have one equivalent of fluoride converted to hydroxide **169** (m/z 1059.1 (100), 1060.1 (47), 1061.1 (8)), (Scheme 85). As no product was observed for rhodium at low temperature and even at high temperature only trace quantities were observed, the reaction was repeated at 150 °C in the microwave with *N*-ethylmorpholine as a base. Silver nitrate was also added to aid in abstraction of the chloride and lower the activation energy of the reaction (Scheme 86). The reaction gave a much larger quantity of complex which could be analysed by NMR. Separation of the largest fraction by column chromatography gave an mixture of complexes which could not

be separated. This was analysed by ^1H and ^{19}F NMR as well as by mass spectrometry. The data would indicate a mixture of bis-heteroleptic cyclorhodate **168** (m/z 1043.5) and bis-homoleptic cyclorhodate **170** (m/z 1025.1).



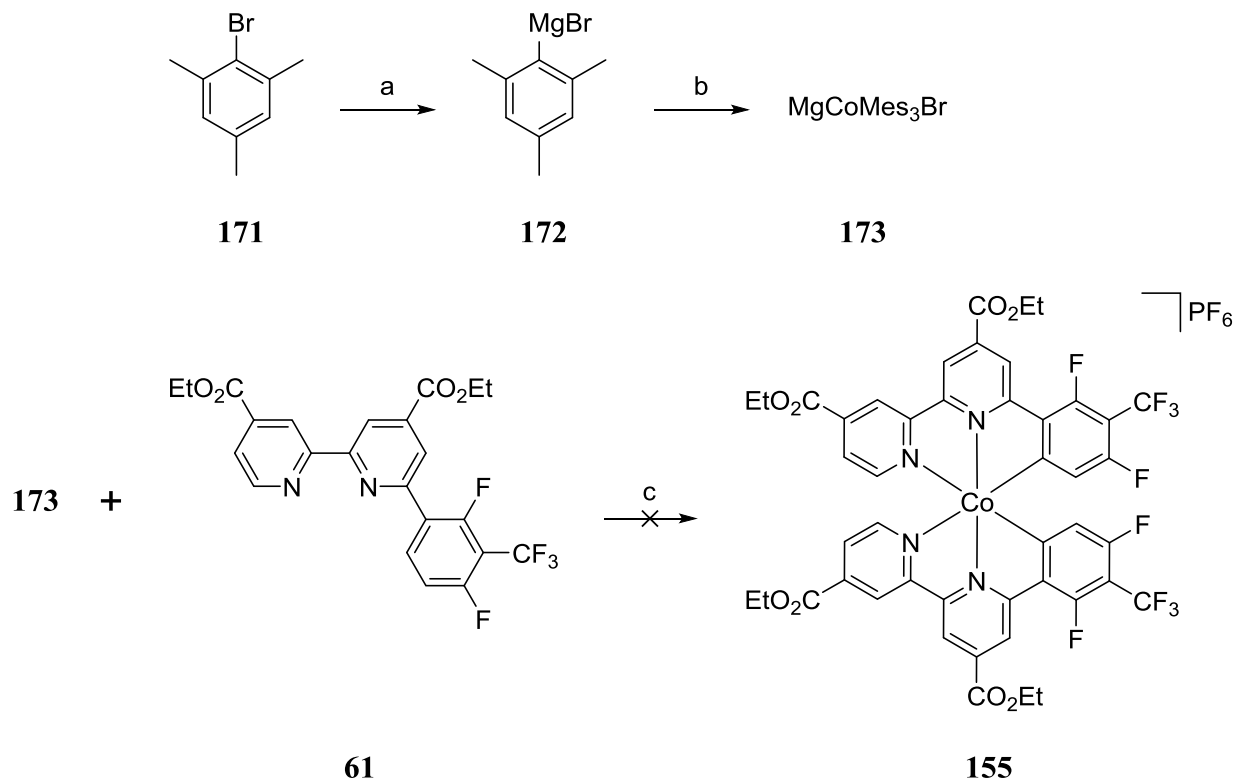
Scheme 86: Synthesis of rhodium complexes **168** and **170**. Reaction conditions: (a) $[\text{Rh}(\text{COD})\text{Cl}]_2$, EtOH, *N*-ethylmorpholine, AgNO_3 , μ -wave, 150°C , 14 h.

3.5 Toward cobalt based complexes

3.5.1 Synthesis of the complexes

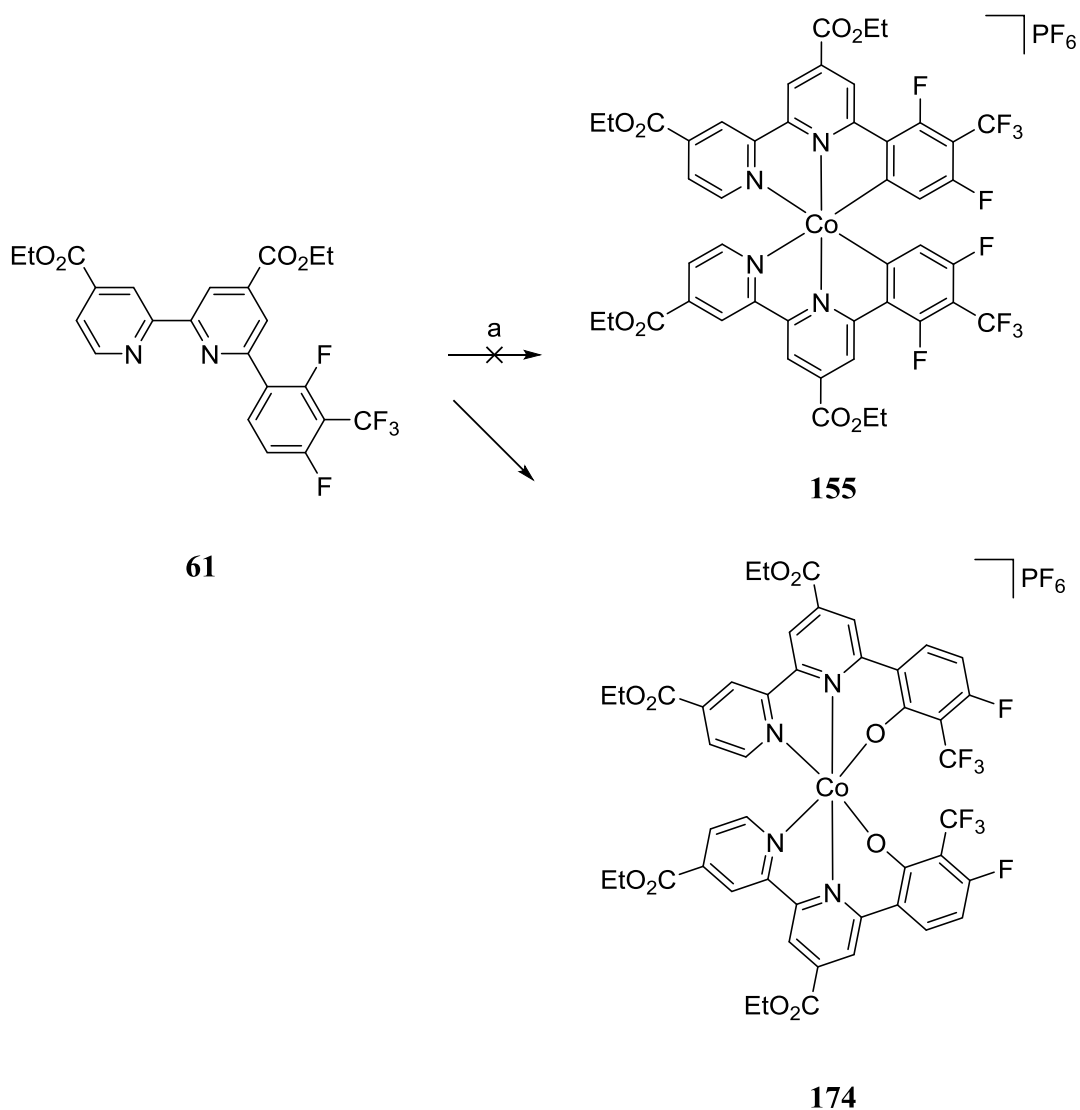
Synthesis of the bis-cyclocobaltate **155** was first attempted *via* the method by Drevs used to access the only other similar literature examples of homoleptic cyclometalated cobalt **7** and **8** the tris-homoleptic cyclometalates described in the General Introduction, section 3. The method involves several steps. First the synthesis of the Grignard of bromomesitylene is made, then this is reacted with CoBr_2 to form the complex $\text{MgCoMes}_3\text{Br}$ (where Mes = mesitylene). This is then

refluxed with the ligand in THF to give the trishomoleptic Co(III) complex. This method was applied to our target with the final step a reflux in *n*PrCN. The reaction mixture was analysed by TLC and mass spectrometry. Only the ligand was observed.



Scheme 87: Synthesis of cobalt complex **155**. Reaction conditions: (a) Mg, I, THF 70 °C, 4h, (b) CoBr₂, -20 °C, 1 h. (c) *n*PrCN, 120 °C, 16 h.

Having had some success with cyclometalation in a microwave reactor for osmium and rhodium which had proven difficult to cyclometalate, this technique was attempted. Using CoBr₂ as the starting material, the reaction was carried out in ethanol with *N*-ethylmorpholine and AgNO₃ at 150 °C for 2 h. The reaction mixture turned a dark brown colour and purification of the mixture by column chromatography gave complex **174** confirmed by ¹H and ¹⁹F NMR as well as mass spectrometry. Rather than the bis-cyclometalate we appear see conversion of the fluoride to hydroxide (as observed for Rh) followed by coordination of the oxygen atoms to cobalt forming an entirely novel bis-homoleptic terdentate cobalt complex.



Scheme 88: Attempted synthesis of complex **155** and unexpected product **174**.

3.5.2 Characterisation of the complexes

The bis-homoleptic cobalt complex **174** was analysed by UV-Vis spectroscopy. Fig 70 shows a comparison with the ruthenium complex **96**. We can see clearly the absorption of **174** is less intense and narrower than **96**. The cobalt complex absorbs strongly between 250 and 500 nm with weak absorption extending up to above 700 nm. Fig. 71 displays the UV-Vis absorption spectra for the literature trishomoleptic cyclocobaltates **7** and **8**. The phenylpyridine complex **7** has the broader absorption profile with a peak at 450 nm and very weak absorption extending up to above 700 nm, very similar to that of the complex terdentate homoleptic complex **174**. The major difference is an additional peak and more intense absorption for **174**.

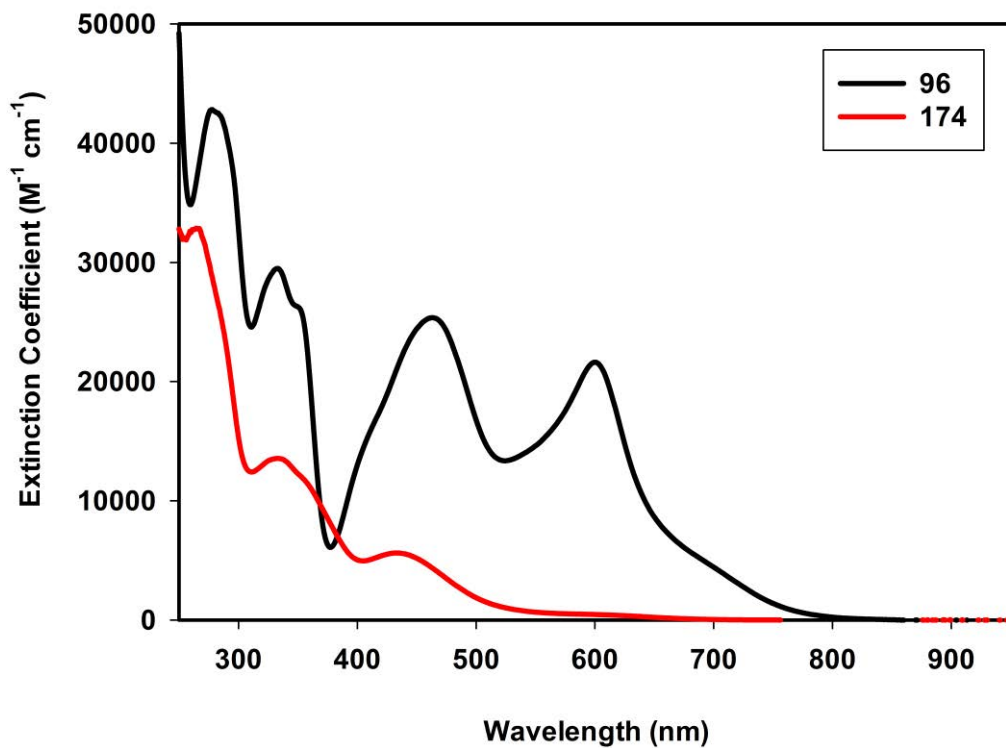


Fig. 70: UV-Vis absorption of homoleptic terdentate cobalt complex **174** compared to the ruthenium complex **96** in CH_2Cl_2 .

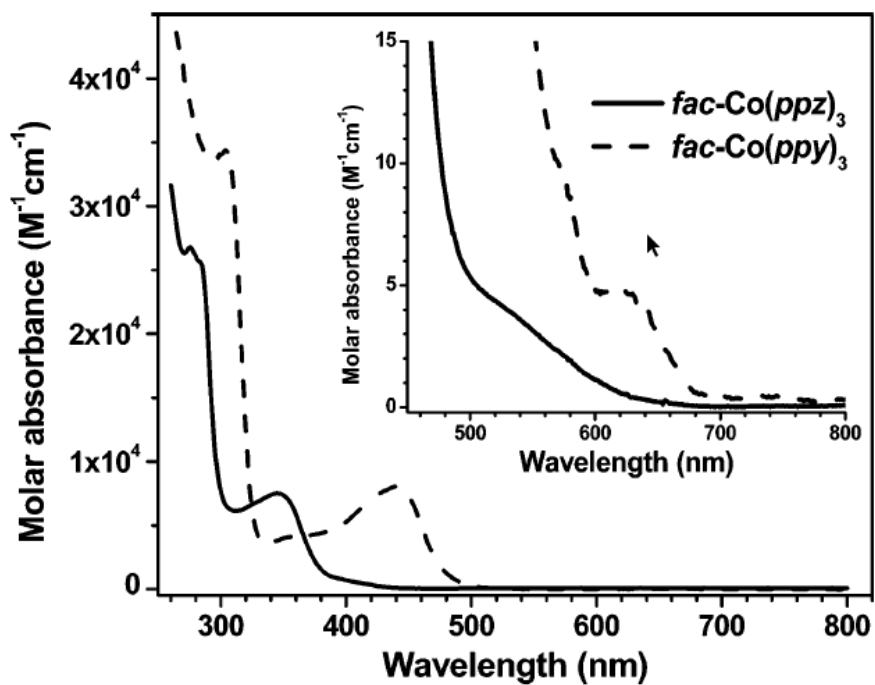


Fig. 71: UV-Vis absorption of literature examples **7** and **8** in CH_2Cl_2 .¹⁵

4 Conclusion

The methods developed in **Chapter 1**, were applied to the synthesis of a novel bis-homoleptic cycloosmate **154**. The method was successful with a low yield of 5%. Optimisation of this reaction led to improvements in efficiency to allow access to **154** in 26% yield. An unexpected C-F insertion side product **161** was also obtained. The optimised method was applied to the synthesis of a second osmium complex **163**. The two complexes were characterised by absorption spectroscopy. Both complexes had excellent absorption properties with intense absorption beyond 900 nm. With the help of a collaboration with Dr Basil Curchod (Bristol University) we identified the cause of the extended breadth of absorption as spin orbit-coupling effects. The oxidation and reduction potentials of **154** were measured by cyclic voltammetry. In comparison with the analogous ruthenium complex **96** the oxidation potential was reduced. Complex **154** was deesterified to give the tetra acid **164** which was tested in a DSSC in collaboration with Dr Allesandro Sinopoli (University of Huddersfield). The device had an efficiency of 0.06%, a slight improvement compared to the analogous ruthenium compound **43**.

An initial experiment to synthesise a cycloferrate was unsuccessful. However cyclometalates of iridium were acquired. The bis-terdentate cycloiridate **165** was however heteroleptic due to a C-F insertion reaction. The absorption and emission spectra for **165** and the monocyclometalate complex **166** were recorded. Both complexes were bright emitters in the yellow and orange respectively.

Attempts to access cyclorhodates eventually led to the production of complexes which were analysed by mass spectrometry. Two bis-heteroleptic terdentate cyclometalates were identified, **168** product of a C-F insertion and **169** the product of a conversion of fluoride to hydroxide. A bis-homoleptic terdentate cyclometalate of rhodium was also identified as **170** the product of two C-F insertions. This complex could not be isolated.

The cyclocobaltate **155** was not obtained by either a classic synthetic route to tris-cyclometalated cobalt, or from the method developed in this work to access cyclometalates of group 8 and 9. An unexpected bis-homoleptic terdentate cobalt complex **174** was created with a NNO coordinating ligand. The complex was characterised by absorption spectroscopy and the absorption profile was comparable to Cobalt(III) tris(phenylpyridine) **7**.

Concluding remarks

In this project we set out to investigate the area of bis-homoleptic terdentate cyclometalates of group 8 and 9. In the first part of the work we developed new synthetic techniques with which we were able to produce a novel first generation of ruthenium complexes with excellent absorption characteristics. Two of these complexes were tested in a DSSC, the best of which gave an efficiency of 4.3%.

Following this successful work a series of investigations into variations of the ligand structure in a second generation of cycloruthenates was undertaken. We were able to access a homoleptic complex with a terpyridyl ligand suitable for the development of DSSCs with a cobalt based electrolyte. Attempts to vary the ligand at the 4-pyridyl position gave limited success and no new complexes were obtained. A new class of quinoline based ligand was synthesised and preliminary results indicate the possibility of a new class of homoleptic cycloruthenates based on a quinolyphenylpyridine ligand.

In the third part of this project we expanded our focus to the other metals of group 8 and 9. An improved method for accessing terdentate cyclometalates was developed and cyclometalates of osmium iridium and rhodium were synthesised. An osmium complex was tested in a DSSC and had an improved efficiency to its ruthenium analogue. Attempts to synthesise cyclometalates of iron and cobalt were unsuccessful, however a new bis-homoleptic complex of cobalt was isolated.

Experimental

1 Instrumentation

Infra-red spectra were recorded neat as thin films on a Perkin Elmer “Spectrum” spectrometer. The intensity of each band is described as s (strong), m (medium) or w (weak) where appropriate.

^1H NMR ^{19}F NMR and ^{13}C NMR spectra were recorded in CDCl_3 unless specified otherwise, on a Bruker AVIII400 (400 and 100 MHz), or a Bruker AVIII300 (300 MHz). Chemical shifts are reported as δ values (ppm) referenced to the following solvent signals: CHCl_3 , δ_{H} 7.26; CDCl_3 , δ_{C} 77.0; CH_3OD , δ_{H} 3.34; CD_3OD , δ_{C} 49.9, CH_3CN , δ_{H} 1.94, CD_3CN , δ_{C} 118.3. Multiplicity of signals and coupling constants were obtained by processing on MestReNova.

Mass spectra were recorded on a Micromass ZABspec spectrometer utilizing electrospray ionization with a MeOH or MeCN mobile phase and are reported as (m/z (%)).

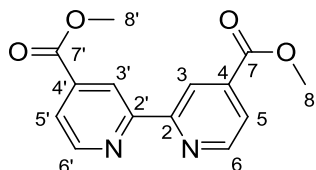
UV-Vis spectra were recorded on a Cary-5000 spectrometer in CH_2Cl_2 solution.

Electrochemical data was obtained using a Metrohm Autolab Pgstat101 potentiostat with a glassy carbon disk as working electrode and Pt wire reference and counter electrodes. Cyclic voltammetry was performed in 0.1 M solutions of $n\text{Bu}_4\text{NPF}_6$ in argon degassed CH_2Cl_2 . The ferrocene/ferrocenium couple (Fc/Fc^+) was used as an internal standard.

Crystallographic data was recorded at the EPSRC UK National Crystallography Service at the University of Southampton by Diamond Light Source on beamline I19.

2 Characterisation-Chapter 1

Dimethyl-2,2'-bipyridine-4,4'-dicarboxylate (49)



2,2'-Bipyridine-4,4'-dicarboxylic acid (5.00 g, 20.5 mmol) was combined with MeOH (300 mL) to form a suspension, to which was added H₂SO₄ (98%, 20 mL) at rt. The mixture was heated to reflux at 85 °C whilst stirred, and the solid dissolved slowly to form a pink solution. The heating continued for 46 h. After cooling to rt an aqueous solution of Na₂CO₃ (20 g Na₂CO₃ in 100 mL H₂O) was added slowly until the pH was increased to 8, causing a white precipitate and evolution of CO₂. The resulting suspension was extracted with CHCl₃ (3 x 300 mL), the organic phases were combined and dried (MgSO₄) and the solvent removed under reduced pressure. Remaining impurities were removed by filtration of the product as a solution in 10% MeOH in CHCl₃ through a pad of silica. Solvent was removed under reduced pressure to afford a white crystalline solid (4.71 g, 17.4 mmol, 85%). *R*_f = 0.90 (10% MeOH in CHCl₃, on silica)

Mp; 205-206 °C;

¹H NMR (300 MHz, CDCl₃) δ 8.95 (dd, *J* 1.5, 0.9 Hz, 2H, H^{3,3'}), 8.86 (dd, *J* = 5.0, 0.9 Hz, 2H, H^{6,6'}), 7.90 (dd, *J* = 5.0, 1.6 Hz, 2H, H^{5,5'}), 3.99 (s, 6H, H^{8,8'});

¹³C NMR (100 MHz, CDCl₃) δ 165.7 (C^{7,7'}), 156.6 (C^{4,4'}), 150.3 (C^{2,2'}), 138.7 (C^{6,6'}), 123.4 (C^{3,3'}), 120.7 (C^{5,5'}), 52.9 (C^{8,8'});

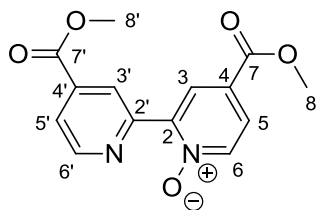
IR(film, cm⁻¹): 2960s (C-H), 2930s (C-H), 2860s (C-H), 1731s (C=O), 1592s (C=C), 1558s (C=C), 1466s (C-H), 1437s (C-H), 1359s (C-H), 1295s (C-O);

MS (TOF ES⁺): *m/z* (%): 295.1 (100) [M+Na]⁺;

HRMS (ES⁺): [M+Na]⁺ calcd. for C₁₄H₁₂N₂O₄Na, 295.0695; found, 295.0694.

Data were in agreement with those reported in the literature.¹²³

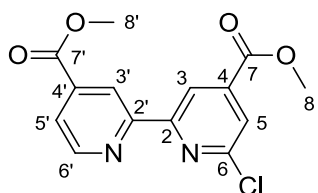
4,4'-Bis(methoxycarbonyl)-2,2'-bipyridine 1-oxide (50)



13 (4.71 g, 17.4 mmol, 1 eq) was dissolved in CHCl_3 (200 mL), to which *m*CPBA (3.00 g, 17.4 mmol, 1 eq) was added slowly at rt producing a yellow solution. After stirring at rt for 10 h the solvent was removed under reduced pressure and the crude product purified by column chromatography on alumina (CH_2Cl_2 :MeOH 50:1), The product proved to be unstable and a mixture of starting material and product along with a yellow impurity was obtained. This crude mixture was carried forward for the next step. $R_f = 0.67$ (CH_2Cl_2 :MeOH, 50:1, on alumina).

^1H NMR (300 MHz, CDCl_3) δ 9.33 (dd, $J = 1.5, 0.9$ Hz, 1H, $\text{H}^{3'}$), 8.91 (dd, $J = 5.0, 0.9$ Hz, 1H, H^6), 8.78 (dd, $J = 2.6, 0.6$ Hz, 1H, H^3), 8.36 (dd, $J = 6.8, 0.6$ Hz, 1H, H^6), 7.95 (dd, $J = 5.0, 1.6$ Hz, 1H, $\text{H}^{5'}$), 7.89 (dd, $J = 6.8, 2.6$ Hz, 1H, H^5), 3.98 (s, 3H, $\text{H}^{8'}$), 3.97 (s, 3H, H^8).

Dimethyl-6-chloro-2,2'-bipyridine-4,4'-dicarboxylate (51)



Crude **14** (1.16 g) was combined with POCl_3 (10 mL), the mixture was stirred and heated to reflux at 120°C and the solid dissolved to form a yellow solution. After 2 h the solution had turned brown. The solution was cooled to rt and the remaining POCl_3 was removed by vacuum distillation at 85°C and 10 mbar. H_2O (50 mL) was added to the remaining solid, which was extracted with CH_2Cl_2 (4 x 50 mL) the organic phases were combined, and dried (MgSO_4), and the solvent removed under reduced pressure. The remaining solid was purified by column chromatography on silica (CHCl_3) to yield a white crystalline solid (0.66 g, 2.15 mmol, 12% over 2 steps). $R_f = 0.79$ (CH_2Cl_2 :MeOH 50:1, on silica);

Mp: $148\text{-}150^\circ\text{C}$;

^1H NMR (300 MHz, CDCl_3) δ 8.86 (dd, $J = 1.6, 0.9$ Hz, 1H, $\text{H}^{3'}$), 8.82 (d, $J = 1.3$ Hz, 1H, H^3), 8.79 (dd, $J = 4.9, 0.9$ Hz, 1H, $\text{H}^{6'}$), 7.86 (stack, 2H, $\text{H}^{5',5''}$), 3.94 (s, 3H, $\text{H}^{8'}$), 3.94 (s, 3H, H^8);

^{13}C NMR (100 MHz, CDCl_3) δ 165.6 ($\text{C}^{7'}$), 164.5 ($\text{C}^{7''}$), 157.1 (C^4), 155.2 ($\text{C}^{4'}$), 152.0 (C^6), 150.3 ($\text{C}^{6'}$), 141.4 (C^2), 138.9 ($\text{C}^{2'}$), 124.4 (C^3), 123.9 ($\text{C}^{3'}$), 121.0 (C^5), 119.4 ($\text{C}^{5'}$), 53.2 (C^8), 53.0 ($\text{C}^{8'}$);

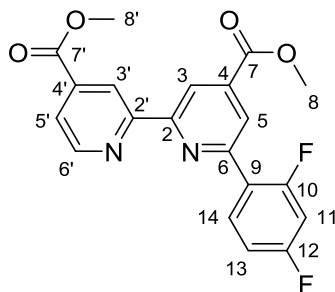
IR(film, cm^{-1}): 3093s (C-H), 3039s (C-H), 2961s (C-H), 1731s (C=O), 1592s (C=C), 1553s (C=C), 1466s (C-H), 1431s (C-H), 1359s (C-H), 1295s (C-O);

MS (TOF ES^+): m/z (%): 329.0 (100) $[\text{M}+\text{Na}]^+$;

HRMS (ES^+): $[\text{M}+\text{Na}]^+$ calcd. for $\text{C}_{14}\text{H}_{11}\text{N}_2\text{O}_4\text{Na}^{35}\text{Cl}$, 329.0305; found, 329.0301.

Data were in agreement with those reported in the literature.⁹⁰

Dimethyl-6-(2,4-difluorophenyl)-2,2'-bipyridine-4,4'-dicarboxylate (**52**)



51 (300 mg, 0.90 mmol, 1 eq), 2,4-difluorophenyl boronic acid (170 mg, 1.08 mmol, 1.1 eq), and Na_2CO_3 (114 mg, 1.08 mmol, 1.1 eq) were combined along with THF (50 mL) and H_2O (10 mL). The solvent was degassed with argon for 20 min. Tetrakis(triphenylphosphine)palladium(0) (51.8 mg 45.0 μmol , 5 mol %) was then added and the mixture degassed with argon for a further 10 min before stirring under argon at 70 $^\circ\text{C}$ for 21 h. After cooling to rt the solvent was removed under reduced pressure and CH_2Cl_2 (50 mL) and H_2O (50 mL) were added. The organic phase was separated and dried (MgSO_4) and the solvent was removed under reduced pressure. The resulting solid was purified by filtration through a pad of silica followed by column

chromatography on silica (CH₂Cl₂:Et₂O 9:1), to afford a white crystalline solid (205 mg, 0.53 mmol, 60%). *R_f* = 0.73 (CH₂Cl₂:Et₂O 9:1, on silica).

Mp: 163-164 °C;

¹H NMR (300 MHz, CDCl₃) δ 9.04 (dd, *J* = 1.6, 0.8 Hz, 1H, H^{3'}), 8.95 (d, *J* = 1.4 Hz, 1H, H³), 8.89 (dd, *J* = 5.0, 0.9 Hz, 1H, H^{6'}), 8.40 (dd, *J* = 2.0, 1.3 Hz, 1H, H⁵), 8.33 – 8.18 (m, 1H, H¹²), 7.93 (dd, *J* = 5.0, 1.6 Hz, 1H, H^{5'}), 7.16 – 7.04 (m, 1H, H¹³), 7.04 – 6.91 (ddd, *J* = 11.3, 8.8, 2.5 Hz, 1H, H¹¹), 4.02 (s, 3H, H^{8'}), 4.02 (s, 3H, H⁸);

¹³C NMR (100 MHz, CDCl₃) δ 165.9 (s, C⁷), 165.8 (s, C^{7'}), 163.8 (dd, *J* = 251.8, 11.8 Hz, C¹⁰), 161.1 (dd, *J* = 253.5, 11.9 Hz, C¹²), 156.6 (s, C⁴), 156.6 (s, C^{4'}), 153.1 (d, *J* = 1.9 Hz, C⁶), 150.2 (s, C^{6'}), 139.5 (s, C²), 138.7 (s, C^{2'}), 132.6 (dd, *J* = 9.6, 4.0 Hz, C¹⁴), 123.8 (d, *J* = 10.6 Hz, C⁵), 123.4 (s, C^{5'}), 123.1 (dd, *J* = 11.5, 4.5 Hz, C⁹), 120.8 (s, C³), 119.5 (s, C^{3'}), 112.3 (dd, *J* = 21.2, 3.3 Hz, C¹³), 104.7 (t, *J* = 26.2 Hz, C¹¹), 53.0 (s, 2C, C^{8,8'});

¹⁹F NMR (282 MHz, CDCl₃) δ -108.10 (d, *J* = 9.1 Hz, F¹⁷), -111.73 (d, *J* = 9.1 Hz, F¹⁸);

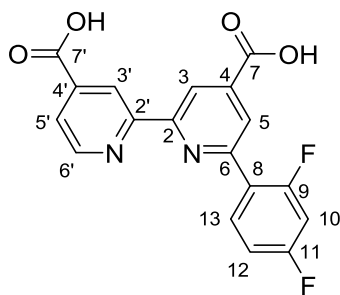
IR(film, cm⁻¹): 3089s (C-H), 3047s (C-H), 2964s (C-H), 1729 (C=O), 1616s (C=C), 1599 (C=C), 1559s (C=C), 1505s (C=C), 1443s (C-H), 1433s (C-H), 1382s (C-H), 1340s (C-H), 1299 (C-O);

MS (TOF ES⁺): *m/z* (%): 407.1 (100) [M+Na]⁺;

HRMS (ES⁺): [M+Na]⁺ calcd. for C₂₀H₁₄N₂O₄NaF₂, 407.0819; found, 407.0836.

Data were in agreement with those reported in the literature.⁹⁰

6-(2,4-Difluorophenyl)-2,2'-bipyridine-4,4'-dicarboxylic acid (54)



16 (205 mg, 0.53 mmol, 1 eq) and KOH (120 mg, 2.13 mmol, 4 eq), were combined with MeOH (10 mL) and H₂O (2 mL), and the resulting mixture was heated to 85 °C and stirred for 18 h. The solution was cooled to rt and neutralised with 2 M HCl solution (0.75 mL), causing a white precipitate to form. The precipitate was filtered and washed with H₂O (5 mL) followed by MeOH (5 mL) and dried under air and then under reduced pressure to yield a white solid (149 mg, 0.42 mmol, 79%).

Mp: >300 °C;

¹H NMR (400 MHz, DMSO) δ; 8.94 (d, *J* = 4.9 Hz, 1H, H^{6'}), 8.88 (s, 1H, H³), 8.84 (d, *J* = 1.2 Hz, 1H, H^{3'}), 8.25 (s, 1H, H⁵), 8.24 – 8.10 (td, *J* = 8.9, 6.9 Hz, 1H, H¹³), 7.94 (dd, *J* = 4.9, 1.5 Hz, 1H, H^{5'}), 7.54 – 7.43 (ddd, *J* = 11.7, 9.3, 2.4 Hz, 1H, H¹⁰), 7.42 – 7.29 (td, *J* = 8.5, 2.4 Hz, H¹²);

¹³C NMR (100 MHz, DMSO) δ; 166.1 (s, C⁷), 165.8 (s, C^{7'}), 162.7 (dd, *J* = 206.4, 11.4 Hz, C⁹), 160.3 (dd, *J* = 252.2, 12.2 Hz, C¹¹), 155.7 (s, C²), 155.3 (s, C^{2'}), 152.5 (s, C⁶), 150.6 (s, C^{6'}), 140.9 (s, C⁴), 139.8 (s, C^{4'}), 132.4 (dd, *J* = 13.2, 10.1 Hz, C¹³), 123.7 (s, C^{5'}), 123.3 (d, *J* = 8.4 Hz, C⁵), 119.6 (s, C³), 118.8 (s, C^{3'}), 112.5 (dd, *J* = 21.5, 2.9 Hz, C¹²), 104.9 (t, *J* = 26.6 Hz, C¹⁰);

¹⁹F NMR (282 MHz, MeOD) δ -109.14 (d, *J* = 9.0 Hz, 1F, F⁹), -112.64 (d, *J* = 9.0 Hz, 1F, F¹¹);

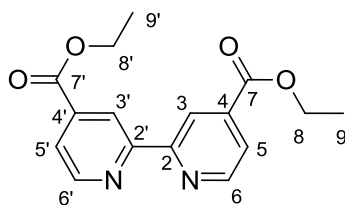
IR(film, cm⁻¹): 3091s (C-H), 1736 (C=O), 1619s (C=C), 1601 (C=C), 1559s (C=C), 1507s (C=C), 1444s (C-H), 1422s (C-H), 1385s (C-H), 1248 (C-O);

MS (TOF ES⁻): *m/z* (%): 377.0 (100) [M+Na-2H]⁻, 355.0 (77) [M-H]⁻, 310.0 (96) [M-CH₂O₂]⁻;

HRMS (ES⁻): [M-H]⁻ calcd. for C₁₈H₉N₂O₄F₂, 355.0529; found, 355.0530.

Data were in agreement with those reported in the literature.⁹⁰

Diethyl-2,2'-bipyridine-4,4'-dicarboxylate (**56**)



2,2'-Bipyridine-4,4'-dicarboxylic acid (4.00 g, 16.4 mmol) was combined with ethanol (60 mL) to form a suspension, to which was added H₂SO₄ (98%, 10 mL). The mixture was heated to reflux at 100 °C whilst stirred, and the solid dissolved slowly to form a pink solution. The heating continued for 72 h. After cooling to rt ethanol (100 mL) was added followed by an aqueous solution of Na₂CO₃ (20 g Na₂CO₃ in 100 mL H₂O) which was added slowly until the pH was increased to 8, causing a white precipitate and evolution of CO₂. The resulting suspension was extracted with CHCl₃ (3 x 300 mL), the organic phases were combined and dried (MgSO₄) and the solvent removed under reduced pressure to afford a white crystalline solid (3.54 g, 11.8 mmol, 72%). *R_f* = 0.93 (CH₂Cl₂, on silica).

Mp: 159-161 °C;

¹H NMR (300 MHz, CDCl₃) δ 8.94 (dd, *J* = 1.7, 0.9 Hz, 1H, H^{3,3'}), 8.87 (dd, *J* = 5.0, 0.9 Hz, 1H, H^{6,6'}), 7.91 (dd, *J* = 5.0, 1.6 Hz, 1H, H^{5,5'}), 4.45 (q, *J* = 7.1 Hz, 4H, H^{8,8'}), 1.43 (t, *J* = 7.1 Hz, 6H, H^{9,9'});

¹³C NMR (100 MHz, CDCl₃) δ 165.2 (C^{7,7'}), 156.5 (C^{4,4'}), 150.1 (C^{2,2'}), 139.2 (C^{6,6'}), 123.4 (C^{3,3'}), 120.8 (C^{5,5'}), 62.1 (C^{8,8'}), 14.4 (C^{9,9'});

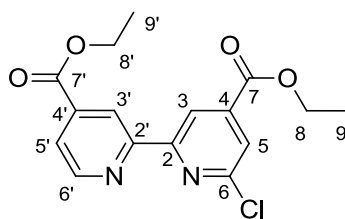
IR(film, cm⁻¹): 2993s (C-H), 2973s (C-H), 2945s (C-H), 2930s (C-H), 2906s (C-H), 2876s (C-H), 1725s (C=O), 1597s (C=C), 1557s (C=C), 1470s (C-H), 1448 (C-H), 1398s (C-H), 1372s (C-H), 1362s (C-H), 1286s (C-O);

MS (TOF EI⁺): *m/z* (%): 228.1 (100), 300.1 (8) [M]⁺;

HRMS (EI⁺): [M]⁺ calcd. for C₁₆H₁₆N₂O₄, 300.1110; found, 300.1109.

Data were in agreement with those reported in the literature.¹²⁴

Diethyl-6-chloro-2,2'-bipyridine-4,4'-dicarboxylate (57)



20 (3.40 g, 11.3 mmol, 1 eq) was dissolved in CHCl₃ (70 mL), to which a solution of *m*CPBA (2.55 g, 14.8 mmol, 1.3 eq) in CHCl₃ (50 mL) was added slowly at rt, producing a yellow solution. After stirring at 30 °C for 36 h the reaction mixture was washed with an aqueous solution Na₂CO₃ (10 g Na₂CO₃ in 100 mL H₂O) followed by 2 x 100 mL H₂O. The organic phase was dried with MgSO₄, and the solvent removed under reduced pressure to yield 3.3 g of the crude oxide as a yellow solid. The crude oxide was then combined with POCl₃ (15 mL), the mixture was stirred and heated to reflux at 120 °C and the solid dissolved to form a yellow solution. After 2.5 h the solution had turned brown. The solution was cooled to rt and the remaining POCl₃ was removed by vacuum distillation at 85 °C and 10 mbar. H₂O (50 mL) was added to the remaining solid, which was extracted with CH₂Cl₂ (4 x 50 mL) the organic phases were combined, and dried (MgSO₄), and the solvent removed under reduced pressure. The remaining solid was purified by column chromatography on silica (CH₂Cl₂:Et₂O 30:1), and washed with hexanes (5 mL) to yield a white crystalline solid (1.34 g, 4.00 mmol, 35% over 2 steps). *R*_f = 0.85 (CH₂Cl₂:Et₂O 9:1, on silica).

Mp: 132-134 °C;

¹H NMR (300 MHz, CDCl₃) δ 8.91 (dd, *J* = 1.6, 0.9 Hz, 1H, H^{3'}), 8.88 (d, *J* = 1.3 Hz, 1H, H³), 8.85 (dd, *J* = 5.0, 0.9 Hz, 1H, H^{6'}), 7.97 – 7.88 (stack, 2H, H^{5,5'}), 4.52 – 4.40 (stack, 4H, H^{8,8'}), 1.52 – 1.39 (stack, 6H, H^{9,9'});

¹³C NMR (100 MHz, CDCl₃) δ 165.2 (C⁷), 164.1 (C^{7'}), 157.2 (C⁴), 155.3 (C^{4'}), 152.0 (C⁶), 150.3 (C^{6'}), 141.9 (C²), 139.3 (C^{2'}), 124.4 (C³), 123.9 (C^{3'}), 121.0 (C⁵), 119.4 (C^{5'}), 62.4 (C⁸), 62.2 (C^{8'}), 14.4 (C⁹), 14.4 (C^{9'});

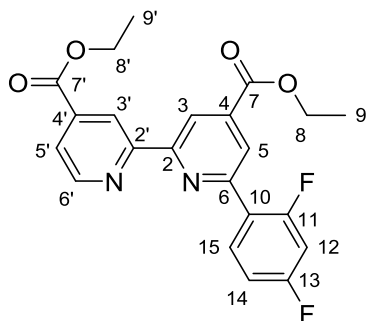
IR(film, cm⁻¹): 3096s (C-H), 3002s (C-H), 2984s (C-H), 2945s (C-H), 2906s (C-H), 1723s (C=O), 1589s (C=C), 1552s (C=C), 1466s (C-H), 1445s (C-H), 1419s (C-H), 1394s (C-H), 1356s (C-H), 1322s (C-H), 1297s (C-O);

MS (TOF ES⁺): *m/z* (%): 357.1 (100) [M+Na]⁺;

HRMS (ES⁺): [M+Na]⁺ calcd. for C₁₆H₁₅N₂O₄Na³⁵Cl, 357.0618; found, 357.0633.

Data were in agreement with those reported in the literature.¹²⁵

Diethyl-6-(2,4-difluorophenyl)-2,2'-bipyridine-4,4'-dicarboxylate (58)



21 (800 mg, 2.39 mmol, 1 eq), 2,4-difluorophenyl boronic acid (453 mg, 2.87 mmol, 1.2 eq), and Na₂CO₃ (304 mg, 2.87 mmol, 1.2 eq) were combined along with THF (50 mL) and H₂O (10 mL). The solvent was degassed with argon for 20 min. Tetrakis(triphenylphosphine)palladium(0) (138 mg 119 μmol, 5 mol %) was then added and the mixture degassed with argon for a further 10 min before stirring under argon at 70 °C for 16 h. After cooling to rt the solvent was removed under reduced pressure and CH₂Cl₂ (100 mL) and H₂O (50 mL) were added and the organic phase extracted. The aqueous phase was extracted with a further 2 portions of CH₂Cl₂ (100 mL). The organic phases were combined and dried (MgSO₄) and the solvent was removed under reduced pressure. The resulting solid was purified by column chromatography on silica (CH₂Cl₂:Et₂O 9:1) followed by a further silica column (CH₂Cl₂), to afford a white crystalline solid (716 mg, 1.74 mmol, 73%). *R_f* = 0.83 (CH₂Cl₂:Et₂O 9:1, on silica).

Mp: 123-125 °C

¹H NMR (400 MHz, CDCl₃) δ 9.03 (s, *J* = 0.7 Hz, 1H, H^{3'}), 8.93 (d, *J* = 1.3 Hz, 1H, H₃), 8.88 (d, *J* = 4.9 Hz, 1H, H^{6'}), 8.39 (t, *J* = 1.5 Hz, 1H, H⁵), 8.25 (td, *J* = 8.8, 6.7 Hz, 1H, H¹⁵), 7.91 (dd, *J* = 5.0, 1.6 Hz, 1H, H^{5'}), 7.08 (td, *J* = 8.3, 2.5 Hz, 1H, H¹⁴), 6.98 (ddd, *J* = 11.3, 8.8, 2.5 Hz, 1H, H¹²), 4.48 (stack, 4H, H^{8,8'}), 1.46 (stack, 6H, H^{9,9'});

¹³C NMR (100 MHz, CDCl₃) δ 165.4 (s, C^{7'}), 165.3 (s, C⁷), 163.8 (dd, *J* = 250.1, 10.2 Hz, C¹¹), 161.1 (dd, *J* = 251.8, 9.9 Hz, C¹³), 156.7 (s, C²), 156.44 (s, C^{2'}), 153.1 (s, C⁶), 150.2 (s, C^{6'}), 140.0 (s, C⁴), 139.1 (s, C^{4'}), 132.6 (dd, *J* = 9.6, 3.9 Hz, C¹⁵), 123.8 (d, *J* = 10.7 Hz, C⁵), 123.4 (s, C^{5'}), 123.1 (dd, *J* = 11.3, 3.6 Hz, C^{3'}), 120.8 (s, C³), 119.4 (s, C¹⁴), 112.2 (dd, *J* = 21.1, 3.4 Hz, C¹²), 104.7 (t, *J* = 26.1 Hz, C¹⁵), 62.1 (s, C^{8'}), 62.08 (s, C⁸), 14.5 (s, C^{9'}), 14.4 (s, C⁹);

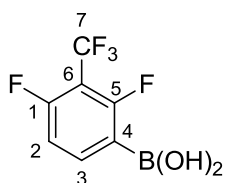
^{19}F NMR (282 MHz, CDCl_3) δ -108.21 (d, $J = 9.0$ Hz, 1F, F^{13}), -111.70 (d, $J = 9.0$ Hz, 1F, F^{11});

IR(film, cm^{-1}): 3095s (C-H), 2987s (C-H), 2948s (C-H), 2906s (C-H), 2882s (C-H), 1731 (C=O), 1719 (C=O), 1620s (C=C), 1597 (C=C), 1560s (C=C), 1506s (C=C), 1478s (C-H), 1441s (C-H), 1382s (C-H), 1368s (C-H), 1275 (C-O);

MS (TOF ES^+): m/z (%): 413.1 (100) $[\text{M}+\text{H}]^+$;

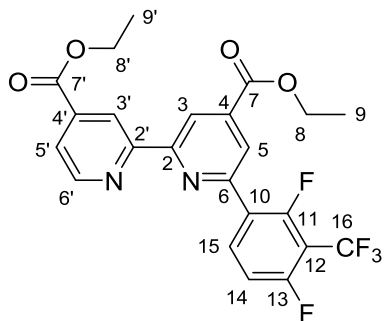
HRMS (ES^+): $[\text{M}+\text{H}]^+$ calcd. for $\text{C}_{22}\text{H}_{19}\text{N}_2\text{O}_4\text{F}_2$, 413.1304; found, 413.1313.

2,4-Difluoro-3-(trifluoromethyl)phenyl boronic acid (60)



A 100 mL 2 neck round bottom flask fitted with addition funnel, septum and stopcock was flame dried under vacuum and filled with argon. 2,6-Difluorobenzotrifluoride (5.00 g, 27.5 mmol, 1 eq) and dry THF (50 mL) were added to the reaction vessel, and the resulting solution cooled to -78 °C. *n*BuLi (1.4 M in toluene, 25.5 mL, 35.8 mmol, 1.3 eq), was then added slowly dropwise to the stirred solution. The resulting dark red solution was stirred at -78 °C for 1 h before the addition of trimethylborate (2.28 g, 41.25 mmol, 1.3 eq). The resulting solution allowed to warm to rt turning pale yellow and was then stirred under argon for 16 h. HCl (3 M, 100 mL) was then added slowly dropwise and the solution stirred for further 1 h. The reaction mixture was then neutralised by careful addition of Na_2CO_3 (20 g in 100 mL H_2O). The organic phase was extracted and the aqueous phase extracted with CH_2Cl_2 (3 x 100 mL). The organic phases were combined dried (MgSO_4) and solvent removed under reduced pressure to yield a crude brown solid (3.57 g) which was carried forward.

Diethyl-6-(2,4-difluoro-3-(trifluoromethyl)phenyl)-2,2'-bipyridine-4,4'-dicarboxylate (61)



57 (500 mg, 1.49 mmol, 1 eq), **60** (506 mg, ≈ 2.24 mmol, ≈ 1.5 eq), and Na_2CO_3 (237 mg, 2.24 mmol, 1.5 eq) were combined along with THF (75 mL) and H_2O (15 mL). The solvent was degassed with argon for 20 min. Tetrakis(triphenylphosphine)palladium(0) (86 mg 74.4 μmol , 5 mol %) was then added and the mixture degassed with argon for a further 10 min before stirring under argon at 70 $^\circ\text{C}$ for 16 h. After cooling to rt the solvent was removed under reduced pressure and CH_2Cl_2 (50 mL) and H_2O (50 mL) were added and the organic phase extracted, dried (MgSO_4) and the solvent was removed under reduced pressure. The resulting solid was purified by column chromatography on silica (CH_2Cl_2 : Et_2O 9:1) to afford a white crystalline solid (481 mg, 1.00 mmol, 67%). $R_f = 0.74$ (CH_2Cl_2 : Et_2O 9:1, on silica);

Mp: 126-128 $^\circ\text{C}$;

^1H NMR (400 MHz, CDCl_3) δ 9.00 (dd, $J = 1.4, 0.8$ Hz, 1H, H^3), 8.98 (d, $J = 1.3$ Hz, 1H, H^3), 8.88 (dd, $J = 5.0, 0.7$ Hz, 1H, H^6), 8.44 – 8.38 (m, 1H, H^{15}), 8.38 (dd, $J = 2.3, 1.3$ Hz, 1H, H^5), 7.92 (dd, $J = 5.0, 1.6$ Hz, 1H, H^5), 7.22 (t, $J = 9.2$ Hz, 1H, H^{14}), 4.48 (m, 4H, $\text{H}^{8,8'}$), 1.46 (m, Hz, 6H, $\text{H}^{9,9'}$);

^{13}C NMR (100 MHz, CDCl_3) δ 165.3 (s, C^7), 165.0 (s, C^7), 160.6 (dd, $J = 258.0, 31.6$ Hz, C^{13}), 158.0 (dd, $J = 259.9, 31.2$ Hz, C^{11}), 156.8 (s, C^2), 156.3 (s, $\text{C}^{2'}$), 151.8 (s, C^6), 150.3 (s, $\text{C}^{6'}$), 140.2 (s, C^4), 139.1 (s, $\text{C}^{4'}$), 135.8 (dd, $J = 10.5, 5.0$ Hz, C^{15}), 124.5 (dd, $J = 12.2, 3.8$ Hz, C^{10}), 124.0 (d, $J = 10.4$ Hz, C^5), 123.5 (s, $\text{C}^{5'}$), 120.8 (s, C^3), 120.12 (s, $\text{C}^{3'}$), 113.4 (dd, $J = 22.3, 3.7$ Hz, C^{14}), 62.3 (s, C^8), 62.1 (s, $\text{C}^{8'}$), 14.4 (s, $\text{C}^{9'}$), 14.4 (s, C^9). Expected signals for C_{12} (approx. 120 (tq, $J = 30, 30$ Hz)) and C_{16} (approx. 120 (tq, $J = 250, 10$ Hz)) not observed due to high level of splitting giving a very weak signal. ^1H , ^{19}F and HRMS confirm structure is correct.

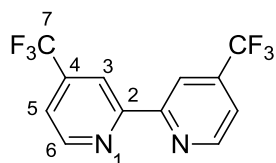
^{19}F NMR (282 MHz, CDCl_3) δ -56.12 (t, $J = 22.9$ Hz, 3F, F^9), -108.72 (qd, $J = 24.0, 3.2$ Hz, 1F, F^{13}), -113.95 (qd, $J = 22.7, 3.2$ Hz, 1F, F^{11});

IR(film, cm^{-1}): 3098w (C-H), 3071w (C-H), 2991s (C-H), 2944w (C-H), 2906w (C-H), 1727s (C=O), 1715s (C=O), 1626s (C=C), 1596s (C=C), 1561s (C=C), 1495s (C-H), 1470s (C-H), 1452s (C-H), 1381s (C-H), 1369s (C-H), 1317s (C-H), 1295s (C-O);

MS (TOF ES^+): m/z (%): 480.1 (100) $[\text{M}]^+$;

HRMS (ES^+): $[\text{M}]^+$ calcd. for $\text{C}_{23}\text{H}_{17}\text{N}_2\text{O}_4\text{F}_5$, 480.1108; found, 480.1109.

4,4'-bis(trifluoromethyl)-2,2'-bipyridine (63)



Activated zinc was prepared by washing ground zinc with 0.5 M HCl followed by water, ethanol, and Et_2O ; the washed zinc and tetraethylammonium iodide were dried under vacuum overnight. The activated zinc (1.09 g, 16.7 mmol, 4.5 eq) and tetraethylammonium iodide (2.22 g, 3.00 mmol, 0.9 eq) were combined with dibromobis(triphenylphosphine)-nickel(II) (2.48 g, 3.30 mmol, 1.0 eq) under argon, to which anhydrous THF (40 mL) was added. After the dark suspension was stirred at room temperature for 30 min, 2-chloro-4-(trifluoromethyl)pyridine (2.00 g, 11.1 mmol, 3.0 eq) was injected by syringe, and the reaction was stirred at 50 °C for an additional 48 h under argon. The black slurry was poured into 2 M ammonium hydroxide (120 mL), mixed with CHCl_3 (120 mL). The organic layer was separated, dried with anhydrous MgSO_4 , and evaporated under reduced pressure. The brown residue was purified by silica gel column chromatography (hexane: CH_2Cl_2 4:1), to afford a white powder (1.81 g, 6.19 mmol, 44%).

Mp: 78-79 °C;

^1H NMR (400 MHz, CDCl_3) δ 8.80 (d, $J = 5.0$ Hz, 2H, H^6), 8.64 (s, 2H, H^3), 7.50 (dd, $J = 5.0, 1.0$ Hz, 2H, H^5);

^{13}C NMR (100 MHz, CDCl_3) δ 156.1 (s, C^2), 150.3 (s, C^6), 139.6 (q, $J = 34.3$ Hz, C^4), 122.8 (q, $J = 273.4$ Hz, C^7), 119.9 (d, $J = 3.3$ Hz, C^5), 117.1 (dd, $J = 6.9, 3.3$ Hz, C^3);

^{19}F NMR (282 MHz, CDCl_3) δ -64.94 (s, 6F, F^7);

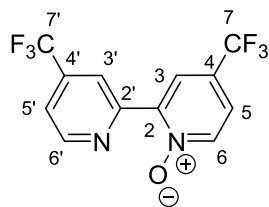
IR(film, cm^{-1}): 3108s (C-H), 3080s (C-H), 3049 (C-H), 1608s (C=C), 1571s (C=C), 1461s (C-H), 1375s (C-H), 1319s (C-H);

MS (TOF ES⁺): m/z (%): 293.1(100) [$\text{M}+\text{H}$]⁺;

HRMS (ES⁺): [$\text{M}+\text{H}$]⁺ calcd. for $\text{C}_{12}\text{H}_7\text{N}_2\text{F}_6$, 293.0513; found, 293.0512.

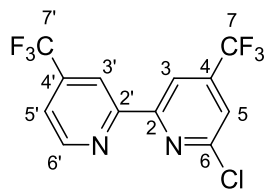
Data were in agreement with those reported in the literature.¹²⁴

4,4'-(Trifluoromethyl)-2,2'-bipyridine-1-oxide (64)



63 (500 mg, 1.71 mmol, 1.0 eq) was dissolved in CHCl_3 (20 mL), to which a solution of *m*CPBA (578 mg, 1.71 mmol, 1.0 eq), in CHCl_3 (10 mL) was added slowly at rt, producing a yellow solution. After stirring at 50 °C for 16 h the reaction mixture was washed with an aqueous solution Na_2CO_3 (10 g Na_2CO_3 in 100 mL H_2O) followed by 2 x 100 mL H_2O . The organic phase was dried with MgSO_4 , and the solvent removed under reduced pressure to yield 500 mg of the crude oxide as a yellow solid.

6-Chloro-4,4'-bis(trifluoromethyl)-2,2'-bipyridine (65)



64 (500 mg, crude) was combined with POCl_3 (10 mL), the mixture was degassed with argon before being stirred and heated to reflux at 120 °C. After 1.5 h the solution was cooled to rt and

the remaining POCl₃ was removed by vacuum distillation at 50 °C and 10⁻³ mbar. H₂O (50 mL) was added to the remaining solid, which was extracted with CH₂Cl₂ (4 x 50 mL) the organic phases were combined, and dried (MgSO₄), and the solvent removed under reduced pressure. The remaining solid was purified by column chromatography on silica (hexane:CH₂Cl₂ 3:1), to yield a white crystalline solid (250 mg, 765 μmol, 45%). *R*_f = 0.30 (hexane:CH₂Cl₂ 3:1, on silica).

Mp: 57-58 °C;

¹H NMR (300 MHz, CDCl₃) δ 8.77 (d, *J* = 5.0 Hz, 1H, H⁶), 8.56 (s, 1H, H^{3'}), 8.55 (s, 1H, H³), 7.51 (s, 2H, H^{5'}, H⁵)

¹³C NMR (100 MHz, CDCl₃) δ 156.72 (s, C⁶), 154.60 (s, C²), 152.05 (s, C^{2'}), 150.35 (s, C^{6'}), 142.13 (q, *J* = 34.8 Hz, C⁷), 139.76 (q, *J* = 34.4 Hz, C^{7'}), 122.37 (q, *J* = 273.6 Hz, C^{4'}), 122.36 (q, *J* = 273.6 Hz, C⁴), 120.93 (d, *J* = 3.4 Hz, C^{3'}), 120.39 (d, *J* = 3.3 Hz, C³), 117.33 (dd, *J* = 6.7, 3.2 Hz, C⁵), 115.78 (dd, *J* = 6.4, 3.1 Hz, C^{5'});

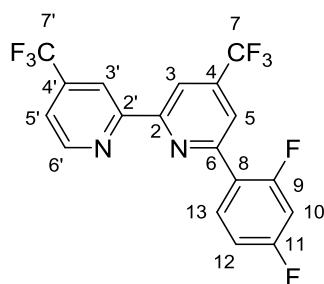
¹⁹F NMR (282 MHz, CDCl₃) δ -64.72 - -64.99 (m, 6F, F^{7,7'});

IR(film, cm⁻¹): 3106s (C-H), 3094s (C-H), 1597s (C=C), 1562s (C=C), 1478s (C=C), 1420s (C=C), 1372s (C-H), 1317s (C-H);

MS (TOF ES⁺): *m/z* (%): 293.1(100) [M+H]⁺;

HRMS (ES⁺): [M+H]⁺ calcd. for C₁₂H₅N₂F₆Cl, 326.0045; found, 326.0051.

6-(2,4-Difluorophenyl)-4,4'-bis(trifluoromethyl)-2,2'-bipyridine (67)



65 (150 mg, 459 μmol, 1.0 eq), 2,4-difluorophenyl boronic acid (156 mg, 689 μmol, 1.5 eq), and Na₂CO₃ (73.0 mg, 689 μmol, 1.5 eq) were combined along with THF (25 mL) and H₂O (5 mL),

The solvent was degassed with argon for 20 min. Tetrakis(triphenylphosphine)palladium(0) (26.6 mg 23.0 μmol , 5 mol%) was then added and the mixture degassed with argon for a further 10 min before stirring under argon at 70 °C for 16 h. After cooling to rt the solvent was removed under reduced pressure and CH_2Cl_2 (50 mL) and H_2O (50 mL) were added and the organic phase extracted, dried (MgSO_4) and the solvent was removed under reduced pressure. The crude product was purified by column chromatography on silica (hexane: CH_2Cl_2 3:1) to afford a white crystalline solid (201 mg, 426 μmol , 93%). $R_f = 0.25$ (hexane: CH_2Cl_2 3:1, on silica).

Mp: 112-114 °C;

^1H NMR (300 MHz, CDCl_3) δ 8.90 (d, $J = 5.0$ Hz, 1H, H^6), 8.83 – 8.72 (m, 1H, H^3), 8.69 (d, $J = 0.6$ Hz, 1H, H^3), 8.22 (td, $J = 8.9, 6.6$ Hz, 1H, H^{13}), 8.06 (s, 1H, H^5), 7.61 (dd, $J = 5.0, 1.0$ Hz, 1H, H^5), 7.18 – 7.06 (m, 1H, H^{12}), 6.99 (ddd, $J = 11.3, 8.7, 2.5$ Hz, 1H, H^{10});

^{13}C NMR (100 MHz, CDCl_3) δ 163.91 (dd, $J = 252.8, 12.3$ Hz, $\text{C}^{9,11}$), 161.04 (dd, $J = 253.8, 12.0$ Hz, $\text{C}^{9,11}$), 156.07 (s, C^2), 155.88 (s, C^2), 153.25 (d, $J = 2.4$ Hz, C^6), 150.32 (s, C^6), 141.15 – 140.00 (m, C^4), 139.98 – 139.01 (m, C^4), 132.32 (dd, $J = 9.7, 3.8$ Hz, C^{13}), 122.23 (d, $J = 7.3$ Hz, $\text{C}^{7,7'}$), 127.76 – 118.19 (m, C^8), 120.22 (dd, $J = 11.2, 3.4$ Hz, C^5), 119.98 (d, $J = 3.4$ Hz, C^5), 117.00 (dd, $J = 6.8, 3.3$ Hz, C^3), 115.82 (d, $J = 3.4$ Hz, C^3), 112.36 (dd, $J = 21.3, 3.3$ Hz, C^{12}), 104.73 (t, $J = 26.3$ Hz, C^{10});

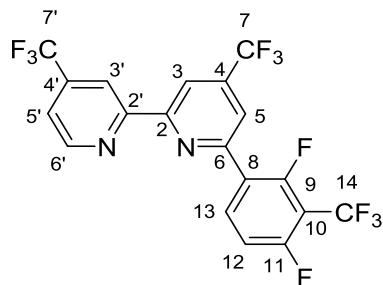
^{19}F NMR (282 MHz, CDCl_3) δ -64.73 (d, $J = 6.6$ Hz, 3F, $\text{F}^{7,7'}$), -89.06 – -109.68 (m, 1F, F^9), -111.72 (dd, $J = 20.3, 9.5$ Hz, 1F, F^{11});

IR(film, cm^{-1}): 3094s (C-H), 3054s (C-H), 2969s (C-H), 1620s (C=C), 1608s (C=C), 1568s (C=C), 1507s (C=C), 1484s (C=C), 1443s (C=C), 1394s (C-H), 1362s (C-H);

MS (TOF ES+): m/z (%): 293.1(100) [$\text{M}+\text{H}$] $^+$;

HRMS (ES+): [$\text{M}+\text{H}$] $^+$ calcd. for $\text{C}_{18}\text{H}_8\text{N}_2\text{F}_8$, 404.0560; found, 404.0558.

6-(2,4-Difluoro-3-(trifluoromethyl)phenyl)-4,4'-bis(trifluoromethyl)-2, 2'-bipyridine (68)



65 (75.0 mg, 0.23 mmol, 1.0 eq), **60** (77.8 mg, 0.34 mmol, 1.5 eq), and Na_2CO_3 (73.0 mg, 689 μmol , 1.5 eq) were combined along with THF (25 mL) and H_2O (5 mL). The solvent was degassed with argon for 20 min. Tetrakis(triphenylphosphine)palladium(0) (14.6 mg, 12.6 μmol , 5 mol%) was then added and the mixture degassed with argon for a further 10 min before stirring under argon at 70 $^\circ\text{C}$ for 16 h. After cooling to rt the solvent was removed under reduced pressure and CH_2Cl_2 (50 mL) and H_2O (50 mL) were added and the organic phase extracted, dried (MgSO_4) and the solvent was removed under reduced pressure. The crude product was purified by column chromatography on silica (hexane: Et_2O 30:1) to afford a white crystalline solid (85.0 mg, 0.18 mmol, 86%). $R_f = 0.30$ (hexane: Et_2O 30:1, on silica).

Mp: 114-115 $^\circ\text{C}$;

^1H NMR (400 MHz, CDCl_3) δ 8.85 (d, $J = 5.0$ Hz, 1H, $\text{H}^{6'}$), 8.68 (s, 1H, H^3), 8.65 (s, 1H, $\text{H}^{3'}$), 8.32 (td, $J = 8.6, 6.3$ Hz, 1H, H^{13}), 8.00 (s, 1H, H^5), 7.56 (d, $J = 4.7$ Hz, 1H, $\text{H}^{5'}$), 7.32 – 6.79 (m, 1H, H^{12});

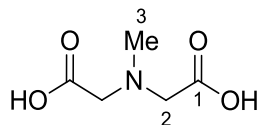
^{13}C NMR (100 MHz, CDCl_3) δ 159.32 (stack, $\text{C}^{9,11}$), 156.26 (s, $\text{C}^{2'}$), 155.73 (s, C^2), 152.02 (s, C^6), 150.44 (s, $\text{C}^{6'}$), 141.36 -140.08 (m, C^4), 140.34 – 138.95 (m, $\text{C}^{4'}$), 135.53 (dd, $J = 10.7, 4.7$ Hz, C^{13}), 123.57 (dd, $J = 11.7, 3.8$ Hz, C^8), 122.77 (q, $J = 273.6$, $\text{C}^{7,7'}$), 120.79 - 120.34 (m, C^5), 120.19 (d, $J = 3.3$ Hz, $\text{C}^{5'}$), 116.98 (d, $J = 3.4$ Hz, C^3), 116.58 (d, $J = 3.4$ Hz, $\text{C}^{3'}$), 113.59 (dd, $J = 22.3, 3.6$ Hz, C^{12}). Expected signals for C^{10} (approx. 120 (tq, $J = 30, 30$ Hz)) and C^{14} (approx. 120 (tq, $J = 250, 10$ Hz)) not observed due to high level of splitting giving a very weak signal;

^{19}F NMR (282 MHz, CDCl_3) δ -56.17 (t, 3F, $J = 23.4$ Hz, F^{14}), -64.60 – -64.72 (m, 3F, F^7), -64.72 – -64.84 (m, 3F, $\text{F}^{7'}$), -105.72-108.90 (m, 1F, F^9), -111.54 – -116.49 (m, 1F, F^{11});

MS (TOF ES+): m/z (%): 293.1(100) $[\text{M}+\text{H}]^+$;

HRMS (ES⁺): [M+H]⁺ calcd. for C₁₉H₇N₂F₁₁, 472.0434.0045; found, 472.0451.

N-Methyliminodiacetic acid (80)



A 250 mL 3 neck round bottom flask fitted with 100 mL addition funnel, thermometer and magnetic stirrer, was charged with iminodiacetic acid (25.0 g, 188 mmol, 1 eq) and formaldehyde solution (37 wt% in H₂O, 21 mL, 282 mmol, 1.5 eq). A reflux condenser was fitted and the white suspension heated to 90 °C and stirred. After 30 min formic acid (14.2 mL, 376 mmol, 2 eq) was added slowly dropwise over 5 min via addition funnel. The resulting mixture was then heated and stirred at 90 °C for a further 1 h. EtOH (190 mL) was added slowly dropwise to the stirred yellow solution causing a white precipitate to form. The solid was collected by vacuum filtration and washed with EtOH (4 x 50 mL). The product was then dried under vacuum to yield a white powder (23.3 g, 157 mmol, 84%).

Mp: 218-219 °C;

¹H NMR (300 MHz, D₂O) δ 3.93 (s, 1H, H²), 2.95 (s, 1H, H³);

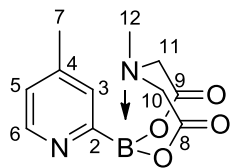
¹³C NMR (100 MHz, D₂O) δ 169.1 (C¹), 57.3 (C²), 42.6 (C³);

IR(film, cm⁻¹): 3000s (C-H), 2968s (C-H), 2792br (O-H) 1685br (C=O), 1329s (C-O);

MS (TOF ES⁺): *m/z* (%): 148.1 (100) [M+H]⁺;

HRMS (ES⁺): [M+H]⁺ calcd. For C₅H₁₀NO₄, 148.0610; found, 148.0613.

4-Methyl-2-pyridylboronic acid MIDA ester (73)



Method 1

A 250 mL 3 neck flask equipped with a tap and stirrer bar was flame dried under vacuum, filled with argon and charged with THF (30 mL), 2-bromo-4-methylpyridine (3.10 g, 18.0 mmol, 1 eq) and triisopropylborate (4.06 g, 21.6 mmol, 1.2 eq) *via* a septum. The resulting mixture was cooled to -78 °C and then *n*BuLi (12.9 mL, 18.0 mmol, 1 eq) was slowly added dropwise with stirring over 20 min, to give a dark red solution. This was stirred at -78 °C for one hour before warming to 23 °C and stirred for a further 3 h. A 250 mL flask fitted with a short path distillation apparatus and a pressure equalising addition funnel was charged with DMSO (30 mL) and **36** (4.50 g, 30.6 mmol, 1.7 eq) and the resulting mixture was heated to 115 °C. The boronate suspension was then added to the addition funnel and combined with the hot DMSO mixture by dropwise addition over one hour. The THF and DMSO were removed by distillation and the remaining orange residue was adsorbed onto celite (15 g) from a suspension in MeCN (200 mL) the solvent was removed under reduced pressure and the resulting celite mixture was left under high vacuum for 15 h. The celite mixture then underwent column chromatography (MeCN:Et₂O, 95:5 → 100:0), to yield a yellow solid (1.6 g). The remaining MIDA boronate by products were removed by recrystallization: The crude yellow solid was dissolved in hot MeCN (28 mL), and cooled to rt. CH₂Cl₂ (100 mL) was added dropwise to the stirred solution followed by Et₂O (300mL). The resulting off white precipitate was collected and dried under vacuum to afford a white solid crystalline product (1.12 g, 4.50 mmol, 25%). *R_f* = 0.29 (MeCN on silica).

Method 2

A 250 mL 3 neck flask equipped with a tap and stirrer bar was flame dried under vacuum, filled with argon and charged with anhydrous THF (70 mL), 2-bromo-4-methylpyridine (5.00 g, 29.1 mmol, 1 eq) and triisopropylborate (6.56 g, 34.9 mmol, 1.2 eq) *via* a septum. The resulting mixture was cooled to -78 °C and then *n*BuLi (1.6 M in hexane, 20 mL, 32.0 mmol, 1.1 eq) was slowly added dropwise with stirring over 20 min, to give a dark red solution. This was stirred at -78 °C for one hour before warming to 23 °C and stirred for a further 3 h. A 250 mL flask fitted with a short path distillation apparatus and a pressure equalising addition funnel was charged with anhydrous DMF (100 mL) and **36** (6.84 g, 46.5 mmol, 1.6 eq) and the resulting mixture was heated to 115 °C. The boronate suspension was then added to the addition funnel and combined with the hot DMF mixture by dropwise addition over one hour. A white precipitate formed, after cooling to rt this was removed by vacuum filtration. The filtrate was concentrated under reduced

pressure and the resulting brown solid was recrystallised by the addition of MeCN (10 mL) followed by CH₂Cl₂ (50 mL) and Et₂O (100 mL). The crude product was then purified by column chromatography on silica (MeCN:Et₂O, 95:5 → 100:0), to yield an off-white solid crystalline product (1.80 g, 7.23 mmol, 25%). *R*_f = 0.29 (MeCN on silica).

¹H NMR (300 MHz, CD₃CN) δ 8.52 (dd, *J* = 5.0, 0.6 Hz, 1H, H⁶), 7.50 – 7.48 (m, 1H, H³), 7.14 (ddd, *J* = 5.0, 1.8, 0.7 Hz, 1H, H⁵), 4.10 (d, *J* = 16.8 Hz, 2H, H¹¹), 3.98 (d, *J* = 16.8 Hz, 2H, H¹⁰), 2.55 (s, 3H, H¹²), 2.34 (s, 3H, H⁷);

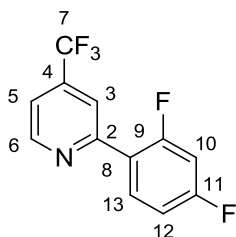
¹³C NMR (100 MHz, CD₃CN) δ 169.6 (C^{8,9}), 150.5 (C⁶), 147.2 (C²), 129.3 (C³), 125.1 (C⁵), 63.1 (C^{10,11}), 47.6 (C¹²), 21.1 (C⁷);

IR(film, cm⁻¹): 3007s (C-H), 2963s (C-H), 1745s (C=O), 1629s (C=C), 1602s (C=C), 1340s (B-O);

MS (TOF ES⁺): *m/z* (%): 249.1 (100) [M+H]⁺, 271.1 (81) [M+Na]⁺;

HRMS (ES⁺): [M+Na]⁺ calcd. For C₁₁H₁₄BN₂O₄, 249.1047; found, 249.1036.

2-(2,4-Difluorophenyl)-4-(trifluoromethyl)pyridine (83)



38 (5.00 g, 27.5 mmol, 1 eq), (2,4-difluorophenyl)boronic acid (5.21 g, 33.0 mmol, 1.2 eq), and Na₂CO₃ (3.50 g, 33.0 mmol, 1.2 eq) were added to a three neck round bottomed flask fitted with reflux condenser and stirrer bar, along with THF (150 mL) and H₂O (30 mL). The resulting mixture was degassed with argon for 30 min. Tetrakis(triphenylphosphine)palladium(0) (159 mg, 138 μmol, 5 mol %) was then added and the mixture degassed for a further 15 min. The solution was then heated to 70 °C and stirred under argon for 20 h. After cooling to rt the solvent was removed under reduced pressure. To the crude residue was added CH₂Cl₂ (100 mL) and H₂O (100 mL). The organic phase was extracted washed with H₂O (2 x 50 mL), dried (MgSO₄) and the solvent removed under reduced pressure. The crude brown solid obtained was purified by

column chromatography on silica (hexanes:Et₂O 10:1) to yield a white crystalline solid (5.04 g, 19.5 mmol, 71%). *R_f* = 0.34 (hexanes:Et₂O 10:1, on silica).

Mp: 35-36 °C;

¹H NMR (400 MHz, CDCl₃) δ 8.88 (d, *J* = 5.1 Hz, 1H, H⁶), 8.07 (td, *J* = 8.9, 6.6 Hz, 1H, H¹³), 7.99 (s, 1H, H³), 7.48 (dd, *J* = 5.1, 0.8 Hz, 1H, H⁵), 7.07 – 6.99 (m, 1H, H¹²), 6.95 (ddd, *J* = 11.3, 8.7, 2.5 Hz, 1H, H¹⁰);

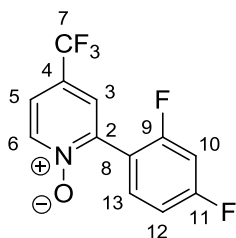
¹³C NMR (100 MHz, CDCl₃) δ 163.9 (dd, *J* = 252.6, 12.2 Hz, C⁹), 160.95 (dd, *J* = 253.4, 12.0 Hz, C¹¹), 153.9 (s, C²), 150.77 (s, C⁶), 139.1 (q, *J* = 34.2 Hz, C⁴), 132.4 (dd, *J* = 9.7, 3.9 Hz, C¹³), 123.0 (q, *J* = 273.3 Hz, C⁷), 122.7 (dd, *J* = 11.2, 3.7 Hz, C⁸), 119.8 (dd, *J* = 10.6, 3.5 Hz, C⁵), 118.1 (d, *J* = 3.2 Hz, C³), 112.4 (dd, *J* = 21.2, 3.4 Hz, C¹²), 104.8 (t, *J* = 26.2 Hz, C¹⁰);

¹⁹F NMR (282 MHz, CDCl₃) δ -63.45 (s, 3F, F⁷), -105.33 (d, *J* = 10.1 Hz 1F, F⁹), -107.05 (d, *J* = 10.0 Hz, 1F, F¹¹);

MS (TOF ES⁺): *m/z* (%): 260.0 (100) [M+H]⁺;

HRMS (ES⁺): [M+H]⁺ calcd. For C₁₂H₇NF₅, 260.0497; found, 260.0499.

2-(2,4-Difluorophenyl)-4-(trifluoromethyl)pyridine (85)



To a round bottom flask charged with **39** (5.01g, 19.3 mmol, 1 eq) and CH₂Cl₂ (50 mL), *m*CPBA (5.00 g, 29.0 mmol, 1.5 eq) was added slowly over 5 min. The resulting mixture was stirred at 30 °C for 16 h. The solvent was removed under reduced pressure and CH₂Cl₂ (100 mL) and Na₂CO₃ solution (10 g in 100 mL H₂O) were added. The organic phase was extracted, washed with H₂O (2 x 50 mL), dried (MgSO₄) and the solvent removed under reduced pressure. The crude solid obtained was then dissolved in Et₂O (10 mL) and the resulting solution was added slowly dropwise to hexanes (150 mL). Large needle like crystals of white solid formed. The crystals

were collected by filtration, washed with hexane (10 mL) and dried under high vacuum to provide a white crystalline solid (4.71 g, 17.1 mmol, 89%).

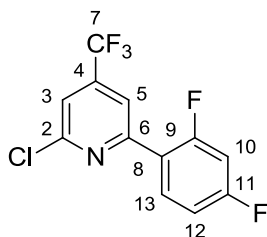
^1H NMR (300 MHz, CDCl_3) δ 8.40 (d, $J = 6.9$ Hz, 1H, H^6), 7.62 (stack, 2H, $\text{H}^{3,13}$), 7.51 (dd, $J = 6.8, 2.6$ Hz, 1H, H^5), 7.01 (stack, 2H, $\text{H}^{12,10}$);

^{13}C NMR (100 MHz, CDCl_3) δ 164.4 (dd, $J = 253.7, 12.0$ Hz, C^9), 160.7 (dd, $J = 254.3, 12.3$ Hz, C^{11}), 145.1 (s, C^2), 140.9 (s, C^6), 132.4 (dd, $J = 10.0, 3.7$ Hz, C^{13}), 126.2 (q, $J = 35.2$ Hz, C^4), 125.2 (s, C^5), 122.5 (q, $J = 272.0$ Hz, C^7), 122.1 (d, $J = 3.4$ Hz, C^3), 115.9 (dd, $J = 14.4, 3.6$ Hz, C^{12}), 112.0 (dd, $J = 21.8, 3.3$ Hz, C^{12}), 104.9 (t, $J = 25.5$ Hz, C^{10}).

MS (TOF ES^+): m/z (%): 294.0 (100) $[\text{M}+\text{H}]^+$;

HRMS (ES^+): $[\text{M}+\text{H}]^+$ calcd. For $\text{C}_{12}\text{H}_6\text{NCIF}_5$, 294.0114; found, 294.0109.

2-Chloro-4-(trifluoromethyl)-6-(2,4-difluorophenyl)pyridine (87)



41 (4.64 g, 21.0 mmol) was combined with POCl_3 (15 mL) in a round bottomed flask fitted with reflux condenser and stirrer bar. The resulting mixture was stirred and heated to 120 $^\circ\text{C}$ for two h. After cooling to rt the condenser was removed. The flask was placed in an ice bath and equipped with an addition funnel. H_2O (70 mL) was added very cautiously. The resulting mixture was extracted with CH_2Cl_2 (2 x 100 mL). The organic phases were combined, dried (MgSO_4), and the solvent removed under reduced pressure. The crude product was purified by column chromatography on silica (hexanes: Et_2O 100:0 \rightarrow 50:1 \rightarrow 20:1) and a subsequent column on silica (hexanes) to yield a white crystalline solid (1.99 g, 6.78 mmol, 40%). $R_f = 0.84$ (hexanes: Et_2O 9:1, on silica).

Mp: 30-31 $^\circ\text{C}$;

^1H NMR (300 MHz, CDCl_3) δ 8.13 (td, $J = 8.9, 6.5$ Hz, 1H, H^{13}), 7.94 (s, 1H, H^3), 7.51 (s, 1H, H^5), 7.10 – 7.00 (m, 1H, H^{12}), 6.95 (ddd, $J = 11.2, 8.6, 2.4$ Hz, 1H, H^{10}).

^{13}C NMR (100 MHz, CDCl_3) δ 164.3 (dd, $J = 254.0, 12.5$ Hz, C^9), 161.1 (dd, $J = 254.4, 12.1$ Hz, C^{11}), 154.3 (d, $J = 2.8$ Hz, C^6), 152.3 (s, C^2), 141.8 (q, $J = 34.4$ Hz, C^4), 132.6 (dd, $J = 9.9, 3.6$ Hz, C^{13}), 122.2 (q, $J = 273.9$ Hz, C^7), 121.1 (dd, $J = 10.6, 3.7$ Hz, C^8), 119.1 (d, $J = 3.3$ Hz, C^3), 118.4 (dd, $J = 12.7, 3.2$ Hz, C^5), 112.6 (dd, $J = 21.3, 3.5$ Hz, C^{12}), 104.9 (t, $J = 26.3$ Hz, C^{10});

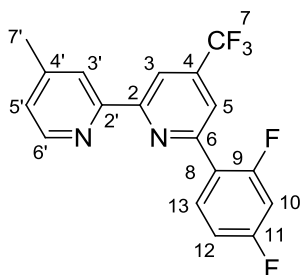
^{19}F NMR (282 MHz, CDCl_3) δ -64.72 (s, 3F, F^7), -106.09 (d, $J = 9.8$ Hz, 1F, F^9), -111.24 (d, $J = 9.8$ Hz, 1F, F^{11}).

IR(film, cm^{-1}): 3169w (C-H), 3126s (C-H), 3105s (C-H), 1616s (C=C), 1599s (C=C), 1568s (C=C) 1504s (C=C);

MS (TOF ES $^+$): m/z (%): 294.0 (100) $[\text{M}+\text{H}]^+$;

HRMS (ES $^+$): $[\text{M}+\text{H}]^+$ calcd. For $\text{C}_{12}\text{H}_6\text{N}^3\text{CF}_5$, 294.0114; found, 294.0109.

4-(Trifluoromethyl)-4'-methyl-6-(2,4-difluorophenyl)-2,2'-bipyridine (75)



A flame dried round bottomed flask (equipped with reflux condenser, tap and stirrer bar) filled with argon was charged with DMF (50 mL) and IPA (12.5 mL). The solvent mixture was degassed with argon for 30 min before the addition of Tris(dibenzylideneacetone)dipalladium(0) (18.3 mg, 20.0 μmol , 15 mol %), and 2-dicyclohexylphosphino-2',4',6'-triisopropylbiphenyl (38.0 mg, 80.0 μmol , 0.06 eq). The resulting black solution was heated to 100 $^\circ\text{C}$ for 5 min turning a dark red colour. A separate flame dried round bottomed flask (equipped with reflux condenser, tap and stirrer bar) filled with argon was charged with **43** (392 mg, 1.33 mmol, 1 eq), **27** (500 mg, 2.00 mmol, 1.5 eq), copper(II) acetate (120 mg, 0.67 mmol, 0.5 eq), and K_2CO_3 (919 mg, 6.65 mmol, 5 eq). The catalytic solution was allowed to cool to 40 $^\circ\text{C}$ and then added to

the second apparatus. The resulting black mixture was heated to 100 °C and stirred under argon for four h. After cooling to rt the solvent was removed under reduced pressure. CH₂Cl₂ (100 mL) and H₂O (100 mL) were added to the crude green solid. The organic phase was separated, dried (MgSO₄) and the solvent removed under reduced pressure. The crude yellow oil obtained was purified by column chromatography on silica (hexanes:Et₂O 10:1) to yield a white crystalline solid (140 mg, 0.40 mmol, 30%). *R*_f = 0.50 (hexanes:Et₂O 10:1, on silica).

Mp: 104-106 °C;

¹H NMR (400 MHz, CDCl₃) δ 8.65 (s, 1H, H^{3'}), 8.58 (d, *J* = 4.9 Hz, 1H, H^{6'}), 8.36 (s, *J* = 0.6 Hz, 1H, H³), 8.24 (td, *J* = 8.9, 6.6 Hz, 1H, H¹³), 7.99 (s, 1H, H⁵), 7.20 (dd, *J* = 4.9, 0.9 Hz, 1H, H^{5'}), 7.09 (tdd, *J* = 8.7, 2.5, 0.9 Hz, 1H, H¹²), 6.97 (ddd, *J* = 11.3, 8.7, 2.5 Hz, 1H, H¹⁰), 2.48 (s, 3H, H^{7'});

¹³C NMR (100 MHz, CDCl₃) δ 163.9 (dd, *J* = 252.4, 12.3 Hz, C⁹), 161.1 (dd, *J* = 253.7, 12.0 Hz, C¹¹), 157.7 (s, C²), 154.6 (s, C^{2'}), 152.9 (s, C^{4'}), 149.32 (s, C^{6'}), 148.5 (s, C⁶), 140.2 (q, *J* = 33.7 Hz, C⁴), 132.5 (dd, *J* = 9.7, 4.0 Hz, C¹³), 125.7 (s, C^{5'}), 123.2 (q, *J* = 273.3 Hz, C⁷), 122.8 (dd, *J* = 11.1, 3.7 Hz, C⁸), 122.3 (s, C³), 119.9 – 119.2 (m, C⁵), 115.8 (d, *J* = 3.3 Hz, C³), 112.3 (dd, *J* = 21.2, 3.3 Hz, C¹²), 104.8 (t, *J* = 26.3 Hz, C¹⁰), 21.4 (s, C^{7'});

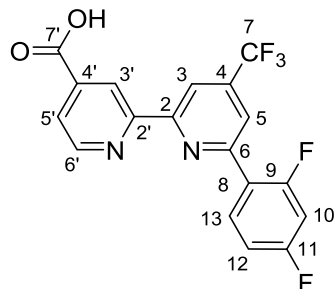
¹⁹F NMR (282 MHz, CDCl₃) δ -64.64 (s, 3F, F⁷), -107.70 (d, *J* = 9.2 Hz, 1F, F⁹), -111.80 (d, *J* = 9.2 Hz, 1F, F¹¹);

IR(film, cm⁻¹): 3106s (C-H), 3056s (C-H), 3000w (C-H), 2964w (C-H), 2927s (C-H), 2865w (C-H), 1617s (C=C), 1601s (C=C), 1574s (C=C) 1501s (C=C);

MS (TOF ES⁺): *m/z* (%): 351.1 (100) [M+H]⁺;

HRMS (ES⁺): [M+H]⁺ calcd. For C₁₈H₁₂N₂F₅, 351.0921; found, 351.0922.

4-(Trifluoromethyl)-6-(2,4-difluorophenyl)-2,2'-bipyridine-4'-carboxylic acid (77)



Potassium dichromate (277 mg, 941 μmol , 3.3 eq) was added slowly to a stirred solution of **45** (100 mg, 285 μmol , 1 eq) in H_2SO_4 (5 mL) cooled by a water bath. The red solution was then heated and stirred at 70 $^\circ\text{C}$ for two h, during which time the solution turned deep green. After cooling to rt the solution was added dropwise to ice water (6 mL) causing a precipitate to form. The flask was washed with a further portion of H_2O (4 mL). The suspension was stirred for a further hour at rt before the precipitate was collected by filtration and washed with H_2O (10 mL) the crude yellow solid obtained was purified by column chromatography on silica ($\text{Et}_2\text{O}:\text{MeOH}$ 10:1) to yield a white solid (37.0 mg, 97.0 μmol , 34%) $R_f = 0.21$ ($\text{Et}_2\text{O}:\text{MeOH}$ 10:1, on silica).

Mp: 248-250 $^\circ\text{C}$;

^1H NMR (400 MHz, 2:1 $\text{CDCl}_3:\text{MeOD}$) δ 8.89 (s, 1H, $\text{H}_{3'}$), 8.69 (d, $J = 4.5$ Hz, 1H, $\text{H}_{6'}$), 8.45 (d, $J = 0.6$ Hz, 1H, H_3), 8.14 (td, $J = 8.9, 6.7$ Hz, 1H, H_{13}), 7.88 (s, 1H, H_5), 7.81 (d, $J = 4.4$ Hz, 1H, $\text{H}_{5'}$), 6.94 (td, $J = 8.3, 2.2$ Hz, 1H, H_{12}), 6.84 (ddd, $J = 11.3, 8.7, 2.4$ Hz, 1H, H_{10});

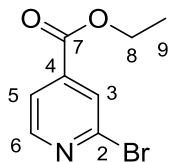
^{13}C NMR (100 MHz, 2:1 $\text{CDCl}_3:\text{MeOD}$) δ 166.9 (s, $\text{C}_{7'}$), 163.8 (dd, $J = 252.6, 12.6$ Hz, C_9), 160.9 (dd, $J = 253.9, 12.1$ Hz, C_{11}), 156.5 (s, C_2), 155.6 (s, $\text{C}_{2'}$), 153.1 (d, $J = 2.1$ Hz, $\text{C}_{4'}$), 149.9 (s, $\text{C}_{6'}$), 148.8 (s, C_6), 139.9 (q, $J = 34.1$ Hz, C_4), 132.4 (dd, $J = 9.9, 3.5$ Hz, C_{13}), 124.2 (q, $J = 273.2$ Hz, C_7), 123.9 (s, $\text{C}_{5'}$), 122.2 (d, $J = 3.5$ Hz, C_8), 121.0 (s, $\text{C}_{3'}$), 119.6 (dd, $J = 11.3, 3.3$ Hz, C_5), 115.4 (d, $J = 3.0$ Hz, C_3), 112.1 (dd, $J = 21.3, 3.1$ Hz, C_{12}), 104.4 (t, $J = 26.4$ Hz, C_{10});

^{19}F NMR (282 MHz, 2:1 $\text{CDCl}_3:\text{MeOD}$) δ -65.08 (s, 3F, F_7), -107.76 (d, $J = 9.3$ Hz, 1F, F_9), -112.18 (d, $J = 9.3$ Hz, 1F, F_{11});

IR(film, cm^{-1}): 3127s (C-H), 2934w (C-H), 1709s (C=O), 1619s (C=C), 1607s (C=C), 1577s (C=C), 1560s (C=C), 1505s (C=C).

MS (TOF ES $^-$): m/z (%): 379.1 (100) $[\text{M}-\text{H}]^-$.

Ethyl-2-bromopyridine-4-carboxylate (89)



49 (97.4%, 5.00 g, 24.0 mmol) was combined with ethanol (30 mL) to form a suspension, to which was added H₂SO₄ (98%, 3.3 mL). The mixture was heated to reflux at 90 °C whilst stirred for 24 h. After an aqueous solution of K₂CO₃ (20 g in 100 mL H₂O) which was added slowly until the pH was increased to 7, causing a white precipitate and evolution of CO₂. The resulting suspension was extracted with Et₂O (3 x 300 mL), the organic phases were combined and dried (MgSO₄) and the solvent removed under reduced pressure to afford a yellow oil. The crude product was purified by column chromatography on silica (hexane:Et₂O 9:1) to yield a colourless oil, (3.46 g, 15. mmol, 63%). *R*_f = 0.33 (hexane:Et₂O 9:1, on silica).

¹H NMR (300 MHz, CDCl₃) δ 8.51 (dd, *J* = 5.0, 0.6 Hz, 1H, H₆), 8.03 (dd, *J* = 1.2, 0.8 Hz, 1H, H₃), 7.80 (dd, *J* = 5.0, 1.4 Hz, 1H, H₅), 4.41 (q, *J* = 7.1 Hz, 2H, H₈), 1.40 (t, *J* = 7.1 Hz, 3H, H₉);

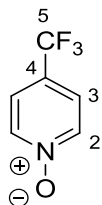
¹³C NMR (100 MHz, CDCl₃) δ 163.6 (C₇), 150.9 (C₆), 142.8 (C₄), 140.2 (C₂), 127.7 (C₃), 121.9 (C₅), 62.3 (C₈), 14.1 (C₉);

IR(film, cm⁻¹): 3096w (C-H), 3062w (C-H), 2983s (C-H), 2934w (C-H), 2906w (C-H), 2875w (C-H), 1726s (C=O), 1588s (C=C), 1548s (C=C), 1459s (C=C) 1360s (C-O);

MS (TOF ES⁺): *m/z* (%): 230.0 (100) [M+H]⁺;

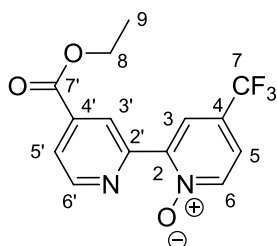
HRMS (ES⁺): [M+H]⁺ calcd. For C₈H₉NO⁷⁹Br, 229.9817; found, 229.9808.

4-Trifluoromethylpyridine-*N*-oxide (90)



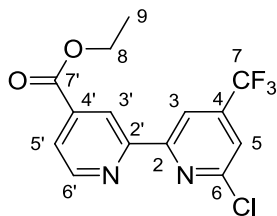
To a 100 mL round bottom flask charged with **50** (2.50 g, 17.0 mmol, 1 eq) and CH₂Cl₂ (50 mL), *m*CPBA (77 %, 5.03 g, 22.4 mmol, 1.3 eq) was added slowly over 5 min. The resulting mixture was stirred at 30 °C for 16 h. The solvent was removed under reduced pressure and CH₂Cl₂ (100 mL) and Na₂CO₃ solution (20 g in 100 mL H₂O) were added. The organic phase was extracted, washed with H₂O (2 x 100 mL), dried (MgSO₄) and the solvent removed under reduced pressure. Crude carried forward without further purification.

4-(Trifluoromethyl)-4'-(ethoxycarbonyl)-2-2'-bipyridine-1-oxide (71)



89 (1.53g, 6.63 mmol, 1 eq), **90** (2.16 g, 13.3 mmol, 2 eq), palladium(II) acetate (74.0 mg, 401 μmol, 5 mol %), tri-*tert*-butylphosphonium tetrafluoroborate (115 mg, 1.20 mmol, 15 mol %), potassium phosphate (2.82 g, 13.3 mmol, 2 eq) and toluene (50 ml) were combined in a 2 neck round bottom flask fitted with condenser, stop cock and magnetic stirrer. The resulting mixture was degassed with argon and heated to 110 °C and stirred for 16 h. After cooling to rt the solvent was removed under reduced pressure. CH₂Cl₂ (50 mL) was added and extracted with H₂O (50 mL). The organic phases was dried (MgSO₄) and the solvent removed under reduced pressure to afford a brown solid. The crude mixture was recrystallised from CH₂Cl₂ (10 mL) by the addition of hexane (100 mL). The precipitate was collected by vacuum filtration and dried under vacuum. The resulting crude yellow solid was carried forward without further purification.

Ethyl-6-chloro-4-(trifluoromethyl)-2-2'-bipyridine-4'-carboxylate (91)



71 (2.30 g, crude) was combined with POCl₃ (10 mL), the mixture was degassed with argon before being stirred and heated to reflux at 120 °C. After 1.5 h the solution was cooled to rt and the remaining POCl₃ was removed by vacuum distillation at 50 °C and 10⁻³ mbar. H₂O (50 mL) was added to the remaining solid, which was extracted with CH₂Cl₂ (4 x 50 mL) the organic phases were combined, and dried (MgSO₄), and the solvent removed under reduced pressure. The remaining solid was purified by column chromatography on silica (CH₂Cl₂:Et₂O 30:1) to yield a white crystalline solid (706 mg, 2.13 mmol, 32% over 2 steps).

Mp: 112-114 °C;

¹H NMR (300 MHz, CDCl₃) δ 8.89 (dd, *J* = 1.5, 0.9 Hz, 1H, H_{3'}), 8.81 (dd, *J* = 4.9, 0.8 Hz, 1H, H_{6'}), 8.60 (d, *J* = 0.6 Hz, 1H, H₃), 7.92 (dd, *J* = 4.9, 1.6 Hz, 1H, H_{5'}), 7.57 (d, *J* = 0.6 Hz, 1H, H₅), 4.46 (q, *J* = 7.1 Hz, 2H, H₈), 1.44 (t, *J* = 7.1 Hz, 4H, H₉);

¹³C NMR (100 MHz, CDCl₃) δ 164.94 (s, C_{7'}), 157.64 (s, C_{2'}), 154.47 (s, C₂), 152.09 (s, C₆), 150.29 (s, C_{6'}), 142.10 (q, *J* = 34.6 Hz, C₄), 139.40 (s, C_{4'}), 124.26 (s, C_{5'}), 122.27 (q, *J* = 273.9 Hz, C₇), 120.96 (s, C_{3'}), 120.63 (q, *J* = 3.4 Hz, C₅), 115.85 (q, *J* = 3.3 Hz, C₃), 62.18 (s, C₈), 14.37 (s, C₉);

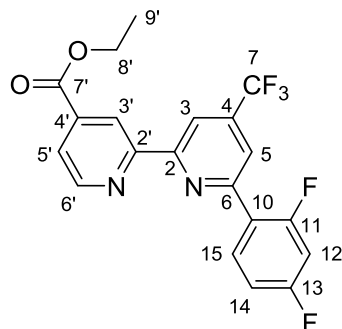
¹⁹F NMR (282 MHz, CDCl₃) δ -64.72 (s, 3F, F⁷);

IR(film, cm⁻¹): 3108s (C-H), 3084s (C-H), 3001s (C-H), 2967s (C-H), 2904s (C-H), 1724s (C=O), 1593s (C=C), 1557s (C=C), 1471s (C-H), 1419s (C-H), 1397s (C-H), 1367s (C-H), 1332s (C-H), 1298s (C-O);

MS (TOF ES⁺): *m/z* (%): 331.0 (100) [M+H]⁺;

HRMS (ES⁺): [M+H]⁺ calcd. For C₁₄H₁₁N₂O₂F₃³⁵Cl, 331.0461; found, 331.0454.

Ethyl-6-(2, 4-difluorophenyl)-4-(trifluoromethyl)-2, 2'-bipyridine-4'-carboxylate (92)



91 (116 mg, 0.90 mmol, 1.0 eq), **66** (60.0 mg, 1.08 mmol, 1.1 eq), and Na₂CO₃ (41.0 mg, 1.08 mmol, 1.1 eq) were combined along with THF (50 mL) and H₂O (10 mL). The solvent was degassed with argon for 20 min. Tetrakis(triphenylphosphine)palladium(0) (22.0 mg 45.0 μmol, 5 mol %) was then added and the mixture degassed with argon for a further 10 min before stirring under argon at 70 °C for 16 h. After cooling to rt the solvent was removed under reduced pressure and CH₂Cl₂ (50 mL) and H₂O (50 mL) were added. The organic phase was separated and dried (MgSO₄) and the solvent was removed under reduced pressure. The resulting solid was purified by column chromatography on silica (hexane:EtOAc 9:1), to afford a white crystalline solid (205 mg, 0.53 mmol, 60%). *R*_f = 0.3 (CH₂Cl₂:Et₂O 9:1, on silica).

Mp: 94-96 °C;

¹H NMR (300 MHz, CDCl₃) δ 9.03 (dd, *J* = 1.5, 0.8 Hz, 1H, H_{3'}), 8.85 (dd, *J* = 5.0 Hz, 1H, H_{6'}), 8.65 (d, *J* = 0.6 Hz, 1H, H₃), 8.27 (td, *J* = 8.9, 6.6 Hz, 1H, H₁₂), 8.03 (s, 1H, H₅), 7.92 (dd, *J* = 5.0, 1.6 Hz, 1H, H_{5'}), 7.13 – 7.04 (m, 1H, H₁₄), 6.97 (ddd, *J* = 11.3, 8.7, 2.5 Hz, 1H, H₁₅), 4.47 (s, *J* = 7.1 Hz, 2H, H₈), 1.45 (t, *J* = 7.1 Hz, 3H, H₉);

¹³C NMR (101 MHz, CDCl₃) δ 165.2 (s, C_{7'}), 163.9 (stack, C₁₁), 161.2 (dd, *J* = 253.6, 12.0 Hz, C₁₃), 156.6 (s, C_{2'}), 155.9 (s, C₂), 153.2 (d, *J* = 2.5 Hz, C₆), 150.2 (s, C_{6'}), 140.3 (q, *J* = 33.9 Hz, C_{4'}), 139.2 (s, C₄), 132.6 (dd, *J* = 9.7, 3.7 Hz, C₁₂), 123.7 (s, C_{5'}), 123.1 (q, *J* = 273.5 Hz, C₇), 122.5 (dd, *J* = 11.0, 3.7 Hz, C₁₀), 120.8 (s, C_{3'}), 120.1 -119.8 (m, C₅), 115.8 (d, *J* = 3.5 Hz, C₃), 112.4 (dd, *J* = 21.2, 3.2 Hz, C₁₄), 104.8 (t, *J* = 26.3 Hz, C₁₅), 62.1 (s, C₈), 14.4 (s, C₉);

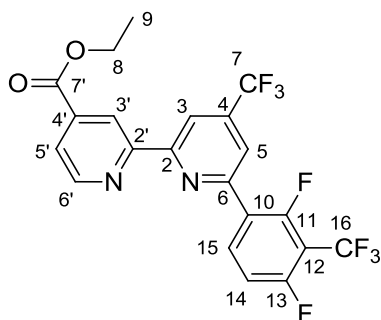
¹⁹F NMR (282 MHz, CDCl₃) δ -64.69 (s, F₇), 107.28–107.46 (m, F₁₁), -111.66 (dd, *J* = 20.4, 9.3 Hz, F₁₃);

IR(film, cm^{-1}): 3097s (C-H), 3080s (C-H), 2994s (C-H), 2951s (C-H), 2913s (C-H), 1731 (C=O), 1618s (C=C), 1597 (C=C), 1574s (C=C), 1505s (C=C), 1474s (C-H), 1443s (C-H), 1388s (C-H), 1356s (C-H), 1274 (C-O);

MS (TOF ES⁺): m/z (%): 431.1 (100) [M+Na]⁺;

HRMS (ES⁺): [M+H]⁺ calcd. for C₂₀H₁₃N₂O₂NaF₅, 431.0795; found, 431.0787.

Ethyl-6-(2,4-difluoro-3-(trifluoromethyl)phenyl)-4-(trifluoromethyl)-2-2'-bipyridine-4'-carboxylate (93)



91 (150 mg, 450 μmol , 1 eq), **60** (154 mg, ≈ 680 μmol , ≈ 1.5 eq), and Na₂CO₃ (72.1 mg, 680 μmol , 1.5 eq) were combined along with THF (20 mL) and H₂O (5 mL). The solvent was degassed with argon for 20 min. Tetrakis(triphenylphosphine)palladium(0) (26.2 mg 22.7 μmol , 5 mol %) was then added and the mixture degassed with argon for a further 10 min before stirring under argon at 70 °C for 16 h. After cooling to rt the solvent was removed under reduced pressure and CH₂Cl₂ (50 mL) and H₂O (50 mL) were added and the organic phase extracted, dried (MgSO₄) and the solvent was removed under reduced pressure. The resulting solid was purified by column chromatography on silica (CH₂Cl₂ followed by hexane:Et₂O 9:1) to afford a white crystalline solid (118 mg, 248 μmol , 55%). R_f = 0.70 (CH₂Cl₂:Et₂O 9:1, on silica).

Mp: 114-116 °C;

¹H NMR (400 MHz, CDCl₃) δ 9.01 (dd, J = 1.5, 0.8 Hz, 1H, H_{3'}), 8.87 (dd, J = 4.9, 0.8 Hz, 1H, H_{6'}), 8.73 (d, J = 0.4 Hz, 1H, H₃), 8.44 (td, J = 8.7, 6.1 Hz, 1H, H₁₅), 8.04 (d, J = 0.4 Hz, 1H, H₅), 7.94 (dd, J = 5.0, 1.6 Hz, 1H, H_{5'}), 7.24 (t, J = 9.6 Hz, 1H, H₁₄), 4.48 (q, J = 7.1 Hz, 2H, H₈), 1.46 (t, J = 7.1 Hz, 3H, H₉);

^{13}C NMR (100 MHz, CDCl_3) δ 165.19 (s, $\text{C}_{7'}$), 160.78 (dd, $J = 244.5, 4.0$ Hz, C_{13}), 158.17 (dd, $J = 244.3, 4.5$ Hz, C_{11}), 157.07 (s, C_2), 155.61 (s, $\text{C}_{2'}$), 151.98 (s, C_6), 150.34 (s, $\text{C}_{6'}$), 140.65 (q, $J = 34.0$ Hz, C_4), 139.27 (s, $\text{C}_{4'}$), 135.81 (dd, $J = 10.7, 4.9$ Hz, C_{15}), 123.91 (s, $\text{C}_{5'}$), 122.95 (q, $J = 273.8$ Hz, C_7), 120.78 (s, $\text{C}_{3'}$), 120.20 (dd, $J = 11.1, 3.3$ Hz, C_5), 116.62 (d, $J = 3.3$ Hz, C_3), 113.63 (dd, $J = 22.2, 3.7$ Hz, C_{14}), 62.20 (s, C_8), 14.36 (s, C_9);

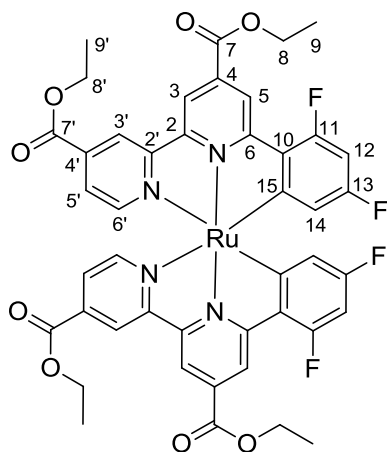
^{19}F NMR (282 MHz, CDCl_3) δ -56.17 (dd, $J = 23.9, 22.8$ Hz, 3F, F_{16}), -64.69 (s, 3F, F_7), -107.85 (qd, $J = 24.0, 3.5$ Hz, 1F, F_{11}), -114.10 (qd, $J = 22.7, 3.5$ Hz, 1F, F_{13});

IR(film, cm^{-1}): 3100s (C-H), 2993s (C-H), 2920s (C-H), 1734 (C=O), 1627s (C=C), 1598 (C=C), 1562s (C=C), 1495s (C=C), 1456s (C-H), 1443s (C-H), 1387s (C-H), 1358s (C-H), 1279 (C-O);

MS (TOF ES^+): m/z (%): 477.1 (100) $[\text{M}+\text{H}]^+$;

HRMS (ES^+): $[\text{M}+\text{H}]^+$ calcd. For $\text{C}_{21}\text{H}_{13}\text{N}_2\text{O}_2\text{F}_8$, 477.0849; found, 477.0839.

Ruthenium(II) bis(diethyl-6-(2,4-difluorophenyl)-2,2'-bipyridine-4,4'-dicarboxylate) (**95**)



A 2 neck round bottom flask fitted with stirrer, condenser and stopcock was charged with **22** (550 mg, 1.33 mmol, 4 eq) and $[\text{Ru}(p\text{-cymene})\text{Cl}_2]_2$ (204 mg, 333 μmol , 1 eq). The apparatus was filled with argon before the addition of $n\text{PrCN}$ (10 mL) and N -ethylmorpholine (2 mL). The resulting orange solution was degassed with argon for 20 min before heating and stirring at 120 $^\circ\text{C}$, for 16 h under argon and reduced light. After cooling to rt solvent was removed under reduced pressure and the crude black solid was dried under high vacuum. Ethylene glycol (10 mL) was added and the resulting mixture degassed for 20 min with argon. The reaction mixture

was then heated and stirred at 200 °C for 2 h under argon and reduced light. After cooling to rt, ethylene glycol was removed by vacuum distillation. The crude black mixture was combined with H₂O (100 mL) and CH₂Cl₂ (100 mL). The organic phase was separated and the aqueous phase extracted with further portions of CH₂Cl₂ (3 x 100 mL). The organic phases were combined, dried (MgSO₄) and solvent removed under reduced pressure. The crude product was purified by column chromatography on silica (CH₂Cl₂:Et₂O 10:0 → 9:1) to yield a black solid (400 mg, 433 μmol, 65%). *R*_f = 0.85 (CH₂Cl₂:Et₂O 9:1, on silica).

¹H NMR (300 MHz, CDCl₃) δ 8.95 (m, 2H, H₅), 8.84 (d, *J* = 1.5 Hz, 2H, H₃'), 8.84 (d, *J* = 1.4 Hz, 2H, H₃), 7.47 (dd, *J* = 5.7, 0.7 Hz, 2H, H₆'), 7.44 (dd, *J* = 5.7, 1.5 Hz, 2H, H₅'), 6.22 (td, *J* = 10.8 Hz, 2.3 Hz, 2H, H₁₂), 5.33 (dd, *J* = 6.8, 1.9 Hz, 2H, H₁₄), 4.64 (q, *J* = 7.1 Hz, 4H, H₈'), 4.43 (q, *J* = 7.1 Hz, 4H), 1.60 (t, *J* = 7.1 Hz, 6H), 1.41 (t, *J* = 7.1 Hz, 6H);

¹³C NMR (100 MHz, CDCl₃) δ 191.73 (s, C₁₅), 165.95 (s, C₇), 164.21 (s, C₇'), 162.45 (dd, *J* = 258.9, 11.1 Hz, C₁₃), 161.31 (dd, *J* = 260.8, 12.5 Hz, C₁₁), 159.34 (s, C₆), 155.74 (s, C₂), 150.85 (s, C₂'), 150.04 (s, C₆'), 135.38 (s, C₄), 130.62 (s, C₄'), 127.12 (s, C₁₀), 124.18 (s, C₅'), 121.71 (s, C₃'), 119.68 (d, *J* = 19.4 Hz, C₅), 117.16 (s, C₃), 114.97 (dd, *J* = 10.8, 6.1 Hz, C₁₄), 96.54 (t, *J* = 26.5 Hz, C₁₂), 62.37 (s, C₈), 62.11 (s, C₈'), 14.66 (s, C₉), 14.41 (s, C₉');

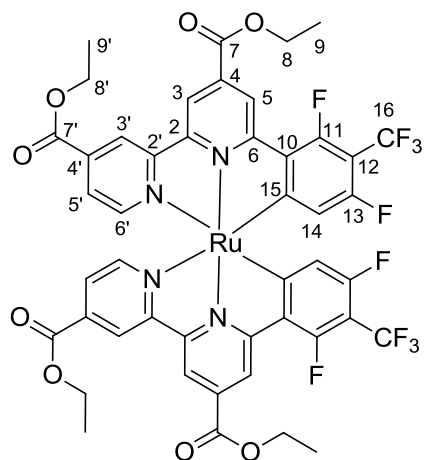
IR(film, cm⁻¹): 3129s (C-H), 3080s (C-H), 2979s (C-H), 2937s (C-H), 2901s (C-H), 1706 (C=O), 1591s (C=C), 1555 (C=C), 1512s (C=C), 1420s (C-H), 1365s (C-H);

¹⁹F NMR (282 MHz, CDCl₃) δ -110.37 (d, *J* = 9.5 Hz, 2F, F₁₃), -110.41 (d, *J* = 9.3 Hz, 2F, F₁₁);

MS (TOF ES⁺): *m/z* (%): 924.1 (100) [M+H]⁺;

HRMS (ES⁺): [M+H]⁺ calcd. For C₄₄H₃₄N₄O₈F₄¹⁰²Ru, 924.1356; found, 924.1372.

Ruthenium(II) bis(diethyl-6-(2,4-difluoro-3-(trifluoromethyl)phenyl)-2,2'-bipyridine-4,4'-dicarboxylate) (96)



Method 1

A 2 neck round bottom flask fitted with stirrer, condenser and stopcock was charged with **61** (50.0 mg, 104 μmol , 2 eq), $[\text{Ru}(p\text{-cymene})\text{Cl}_2]_2$ (32.0 mg, 52.0 μmol , 1 eq), KOH (5.80 mg, 104 μmol , 2 eq) and KPF_6 (19.0 mg, 104 μmol , 2 eq). The apparatus was evacuated and filled with argon before the addition of MeCN (10 mL). The resulting orange solution was degassed with argon for 20 min before heating and stirring at 80 $^\circ\text{C}$, for 72 h under argon and reduced light. After cooling to rt solvent was removed under reduced pressure and the crude brown solid was dried under high vacuum. Crude purification was performed by chromatography on silica ($\text{CHCl}_3:\text{MeOH}$ 100:0 \rightarrow 100:5) The yellow fraction was collected and verified as the trisacetonitrile intermediate, by ^1H NMR and mass spectrometry. $R_f = 0.73$ ($\text{CHCl}_3:\text{MeOH}$ 9:1, on silica). The product was then added to a 2 neck round bottom flask fitted with stirrer, condenser and stopcock which was charged with **61** (50.0 mg, 104 μmol , 2 eq). The apparatus was evacuated and filled with argon before the addition of EtOH (10 mL) and *N*-ethylmorpholine (0.5 mL), and the resulting mixture degassed for 20 min with argon. The reaction mixture was then heated and stirred at 80 $^\circ\text{C}$ for 16 h under argon and reduced light. After cooling to rt, solvent was removed under reduced pressure. The crude black solid was purified by preparative TLC on silica ($\text{CH}_2\text{Cl}_2:\text{Et}_2\text{O}$ 30:1) to yield a black solid (5.70 mg, 5.38 μmol , 5%). $R_f = 0.89$ ($\text{CH}_2\text{Cl}_2:\text{Et}_2\text{O}$ 9:1, on silica).

Method 2

A 2 neck round bottom flask fitted with stirrer, condenser and stopcock was charged with **61** (50.0 mg, 104 μmol , 4 eq) and $[\text{Ru}(p\text{-cymene})\text{Cl}_2]_2$ (16.0 mg, 26.0 μmol , 1 eq). The apparatus evacuated and filled with argon before the addition of MeCN (10 mL) and *N*-ethylmorpholine (0.2 mL). The resulting orange solution was degassed with argon for 20 min before heating and stirring at 80 °C, for 144 h under argon and reduced light. After cooling to rt solvent was removed under reduced pressure and the crude black solid was dried under high vacuum. The crude black solid was purified by preparative TLC on silica ($\text{CH}_2\text{Cl}_2:\text{Et}_2\text{O}$ 30:1) to yield a black solid (12.7 mg, 12.0 μmol , 23%). ($R_f = 0.89$ ($\text{CH}_2\text{Cl}_2:\text{Et}_2\text{O}$ 9:1, on silica). Monocyclometalated by product obtained (15.6 mg, 14.2 μmol , 27%).

Method 3

A 2 neck round bottom flask fitted with stirrer, condenser and stopcock was charged with **61** (100.0 mg, 208 μmol , 4 eq) and $[\text{Ru}(p\text{-cymene})\text{Cl}_2]_2$ (32.0 mg, 52.0 μmol , 1 eq). The apparatus evacuated and filled with argon before the addition of MeCN (10 mL) and NEt_3 (0.5 mL). The resulting orange solution was degassed with argon for 20 min before heating and stirring at 80 °C, for 162 h under argon and reduced light. After cooling to rt solvent was removed under reduced pressure and the crude black solid was dried under high vacuum. The crude black solid was purified by preparative TLC on silica ($\text{CH}_2\text{Cl}_2:\text{Et}_2\text{O}$ 30:1) to yield a black solid (3.0 mg, 12.0 μmol , 2.7%). ($R_f = 0.89$ ($\text{CH}_2\text{Cl}_2:\text{Et}_2\text{O}$ 9:1, on silica). Monocyclometalated by product obtained (1.6 mg, 14.2 μmol , 1.6%).

Method 4

A 2 neck round bottom flask fitted with stirrer, condenser and stopcock was charged with **61** (50.0 mg, 104 μmol , 4 eq) and $[\text{Ru}(p\text{-cymene})\text{Cl}_2]_2$ (16.0 mg, 26.0 μmol , 1 eq). The apparatus evacuated and filled with argon before the addition of *n*PrCN (10 mL) and *N*-ethylmorpholine (0.2 mL). The resulting orange solution was degassed with argon for 20 min before heating and stirring at 120 °C, for 96 h under argon and reduced light. After cooling to rt solvent was removed under reduced pressure and the crude black solid was dried under high vacuum. The crude black solid was purified by preparative TLC on silica ($\text{CH}_2\text{Cl}_2:\text{Et}_2\text{O}$ 30:1) to yield a black

solid (6.1 mg, 5.76 μmol , 11%). ($R_f = 0.89$ ($\text{CH}_2\text{Cl}_2:\text{Et}_2\text{O}$ 9:1, on silica). Monocyclometalated by product obtained (42.1 mg, 38.4 μmol , 74%).

Method 5

Monocyclometalated product **99** from **Method 4** (42.1 mg, 38.4 μmol) was added to a 2 neck round bottom flask fitted with stirrer, condenser and stopcock. The apparatus evacuated and filled with argon before the addition of ethylene glycol (10 mL). was added and the resulting mixture degassed for 20 min with argon. The reaction mixture was then heated and stirred at 200 °C for 2 h under argon and reduced light. After cooling to rt, the crude black mixture was combined with H_2O (50 mL) and CH_2Cl_2 (50 mL). The organic phase was separated and the aqueous phase extracted with further portions of CH_2Cl_2 (2 x 50 mL). The organic phases were combined, dried (MgSO_4) and solvent removed under reduced pressure. The crude product was purified by preparative TLC on silica ($\text{CH}_2\text{Cl}_2:\text{Et}_2\text{O}$ 30:1) to yield a black solid (36.6 mg, 34.6 μmol , 90%). ($R_f = 0.89$ ($\text{CH}_2\text{Cl}_2:\text{Et}_2\text{O}$ 9:1, on silica).

Method 6

A 2 neck round bottom flask fitted with stirrer, condenser and stopcock was charged with **61** (387 mg, 806 μmol , 4 eq) and $[\text{Ru}(p\text{-cymene})\text{Cl}_2]_2$ (123 mg, 202 μmol , 1 eq). The apparatus evacuated and filled with argon before the addition of *n*-PrCN (10 mL) and *N*-ethylmorpholine (2 mL). The resulting orange solution was degassed with argon for 20 min before heating and stirring at 120 °C, for 16 h under argon and reduced light. After cooling to rt solvent was removed under reduced pressure and the crude black solid was dried under high vacuum. Ethylene glycol (10 mL) was added and the resulting mixture degassed for 20 min with argon. The reaction mixture was then heated and stirred at 200 °C for 2 h under argon and reduced light. After cooling to rt, ethylene glycol was removed by vacuum distillation. The crude black mixture was combined with H_2O (100 mL) and CH_2Cl_2 (100 mL). The organic phase was separated and the aqueous phase extracted with further portions of CH_2Cl_2 (3 x 100 mL). The organic phases were combined, dried (MgSO_4) and solvent removed under reduced pressure. The crude product was purified by column chromatography on silica ($\text{CH}_2\text{Cl}_2:\text{Et}_2\text{O}$ 10:0 \rightarrow 9:1) to yield a black solid (175 mg, 161 μmol , 65%). $R_f = 0.89$ ($\text{CH}_2\text{Cl}_2:\text{Et}_2\text{O}$ 9:1, on silica).

^1H NMR (400 MHz, CDCl_3) δ 8.99 (s, 2H, H_5), 8.89 (d, $J = 1.2$ Hz, 2H, H_3), 8.86 (d, $J = 0.7$ Hz, 2H, H_3'), 7.50 (dd, $J = 5.7, 1.6$ Hz, 2H, H_5'), 7.44 (d, $J = 5.7$ Hz, 2H, H_6), 5.45 (d, $J = 10.0$ Hz, 2H, H_{14}), 4.63 (q, $J = 7.1$ Hz, 4H, H_8), 4.43 (q, $J = 7.1$ Hz, 4H, H_8'), 1.59 (t, $J = 7.1$ Hz, 6H, H_9), 1.39 (t, $J = 7.1$ Hz, 6H, H_9');

^{13}C NMR (100 MHz, CDCl_3) δ 197.6 (s, C_{15}), 165.5 (s, C_7), 163.9 (s, $\text{C}_{7'}$), 159.0 (s, C_6), 158.6 (d, $J = 267.7$ Hz, C_{13}), 157.7 (d, $J = 281.0$ Hz, C_{11}), 155.8 (s, C_2), 151.3 (s, $\text{C}_{2'}$), 150.1 (s, C_6'), 136.4 (s, C_4), 131.64 (s, $\text{C}_{4'}$), 128.2 (s, C_{10}), 124.7 (s, $\text{C}_{5'}$), 122.0 (s, $\text{C}_{3'}$), 120.7 (d, $J = 19.5$ Hz, C_5), 118.2 (s, C_3), 116.4 (d, $J = 15.1$ Hz, C_{14}) 62.58 (s, $\text{C}_{8'}$), 62.40 (s, C_8), 14.65 (s, C_9), 14.40 (s, C_9'). Expected signals for C_{12} (approx. 120 (tq, $J = 30, 30$ Hz)) and C_{16} (approx. 120 (tq, $J = 250, 10$ Hz)) not observed due to high level of splitting giving a very weak signal. ^1H , ^{19}F , HRMS and crystal data confirm structure is correct;

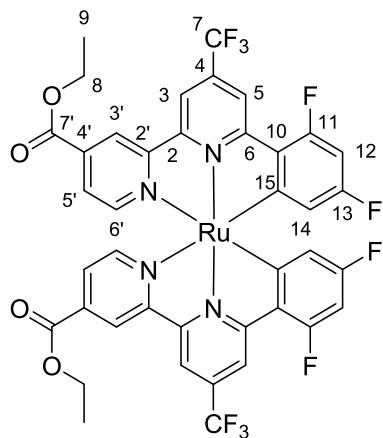
^{19}F NMR (282 MHz, CDCl_3) δ -54.92 (t, $J = 22.6$ Hz, 6F, F_{12}), -113.32 (qd, $J = 22.6, 4.1$ Hz, 2F, F_{13}), -113.75 (qd, $J = 22.7, 4.2$ Hz, 2F, F_{11});

IR(film, cm^{-1}): 3208w (C-H), 3074w (C-H), 2989s (C-H), 2957s (C-H), 2908w (C-H), 1710s (C=O), 1603s (C=C), 1535s (C=C), 1444s (C=C), 1300 (C-O);

MS (TOF ES^+): m/z (%): 1060.1 (100) $[\text{M}+\text{H}]^+$;

HRMS (ES^+): $[\text{M}+\text{H}]^+$ calcd. For $\text{C}_{46}\text{H}_{32}\text{N}_4\text{O}_8\text{F}_{10}^{102}\text{Ru}$, 1060.1104; found, 1060.1080.

Ruthenium(II) bis(ethyl-6-(2,4-difluorophenyl)-4-(trifluoromethyl)-2'-bipyridine-4'-carboxylate) (97)



A 2 neck round bottom flask fitted with stirrer, condenser and stopcock was charged with **92** (33.0 mg, 81.0 μmol , 4.0 eq) and $[\text{Ru}(p\text{-cymene})\text{Cl}_2]_2$ (12.0 mg, 20.0 μmol , 1.0 eq). The apparatus evacuated and filled with argon before the addition of *n*PrCN (5 mL) and *N*-ethylmorpholine (0.5 mL). The resulting orange solution was degassed with argon for 20 min before heating and stirring at 120 °C, for 16 h under argon and reduced light. After cooling to rt solvent was removed under reduced pressure and the crude black solid was dried under high vacuum. Ethylene glycol (5 mL) was added and the resulting mixture degassed for 20 min with argon. The reaction mixture was then heated and stirred at 200 °C for 2 h under argon and reduced light. After cooling to rt, ethylene glycol was removed by vacuum distillation. The crude black mixture was combined with H₂O (50 mL) and CH₂Cl₂ (50 mL). The organic phase was separated and the aqueous phase extracted with further portions of CH₂Cl₂ (3 x 50 mL). The organic phases were combined, dried (MgSO₄) and solvent removed under reduced pressure. The crude product was purified by column chromatography on silica (CH₂Cl₂ and then hexane:EtOAc 8:2) to yield a black solid (10.2 mg, 11.1 μmol , 27%). $R_f = 0.31$ (hexane:EtOAc 8:2 on silica).

¹H NMR (400 MHz, CDCl₃) δ 8.76 (t, $J = 1.1$ Hz, 2H, H^{3'}), 8.57 (s, 2H, H⁵), 8.39 (s, 2H, H³), 7.48 (d, $J = 1.2$ Hz, 4H, H^{5'} H^{6'}), 6.29 – 6.13 (m, 2H, H₁₄), 5.32 (dd, $J = 7.8, 2.3$ Hz, 2H, H¹²), 4.42 (q, $J = 7.1$ Hz, 4H, H⁸), 1.39 (t, $J = 7.1$ Hz, 6H, H⁹);

¹³C NMR (100 MHz, CDCl₃) δ 192.12 (s, C¹⁵), 163.90 (s, C^{7'}), 162.64 (dd, C¹¹), 161.32 (dd, $J = 293.5, 9.6$ Hz, C¹³), 154.97 (s, C^{2'}), 151.20 (s, C²), 150.06 (s, C^{6'}), 149.79 (s, C⁶), 135.24 (s, C^{4'}), 130.96 (q, $J = 53.8$ Hz, C⁴), 126.65 (s, C¹⁰), 124.45 (s, C^{5'}), 123.87 (q, C⁷), 121.70 (s, C^{3'}), 115.78 (dd, $J = 18.3, 3.5$ Hz, C¹²), 114.92 (d, $J = 14.9$ Hz, C⁵), 112.85 (d, $J = 3.0$ Hz, C³), 96.55 (t, $J = 27.1$ Hz, C¹⁴), 62.32 (s, C⁸), 14.25 (s, C⁹);

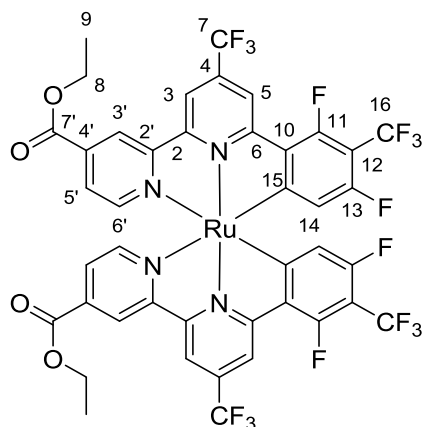
¹⁹F NMR (282 MHz, CDCl₃) δ -63.04 (s, 6F, F⁷), -109.44 (dd, $J = 17.5, 9.3$ Hz, 2F, F¹¹), -109.95 (t, $J = 11.9$ Hz, 2F, F¹³);

IR(film, cm⁻¹): 3089s (C-H), 2989s (C-H), 2944s (C-H), 2910s (C-H), 2861s (C-H), 1713 (C=O), 1595s (C=C), 1554 (C=C), 1539s (C=C), 1431s (C-H), 1395s (C-H), 1324s (C-H), 1252 (C-O);

MS (TOF ES⁺): m/z (%): 916.6 (100) [M+H]⁺;

HRMS (ES⁺): [M+H]⁺ calcd. for C₄₀H₂₄N₄O₄F₁₀, 916.0681; found, 916.0695.

Ruthenium(II) bis(ethyl-6-(2,4-difluoro-3-(trifluoromethyl)phenyl)-4-(trifluoromethyl)-2'-bipyridine-4'-carboxylate) (98)



A 2 neck round bottom flask fitted with stirrer, condenser and stopcock was charged with **93** (50 mg, 105 μ mol, 4 eq) and [Ru(*p*-cymene)Cl₂]₂ (15.9 mg, 26 μ mol, 1 eq). The apparatus was evacuated and filled with argon before the addition of *n*PrCN (10 mL) and *N*-ethylmorpholine (2 mL). The resulting orange solution was degassed with argon for 20 min before heating and stirring at 120 °C, for 16 h under argon and reduced light. After cooling to rt solvent was removed under reduced pressure and the crude black solid was dried under high vacuum. Ethylene glycol (10 mL) was added and the resulting mixture degassed for 20 min with argon. The reaction mixture was then heated and stirred at 200 °C for 2 h under argon and reduced light. The crude black mixture was combined with H₂O (100 mL) and CH₂Cl₂ (100 mL). The organic phase was separated and the aqueous phase extracted with further portions of CH₂Cl₂ (3 x 100 mL). The organic phases were combined, dried (MgSO₄) and solvent removed under reduced pressure. The crude product was purified by column chromatography on silica (CH₂Cl₂:Et₂O 10:0 → 9:1) to yield a black solid (44 mg, 41.9 μ mol, 80%). *R*_f = 0.91 (CH₂Cl₂:Et₂O 9:1, on silica).

¹H NMR (400 MHz, CDCl₃) δ 8.81 (s, 2H, H^{3'}), 8.64 (s, 2H, H⁵), 8.46 (s, 2H, H³), 7.56 (dd, *J* = 5.7, 1.5 Hz, 1H, H^{5'}), 7.47 (d, *J* = 5.7 Hz, 2H, H^{6'}), 5.47 (d, *J* = 10.0 Hz, 2H, H¹⁴), 4.43 (q, *J* = 7.1 Hz, 4H, H⁸), 1.39 (t, *J* = 7.1 Hz, 6H, H⁹);

^{13}C NMR (100 MHz, CDCl_3) δ 197.88 (d, $J = 5.1$ Hz, C^{15}), 163.69 (s, C^7), 159.69 (d, $J = 5.9$ Hz, C^6), 158.80 (d, $J = 270.9$ Hz, C^{13}), 157.95 (d, $J = 273.2$ Hz, C^{11}), 155.15 (s, $\text{C}^{2'}$), 151.75 (s, C^2), 150.23 (s, C^6), 136.53 (s, C^4), 132.16 (q, $J = 34.0$ Hz, C^4), 125.13 (s, $\text{C}^{5'}$), 127.89 – 122.24 (m, C^{10}), 122.64 (q, $J = 272.9$ Hz, C^7), 122.12 (s, $\text{C}^{3'}$), 117.05 (d, $J = 19.2$ Hz, C^5), 116.52 (d, $J = 14.7$ Hz, C^{14}), 114.12 (s, C^3), 62.69 (s, C^8), 14.36 (s, C^9). Expected signals for C_{12} (approx. 120 (tq, $J = 30, 30$ Hz)) and C_{16} (approx. 120 (tq, $J = 250, 10$ Hz)) not observed due to high level of splitting giving a very weak signal. ^1H , ^{19}F , HRMS and crystal data confirm structure is correct;

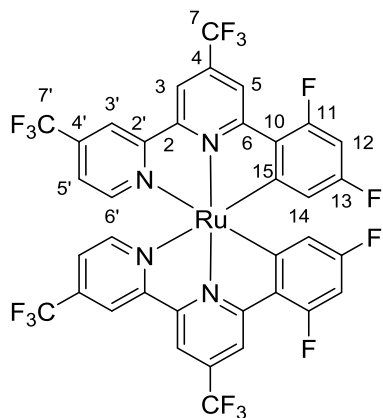
^{19}F NMR (282 MHz, CDCl_3) δ -55.03 (t, $J = 22.7$ Hz, 6F, F^{16}), -63.21 (s, $J = 6.4$ Hz, 6F, F^7), -112.39 (qd, $J = 22.4, 4.6$ Hz, 2F, F^{11}), -113.26 (qd, $J = 22.9, 4.6$ Hz, 2F, F^{13});

IR(film, cm^{-1}): 3129w (C-H), 3097w (C-H), 2986s (C-H), 2930s (C-H), 2867s (C-H), 1725 (C=O), 1604s (C=C), 1538(C=C), 1467w (C-H), 1432s (C-H), 1403s (C-H), 1369s (C-H), 1305s (C-H), 1241 (C-O);

MS (TOF ES^+): m/z (%): 1052.0 (100) $[\text{M}]^+$;

HRMS (ES^+): $[\text{M}+\text{H}]^+$ calcd. For $\text{C}_{42}\text{H}_{22}\text{N}_4\text{O}_4\text{F}_{16}^{102}\text{Ru}$, 1052.0429; found, 1052.0424.

Ruthenium(II) bis(6-(2,4-difluorophenyl)-4,4'-bis(trifluoromethyl)-2,2'-bipyridine) (46)



A 2 neck round bottom flask fitted with stirrer, condenser and stopcock was charged with **67** (70.0 mg, 170 μmol , 4.0 eq), and $[\text{Ru}(p\text{-cymene})\text{Cl}_2]_2$ (26.5 mg, 42.5 μmol , 1.0 eq). The apparatus evacuated and filled with argon before the addition of $n\text{PrCN}$ (5 mL) and N -ethylmorpholine (0.5 mL). The resulting orange solution was degassed with argon for 20 min before heating and stirring at 120 $^\circ\text{C}$, for 16 h under argon and reduced light. After cooling to rt

solvent was removed under reduced pressure and the crude black solid was dried under high vacuum. Ethylene glycol (5 mL) was added and the resulting mixture degassed for 20 min with argon. The reaction mixture was then heated and stirred at 200 °C for 2 h under argon and reduced light. After cooling to rt, ethylene glycol was removed by vacuum distillation. The crude black mixture was combined with H₂O (50 mL) and CH₂Cl₂ (50 mL). The organic phase was separated and the aqueous phase extracted with further portions of CH₂Cl₂ (3 x 50 mL). The organic phases were combined, dried (MgSO₄) and solvent removed under reduced pressure. The crude product was purified by chromatography on silica (hexane: CH₂Cl₂ 3:0 → 3:1) to yield a black solid (22.6 mg, 24.9 μmol, 32%). *R_f* = 0.35 (hexane: CH₂Cl₂ 3:1, on silica).

¹H NMR (300 MHz, CDCl₃) δ 8.52 (s, 2H, H³), 8.34 (s, 2H, H³), 8.28 (s, 2H⁵), 7.48 (d, *J* = 5.8 Hz, 2H, H⁶), 7.09 (dd, *J* = 5.8, 1.3 Hz, 2H, H⁵), 6.16 (ddd, *J* = 12.4, 9.2, 2.3 Hz, 2H, H¹²), 5.25 (dd, *J* = 7.8, 2.3 Hz, 2H, H¹⁴);

¹³C NMR (100 MHz, CDCl₃) δ 191.5 (s, C¹⁵), 162.7 (dd, *J* = 258.8, 11.1 Hz, C¹¹), 161.6 (dd, *J* = 260.8, 12.1 Hz, C¹³), 160.1 – 159.9 (m, C²), 155.3 (s, C²), 150.7 (s, C⁶), 150.6 (s, C⁶), 136.8 – 134.8 (m, C⁴), 131.2 (q, *J* = 34.1 Hz, C⁴), 125.8 (q, *J* = 281.6 Hz, C⁷), 124.4 (q, *J* = 273.0 Hz, C⁷), 121.0 (s, C¹⁰), 118.0 (s, C⁵), 116.1 (dd, *J* = 18.8, 3.1 Hz, C¹²), 115.0 (dd, *J* = 14.5, 1.8 Hz), 113.1 (d, *J* = 2.9 Hz), 96.8 (t, *J* = 26.7 Hz, C¹²);

¹⁹F NMR (282 MHz, CDCl₃) δ -63.12 (s, 6F, F⁷), -64.39 (s, 6F, F⁷), -108.89 (dd, *J* = 17.5, 9.5 Hz, 2F, F¹¹), -109.61 (ddd, *J* = 12.3, 10.0, 2.1 Hz, 2F, F¹³);

IR(film, cm⁻¹): 3113s (C-H), 3052s (C-H), 2920s (C-H), 2851s (C-H), 1593s (C=C), 1548 (C=C), 1432s (C-H), 1393s (C-H);

MS (TOF ES⁺): *m/z* (%): 907.9 (100) [M]⁺;

HRMS (ES⁺): [M+H]⁺ calcd. for C₃₆H₁₄N₄F₁₆¹⁰²Ru, 908.0006; found, 908.0031.

Ruthenium(II) bis(6-(2,4-difluoro-3-(trifluoromethyl)phenyl)-4,4'-bis(trifluoromethyl)-2,2'-bipyridine) (47)

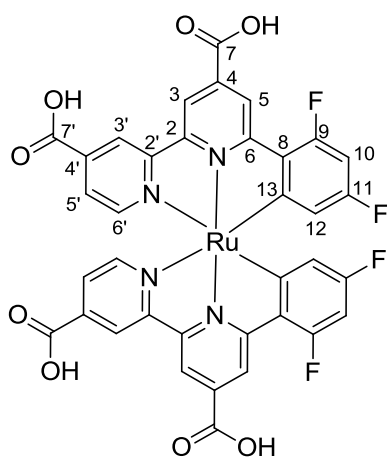
^{19}F NMR (282 MHz, $\text{CD}_3\text{CN}:\text{CDCl}_3$, 2:1) δ -55.09 (t, $J = 22.8$ Hz, 6F, F^{16}), -63.46 (s, 6F, F^7), -64.61 (s, 6F, $\text{F}^{7'}$), -114.40 (qd, $J = 22.4, 3.9$ Hz, 2F, F^{11}), -114.73 (qd, $J = 23.2, 3.9$ Hz, 2F, F^{13});

IR(film, cm^{-1}): 3219w (C-H), 3128w (C-H), 2925s (C-H), 2857s (C-H), 1607s (C=C), 1539 (C=C), 1435s (C-H), 1404s (C-H);

MS (TOF ES $^+$): m/z (%): 1043.8 (100) $[\text{M}]^+$;

HRMS (ES $^+$): $[\text{M}+\text{H}]^+$ calcd. for $\text{C}_{38}\text{H}_{12}\text{N}_4\text{F}_{22}^{102}\text{Ru}$, 1043.9754; found, 1043.9761.

Ruthenium(II) bis(6-(2,4-difluorophenyl)-2,2'-bipyridine-4,4'-dicarboxylic acid) (42)



Method 1

A 50 mL 2 neck round bottom flask fitted with condenser, stopcock and stirrer, was charged with **54** (23.2 mg, 65.0 μmol , 4 eq), and $[\text{Ru}(p\text{-cymene})\text{Cl}_2]_2$ (10.0 mg, 16.3 μmol , 1 eq). The apparatus was then evacuated and filled with argon. DMF (10 mL) was added and the resulting solution was degassed with argon for 20 min before heating to 80 $^\circ\text{C}$ and stirring for 4 h then at 160 $^\circ\text{C}$ for 4 h under argon and reduced light. After cooling to rt the solvent was removed under reduced pressure. Purification was performed by column chromatography on sephadex LH-20 (MeOH). Product not observed.

Method 2

A 50 mL 2 neck round bottom flask fitted with condenser, stopcock and stirrer, was charged with **54** (20.0 mg, 56.0 μmol , 4 eq), and $[\text{Ru}(p\text{-cymene})\text{Cl}_2]_2$ (8.60 mg, 14.0 μmol , 1 eq). The

apparatus was then evacuated and filled with argon. DMF (5 mL) was added and the resulting solution was degassed with argon for 20 min before heating to 80 °C and stirring for 2 h then at 160 °C for 4 h under argon and reduced light. After cooling to rt the solvent was removed under reduced pressure. Ethylene glycol (5 mL) was added and the resulting black solution was degassed with argon for 20 min before heating to 160 °C and stirring under argon and reduced light. After 2 h TBOH (99.0 mg, 123 µmol, 8.8 eq) was added and the reaction continued at 160 °C under argon and reduced light for a further 4 h. Purification was performed by column chromatography on sephadex LH-20 (MeOH). Product not observed.

Method 3

A 50 mL 2 neck round bottom flask fitted with condenser, stopcock and stirrer, was charged with **54** (13.0 mg, 36.5 µmol, 4 eq), and [Ru(*p*-cymene)Cl₂]₂ (5.6 mg, 9.1 µmol, 1 eq). The apparatus was then evacuated and filled with argon. DMF (5 mL) was added and the resulting solution was degassed with argon for 20 min before heating and stirring at 160 °C for 48 h under argon and reduced light. After cooling to rt the solvent was removed under reduced pressure. Purification was performed by column chromatography on sephadex LH-20 (MeOH). Product not observed.

Method 4

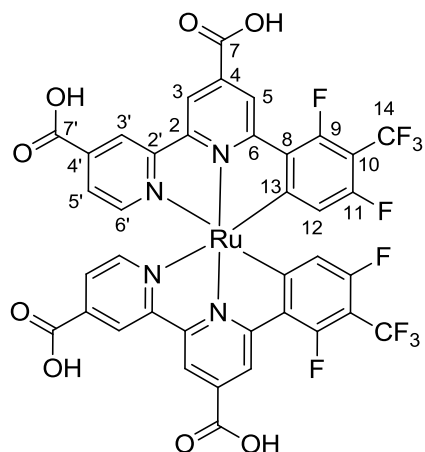
A 2 neck round bottom flask fitted with stirrer, condenser and stopcock was charged with **54** (387 mg, 806 µmol, 4 eq) and [Ru(*p*-cymene)Cl₂]₂ (123 mg, 202 µmol, 1 eq). The apparatus evacuated and filled with argon before the addition of *n*PrCN (10 mL) and *N*-ethylmorpholine (2 mL). The resulting orange solution was degassed with argon for 20 min before heating and stirring at 120 °C, for 16 h under argon and reduced light. After cooling to rt solvent was removed under reduced pressure and the crude black solid was dried under high vacuum. Ethylene glycol (10 mL) was added and the resulting mixture degassed for 20 min with argon. The reaction mixture was then heated and stirred at 200 °C for 2 h under argon and reduced light. After cooling to rt, ethylene glycol was removed by vacuum distillation. The crude black mixture was combined with H₂O (10 mL) and TBAOH (380 mg, 350 µmol, 10 eq). The resulting dark purple solution was treated with HNO₃ (0.01 M) to a pH of 3. The resulting precipitate was collected by vacuum filtration and washed with H₂O. The black solid was dried under vacuum.

Purification was performed by column chromatography on sephadex LH-20 (MeOH). Product not observed.

Method 5

A 50 mL 2 neck round bottom flask fitted with condenser, stopcock and stirrer, was charged with **95** (19.6 mg, 21.2 μmol). The apparatus was then evacuated and filled with argon. DMF (18 mL), H_2O (6 mL) and NEt_3 (6 mL) were added and the resulting black solution was degassed with argon for 20 min before heating to 110 $^\circ\text{C}$ and stirring for 16 h under argon and reduced light conditions. After cooling to rt the solvent and base was removed under reduced pressure. Purification was performed by column chromatography on sephadex LH-20 (MeOH: H_2O 7:3). Some impurities remained.

Ruthenium(II) bis(6-(2,4-difluoro-3-(trifluoromethyl)phenyl)-2,2'-bipyridine-4,4'-dicarboxylic acid) (**43**)



Method 1

A 50 mL 2 neck round bottom flask fitted with condenser, stopcock and stirrer, was charged with **96** (30.1 mg, 28.1 μmol). The apparatus was then evacuated and filled with argon. DMF (18 mL), H_2O (6 mL) and NEt_3 (6 mL) were added and the resulting black solution was degassed with argon for 20 min before heating to 110 $^\circ\text{C}$ and stirring for 16 h under argon and reduced light conditions. After cooling to rt the solvent and base was removed under reduced pressure. Purification was performed by column chromatography on sephadex LH-20 (MeOH: H_2O 7:3). Some impurities remained.

Method 2

A 50 mL 2 neck round bottom flask fitted with condenser, stopcock and stirrer, was charged with **96** (20.0 mg, 18.9 μmol). The apparatus was then evacuated and filled with argon. KOH (2M, aq, 1 mL) and acetone (5 mL) were added and the resulting mixture was degassed with argon for 20 min before heating to 60 °C and stirring for 16 h under argon and reduced light conditions. After cooling to rt the mixture was treated with HCl (1M) until a black precipitate formed. The solid was collected by filtration, washed with H₂O, hexane, and CH₂Cl₂. After drying the filtrand was removed from the filter by dissolving in MeOH. Solvent was removed under reduced pressure to yield a black solid (15.5 mg, 16.3 μmol , 86%).

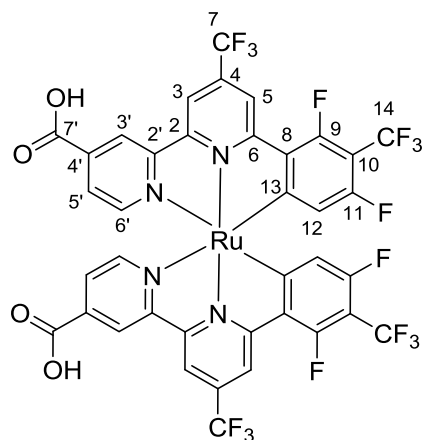
¹H NMR (300 MHz, MeOD) δ 8.95 (d, J = 6.0 Hz, 2H), 8.88 (s, 1H), 7.58 (d, J = 5.7 Hz, 1H), 7.50 (d, J = 5.4 Hz, 1H), 5.45 (d, J = 10.3 Hz, 1H).

¹⁹F NMR (282 MHz, MeOD) δ -56.17 (t, J = 22.9 Hz, 6F, F¹⁴), -116.38 (qd, J = 22.4, 2.3 Hz, 2F, F⁹), -116.76 (qd, J = 23.3, 2.1 Hz, 2F, F¹¹).

MS (TOF ES⁻): m/z (%): 946.97 (100) [M-H]⁻;

HRMS (ES⁻): [M-H]⁻ calcd. for C₃₈H₁₅N₄F₁₀¹⁰²Ru, 946.9774; found, 946.9769.

Ruthenium(II) bis(6-(2,4-difluoro-3-(trifluoromethyl)phenyl)-4-(trifluoromethyl)-2,2'-bipyridine-4'-carboxylic acid) (45)



A 50 mL 2 neck round bottom flask fitted with condenser, stopcock and stirrer, was charged with **98** (16.0 mg, 15.2 μmol). The apparatus was then evacuated and filled with argon. KOH (2M, aq,

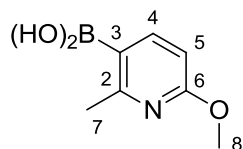
1 mL) and acetone (5 mL) were added and the resulting mixture was degassed with argon for 20 min before heating to 60 °C and stirring for 16 h under argon and reduced light conditions. After cooling to rt the mixture was treated with HCl (1M) until a black precipitate formed. The solid was collected by filtration, washed with H₂O, hexane, and CH₂Cl₂. After drying the filtrand was removed from the filter by dissolving in MeOH. Solvent was removed under reduced pressure to yield a black solid (12.1 mg, 12.9 μmol, 85%).

¹H NMR (300 MHz, MeOD) δ 9.27 (s, 2H, H^{3'}), 8.90 (s, 4H, H^{3,5}), 7.93 (d, *J* = 5.6 Hz, 2H, H^{6'}), 7.85 (d, *J* = 5.8 Hz, 2H, H^{5'}), 5.79 (d, *J* = 10.0 Hz, 2H, H¹²);

¹⁹F NMR (282 MHz, MeOD) δ -55.43 (t, *J* = 22.7 Hz, 6F, F¹⁴), -63.77 (s, 6F, F⁷), -113.50 (qd, *J* = 22.3, 4.1 Hz, 2F, F⁹), -113.97 – -114.61 (m, 2F, F¹¹).

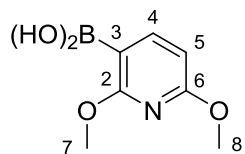
3 Characterisation-Chapter 2

2-Methyl-6-methoxypyridyl-3-boronic acid (109)



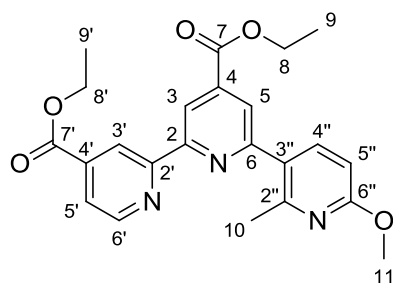
A flame dried 2 neck 100 mL flask fitted with stop-cock septum and stirrer bar was filled with argon and charged with 3-bromo-6-methoxy-2-methylpyridine (1.00 g, 4.98 mmol, 1eq) and anhydrous THF (20 mL). The resulting solution was cooled to -78 °C and stirred before the slow dropwise addition of *n*BuLi (1.6 M in hexane, 4.67 mL, 7.47 mmol, 1.5 eq). The resulting orange solution was stirred for 1 h. triisopropylborate (1.40 g, 7.46 mmol, 1.5 eq) was added and the solution allowed to warm to rt. After 2 h HCl (1 M, 30 mL) was added slowly dropwise. The organic phase was extracted and the aqueous phase neutralised with KOH (2 M), causing a white precipitate. The suspension was then extracted with CH₂Cl₂ (2 x 100 mL). Organic phases were dried (MgSO₄) and solvent removed under reduced pressure to yield a white solid (616 mg) the crude was carried forward without further purification.

2,6-Dimethoxypyridyl-3-boronic acid (110)



A flame dried 250 mL 3 neck flask fitted with stirrer bar, stopcock and pressure equalising addition funnel was filled with argon and charged with 3-bromo-2,6-dimethoxypyridine (2.00 g, 9.17 mmol, 1eq) and anhydrous THF (20 mL). The resulting solution was cooled to $-78\text{ }^{\circ}\text{C}$. *n*BuLi (1.4 M in PhMe, 7.2 mL, 10.1 mmol, 1.1 eq) was then added slowly dropwise to the stirred solution over 30 min. The resulting solution was stirred at $-78\text{ }^{\circ}\text{C}$ under argon for 3 h. $\text{B}(\text{O}^i\text{Pr})_3$ (2.59 g, 13.76 mmol, 1.5 eq) was then added and the solution was stirred for a further 5 h at $-78\text{ }^{\circ}\text{C}$ before warming to rt and stirring for a further 16 h. AcOH (1.5 mL) and H_2O (4 mL) were added and the mixture stirred at rt for 2 h. The solvent was removed under reduced pressure. Residual acetic acid was removed by distillation with the aid of propan-2-ol (3 x 15 mL aliquots). The off white solid obtained was triturated with Et_2O , filtered and dried under vacuum. The crude solid was carried forward without further purification.

Diethyl-2''-methyl-6''-methoxy-2,2',6,3''-terpyridine-4, 4'-dicarboxylate (**113**)



57 (251 mg, 749 μmol , 1 eq), **111** (150 mg, 898 μmol , 1.2 eq), and Na_2CO_3 (95 mg, 898 μmol , 1.2 eq) were combined along with THF (25 mL) and H_2O (5 mL), The solvent was degassed with argon for 20 min. Tetrakis(triphenylphosphine)palladium(0) (43.0 mg 37.0 μmol , 5 mol %) was then added and the mixture degassed with argon for a further 10 min before stirring under argon at $70\text{ }^{\circ}\text{C}$ for 16 h. After cooling to rt the solvent was removed under reduced pressure and CH_2Cl_2 (50 mL), HCl (2 M, 0.5 mL) and H_2O (50 mL) were added. The organic phase was separated and dried (MgSO_4) and the solvent was removed under reduced pressure. The resulting solid was purified by column chromatography on silica ($\text{CH}_2\text{Cl}_2:\text{Et}_2\text{O}$ 20:1), to afford a white crystalline solid (270 mg, 641 μmol , 86%). $R_f = 0.38$ ($\text{CH}_2\text{Cl}_2:\text{Et}_2\text{O}$ 20:1, on silica).

Mp: 145-147 °C;

¹H NMR (300 MHz, CDCl₃) δ 8.97 (dd, *J* = 1.5, 0.8 Hz, 1H, H^{3'}), 8.87 (d, *J* = 1.4 Hz, 1H, H³), 8.85 (dd, *J* = 5.0, 0.7 Hz, 1H, H^{6'}), 8.01 (d, *J* = 1.4 Hz, 1H, H⁵), 7.88 (dd, *J* = 5.0, 1.6 Hz, 1H, H^{5'}), 7.81 (d, *J* = 8.4 Hz, 1H, H^{4''}), 6.70 (d, *J* = 8.4 Hz, 1H, H^{6''}), 4.44 (stack, 4H, H^{8,8'}), 3.99 (s, 3H, H¹¹), 2.66 (s, *J* = 5.4 Hz, 3H, H¹⁰), 1.42 (stack, 6H, H^{9,9'});

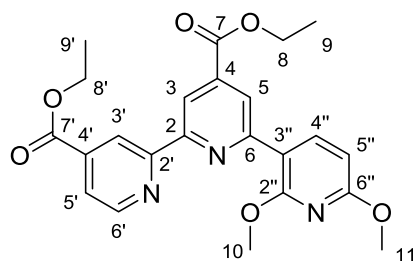
¹³C NMR (100 MHz, CDCl₃) δ 165.3 (C^{7'}), 165.2 (C⁷), 163.4 (C^{6''}), 158.9 (C⁶), 156.7 (C^{2'}), 156.1 (C²), 154.8 (C^{3''}), 150.1 (C^{6'}), 140.5 (C^{4''}), 139.6 (C⁴), 139.0 (C^{4'}), 127.8 (C^{2''}), 123.4 (C⁵), 123.3 (C^{5'}), 120.7 (C^{3'}), 118.3 (C³), 107.9 (C^{5''}), 62.0 (C⁸), 62.0 (C^{8'}), 53.6 (C¹¹), 23.7 (C¹⁰), 14.4 (C⁹), 14.3 (C^{9'});

IR(film, cm⁻¹): 3097w (C-H), 3073w (C-H), 2991s (C-H), 2946s (C-H), 2913s (C-H), 1728 (C=O), 1598 (C=C), 1558s (C=C), 1476s (C-H), 1443s (C-H), 1377s (C-H), 1365s (C-H), 1299 (C-O), 1259 (C-O);

MS (TOF ES⁺): *m/z* (%): 422.1 (100) [M+H]⁺;

HRMS (ES⁺): [M+H]⁺ calcd. for C₂₃H₂₄N₃O₅, 422.1716; found, 422.1717.

Diethyl-2'',6''-dimethoxy-2,2',6,3''-terpyridine-4,4'-dicarboxylate (**114**)



57 (235 mg, 701 μmol, 1 eq), **112** (100 mg, 841 μmol, 1.2 eq), and Na₂CO₃ (89.1 mg, 841 μmol, 1.2 eq) were combined along with THF (25 mL) and H₂O (5 mL). The solvent was degassed with argon for 20 min. Tetrakis(triphenylphosphine)palladium(0) (40.5 mg 35.1 μmol, 5 mol %) was then added and the mixture degassed with argon for a further 10 min before stirring under argon at 70 °C for 16 h. After cooling to rt the solvent was removed under reduced pressure and CH₂Cl₂ (50 mL), HCl (2 M, 0.5 mL) and H₂O (50 mL) were added. The organic phase was separated and dried (MgSO₄) and the solvent was removed under reduced pressure. The resulting

solid was purified by column chromatography on silica (Hexane:EtOAc 8:2), to afford a white crystalline solid (218 mg, 498 μmol , 71%). $R_f = 0.33$ (Hexane:EtOAc 8:2, on silica).

Mp: 141-143 $^{\circ}\text{C}$;

^1H NMR (300 MHz, CDCl_3) δ 9.03 (dd, $J = 1.4, 0.8$ Hz, 1H, $\text{H}^{3'}$), 8.85 (dd, $J = 5.0, 0.7$ Hz, 1H, $\text{H}^{6'}$), 8.79 (d, $J = 1.4$ Hz, 1H, H^3), 8.66 (d, $J = 1.4$ Hz, 1H, H^5), 8.55 (d, $J = 8.3$ Hz, 1H, $\text{H}^{4''}$), 7.88 (dd, $J = 5.0, 1.6$ Hz, 1H, $\text{H}^{5'}$), 6.53 (d, $J = 8.3$ Hz, 1H, $\text{H}^{5''}$), 4.47 (q, $J = 7.1$ Hz, 2H, H^8), 4.46 (q, $J = 7.1$ Hz, 2H, $\text{H}^{8'}$), 4.10 (s, $J = 6.2$ Hz, 3H, H^{10}), 4.01 (s, 3H, H^{11}), 1.46 (t, $J = 7.1$ Hz, 3H, H^9), 1.44 (t, $J = 7.1$ Hz, 3H, $\text{H}^{9'}$);

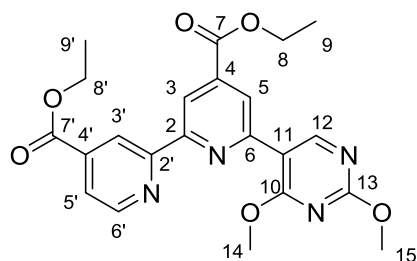
^{13}C NMR (100 MHz, CDCl_3) δ 165.84 (C^7), 165.47 ($\text{C}^{7'}$), 163.56 ($\text{C}^{6''}$), 160.47 ($\text{C}^{2''}$), 157.17 ($\text{C}^{2'}$), 155.68 (C^2), 154.81 (C^6), 150.05 ($\text{C}^{6'}$), 142.61 ($\text{C}^{4''}$), 139.33 (C^4), 138.94 ($\text{C}^{4'}$), 123.71 (C^5), 123.05 ($\text{C}^{5'}$), 120.75 (C^3), 117.97 (C^3), 113.47 ($\text{C}^{3''}$), 102.33 ($\text{C}^{5''}$), 61.99 (C^8), 61.86 ($\text{C}^{8'}$), 53.88 (C^{10}), 53.74 (C^{11}), 14.45 (C^9), 14.38 ($\text{C}^{9'}$);

IR(film, cm^{-1}): 3125w (C-H), 3089w (C-H), 2988s (C-H), 2947s (C-H), 2902s (C-H), 2860s (C-H), 1716 (C=O), 1596 (C=C), 1580s (C=C), 1556s (C=C), 1488s (C-H), 1479s (C-H), 1457s (C-H), 1365s (C-H), 1321s (C-H), 1295 (C-O), 1260 (C-O);

MS (TOF ES^+): m/z (%): 438.2 (100) $[\text{M}+\text{H}]^+$;

HRMS (ES^+): $[\text{M}+\text{H}]^+$ calcd. for $\text{C}_{23}\text{H}_{24}\text{N}_3\text{O}_6$, 438.1665; found, 438.1662.

Diethyl-6-(2,6-dimethoxypyrimidyl)-2,2'-bipyridine-4,4'-dicarboxylate (**116**)



Method 1

57 (250 mg, 747 μmol , 1 eq), **115** (174 mg, 896 μmol , 1.2 eq), and K_2CO_3 (123 mg, 89.6 μmol , 1.2 eq) were combined along with dioxane (20 mL) and H_2O (10 mL). The solvent was degassed

with argon for 20 min. Tetrakis(triphenylphosphine)palladium(0) (43.2 mg 37.3 μmol , 5 mol %) was then added and the mixture degassed with argon for a further 10 min before stirring under argon at 70 °C for 16 h. After cooling to rt the solvent was removed under reduced pressure and CH_2Cl_2 (50 mL), HCl (2 M, 0.5 mL) and H_2O (50 mL) were added. The organic phase was separated and dried (MgSO_4) and the solvent was removed under reduced pressure. The resulting solid was purified by column chromatography on silica (CH_2Cl_2 :EtOAc 8:2), to afford a white crystalline solid (28.0 mg, 63.9 μmol , 8.5%). R_f = 0.19 (CHCl_3 :EtOAc 9:1, on silica).

Method 2

57 (100 mg, 299 μmol , 1 eq), **115** (69.4 mg, 358 μmol , 1.2 eq), and Na_2CO_3 (37.9 mg, 358 μmol , 1.2 eq) were combined along with THF (25 mL) and H_2O (5 mL), The solvent was degassed with argon for 20 min. Tetrakis(triphenylphosphine)palladium(0) (17.3 mg 15.0 μmol , 5 mol %) was then added and the mixture degassed with argon for a further 10 min before stirring under argon at 70 °C for 16 h. After cooling to rt the solvent was removed under reduced pressure and CH_2Cl_2 (50 mL), HCl (2 M, 0.5 mL) and H_2O (50 mL) were added. The organic phase was separated and dried (MgSO_4) and the solvent was removed under reduced pressure. The resulting solid was purified by column chromatography on silica (CH_2Cl_2 :EtOAc 8:2), to afford a white crystalline solid (112 mg, 255 μmol , 85%). R_f = 0.19 (CHCl_3 :EtOAc 9:1, on silica).

Mp: 150-151 °C;

^1H NMR (300 MHz, CDCl_3) δ 9.22 (s, J = 5.0 Hz, 1H, H^{12}), 8.99 (dd, J = 1.4, 0.8 Hz, 1H, $\text{H}^{3'}$), 8.88 (d, J = 1.4 Hz, 1H, H^3), 8.86 (dd, J = 5.0, 0.8 Hz, 1H, $\text{H}^{6'}$), 8.52 (d, J = 1.4 Hz, 1H, H^5), 7.91 (dd, J = 5.0, 1.6 Hz, 1H, $\text{H}^{5'}$), 4.47 (q, J = 7.1 Hz, 4H, $\text{H}^{8,8'}$), 4.15 (s, 3H, H, H^{14}), 4.10 (s, 3H, H^{15}), 1.46 (t, J = 7.1 Hz, 3H, H^9), 1.44 (t, J = 7.1 Hz, 3H, $\text{H}^{9'}$);

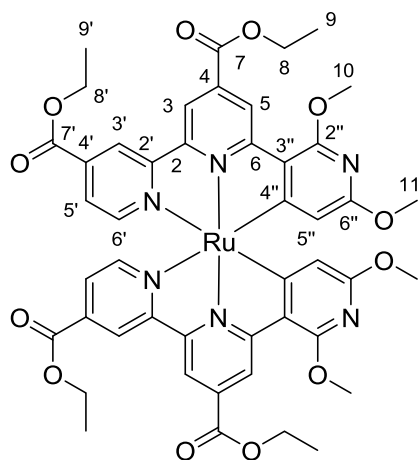
^{13}C NMR (100 MHz, CDCl_3) δ 168.59 (C^{13}), 165.51 (C^7), 165.46 ($\text{C}^{7'}$), 165.32 (C^{10}), 160.47 (C^{12}), 156.67 ($\text{C}^{2'}$), 156.15 (C^2), 152.28 (C^6), 150.11 ($\text{C}^{6'}$), 139.62 (C^4), 139.14 ($\text{C}^{4'}$), 123.58 (C^5), 123.40 ($\text{C}^{5'}$), 120.64 (C^3), 119.01 (C^3), 113.89 (C^{11}), 62.08 (C^8), 62.05 ($\text{C}^{8'}$), 55.25 (C^{14}), 54.51 (C^{15}), 14.43 ($\text{C}^{9,9'}$);

IR(film, cm^{-1}): 3101w (C-H), 3004s (C-H), 2966s (C-H), 2907s (C-H), 1728 (C=O), 1599 (C=C), 1557s (C=C), 1476s (C-H), 1448s (C-H), 1386s (C-H), 1365s (C-H), 1338s (C-H), 1291 (C-O), 1266 (C-O);

MS (TOF ES⁺): m/z (%): 439.4 (100) [M+H]⁺;

HRMS (ES⁺): [M+H]⁺ calcd. for $\text{C}_{22}\text{H}_{23}\text{N}_4\text{O}_6$, 439.1618; found, 439.1619.

Ruthenium(II) bis(diethyl-2'',6''-dimethoxy-2,2',6,3''-terpyridine-4,4'-dicarboxylate) (107)



A 10 mL microwave reactor vial fitted with a septum, was charged with **114** (50.0 mg, 114 μmol , 4 eq) and $[\text{Ru}(p\text{-cymene})\text{Cl}_2]_2$ (17.5 mg, 28.6 μmol). The apparatus was then evacuated and filled with argon. EtOH (2.5 mL) and *N*-ethylmorpholine (0.1 mL) (6 mL) were added and the resulting mixture was degassed with argon for 20 min before heating to 150 $^\circ\text{C}$ and stirring for 14 h under in a microwave reactor. After cooling to rt the solvent and base were removed under reduced pressure. Purification was performed by column chromatography on alumina (Hexane:EtOAc 9:1) to yield a black solid (8.1 mg, 8.32 μmol , 14.6%). $R_f = 0.41$ (Hexane:EtOAc 7:3, on alumina).

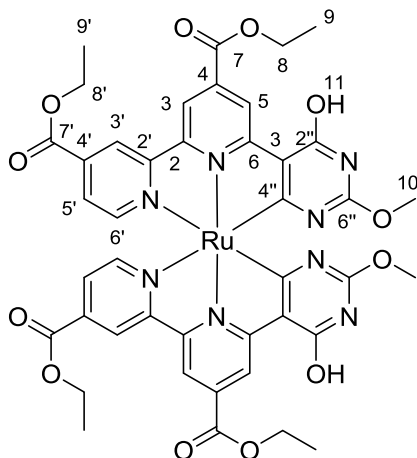
^1H NMR (300 MHz, CDCl_3) δ 9.12 (d, $J = 1.5$ Hz, 2H), 8.78 (dd, $J = 1.6, 0.7$ Hz, 2H), 8.69 (d, $J = 1.5$ Hz, 2H), 7.42 (dd, $J = 5.7, 0.5$ Hz, 2H), 7.36 (dd, $J = 5.7, 1.6$ Hz, 2H), 4.88 (s, 2H), 4.61 (q, $J = 7.1$ Hz, 4H), 4.40 (q, $J = 7.1$ Hz, 4H), 4.05 (s, 6H), 3.58 (s, 6H), 1.58 (t, $J = 7.1$ Hz, 6H), 1.38 (t, $J = 7.1$ Hz, 6H);

^{13}C NMR (100 MHz, CDCl_3) δ 205.22 ($\text{C}^{4''}$), 166.51 (C^7), 164.44 ($\text{C}^{7'}$), 160.60 (C^6), 160.50 ($\text{C}^{6''}$), 159.63 ($\text{C}^{2''}$), 156.00 ($\text{C}^{2'}$), 150.44 (C^2), 149.88 (C^6'), 134.95 ($\text{C}^{4'}$), 130.09 (C^4), 123.69 (C^5), 121.42 (C^3), 120.34 ($\text{C}^{3''}$), 119.07 (C^3), 115.63 (C^5), 105.45 ($\text{C}^{5''}$), 62.23 ($\text{C}^{8'}$), 61.80 (C^8), 52.99 (C^{10}), 52.94 (C^{11}), 14.67 (C^9), 14.41 (C^9');

MS (TOF ES^+): m/z (%): 974.2 (100) [M] $^+$;

HRMS (ES^+): [M] $^+$ calcd. for $\text{C}_{46}\text{H}_{44}\text{N}_6\text{O}_{12}^{102}\text{Ru}$, 974.2061; found, 974.2063.

Ruthenium(II) bis(diethyl 6-(4-hydroxy-2-methoxypyrimidyl)-2,2'-bipyridine-4,4'-dicarboxylate) (117)

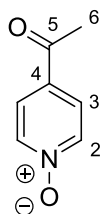


A 10 mL microwave reactor vial fitted with a septum, was charged with **116** (50.0 mg, 114 μmol , 4 eq) and $[\text{Ru}(p\text{-cymene})\text{Cl}_2]_2$ (17.5 mg, 28.6 μmol , 1eq). The apparatus was then evacuated and filled with argon. EtOH (2.5 mL) and *N*-ethylmorpholine (0.1 mL) (6 mL) were added and the resulting mixture was degassed with argon for 20 min before heating to 150 $^\circ\text{C}$ and stirring for 14 h under in a microwave reactor. After cooling to rt the solvent and base were removed under reduced pressure. Purification was performed by column chromatography on alumina (Hexane:EtOAc 9:1) to yield a black solid (8.1 mg, 8.32 μmol , 14.6%). $R_f = 0.41$ (Hexane:EtOAc 7:3, on silica).

^1H NMR (300 MHz, CDCl_3) δ 8.85 (d, $J = 14.6$ Hz, 2H, $\text{H}^{5'}$), 8.80 (s, 2H, $\text{H}^{3'}$), 8.59 (s, 2H, H^3), 7.79 (s, 2H, H^{11}), 7.60 (d, $J = 5.4$ Hz, 2H, H^6), 7.32 (d, $J = 5.5$ Hz, 2H, $\text{H}^{5''}$), 4.64 (q, $J = 6.8$ Hz, 4H, H^8), 4.47 (q, $J = 7.0$ Hz, 4H, $\text{H}^{8'}$), 1.60 (t, $J = 7.0$ Hz, 6H, H^9), 1.43 (t, $J = 7.0$ Hz, 6H, $\text{H}^{9'}$);

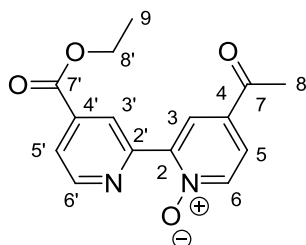
MS (TOF ES⁺): *m/z* (%): 971.1 (100) [M+Na]⁺.

4-Acetylpyridine-1-oxide (121)



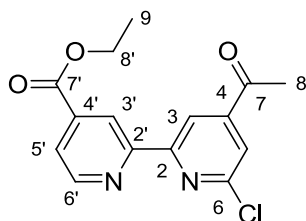
To a 100 mL round bottom flask charged with 4-acetylpyridine (2.10 g, 17.0 mmol, 1 eq) and CH₂Cl₂ (50 mL), *m*CPBA (75 %, 5.15 g, 22.4 mmol, 1.3 eq) was added slowly over 5 min. The resulting mixture was stirred at 30 °C for 16 h. The solvent was removed under reduced pressure and CH₂Cl₂ (100 mL) and Na₂CO₃ solution (20 g in 100 mL H₂O) were added. The organic phase was extracted, washed with H₂O (2 x 100 mL), dried (MgSO₄) and the solvent removed under reduced pressure. Crude carried forward without further purification.

4-Acetyl-4'-(ethoxycarbonyl)-2-2'-bipyridine-1-oxide (122)



89 (1.85g, 8.04 mmol, 1 eq), **121** (2.20 g, 137.14 mmol, 2 eq), palladium(II) acetate (90.0 mg, 401 μmol, 5 mol %), tri-*tert*-butylphosphonium tetrafluoroborate (348 mg, 401 μmol, 0.15 mol %), potassium phosphate (3.4 g, 16.0 mmol, 2 eq) and toluene (20 ml) were combined in a 2 neck round bottom flask fitted with condenser, stop cock and magnetic stirrer. The resulting mixture was degassed with argon and heated to 110 °C and stirred for 16 h. After cooling to rt the solvent was removed under reduced pressure. CH₂Cl₂ (50 mL) was added and extracted with H₂O (50 mL). The organic phases were dried (MgSO₄) and the solvent removed under reduced pressure to afford a brown solid. The crude mixture was recrystallized from CH₂Cl₂ (10 mL) by the addition of hexane (100 mL). The precipitate was collected by vacuum filtration and dried under vacuum. The resulting crude yellow solid was carried forward without further purification.

Ethyl-6-chloro-4-acetyl-2-2'-bipyridine-4'-carboxylate (123)



122 (1.40 g, crude) was combined with POCl₃ (10 mL), the mixture was degassed with argon before being stirred and heated to reflux at 120 °C. After 1.5 h the solution was cooled to rt and the remaining POCl₃ was removed by vacuum distillation at 50 °C and 10⁻³ mbar. H₂O (50 mL) was added to the remaining solid, which was extracted with CH₂Cl₂ (4 x 50 mL) the organic phases were combined, and dried (MgSO₄), and the solvent removed under reduced pressure. The remaining solid was purified by column chromatography on silica (CH₂Cl₂:Et₂O 9:1 and then hexane:EtOAc 5:2) to yield a white crystalline solid (40.0 mg, 131 μmol, 1.6 % over 2 steps). *R*_f = 0.34 (CH₂Cl₂:Et₂O 9:1, on silica).

Mp: 140-142 °C;

¹H NMR (400 MHz, CDCl₃) δ 8.92 (dd, *J* = 1.4, 0.8 Hz, 1H, H^{3'}), 8.84 (dd, *J* = 4.9, 0.7 Hz, 1H, H^{6'}), 8.79 (d, *J* = 1.3 Hz, 1H, H³), 7.93 (dd, *J* = 4.9, 1.6 Hz, 1H, H^{5'}), 7.81 (d, *J* = 1.3 Hz, 1H, H⁵), 4.47 (q, *J* = 7.1 Hz, 2H, H^{8'}), 2.71 (s, *J* = 5.9 Hz, 4H, H⁸), 1.45 (t, *J* = 7.1 Hz, 3H, H⁹);

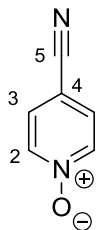
¹³C NMR (100 MHz, CDCl₃) δ 196.12 (C⁷), 165.11 (C^{7'}), 157.62 (C²), 155.15 (C²), 152.53 (C⁶), 150.25 (C^{6'}), 146.83 (C⁴), 139.38 (C^{4'}), 124.01 (C^{5'}), 122.49 (C⁵), 120.98 (C^{3'}), 118.04 (C³), 62.18 (C^{8'}), 27.18 (C⁸), 14.42 (C⁹);

IR(film, cm⁻¹): 3092s (C-H), 2998s (C-H), 2925s (C-H), 2854 (C-H), 1719 (C=O), 1704 (C=O), 1585 (C=C), 1544s (C=C), 1469s (C-H), 1417s (C-H), 1396s (C-H), 1367s (C-H), 1285 (C-O), 1253 (C-O);

MS (TOF ES⁺): *m/z* (%): 305.1 (100) [M+H]⁺;

HRMS (ES⁺): [M+H]⁺ calcd. For C₁₅H₁₄N₂O₃³⁵Cl, 305.0693; found, 305.0691.

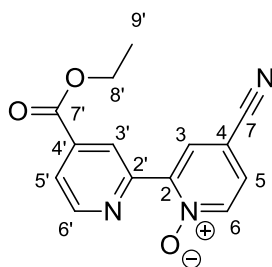
4-Cyanopyridine-*N*-oxide (126)



4-Cyanopyridine 98% (2.30g, 21.7 mmol, 1 eq) was combined with CH₂Cl₂ (50 mL) in a 100 mL flask fitted with magnetic stirrer and condenser. *m*-CPBA 75% (5.00 g, 21.7 mmol, 1 eq) was added slowly to the stirred solution. The resulting solution was stirred for 16 h at rt. A white precipitate was formed. Solvent was removed under reduced pressure and the crude white solid was combined with silica (15 g) and CHCl₃ (50 mL). Solvent was removed under reduced pressure and the solid purified by column chromatography on silica (CH₂Cl₂:Et₂O 5:2, CH₂Cl₂:MeOH 9:1), to afford a white crystalline solid (1.80 g, 15.0 mmol, 69%). *R*_f = 0.16 (CH₂Cl₂:Et₂O 5:2, on silica).

¹H NMR (300 MHz, CDCl₃) δ 8.25 (d, *J* = 7.4 Hz, 1H, H²), 7.53 (d, *J* = 7.3 Hz, 1H, H³).

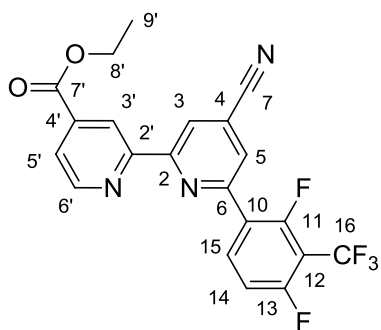
4-Cyano-4'-(ethoxycarbonyl)-2,2'-bipyridine-*N*-oxide (**127**)



89 (1.80 g, 15.0 mmol, 2 eq), **126** (1.72 g, 7.5 mmol, 1 eq), palladium(II) acetate (84 mg, 375 μmol, 5 mol%), PtBu₃-HBF₄ (131 mg, 450 μmol, 6 mol%), and K₂PO₄ (2.07 g, 9.75 mmol, 1.3 eq) were combined in a 100 mL 2 neck flask fitted with magnetic stirrer, condenser and stopcock. The apparatus was evacuated and filled with argon before the addition of toluene (50 mL). The resulting solution was degassed with argon before heating to 110 °C under argon for 14 h. After cooling to rt, solvent was removed under reduced pressure. Saturated NH₄Cl solution (75 mL) was added along with CH₂Cl₂ (100 mL). The resulting mixture was filtered through celite (10 g) The resulting biphasic filtrate was separated and the aqueous phase extracted with

further portions of CH₂Cl₂ (2 x 100 mL). The filtrand was washed with H₂O (50 mL) and CH₂Cl₂ (100 mL) and the resulting mixture separated. The organic phases were combined and dried (MgSO₄) and the solvent removed under reduced pressure to yield a crude yellow solid (2.98 g) which was carried forward without further purification.

Ethyl-6-(2,4-difluoro-3-(trifluoromethyl)phenyl)-4-Cyano-2,2'-bipyridine-4'-carboxylate (131)



A mixture of **130** (49.1 mg, 354 μ mol, 0.67 eq), and **131** (50.9 mg, 177 μ mol, 0.33 eq) was combined with **60** (180 mg, 797 μ mol, 1.5 eq), and Na₂CO₃ (84.5 mg, 797 μ mol, 1.5 eq) were combined along with THF (25 mL) and H₂O (5 mL). The solvent was degassed with argon for 20 min. Tetrakis(triphenylphosphine)palladium(0) (30.7 mg 26.6 μ mol, 5 mol %) was then added and the mixture degassed with argon for a further 10 min before stirring under argon at 70 °C for 16 h. After cooling to rt the solvent was removed under reduced pressure and CH₂Cl₂ (50 mL), HCl (2 M, 0.5 mL) and H₂O (50 mL) were added. The organic phase was separated and dried (MgSO₄) and the solvent was removed under reduced pressure. The resulting solid was purified by column chromatography on silica (CH₂Cl₂:Hexane 8:2), to afford a white crystalline solid (64 mg, 148 μ mol, 84%). *R*_f = 0.53 (CH₂Cl₂:Hexane 8:2, on silica).

¹H NMR (300 MHz, CDCl₃) δ 8.98 (dd, *J* = 1.5, 0.8 Hz, 1H, H^{3'}), 8.87 (dd, *J* = 5.0, 0.8 Hz, 1H, H^{6'}), 8.73 (d, *J* = 1.2 Hz, 1H, H³), 8.44 (td, *J* = 8.7, 6.1 Hz, 1H, H¹⁵), 8.07 – 8.04 (m, 1H, H₅), 7.96 (dd, *J* = 4.9, 1.6 Hz, 1H, H^{5'}), 7.25 (t, *J* = 9.1 Hz, 1H, H¹⁴), 4.48 (q, *J* = 7.1 Hz, 2H, H^{8'}), 1.45 (t, *J* = 7.1 Hz, 3H, H^{9'});

¹³C NMR (100 MHz, CDCl₃) δ 165.09 (s, C^{7'}), 163.53 (dd, *J* = 270.3, 4.4 Hz, C¹¹), 159.70 – 156.76 (m, C¹³), 157.04 (s, C^{2'}), 155.01 (s, C²), 151.92 (s, C⁶), 150.47 (s, C^{6'}), 139.36 (s, C^{4'}),

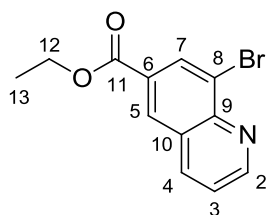
135.66 (d, $J = 10.8$ Hz, C¹⁵), 125.85 (s, C⁴), 125.73 (s, C⁵), 124.19 (s, C^{5'}), 122.72 (s, C¹⁰), 122.44 (s, C³), 120.74 (s, C^{3'}), 116.54 (s, C⁷), 113.80 (dd, $J = 22.3, 3.8$ Hz, C¹⁴), 62.26 (s, C^{8'}), 14.36 (s, C^{9'}), Expected signals for C¹² (approx. 120 (tq, $J = 30, 30$ Hz)) and C¹⁶ (approx. 120 (tq, $J = 250, 10$ Hz)) not observed due to high level of splitting giving a very weak signal. ¹H, ¹⁹F and HRMS confirm structure is correct;

¹⁹F NMR (282 MHz, CDCl₃) δ -56.17 (dd, $J = 23.8, 23.1$ Hz, 3F, F¹⁶), -107.08 (qd, $J = 24.0, 3.8$ Hz, 1F, F¹³), -113.91 (qd, $J = 22.8, 3.8$ Hz, 1F, F¹¹);

MS (TOF ES⁺): m/z (%): 434.11 (100) [M+H]⁺;

HRMS (ES⁺): [M+H]⁺ calcd. for C₂₁H₁₃N₃O₂F₅, 434.0928; found, 434.0919.

Ethyl-8-bromoquinoline-6-carboxylate (134)



4-Amino-3-bromobenzoic acid (5.00 g, 23.1 mmol, 1 eq) was combined with sodium *m*-nitrobenzene sulfonate (5.20 g, 23.1 mmol, 1 eq), glycerol (9.60 g) and H₂SO₄ (75%, 60 mL) in a 250 mL flask fitted with magnetic stirrer and condenser. The resulting solution was stirred for 3 h at 100 °C and then 4 h at 140 °C. After cooling to 60 °C EtOH (60 mL) was added and the reaction stirred at 60 °C for 12 h. The pH of the resulting solution was adjusted to 7 with saturated Na₂CO₃ solution causing a precipitate to form. The resulting suspension was extracted with EtOAc (3 x 500 mL). The organic phases were combined, dried (MgSO₄) and solvent was removed under reduced pressure. The crude brown solid was purified by column chromatography on silica (CH₂Cl₂, CHCl₃:MeOH 9:1) followed by recrystallization from acetone using the following method: The crude solid was combined with 50 mL acetone and heated with stirring to 50 °C for 30 min. The resulting solution was cooled to 0 °C for 30 min and the resulting crystals collected by vacuum filtration and washed with -20 °C acetone. The

crystals were dried under vacuum to afford a white crystalline solid (2.71 g, 9.67 mmol, 42%). $R_f = 0.51$ (CH_2Cl_2 on silica).

Mp: 129-131 °C;

^1H NMR (400 MHz, CDCl_3) δ 9.15 (dd, $J = 4.2, 1.7$ Hz, 1H, H^2), 8.66 (d, $J = 1.8$ Hz, 1H, H^7), 8.57 (d, $J = 1.8$ Hz, 1H, H^5), 8.30 (dd, $J = 8.3, 1.7$ Hz, 1H, H^4), 7.56 (dd, $J = 8.3, 4.2$ Hz, 1H, H^3), 4.47 (q, $J = 7.1$ Hz, 2H, H^{12}), 1.46 (t, $J = 7.1$ Hz, 3H, H^{13});

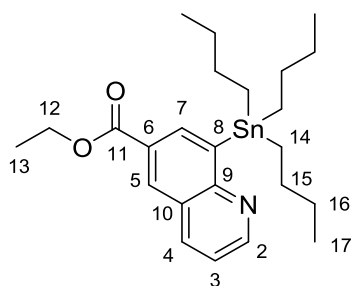
^{13}C NMR (100 MHz, CDCl_3) δ 165.11 (C^{11}), 153.37 (C^2), 147.24 (C^9), 138.13 (C^4), 132.75 (C^7), 130.71 (C^5), 129.20 (C^{10}), 128.68 (C^6), 125.29 (C^8), 122.79 (C^3), 61.94 (C^{12}), 14.49 (C^{13});

IR(film, cm^{-1}): 3076s (C-H), 2981s (C-H), 2948s (C-H), 2904 (C-H), 1709 (C=O), 1594 (C=C), 1556s (C=C), 1486s (C-H), 1475s (C-H), 1416s (C-H), 1367s (C-H), 1321s (C-H), 1267 (C-O);

MS (TOF ES^+): m/z (%): 280.0 (100) [$\text{M}+\text{H}$] $^+$;

HRMS (ES^+): [$\text{M}+\text{H}$] $^+$ calcd. for $\text{C}_{12}\text{H}_{11}\text{NO}_2\text{Br}$, 279.9973; found, 279.9972.

Ethyl-8-(tributylstannyl)quinoline-6-carboxylate (**142**)



134 (250 mg, 892 μmol , 1 eq), was combined with hexabutyliditin (98%, 569 mg, 981 μmol , 1.1 eq) along with PhMe (25 mL). The solvent was degassed with argon for 20 min. Bis(triphenylphosphine)palladium(II) dichloride (18.8 mg 26.6 μmol , 3 mol %) was then added and the mixture degassed with argon for a further 10 min before stirring under argon at 110 °C for 24 h. After cooling to rt the solvent was removed under reduced pressure and CH_2Cl_2 (50 mL), and H_2O (50 mL) were added. The organic phase was separated and dried (MgSO_4) and the solvent was removed under reduced pressure. The resulting solid was purified by column chromatography on silica (CH_2Cl_2), to afford colourless oil (260 mg, 530 μmol , 59%). $R_f = 0.74$ (CH_2Cl_2 on silica).

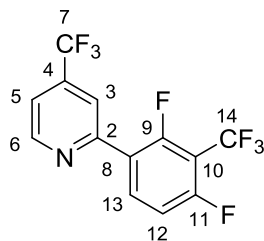
^1H NMR (300 MHz, CDCl_3) δ 8.94 (dd, $J = 4.2, 1.8$ Hz, 1H, H^2), 8.48 (dd, $J = 19.1, 1.9$ Hz, 1H, H^5), 8.21 (dd, $J = 8.3, 1.8$ Hz, 1H, H^4), 7.40 (dd, $J = 8.2, 4.2$ Hz, 1H, H^3), 7.30 – 7.11 (m, 3H, H^7), 4.46 (q, $J = 7.1$ Hz, 2H, H^{12}), 1.63 – 1.50 (m, 6H, H^{14}), 1.46 (t, $J = 7.1$ Hz, 3H, H^{13}), 1.40 – 1.23 (m, 6H, H^{15}), 1.22 – 1.11 (m, 6H, H^{16}), 0.90 – 0.81 (m, 9H, H^{17}).

IR(film, cm^{-1}): 2955s (C-H), 2921s (C-H), 2852s (C-H), 2871 (C-H), 1719 (C=O), 1609 (C=C), 1555s (C=C), 1478s (C-H), 1460s (C-H), 1417s (C-H), 1365s (C-H), 1315s (C-H), 1253 (C-O);

MS (TOF ES $^+$): m/z (%): 514.2 (100) $[\text{M}+\text{Na}]^+$;

HRMS (ES $^+$): $[\text{M}+\text{Na}]^+$ calcd. for $\text{C}_{24}\text{H}_{37}\text{NO}_2^{23}\text{Na}^{120}\text{Sn}$, 514.1744; found, 514.1746.

2-(2,4-Difluoro-3-(trifluoromethyl)phenyl)-4-(trifluoromethyl)pyridine (84)



2-Chloro-4-trifluoromethylpyridine (3.47 g, 19.1 mmol, 1 eq), **60** (5.18 g, 22.9 mmol, 1.2 eq), and Na_2CO_3 (2.43mg, 22.9 mmol, 1.2 eq) were combined along with THF (150 mL) and H_2O (30 mL). The solvent was degassed with argon for 20 min. Tetrakis(triphenylphosphine)palladium(0) (441 mg, 382 μmol , 5 mol %) was then added and the mixture degassed with argon for a further 10 min before stirring under argon at 70 $^\circ\text{C}$ for 20 h. After cooling to rt the solvent was removed under reduced pressure and CH_2Cl_2 (100 mL) and H_2O (100 mL) were added. The organic phase was separated and dried (MgSO_4) and the solvent was removed under reduced pressure. The resulting solid was purified by column chromatography on silica (hexane: Et_2O 10:1), to afford a white crystalline solid (3.87 g, 11.8 mmol, 62%). $R_f = 0.21$ (hexane: Et_2O 10:1, on silica).

Mp: 38-39 $^\circ\text{C}$

^1H NMR (300 MHz, CDCl_3) δ 8.91 (d, $J = 5.1$ Hz, 1H, H^6), 8.27 (td, $J = 8.7, 6.1$ Hz, 1H, H^{13}), 8.01 (d, $J = 0.7$ Hz 1H, H^3), 7.54 (dd, $J = 5.0, 0.7$ Hz, 1H, H^5), 7.23 – 7.11 (m, 1H, H^{12});

^{13}C NMR (75 MHz, CDCl_3) δ 160.65 (dd, $J = 263.3, 4.0$ Hz, C^9), 157.48 (dd, $J = 263.6, 4.0$ Hz, C^{11}), 152.64 (s, C^2), 151.02 (s, $J = 8.8$ Hz, C^6), 139.41 (q, $J = 34.3$ Hz, C^4), 135.66 (dd, $J = 10.8, 5.0$ Hz, C^{12}), 123.89 (dd, $J = 12.0, 3.8$ Hz, C^8), 122.83 (q, $J = 273.3$ Hz, C^7), 127.37 – 116.21 (m, C^{14}), 120.47 – 119.76 (m, C^3), 119.04 – 118.61 (m, C^5), 113.48 (dd, $J = 22.3, 3.8$ Hz C^{13}), 109.53 – 107.53 (m, C^{10}).

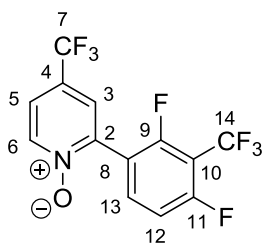
^{19}F NMR (282 MHz, CDCl_3) δ -56.19 (dd, $J = 23.9, 22.7$ Hz, 3F, F^{14}), -64.81 (s, 3F, F^7), -107.91 (qd, $J = 24.0, 3.5$ Hz, 1F, F^9), -114.54 (qd, $J = 22.7, 3.5$ Hz, 1F, F^{11}).

IR(film, cm^{-1}): 3085s (C-H), 3066s (C-H), 1627 (C=C), 1594s (C=C), 1500s (C-H), 1437s (C-H), 1409s (C-H), 1338s (C-H), 1309s (C-H);

MS (TOF ES^+): m/z (%): 328.0 (100) $[\text{M}+\text{H}]^+$;

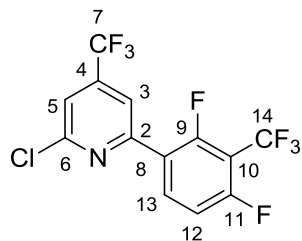
HRMS (ES^+): $[\text{M}+\text{H}]^+$ calcd. for $\text{C}_{13}\text{H}_6\text{NF}_8$, 328.0372; found, 328.0373.

2-(2,4-Difluoro-3-(trifluoromethyl)phenyl)-4-(trifluoromethyl)pyridine-*N*-oxide (86)



To a round bottom flask charged with **84** (2.00 g, 6.11 mmol, 1 eq) and CHCl_3 (50 mL), *m*CPBA (75%, 1.69 g, 7.34 mmol, 1.2 eq) was added slowly over 5 min. The resulting mixture was stirred at 50 °C for 16 h. After cooling to rt, Na_2CO_3 solution (1 M, 50 mL) was added. The organic phase was extracted, washed with H_2O (2 x 50 mL), dried (MgSO_4) and the solvent removed under reduced pressure. The crude solid (1.53 g) was carried forward.

2-Chloro-6-(2,4-Difluoro-3-(trifluoromethyl)phenyl)-4-(trifluoromethyl)pyridine (88)



Crude **86** (1.00 g) was combined with POCl₃ (10 mL), the mixture was stirred and heated to reflux at 120 °C and the solid dissolved to form a yellow solution. After 2 h the solution had turned brown. The solution was cooled to rt and the remaining POCl₃ was removed by vacuum distillation at 85 °C and 10 mbar. H₂O (50 mL) was added to the remaining solid, which was extracted with CH₂Cl₂ (4 x 50 mL) the organic phases were combined, and dried (MgSO₄), and the solvent removed under reduced pressure. The remaining solid was purified by column chromatography on silica (hexane:CH₂Cl: 8:2) to yield a white oil (350 mg, 970 μmol, 24% over 2 steps). *R_f* = 0.26 (hexane:CH₂Cl: 8:2, on silica);

¹H NMR (300 MHz, CDCl₃) δ 8.32 (td, *J* = 8.7, 6.0 Hz, 1H, H¹²), 7.96 (s, 1H, H³), 7.58 (s, 1H, H⁵), 7.23 – 7.13 (m, 1H, H¹³);

¹³C NMR (100 MHz, CDCl₃) δ 162.25 – 159.27 (m, C⁹), 159.60 – 156.64 (m, C¹¹), 152.81 (s, C²), 152.44 (s, C⁶), 141.94 (q, *J* = 34.4 Hz, C⁴), 135.59 (dd, *J* = 10.8, 4.4 Hz, C¹²), 122.21 (dd, *J* = 11.7, 3.9 Hz, C⁸), 121.89 (q, *J* = 274.0 Hz, C⁷), 120.18 – 119.55 (m, C³), 125.40 – 117.05 (m, C¹⁴), 118.99 – 118.05 (m, C⁵), 113.61 (dd, *J* = 22.3, 3.8 Hz C¹³). C¹⁰ too heavily split to be observed expected at around 110 ppm;

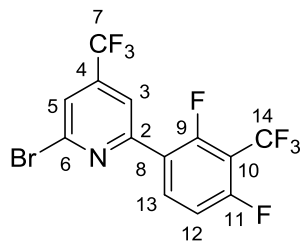
¹⁹F NMR (282 MHz, CDCl₃) δ -56.23 (dd, *J* = 23.8, 23.0 Hz, 3F, F¹⁴), -64.70 (s, 3F, F⁷), -106.52 (qd, *J* = 24.0, 4.1 Hz, 1F, F⁹), -113.58 (qd, *J* = 22.8, 4.1 Hz, 1F, F¹¹);

IR(film, cm⁻¹): 3100s (C-H), 1627 (C=C), 1608s (C=C), 1564s (C-H), 1498s (C-H), 1456s (C-H), 1405s (C-H), 1338s (C-H) 1310s (C-H);

MS (TOF ES⁺): *m/z* (%): 360.91 (100) [M]⁺;

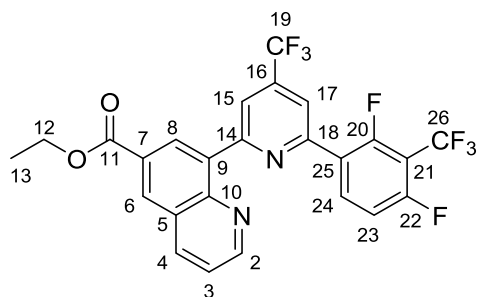
HRMS (ES⁺): [M]⁺ calcd. for C₁₃H₄NF₈³⁵Cl, 360.9905; found, 360.9897.

2-Bromo-6-(2,4-Difluoro-3-(trifluoromethyl)phenyl)-4-(trifluoromethyl)pyridine (141)



88 (100 mg, 277 μmol , 1 eq), bromotrimethylsilane (340 mg, 2.22 mmol, 8 eq), and anhydrous *i*PrCN (10 mL) were combined. The resulting mixture degassed with argon before heating to 80 $^{\circ}\text{C}$ for 100 h. After cooling to rt solvent was removed under reduced pressure and the mixture combined with CH_2Cl_2 (50 mL) and Na_2CO_3 (aq, 2M, 50 ml). The organic phase was extracted and washed with H_2O (50 mL) before drying with MgSO_4 . The solvent was removed under reduced pressure to produce a colourless oil (150 mg) which was carried forward to the next step.

Ethyl 8-(6-(2,4-difluoro-3-(trifluoromethyl)phenyl)-4-(trifluoromethyl)pyridin-2-yl)quinoline-6-carboxylate (137)



88 (50 mg, 130 μmol , 1 eq), **142** (68.8 mg, 143 μmol , 1.1 eq) and Bis(triphenylphosphine)palladium(II) dichloride (4.6 mg 6.50 μmol , 5 mol %) were added to a flame dried 2-neck flask fitted with stopcock septum and condenser. The reaction vessel was evacuated and refilled with argon after which anhydrous DMF (10 mL) was then added and the mixture degassed with argon for a further 10 min before stirring under argon at 110 $^{\circ}\text{C}$ for 24 h. After cooling to rt the solvent was removed under reduced pressure and CH_2Cl_2 (50 mL), and H_2O (50 mL) were added. The organic phase was separated and dried (MgSO_4) and the solvent was removed under reduced pressure. The resulting solid was purified by column chromatography on silica (hexane:EtOAc 8:2), to afford a white solid (8.8 mg, 16.7 μmol , 13%). $R_f = 0.33$ (hexane:EtOAc 8:2 on silica).

^1H NMR (300 MHz, CDCl_3) δ 9.08 (dd, $J = 4.2, 1.8$ Hz, 1H, H^2), 8.84 (d, $J = 2.0$ Hz, 1H, H^6), 8.71 (d, $J = 2.0$ Hz, 1H, H^8), 8.48 (s, 1H, H^{15}), 8.47 – 8.41 (m, 1H, H^{23}), 8.39 (dd, $J = 8.4, 1.9$ Hz, 1H, H^4), 8.04 (s, 1H, H^{17}), 7.57 (dd, $J = 8.3, 4.2$ Hz, 1H, H^3), 7.22 – 7.13 (m, 1H, H^{24}), 4.49 (q, $J = 7.1$ Hz, 2H, H^{12}), 1.47 (t, $J = 7.1$ Hz, 3H, H^{13});

Insufficient quantity for ^{13}C NMR;

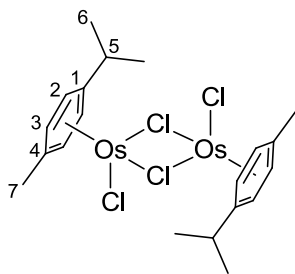
^{19}F NMR (282 MHz, CDCl_3) δ -56.11 (dd, $J = 23.7, 22.9$ Hz, 3F, F^{26}), -64.39 (s, 3F, F^{19}), -108.41 (qd, $J = 24.0, 3.3$ Hz, 1F, F^{20}), -114.39 (qd, $J = 22.7, 3.3$ Hz, 1F, F^{22});

MS (TOF ES^+): m/z (%): 527.1 (100) $[\text{M}+\text{H}]^+$;

HRMS (ES^+): $[\text{M}+\text{H}]^+$ calcd. for $\text{C}_{25}\text{H}_{15}\text{N}_2\text{O}_2\text{F}_8$, 527.1006; found, 527.1008.

4 Characterisation-Chapter 3

Dichloro(*p*-cymene)osmium(II) dimer (160)



A 10 mL microwave reactor vial fitted with a septum, was charged with sodium hexachloroosmate dihydrate (200 mg, 412 μmol , 1eq) and α -phellandrene (0.5 mL). The apparatus was then evacuated and filled with argon. EtOH (2.5 mL) and H_2O (0.1 mL) were added and the resulting mixture was degassed with argon for 20 min before heating to 100 $^\circ\text{C}$ and stirring for 3 h in a microwave reactor. After cooling to rt the resulting suspension was cooled to 5 $^\circ\text{C}$ overnight. The resulting orange precipitate was collected by vacuum filtration, washed with ice-cold EtOH (2 x 10 mL) and diethyl ether (2 x 10 mL), and dried under vacuum to yield an orange solid, (93.0 mg, 118 μmol , 57%).

^1H NMR (400 MHz, CDCl_3) δ 6.18 (d, $J = 5.7$ Hz, 2H, H^3), 6.02 (d, $J = 5.7$ Hz, 2H, H^2), 2.78 (sep, $J = 6.9$ Hz, 1H, H^5), 2.20 (s, 3H, H^7), 1.28 (d, $J = 6.9$ Hz, 6H, H^6);

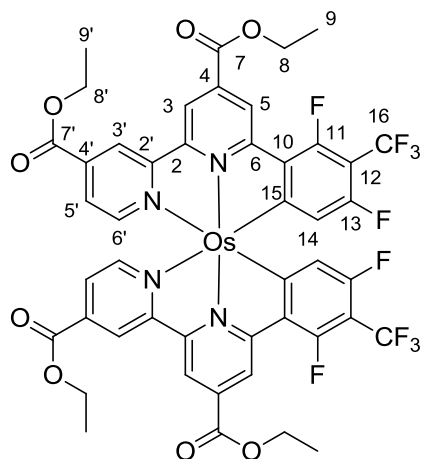
^{13}C NMR (100 MHz, CDCl_3) δ 92.6 (C^4), 89.3 (C^1), 74.2 (C^3), 72.6 (C^2), 31.5 (C^5), 22.6 (C^6), 19.6 (C^7);

IR(film, cm^{-1}): 3045s (C-H), 2961s (C-H), 2925s (C-H), 2868s (C-H), 1448s (C=C), 1387s (C-H), 876s (Os-Cl);

MS (TOF ES $^+$): m/z (%): 755.2 (100) $[\text{M}+\text{H}]^+$;

HRMS (ES $^+$): $[\text{M}+\text{H}]^+$ calcd. For $\text{C}_{20}\text{H}_{28}\text{Cl}_3^{190}\text{Os}^{192}\text{Os}$, 755.0456; found, 755.0424.

Osmium(II) bis(diethyl-6-(2,4-difluoro-3-(trifluoromethyl)phenyl)-2-2'-bipyridine-4,4'-dicarboxylate) (154)



Standard procedure

A 2 neck round bottom flask fitted with stirrer, condenser and stopcock was charged with **61** (97.2 mg, 202 μmol , 4 eq) and **160** (41 mg, 50.6 mmol, 1 eq). The apparatus was evacuated and filled with argon before the addition of *n*PrCN (10 mL) and *N*-ethylmorpholine (0.2 mL). The resulting orange solution was degassed with argon for 20 min before heating and stirring at 120 $^{\circ}\text{C}$, for 16 h under argon and reduced light. After cooling to rt solvent was removed under reduced pressure and the crude black solid was dried under high vacuum. Ethylene glycol (10 mL) was added and the resulting mixture degassed for 20 min with argon. The reaction mixture was then heated and stirred at 200 $^{\circ}\text{C}$ for 2 h under argon and reduced light. The crude black mixture was combined with H_2O (50 mL) and CH_2Cl_2 (50 mL). The organic phase was separated and the aqueous phase extracted with further portions of CH_2Cl_2 (3 x 50 mL). The organic phases were combined, dried (MgSO_4) and solvent removed under reduced pressure. The crude

product was purified by column chromatography on silica (Hexane:EtOAc 7:3) to yield a black solid (5.8 mg, 5.05 μmol , 5.7%). $R_f = 0.24$ (Hexane:EtOAc 7:3, on silica).

Microwave procedure

A 10 mL microwave reactor vial fitted with a septum, was charged with **61** (100 mg, 208 μmol , 4eq) and **160** (41.2 mg, 52.0 μmol , 1 eq). The apparatus was then evacuated and filled with argon. EtOH (2.5 mL) and *N*-ethylmorpholine (0.1 mL) were added and the resulting mixture was degassed with argon for 20 min before heating to 100 °C and stirring for 14 h in a microwave reactor. After cooling to rt solvent was removed under reduced pressure and the crude black solid was purified by column chromatography on silica (Hexane:CH₂Cl₂ 7:1) to yield a black solid (31.0 mg, 27.0 μmol , 26%). $R_f = 0.24$ (Hexane:EtOAc 7:3, on silica).

¹H NMR (400 MHz, CDCl₃) δ 8.99 (s, 2H, H³), 8.97 (d, $J = 1.4$ Hz, 2H, H⁵), 8.89 (dd, $J = 1.6, 0.6$ Hz, 2H, H^{3'}), 7.33 (dd, $J = 5.9, 0.6$ Hz, 2H, H^{6'}), 7.29 (dd, $J = 5.9, 1.6$ Hz, 2H, H^{5'}), 5.32 (d, $J = 10.3$ Hz, 2H, H¹⁴), 4.64 (q, $J = 7.1$ Hz, 4H, H⁸), 4.43 (q, $J = 7.1$ Hz, 4H, H^{8'}), 1.59 (t, $J = 7.1$ Hz, 6H, H⁹), 1.39 (t, $J = 7.1$ Hz, 6H, H^{9'});

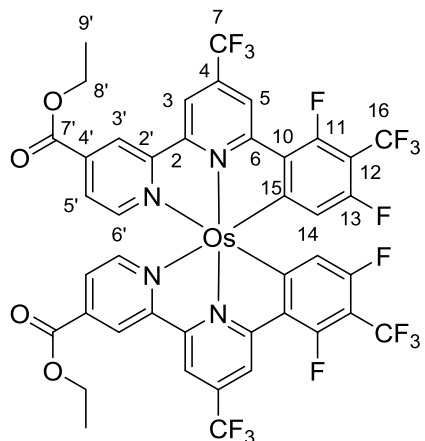
¹⁹F NMR (282 MHz, CDCl₃) δ -55.02 (dd, $J = 29.2, 16.1$ Hz, 6F, F¹⁶), -112.61 (qd, $J = 22.4, 4.5$ Hz, 2F, F¹¹), -113.54 (qd, $J = 22.8, 4.6$ Hz, 2F, F¹³);

¹³C NMR (100 MHz, CDCl₃) δ 179.27 (d, $J = 6.5$ Hz, C¹⁵), 164.89 (s, C^{7'}), 163.57 (s, C⁷), 160.80 (d, $J = 265.5$ Hz, C¹¹), 158.78 (d, $J = 270.7$ Hz, C¹³), 158.45 (d, $J = 6.3$ Hz, C⁶), 157.63 (s, C²), 149.89 (s, C⁶), 149.74 (s, C^{2'}), 135.61 (s, C⁴), 130.83 (s, C^{4'}), 128.43 (s, C⁵), 125.36 (s, C^{3'}), 122.90 (q, $J = 272.2$ Hz), 122.43 (s, C⁵), 119.62 (d, $J = 19.9$ Hz, C¹⁰), 117.87 (s, C³), 116.03 (d, $J = 14.5$ Hz, C¹⁴), 62.56 (s, C^{8'}), 62.26 (s, C⁸), 14.71 (s, C⁹), 14.42 (s, C^{9'});

IR(film, cm⁻¹): 3052w (C-H), 2968s (C-H), 2927s (C-H), 2855s (C-H), 2027s (Os-C), 1961s (Os-C), 1721s (C=O), 1704s (C=O), 1606s (C=C), 1537s (C=C), 1465s (C-H), 1448s (C-H), 1432s (C-H), 1366s (C-H), 1303 (C-O);

MS (TOF ES⁺): m/z (%): 1150.6 (100) [M+H]⁺;

Osmium(II) bis(ethyl-6-(2,4-difluoro-3-(trifluoromethyl)phenyl)-4-(trifluoromethyl)-2,2'-bipyridine-4'-carboxylate) (163)



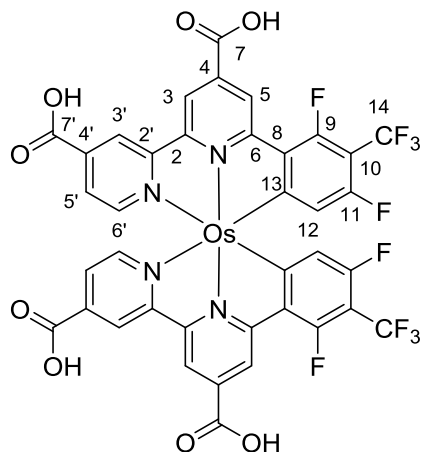
A 10 mL microwave reactor vial fitted with a septum, was charged with **68** (30.1 mg, 63.2 μmol , 4 eq) and **160** (12.5 mg, 15.8 μmol , 1eq). The apparatus was then evacuated and filled with argon. EtOH (2.5 mL) and *N*-ethylmorpholine (0.1 mL) (6 mL) were added and the resulting mixture was degassed with argon for 20 min before heating to 150 $^{\circ}\text{C}$ and stirring for 14 h under in a microwave reactor. After cooling to rt the solvent and base were removed under reduced pressure. Purification was performed by column chromatography on silica (Hexane:EtOAc 7:3) to yield a black solid (5.41 mg, 4.74 μmol , 15%). $R_f = 0.31$ (Hexane:EtOAc 7:3, on silica).

^1H NMR (300 MHz, CDCl_3) δ 8.81 (s, 2H, H^3), 8.66 (s, 2H, H^5), 8.55 (s, 2H, $\text{H}^{3'}$), 7.38 – 7.29 (m, 4H, $\text{H}^{5',6'}$), 5.32 (d, $J = 10.2$ Hz, 2H, H^{14}), 4.43 (q, $J = 7.1$ Hz, 4H, H^8), 1.39 (t, $J = 7.1$ Hz, 6H, H^9);

^{19}F NMR (282 MHz, CDCl_3) δ -55.13 (t, $J = 22.7$ Hz), -62.57 (s, $J = 7.1$ Hz), -111.58 (qd, $J = 22.2, 5.0$ Hz), -113.02 (qd, $J = 23.2, 5.1$ Hz);

MS (TOF ES^+): m/z (%): 1141.5 (100) $[\text{M}+\text{H}]^+$.

Osmium(II) bis(6-(2,4-difluoro-3-(trifluoromethyl)phenyl)-2,2'-bipyridine-4,4'-dicarboxylic acid) (164)

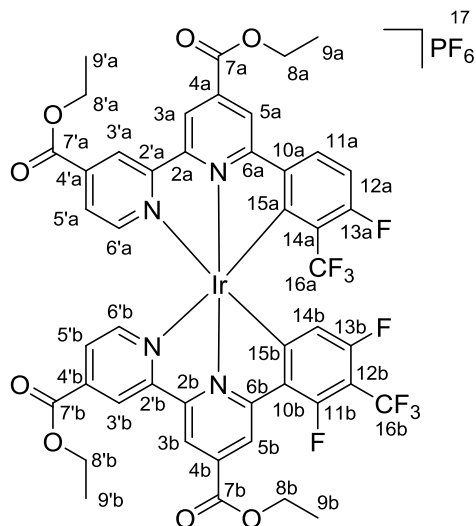


A 50 mL 2 neck round bottom flask fitted with condenser, stopcock and stirrer, was charged with **154** (10.0 mg, 8.70 μmol). The apparatus was then evacuated and filled with argon. KOH (2M, aq, 1 mL) and acetone (5 mL) were added and the resulting mixture was degassed with argon for 20 min before heating to 60 $^{\circ}\text{C}$ and stirring for 16 h under argon and reduced light conditions. After cooling to rt the mixture was treated with HCl (1M) until a black precipitate formed. The solid was collected by filtration, washed with H_2O , hexane, and CH_2Cl_2 . After drying the filtrand was removed from the filter by dissolving in MeOH. Solvent was removed under reduced pressure to yield a black solid (9.00 mg, 7.52 μmol , 86%).

^1H NMR (300 MHz, MeOD) δ 9.01 (d, $J = 7.4$ Hz, 2H, $\text{H}^{3'}$), 8.90 (s, 2H, H^3), 7.57 (d, $J = 5.0$ Hz, 2H, $\text{H}^{6'}$), 7.40 (d, $J = 5.3$ Hz, 2H, $\text{H}^{5'}$), 5.22 (d, $J = 9.3$ Hz, 2H, H^{12}).

^{19}F NMR (282 MHz, MeOD) δ -56.15 (t, $J = 22.3$ Hz, F6, F^{14}), -115.15 – -116.21 (m, F2, F^9), -116.21 – -117.83 (m, F2, F^{11}).

Iridium(III) (diethyl-6-(2,4-difluoro-3-(trifluoromethyl)phenyl)-2-2'-bipyridine-4,4'-dicarboxylate) (diethyl-6-(4-fluoro-3-(trifluoromethyl)phenyl)-2-2'-bipyridine-4,4'-dicarboxylate) hexafluorophosphate (165)



A 2 neck round bottom flask fitted with stirrer, condenser and stopcock was charged with **61** (100 mg, 208 μmol , 4 eq) and $[\text{Ir}(\text{COD})\text{Cl}]_2$ (35.0 mg, 52.0 μmol , 1 eq). The apparatus was evacuated and filled with argon before the addition of *n*PrCN (10 mL). The resulting yellow solution was degassed with argon for 20 min before heating and stirring at 120 $^\circ\text{C}$, for 16 h under argon and reduced light. After cooling to rt solvent was removed under reduced pressure and the crude brown solid was purified by column chromatography on silica (CH_2Cl_2 :MeCN 9:1 then CH_2Cl_2 :Et₂O 8:2) to yield a yellow solid (9.4 mg, 7.36 μmol , 7%). $R_f = 0.32$ (CH_2Cl_2 :Et₂O 8:2, on silica).

^1H NMR (300 MHz, CDCl_3) δ 8.88 (s, 1H), 8.77 (s, 2H), 8.74 (d, $J = 1.1$ Hz, 1H), 8.72 (s, 2H), 8.13 – 8.08 (m, 1H), 8.07 (d, $J = 5.5$ Hz, 1H), 7.84 (dd, $J = 5.6, 1.6$ Hz, 1H), 7.80 (dd, $J = 5.7, 1.6$ Hz, 1H), 6.97 – 6.88 (m, 2H), 5.48 (d, $J = 9.7$ Hz, 1H), 4.60 (qd, $J = 7.1, 2.7$ Hz, 4H), 4.44 – 4.18 (m, 5H), 1.53 (td, $J = 7.1, 5.3$ Hz, 13H), 1.30 (td, $J = 7.1, 2.8$ Hz, 7H).

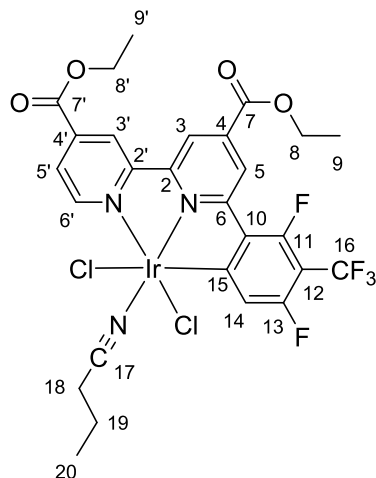
^{19}F NMR (282 MHz, CDCl_3) δ -55.69 (t, $J = 22.8$ Hz), -55.98 (d, $J = 41.6$ Hz), -73.04 (d, $J = 713.6$ Hz), -103.10 (q, $J = 41.6$ Hz), -105.20 (qd, $J = 22.8, 5.9$ Hz), -110.54 (ddd, $J = 45.5, 22.8, 6.0$ Hz);

MS (TOF ES⁺): m/z (%): 1134.5 (100) $[\text{M}+\text{H}]^+$;

HRMS (ES⁺): $[\text{M}+\text{H}]^+$ calcd. For $\text{C}_{46}\text{H}_{33}\text{N}_4\text{O}_8\text{F}_9$ ^{139}Ir , 1133.1784; found, 1133.1753.

Iridium(III) (diethyl-6-(2,4-difluoro-3-(trifluoromethyl)phenyl)-2,2'-bipyridine-4,4'-dicarboxylate) (butyronitrile) dichloride (166)

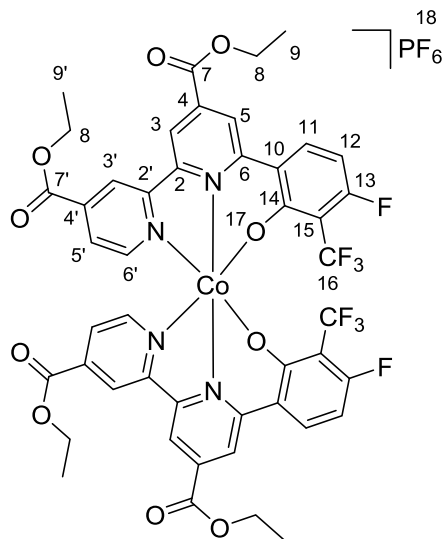
Side product of the above reaction. Orange solid, (5.40 mg, 5.66 μmol , 5%), $R_f = 0.62$ ($\text{CH}_2\text{Cl}_2:\text{Et}_2\text{O}$ 8:2, on silica).



^1H NMR (300 MHz, CDCl_3) δ 9.08 (dd, $J = 5.5, 0.5$ Hz, 1H, $\text{H}^{6'}$), 8.76 (d, $J = 0.8$ Hz, 1H, $\text{H}^{3'}$), 8.69 (d, $J = 1.1$ Hz, 1H, $\text{H}^{3'}$), 8.51 (d, $J = 1.3$ Hz, 1H, $\text{H}^{5'}$), 8.25 (dd, $J = 5.5, 1.6$ Hz, 1H, $\text{H}^{5'}$), 7.19 (d, $J = 10.2$ Hz, 1H, H^{13}), 4.56 (m, 4H, $\text{H}^{8,8'}$), 3.19 (t, $J = 7.1$ Hz, 2H, H^{18}), 2.13 – 1.93 (m, 2H, H^{19}), 1.55 – 1.42 (m, 7H, $\text{H}^{9,20}$), 1.36 – 1.20 (m, 3H, H^9);

^{19}F NMR (282 MHz, CDCl_3) δ -55.47 (t, $J = 22.7$ Hz, 3F, F^{16}), -105.87 (qd, $J = 22.8, 5.6$ Hz, 1F, F^{11}), -112.30 (qd, $J = 22.6, 5.6$ Hz, 1F, F^{13}).

Cobalt (III) bis(diethyl 6-(4-fluoro-2-oxy-3-(trifluoromethyl)phenyl)-2,2'-bipyridine-4,4'-dicarboxylate) (174)



A 10 mL microwave reactor vial fitted with a septum, was charged with **61** (50.0 mg, 104 μmol , 2 eq), CoBr_2 (11.4 mg, 52.8 μmol , 1eq), and AgNO_3 (17.7 mg, 104 μmol , 2 eq). The apparatus was then evacuated and filled with argon. EtOH (2.5 mL) and *N*-ethylmorpholine (0.1 mL) (6 mL) were added and the resulting mixture was degassed with argon for 20 min before heating to 150 °C and stirring for 14 h under in a microwave reactor. After cooling to rt the solvent and base were removed under reduced pressure. Purification was performed by column chromatography on silica (CH_2Cl_2 :MeOH 9:1) to yield a brown solid (14.3 mg, 14.1 μmol , 27%). $R_f = 0.26$ (Hexane:EtOAc 7:3, on silica).

^1H NMR (300 MHz, CDCl_3) δ 8.91 (d, $J = 1.2$ Hz, 2H, H^3), 8.87 (d, $J = 1.2$ Hz, 2H, H^5), 8.86 (d, $J = 1.1$ Hz, 2H, $\text{H}^{3'}$), 8.04 (dd, $J = 9.3, 5.9$ Hz, 2H, H^{11}), 7.74 (dd, $J = 5.9, 1.6$ Hz, 2H, $\text{H}^{5'}$), 7.65 (d, $J = 5.8$ Hz, 2H, H^6), 6.54 (t, $J = 9.7$ Hz, 2H, H^{12}), 4.68 (q, $J = 7.1$ Hz, 4H, H^8), 4.43 (q, $J = 7.1$ Hz, 4H, $\text{H}^{8'}$), 1.60 (t, $J = 7.2$ Hz, 6H, H^9), 1.46 – 1.33 (m, 3H, $\text{H}^{9'}$);

^{13}C NMR (101 MHz, CDCl_3) δ 192.33 (d, $J = 58.6$ Hz C^{14}), 163.29 (d, $J = 265.7$ Hz, C^{13}), 162.88 (s, C^7), 162.38 (s, $\text{C}^{7'}$), 157.73 (s, C^2), 157.30 (s, $\text{C}^{2'}$), 156.52 (s, C^6), 152.53 (s, $\text{C}^{6'}$), 142.80 (s, C^4), 142.27 (s, $\text{C}^{4'}$), 134.10 (d, $J = 13.5$ Hz, C^{11}), 127.04 (s, $\text{C}^{5'}$), 124.05 (s, $\text{C}^{3'}$), 123.34 (s, C^5), 119.86 (s, C^3), 117.85 (s, C^{10}), 106.46 (d, $J = 25.4$ Hz, C^{12});

^{19}F NMR (282 MHz, CDCl_3) δ -57.26 (d, $J = 31.3$ Hz, 6F, F^{16}), -73.15 (d, $J = 713.8$ Hz, 6F, F^{18}), -104.70 (q, $J = 31.3$ Hz, 2F, F^{13});

MS (TOF ES⁺): m/z (%): 1013.2 (100) $[\text{M}]^+$

5 Crystallographic data

Table 15: Crystal data and structure refinement for **95**

Identification code	TXR056
Empirical formula	C ₄₆ H ₃₂ F ₁₀ N ₄ O ₈ Ru, 0.2(CH ₂ Cl ₂)
Formula weight	1076.81
Temperature/K	100.00(10)
Crystal system	triclinic
Space group	P-1
a/Å	12.973(14)
b/Å	13.419(15)
c/Å	16.677(18)
α/°	100.695(3)
β/°	109.451(13)
γ/°	109.473(11)
Volume/Å ³	2433(5)
Z	2
ρ _{calc} /cm ³	1.470
μ/mm ⁻¹	3970
F(000)	1084.8
Crystal size/mm ³	0.050 x 0.010 x 0.010
Radiation	CuKα (λ = 1.54184)
2θ range for data collection/°	6.87 to 148.816
Index ranges	-16 ≤ h ≤ 12, -16 ≤ k ≤ 16, -18 ≤ l ≤ 20
Reflections collected	22115
Independent reflections	9576 [R(int) = 0.0748]
Data/restraints/parameters	9576 / 78 / 660
Goodness-of-fit on F ²	1.118
Final R indexes [I ≥ 2σ (I)]	R1 = 0.0866, wR2 = 0.2334
Final R indexes [all data]	R1 = 0.1132, wR2 = 0.2597
Largest diff. peak/hole / e Å ⁻³	1.277 and -1.276

Notes:

The ethyl group C(109)-C(110)/C(09')-C(10') is disordered over two positions with the refined percentage occupancy ratio of 56(2):44(2).

A molecule of dichloromethane solvent is present at 20 % occupancy and is disordered over two positions. It was only possible to refine this group isotropically.

Table 16: Crystal data and structure refinement for **96**

Identification code	TXR054
Empirical formula	C ₄₄ H ₃₄ N ₄ O ₈ F ₄ Ru
Formula weight	923.82
Temperature/K	100.00(10)
Crystal system	triclinic
Space group	P-1
a/Å	12.8716(4)
b/Å	13.0639(4)
c/Å	23.1946(7)
α/°	101.138(3)
β/°	90.227(2)
γ/°	91.197(3)
Volume/Å ³	3825.8(2)
Z	4
ρ _{calc} /cm ³	1.604
μ/mm ⁻¹	4.035
F(000)	1880.0
Crystal size/mm ³	0.186 × 0.128 × 0.0733
Radiation	CuKα (λ = 1.54184)
2Θ range for data collection/°	6.87 to 148.816
Index ranges	-15 ≤ h ≤ 16, -14 ≤ k ≤ 16, -26 ≤ l ≤ 28
Reflections collected	28056
Independent reflections	15085 [R _{int} = 0.0324, R _{sigma} = 0.0458]
Data/restraints/parameters	15085/39/1127
Goodness-of-fit on F ²	1.101
Final R indexes [I ≥ 2σ (I)]	R ₁ = 0.0623, wR ₂ = 0.1653
Final R indexes [all data]	R ₁ = 0.0679, wR ₂ = 0.1686
Largest diff. peak/hole / e Å ⁻³	4.35/-1.17

Table 17: Crystal data and structure refinement for **98**.

Identification code	TXR087
Empirical formula	C ₄₂ H ₂₂ F ₁₆ N ₄ O ₄ Ru
Formula weight	1051.70
Temperature/K	100
Crystal system	monoclinic
Space group	P2 ₁ /c
a/Å	13.0873(9)
b/Å	13.9901(10)
c/Å	22.8552(16)
α/°	90
β/°	91.0505(15)
γ/°	90
Volume/Å ³	4183.9(5)
Z	4
ρ _{calc} /cm ³	1.670
μ/mm ⁻¹	0.494
F(000)	2088.0
Crystal size/mm ³	0.34 × 0.09 × 0.01
Radiation	MoKα (λ = 0.71075)
2θ range for data collection/°	5.824 to 51.364
Index ranges	-15 ≤ h ≤ 15, -15 ≤ k ≤ 16, -24 ≤ l ≤ 27
Reflections collected	26519
Independent reflections	7816 [R _{int} = 0.0989, R _{sigma} = 0.0686]
Data/restraints/parameters	7816/30/634
Goodness-of-fit on F ²	1.052
Final R indexes [I ≥ 2σ (I)]	R ₁ = 0.0778, wR ₂ = 0.2031
Final R indexes [all data]	R ₁ = 0.0926, wR ₂ = 0.2209
Largest diff. peak/hole / e Å ⁻³	2.33/-1.64

References

1. M. Albrecht, *Chem. Rev.*, 2010, **110**, 576-623.
2. P. G. Bomben, K. C. D. Robson, B. D. Koivisto and C. P. Berlinguette, *Coord. Chem. Rev.*, 2012, **256**, 1438-1450.
3. M. I. Bruce, *Angew. Chem. Int. Ed.*, 1977, **16**, 73-86.
4. M. E. van der Boom and D. Milstein, *Chem. Rev.*, 2003, **103**, 1759-1792.
5. S. Hosokawa, J.-i. Ito and H. Nishiyama, *Organometallics*, 2010, **29**, 5773-5775.
6. S. Jiang, S. Quintero-Duque, T. Roisnel, V. Dorcet, M. Grellier, S. Sabo-Etienne, C. Darcel and J.-B. Sortais, *Dalton Trans.*, 2016, **45**, 11101-11108.
7. H.-F. Klein, S. Camadanli, R. Beck and U. Florke, *Chem. Commun.*, 2005, 381-382.
8. S. Hosokawa, J.-i. Ito and H. Nishiyama, *Organometallics*, 2013, **32**, 3980-3985.
9. M. A. Kent, C. H. Woodall, M. F. Haddow, C. L. McMullin, P. G. Pringle and D. F. Wass, *Organometallics*, 2014, **33**, 5686-5692.
10. H. Zhou, H. Sun, S. Zhang and X. Li, *Organometallics*, 2015, **34**, 1479-1486.
11. S. Decurtins, F. Felix, J. Ferguson, H. U. Guedel and A. Ludi, *J. Am. Chem. Soc.*, 1980, **102**, 4102-4106.
12. W. Liu, W. Xu, J.-L. Lin and H.-Z. Xie, *Acta. Cryst. E.*, 2008, **64**, m1586-m1586.
13. Y. Kazunori, O. Yuji, S. Yoshio, K. Youkoh and K. Hiroshi, *Bull. Chem. Soc. Jpn.*, 1981, **54**, 118-126.
14. H. Dreves, *Z. Anorg. Allg. Chem.*, 1991, **605**, 145-150.
15. X. Ren, B. D. Alleyne, P. I. Djurovich, C. Adachi, I. Tsyba, R. Bau and M. E. Thompson, *Inorg. Chem.*, 2004, **43**, 1697-1707.
16. J.-P. Djukic, J.-B. Sortais, L. Barloy and M. Pfeffer, *Eur. J. Inorg. Chem.*, 2009, **2009**, 817-853.
17. J.-i. Ito, S. Ujiie and H. Nishiyama, *Chem. Commun.*, 2008, 1923-1925.
18. D. Conner, K. N. Jayaprakash, T. R. Cundari and T. B. Gunnoe, *Organometallics*, 2004, **23**, 2724-2733.
19. M. Poyatos, J. A. Mata, E. Falomir, R. H. Crabtree and E. Peris, *Organometallics*, 2003, **22**, 1110-1114.

20. H. Rudmann, S. Shimada and M. F. Rubner, *J. Am. Chem. Soc.*, 2002, **124**, 4918-4921.
21. G. Ciantelli, P. Legittimo and F. Pantani, *Anal. Chim. Acta*, 1971, **53**, 303-308.
22. A. Juris, V. Balzani, F. Barigelletti, S. Campagna, P. Belser and A. von Zelewsky, *Coord. Chem. Rev.*, 1988, **84**, 85-277.
23. E. C. Constable and J. M. Holmes, *J. Organomet. Chem.*, 1986, **301**, 203-208.
24. E. C. Constable and M. J. Hannon, *Inorg. Chim. Acta*, 1993, **211**, 101-110.
25. T. Matsui, H. Sugiyama, M. Nakai and Y. Nakabayashi, *Chem. Pharm. Bull.*, 2016, **64**, 282-286.
26. H. Huang, P. Zhang, B. Yu, Y. Chen, J. Wang, L. Ji and H. Chao, *J. Med. Chem.*, 2014, **57**, 8971-8983.
27. L. Zeng, Y. Chen, H. Huang, J. Wang, D. Zhao, L. Ji and H. Chao, *Chem. Eur. J.*, 2015, **21**, 15308-15319.
28. S. Blanck, T. Cruchter, A. Vultur, R. Riedel, K. Harms, M. Herlyn and E. Meggers, *Organometallics*, 2011, **30**, 4598-4606.
29. L. Fetzer, B. Boff, M. Ali, M. Xiangjun, J.-P. Collin, C. Sirlin, C. Gaiddon and M. Pfeffer, *Dalton Trans.*, 2011, **40**, 8869-8878.
30. K. C. D. Robson, B. D. Koivisto, A. Yella, B. Sporinova, M. K. Nazeeruddin, T. Baumgartner, M. Grätzel and C. P. Berlinguette, *Inorg. Chem.*, 2011, **50**, 5494-5508.
31. C.-C. Chou, K.-L. Wu, Y. Chi, W.-P. Hu, S. J. Yu, G.-H. Lee, C.-L. Lin and P.-T. Chou, *Angew. Chem. Int. Ed.*, 2011, **50**, 2054-2058.
32. C. Patoux, J.-P. Launay, M. Beley, S. Chodorowski-Kimmes, J.-P. Collin, S. James and J.-P. Sauvage, *J. Am. Chem. Soc.*, 1998, **120**, 3717-3725.
33. A. Harriman and R. Ziessel, *Chem. Commun.*, 1996, 1707-1716.
34. R. M. Gauvin, H. Rozenberg, L. J. W. Shimon and D. Milstein, *Organometallics*, 2001, **20**, 1719-1724.
35. C.-Y. Wong, L.-M. Lai, P.-K. Pat and L.-H. Chung, *Organometallics*, 2010, **29**, 2533-2539.
36. R. Cerón-Camacho, D. Morales-Morales, S. Hernandez, R. Le Lagadec and A. D. Ryabov, *Inorg. Chem.*, 2008, **47**, 4988-4995.
37. B. Boff, C. Gaiddon and M. Pfeffer, *Inorg. Chem.*, 2013, **52**, 2705-2715.
38. M. Beley, J. P. Collin and J. P. Sauvage, *Inorg. Chem.*, 1993, **32**, 4539-4543.

39. J.-J. Shen, J.-Y. Shao, Z.-L. Gong and Y.-W. Zhong, *Inorg. Chem.*, 2015, **54**, 10776-10784.
40. M.-J. Sun, H.-J. Nie, J.-N. Yao and Y.-W. Zhong, *Chin. Chem. Lett.*, 2015, **26**, 649-652.
41. K.-C. Hwang, J.-L. Chen, Y. Chi, C.-W. Lin, Y.-M. Cheng, G.-H. Lee, P.-T. Chou, S.-Y. Lin and C.-F. Shu, *Inorg. Chem.*, 2008, **47**, 3307-3317.
42. T. Wang, X.-Q. Hao, J.-J. Huang, J.-L. Niu, J.-F. Gong and M.-P. Song, *J. Org. Chem.*, 2013, **78**, 8712-8721.
43. M. E. van der Boom, S.-Y. Liou, Y. Ben-David, L. J. W. Shimon and D. Milstein, *J. Am. Chem. Soc.*, 1998, **120**, 6531-6541.
44. M. Poyatos, E. Mas-Marzá, José A. Mata, M. Sanaú and E. Peris, *Eur. J. Inorg. Chem.*, 2003, **2003**, 1215-1221.
45. U. Mäder, A. Von Zelewsky and T. Jenny, *Helv. Chim. Acta*, 1986, **69**, 1085-1087.
46. M. G. Colombo, T. C. Brunold, T. Riedener, H. U. Guedel, M. Fortsch and H.-B. Büergi, *Inorg. Chem.*, 1994, **33**, 545-550.
47. Y. Ohsawa, S. Sprouse, K. A. King, M. K. DeArmond, K. W. Hanck and R. J. Watts, *J. Phys. Chem.*, 1987, **91**, 1047-1054.
48. C. M. Jensen, *Chem. Commun.*, 1999, 2443-2449.
49. J. Yang and M. Brookhart, *J. Am. Chem. Soc.*, 2007, **129**, 12656-12657.
50. K. A. King, P. J. Spellane and R. J. Watts, *J. Am. Chem. Soc.*, 1985, **107**, 1431-1432.
51. M. A. Baldo, S. Lamansky, P. E. Burrows, M. E. Thompson and S. R. Forrest, *Appl. Phys. Lett.*, 1999, **75**, 4-6.
52. C. Adachi, M. A. Baldo, S. R. Forrest and M. E. Thompson, *Appl. Phys. Lett.*, 2000, **77**, 904-906.
53. E. C. Constable, R. P. G. Henney, T. A. Leese and D. A. Tocher, *J. Chem. Soc., Dalton Trans.*, 1990, 443-449.
54. D. A. Bardwell, J. C. Jeffery, E. Schatz, E. E. M. Tilley and M. D. Ward, *J. Chem. Soc., Dalton Trans.*, 1995, 825-834.
55. E. C. Constable and C. E. Housecroft, *Polyhedron*, 1990, **9**, 1939-1947.
56. C. M. A. Ollagnier, S. D. Perera, C. M. Fitchett and S. M. Draper, *Dalton Trans.*, 2008, 283-290.
57. L. L. Tinker and S. Bernhard, *Inorg. Chem.*, 2009, **48**, 10507-10511.

58. 2014 *The Outlook for Energy: A View to 2040-Exxon Mobil Energy report*, <http://cdn.exxonmobil.com/~media/Reports/Outlook%20For%20Energy/2014/2014-Outlook-for-Energy-print-resolution.pdf>, Accessed 21/02/14, 2014.
59. J. Goldenberg and T. B. Johansson, *World Energy Assessment Overview, 2004 Update*, <http://www.undp.org/content/dam/aplaws/publication/en/publications/environment-energy/www-ee-library/sustainable-energy/world-energy-assessment-overview-2004-update/World%20Energy%20Assessment%20Overview-2004%20Update.pdf>, Accessed 21/02/2014.
60. J. Koepke, X. Hu, C. Muenke, K. Schulten and H. Michel, *Structure*, 1996, **4**, 581-597.
61. M. Kopczynski, T. Lenzer, K. Oum, J. Seehusen, M. T. Seidel and V. G. Ushakov, *Phys. Chem. Chem. Phys.*, 2005, **7**, 2793-2803.
62. R. C. Davis, S. L. Ditson, A. F. Fentiman and R. M. Pearlstein, *J. Am. Chem. Soc.*, 1981, **103**, 6823-6826.
63. *US Pat.*, 2,402,662, 1946.
64. D. M. Chapin, C. S. Fuller and G. L. Pearson, *J. App. Phys.*, 1954, **25**, 676-677.
65. T. Markvart and L. Castañer, in *Practical Handbook of Photovoltaics (Second Edition)* (Eds.: A. McEvoy, T. Markvart and L. Castañer), Academic Press, Boston, 2012, 7-31.
66. M. A. Green, K. Emery, Y. Hishikawa, W. Warta and E. D. Dunlop, *Prog. Photovoltaics: Res. Appl.*, 2012, **20**, 12-20.
67. D. Chianese, A. Realini, N. Cereghetti, A. Rezzonico, E. Bura, G. Friesen and A. Bernasconi, Proceedings of 3rd World Conference on Photovoltaic Energy Conversion 2003.
68. J. W. Morgan and E. Anders, *Proc. Natl. Acad. Sci.*, 1980, **77**, 6973-6977.
69. A. E. Curtright and J. Apt, *Prog. Photovoltaics: Res. Appl.*, 2008, **16**, 241-247.
70. Y. Zhao, *Phys. Status Solidi C*, 2009, **6**, 744-747.
71. H. J. Möller, C. Funke, M. Rinio and S. Scholz, *Thin Solid Films*, 2005, **487**, 179-187.
72. K. P. Bhandari, J. M. Collier, R. J. Ellingson and D. S. Apul, *Renew. Sustainable Energy Rev.*, 2015, **47**, 133-141.
73. K. L. Chopra, P. D. Paulson and V. Dutta, *Prog. Photovoltaics: Res. Appl.*, 2004, **12**, 69-92.
74. B. O'Regan and M. Grätzel, *Nature*, 1991, **353**, 737-740.

75. R. Garcia-Valverde, J. A. Cherni and A. Urbina, *Prog. Photovoltaics*, 2010, **18**, 535-558.
76. M. Grätzel, *J. Photochem. Photobio. C: Photochem. Rev.*, 2003, **4**, 145-153.
77. M. K. Nazeeruddin, A. Kay, I. Rodicio, R. Humphry-Baker, E. Mueller, P. Liska, N. Vlachopoulos and M. Grätzel, *J. Am. Chem. Soc.*, 1993, **115**, 6382-6390.
78. M. K. Nazeeruddin, F. De Angelis, S. Fantacci, A. Selloni, G. Viscardi, P. Liska, S. Ito, B. Takeru and M. Grätzel, *J. Am. Chem. Soc.*, 2005, **127**, 16835-16847.
79. M. K. Nazeeruddin, R. Humphry-Baker, P. Liska and M. Grätzel, *J. Phys. Chem. B*, 2003, **107**, 8981-8987.
80. Y. J. Hou, P. H. Xie, B. W. Zhang, Y. Cao, X. R. Xiao and W. B. Wang, *Inorg. Chem.*, 1999, **38**, 6320-6322.
81. M. K. Nazeeruddin, P. Pechy, T. Renouard, S. M. Zakeeruddin, R. Humphry-Baker, P. Comte, P. Liska, L. Cevey, E. Costa, V. Shklover, L. Spiccia, G. B. Deacon, C. A. Bignozzi and M. Grätzel, *J. Am. Chem. Soc.*, 2001, **123**, 1613-1624.
82. M. I. Asghar, K. Miettunen, J. Halme, P. Vahermaa, M. Toivola, K. Aitola and P. Lund, *Energy Environ. Sci.*, 2010, **3**, 418-426.
83. T. Bessho, E. Yoneda, J.-H. Yum, M. Guglielmi, I. Tavernelli, H. Imai, U. Rothlisberger, M. K. Nazeeruddin and M. Grätzel, *J. Am. Chem. Soc.*, 2009, **131**, 5930-5934.
84. S. Campagna, F. Puntoriero, F. Nastasi, G. Bergamini and V. Balzani, in *Photochemistry and Photophysics of Coordination Compounds I, Vol. 280* (Eds.: V. Balzani and S. Campagna), 2007, 117-214.
85. P. G. Bomben, K. C. D. Robson, P. A. Sedach and C. P. Berlinguette, *Inorg. Chem.*, 2009, **48**, 9631-9643.
86. S. H. Wadman, J. M. Kroon, K. Bakker, M. Lutz, A. L. Spek, G. P. M. van Klink and G. van Koten, *Chem. Commun.*, 2007, 1907-1909.
87. P. G. Bomben, B. D. Koivisto and C. P. Berlinguette, *Inorg. Chem.*, 2010, **49**, 4960-4971.
88. B. D. Koivisto, K. C. D. Robson and C. P. Berlinguette, *Inorg. Chem.*, 2009, **48**, 9644-9652.
89. K. C. D. Robson, B. Spornova, B. D. Koivisto, E. Schott, D. G. Brown and C. P. Berlinguette, *Inorg. Chem.*, 2011, **50**, 6019-6028.
90. J.-J. Kim, H. Choi, S. Paek, C. Kim, K. Lim, M.-J. Ju, H. S. Kang, M.-S. Kang and J. Ko, *Inorg. Chem.*, 2011, **50**, 11340-11347.

91. K. S. Finnie, J. R. Bartlett and J. L. Woolfrey, *Langmuir*, 1998, **14**, 2744-2749.
92. C. Hansch, A. Leo and R. W. Taft, *Chem. Rev.*, 1991, **91**, 165-195.
93. G. R. Dick, D. M. Knapp, E. P. Gillis and M. D. Burke, *Org. Lett.*, 2010, **12**, 2314-2317.
94. D. M. Knapp, E. P. Gillis and M. D. Burke, *J. Am. Chem. Soc.*, 2009, **131**, 6961-6963.
95. L. C. Campeau, S. Rousseaux and K. Fagnou, *J. Am. Chem. Soc.*, 2005, **127**, 18020-18021.
96. Y. Koga, M. Kamo, Y. Yamada, T. Matsumoto and K. Matsubara, *Eur. J. Inorg. Chem.*, 2011, **2011**, 2869-2878.
97. *WIPO Pat.*, WO2012EP73363 20121122, 2013.
98. C. C. Chou, F. C. Hu, H. H. Yeh, H. P. Wu, Y. Chi, J. N. Clifford, E. Palomares, S. H. Liu, P. T. Chou and G. H. Lee, *Angew. Chem. Int. Ed.*, 2014, **53**, 178-183.
99. G. Boschloo and A. Hagfeldt, *Acc. Chem. Res.*, 2009, **42**, 1819-1826.
100. S. Ferrere, A. Zaban and B. A. Gregg, *J. Phys. Chem. B*, 1997, **101**, 4490-4493.
101. G. Oskam, B. V. Bergeron, G. J. Meyer and P. C. Searson, *J. Phys. Chem. B*, 2001, **105**, 6867-6873.
102. S. Hattori, Y. Wada, S. Yanagida and S. Fukuzumi, *J. Am. Chem. Soc.*, 2005, **127**, 9648-9654.
103. H. Nusbaumer, J.-E. Moser, S. M. Zakeeruddin, M. K. Nazeeruddin and M. Grätzel, *J. Phys. Chem. B*, 2001, **105**, 10461-10464.
104. A. Yella, H.-W. Lee, H. N. Tsao, C. Yi, A. K. Chandiran, M. K. Nazeeruddin, E. W.-G. Diau, C.-Y. Yeh, S. M. Zakeeruddin and M. Grätzel, *Science*, 2011, **334**, 629-634.
105. L. E. Polander, A. Yella, B. F. E. Curchod, N. Ashari Astani, J. Teuscher, R. Scopelliti, P. Gao, S. Mathew, J.-E. Moser, I. Tavernelli, U. Rothlisberger, M. Grätzel, M. K. Nazeeruddin and J. Frey, *Angew. Chem. Int. Ed.*, 2013, **52**, 8731-8735.
106. S.-H. Yang, K.-L. Wu, Y. Chi, Y.-M. Cheng and P.-T. Chou, *Angew. Chem. Int. Ed.*, 2011, **50**, 8270-8274.
107. H.-W. Lin, Y.-S. Wang, Z.-Y. Huang, Y.-M. Lin, C.-W. Chen, S.-H. Yang, K.-L. Wu, Y. Chi, S.-H. Liu and P.-T. Chou, *Phys. Chem. Chem. Phys.*, 2012, **14**, 14190-14195.
108. N. Onozawa-Komatsuzaki, M. Yanagida, T. Funaki, K. Kasuga, K. Sayama and H. Sugihara, *Inorg. Chem. Commun.*, 2009, **12**, 1212-1215.

109. N. Onozawa-Komatsuzaki, M. Yanagida, T. Funaki, K. Kasuga, K. Sayama and H. Sugihara, *Sol. Energ. Mat. Sol. Cells*, 2011, **95**, 310-314.
110. C.-C. Chou, F.-C. Hu, H.-H. Yeh, H.-P. Wu, Y. Chi, J. N. Clifford, E. Palomares, S.-H. Liu, P.-T. Chou and G.-H. Lee, *Angew. Chem. Int. Ed.*, 2014, **53**, 178-183.
111. T. Nagashima, T. Nakabayashi, T. Suzuki, K. Kanaizuka, H. Ozawa, Y.-W. Zhong, S. Masaoka, K. Sakai and M.-a. Haga, *Organometallics*, 2014, **33**, 4893-4904.
112. J.-Y. Shao and Y.-W. Zhong, *Inorg. Chem.*, 2013, **52**, 6464-6472.
113. I. M. Dixon, S. Khan, F. Alary, M. Boggio-Pasqua and J. L. Heully, *Dalton Trans.*, 2014, **43**, 15898-15905.
114. A. J. Wilkinson, A. E. Goeta, C. E. Foster and J. A. G. Williams, *Inorg. Chem.*, 2004, **43**, 6513-6515.
115. V. L. Whittle and J. A. G. Williams, *Dalton Trans.*, 2009, 3929-3940.
116. A. S. Romanov, D. V. Muratov and A. R. Kudinov, *J. Organomet. Chem.*, 2013, **724**, 177-179.
117. J. L. Kiplinger, T. G. Richmond and C. E. Osterberg, *Chem. Rev.*, 1994, **94**, 373-431.
118. P. Barrio, R. Castarlenas, M. A. Esteruelas, A. Lledós, F. Maseras, E. Oñate and J. Tomàs, *Organometallics*, 2001, **20**, 442-452.
119. W.-H. Zhang, X.-H. Zhang, A. L. Tan, M. A. Yong, D. J. Young and T. S. A. Hor, *Organometallics*, 2012, **31**, 553-559.
120. L. Li, F. Wu, S. Zhang, D. Wang, Y. Ding and Z. Zhu, *Dalton Trans.*, 2013, **42**, 4539-4543.
121. M. Lepeltier, F. Dumur, J. Marrot, E. Contal, D. Bertin, D. Gigmes and C. R. Mayer, *Dalton Trans.*, 2013, **42**, 4479-4486.
122. Y. Zheng, A. S. Batsanov, R. M. Edkins, A. Beeby and M. R. Bryce, *Inorg. Chem.*, 2012, **51**, 290-297.
123. G. Vériot, J.-P. Dutasta, G. Matouzenko and A. Collet, *Tetrahedron*, 1995, **51**, 389-400.
124. D. M. Schultz, J. W. Sawicki and T. P. Yoon, *Beilstein J. Org. Chem.*, 2015, **11**, 61-65.
125. K.-L. Wu, C.-H. Li, Y. Chi, J. N. Clifford, L. Cabau, E. Palomares, Y.-M. Cheng, H.-A. Pan and P.-T. Chou, *J. Am. Chem. Soc.*, 2012, **134**, 7488-7496.